Spring 2020

The Use of Natural Anthraquinone Emodin as a Primary and Complementary Therapeutic in the Treatment of Colorectal Cancer

Alexander-Jacques Theodore Sougiannis

THE USE OF NATURAL ANTHRAQUINONE EMODIN AS A PRIMARY AND COMPLEMENTARY THERAPEUTIC IN THE TREATMENT OF COLORECTAL CANCER

by

Alexander-Jacques Theodore Sougiannis

Bachelor of Science
Southern Illinois University, 2013

Master of Science
University of South Carolina, 2015

Submitted in Partial Fulfillment of the Requirements

For the Degree of Doctor of Philosophy in

Biomedical Science

School of Medicine

University of South Carolina

2020

Accepted by:

E. Angela Murphy, Major Professor

Mitzi Nagarkatti, Committee Chair

Daping Fan, Committee Member

Traci Testerman, Committee Member

James A. Carson, Committee Member

Cheryl L. Addy, Vice Provost and Dean of the Graduate School

DEDICATION

This dissertation is dedicated in loving memory of my friend Alexi Pavlov and my grandfather Jacques Oltheten.

ACKNOWLEDGEMENTS

I first need to thank my parents Theodore and Elisabeth and my brother Nick for their incredible support during the last five years. Without you three, I know I would not have made it this far.

I also need to thank my mentor Dr. Angela Murphy. She believed in me from the beginning and always gave me opportunities to continue to grow. The awards I have received and the success I have had in graduate school are because of her faith and confidence in me. I will always be proud to have been your student and I hope we continue to work together for many years to come.

I would also like to acknowledge the faculty and staff of the PMI department, especially Nicki Holt, Maggie Whisenant, Tina Akers. They work to keep the busy lives of scientists just a little less hectic and have always supported my endeavors. I also need to thank Dr. Ioulia Chatzistamou for her friendship and guidance through my PhD and her help in my process in applying to medical school.

Finally, I need to mention my friends Milto and Despoina Stamatopoulos, Christos Stamatopoulos, and Katie and Chrysoula Chulkas, they have been my family away from family and have always supported me. I love you all and I am glad to have had you with me on this journey.

ABSTRACT

5 Fluorouracil (5FU) chemotherapy is widely used in the treatment of colorectal cancer (CRC), and has been the first-choice chemotherapy drug for CRC for many years. However, nearly 10% of patients receiving chemotherapy die during the first 30 days of treatment. Further, it is estimated that 70% of surviving patients will develop non-specific toxicities as a result of chemotherapy treatment. We characterize these toxicities in an animal model of chemotherapy treatment and show that perturbations in the gut microbiome might be exacerbate the prolonged effects of chemotherapy. A compound that could attenuate the multiple non-selective toxicities associated with chemotherapy could have great clinical potential. Emodin is a trihydroxy-anthraquinone found in several Chinese herbs, including *Rheum palmatum* and *Polygonum multiflorum*. Emodin has been shown to attenuate the severity of multiple experimental disease models including arthritis, liver damage, atherosclerosis, myocardial ischemia, and cancer by reducing the inflammatory cascades associated with these conditions. We illustrate that emodin is poorly absorbed when given orally or intraperitoneally and is cleared from systemic circulation by 12 hours. However, we did discover that emodin is more bioavailable in female mice 1 hour after dosing. We also demonstrate that emodin is safe in mice when given through the diet for 3 months and does not cause any physiological or pathological perturbations. When pairing emodin with 5FU, we were able to attenuate functional toxicities associated with chemotherapy and ameliorate the lymphocytopenia associated with chronic and acute chemotherapy. Further, we demonstrate that emodin

can improve gut resilience to 5FU and reduce aberrations in bacterial spatial arrangement. In addition, we examined the ability for emodin to be used as a preventative treatment for colorectal and intestinal cancer. We show that emodin treatment reduces tumor burden in both the AOM/DSS and $Apc^{min/+}$ models of sporadic cancer development. In the AOM/DSS model we show that emodin reduces pro-tumorigenic M2-type macrophages in the colon. Further, we show that there is amelioration of the pro-inflammatory niche that exists in the bone marrow which might contribute to the improved survival outcome and quality of life during cancer treatment. The findings presented in this document show significant promise for the potential use of emodin as a primary and complementary therapeutic in the treatment of colorectal cancer.

PREFACE

The need for physician-scientists has never been greater. As the world enters the next industrial revolution, biomedicine will be at the forefront of the most unprecedented discoveries. With new medical technology and an evolving understanding of nature, so must come a new approach to medicine. Chemically derived therapeutic interventions will be able to optimize physiological interactions to achieve the maximal result during treatment. The goal of this dissertation is to investigate the interaction between three characters in medical treatment; the inflammatory response, the gut microbiota, and the drug itself. Through the course of my work, I will demonstrate how all three of these components of medicine can interact to improve the efficacy, fine tune the pharmacokinetics, and reduce non-specific toxicity to idealize the personalized approach to medicine. While I know that I am not the only one to propose this approach to medicine, I hope these ideas will prove to be fruitful in the evolution of modern medicine and lead to safer and more effective treatments in all fields of medicine.

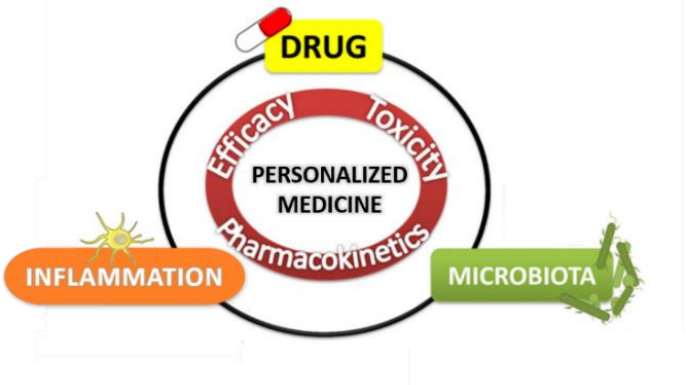

Figure P1.1 The microbiota-immune-drug axis in the development of personalized medicine.

TABLE OF CONTENTS

LIST OF TABLES

LIST OF FIGURES

LIST OF ABBREVIATIONS

5FU ..... 5 Fluorouracil

AKT ..... Protein Kinase B

AOM ..... Azoxymethane

Apc ..... Adenomatous polyposis coli

CRC ..... Colorectal Cancer

DEXA ..... Dual energy X-ray absorptiometry

DMH 1,2-dimethylhydrazine

dMMR ..... deficient mismatch repair

DNA ..... Deoxyribonucleic acid

EPO ..... Erythropoietin

FDA ..... US Food and Drug Administration

FSIG ..... Flexible sigmoidoscopy

GLUT1 ..... Glucose Transporter-1

HIF-1 ..... Hypoxia Inducible Factor-1

Hr ..... hours

IFN-γ ..... Interferon Gamma

IL ..... Interleukin

IP ..... Intraperitoneally

IV ..... Intravenously

JNK ..... Jun Amino-terminal Kinase

kDa ..... Kilodalton

M1 Macrophage ..... Pro-inflammatory Type Macrophage

M2 Macrophage ..... Anti-inflammatory Type Macrophage

MCP-1 ..... Monocyte Chemoattractant Protein 1

mg/kg ..... milligrams per kilogram

min ..... minute

min ..... multiple intestinal neoplasia

MoM ..... Modifiers of Min

mRNA ..... messenger RNA

MSI-H ..... Microsatellite Instability-High

NFκB ..... Nuclear Factor-kappa B

NOS ..... Nitric Oxide Synthase

PBS ..... Phosphate Buffered Saline

PBS-T ..... Phosphate buffered saline and tween

PICRUSt ..... Phylogenetic Investigation of Communities by Reconstruction of Unobserved States

SDS ..... Sodium dodecyl sulfate

TAM ..... Tumor Associated Macrophage

TNFα ..... Tumor Necrosis Factor alpha

WHO ..... World Health Organization

V ..... Volts

VEGF ..... Vascular Endothelial Growth Factor

CHAPTER 1

INTRODUCTION AND AIMS

The WHO has reported cancer as the second leading cause of death, accounting for nearly 9.6 million deaths worldwide per year. This amounts to nearly 1 in 6 deaths being due to cancer. In the United States, the National Cancer Institute estimates that over 1.7 million new cases of cancer will be diagnosed in 2020 and over 600 thousand people will die from the disease. Within this statistic, the American Cancer Society estimated that in 2019 there were over 100 thousand new cases of colon cancer and over 40 thousand new cases of rectal cancer while there were over 51 thousand deaths associated to colorectal cancer alone. It is estimated that the average American has a 5% lifetime risk of developing colorectal cancer (CRC) with men having a greater mortality rate of 59 per 100 thousand versus 44 per 100 thousand in women. The incidence of colorectal cancer increases with advancing age in both genders, with the highest risk occurring in those over 69 years of age. The financial burden of colorectal cancer has had a large impact on the current health care system. In 2010, the estimated direct cost of colorectal cancer was over $14 billion, with over $11 billion resulting from lost productivity and premature death. Thus, colorectal cancer has had, and is continuing, to have a major impact on both the population and economy of the United States.[1]

5 Fluorouracil (5FU) chemotherapy is widely used in the treatment of CRC and has been the first-choice chemotherapy drug for CRC for many years. However, its

clinical utility remains hampered by acquired resistance and hematopoietic and gastrointestinal toxicities resulting from its non-selectivity. 5FU functions as a thymidylate synthase inhibitor with a half-life of approximately 15 min when injected intravenously (IV).

When used in the treatment of CRC, it is estimated that approximately 1% of the injected compound reaches the colon to induce a potential anti-tumor effect. This translates to a 10-15% success rate in the clinic. Currently, there is no standard prescription of 5FU therapy. The most common regimen involves 4 consecutive days of a moderate dose with daily monitoring of behavior and phenotypic changes in the patient. If the patient is described as well adapted and responsive to the treatment, a fifth day of treatment will be given and then will be delivered every other day until the patient begins to show symptoms of non-specific toxicity. As such, many side effects are associated with 5FU treatment; the most common including fatigue, loss of appetite, and diarrhea, all of which can lead to a reduced quality of life. Beyond this, it is estimated that over 7% percent of cancer patients treated with chemotherapy die as a result of non-selective toxicities rather than the cancer itself.

Alternative and complementary medicine has been used in many aspects of both western and eastern medicine. Attenuating inflammation and disease pathology with these compounds is an age-old practice but has recently entered the spotlight in modern experimental medicine. Unfortunately, many natural compounds are sold as supplements and are therefore at risk for being improperly used. This, however, presents the opportunity to investigate the efficacy and applicability of these natural compounds to clinical settings as potential primary or complementary therapeutics.

Emodin (1,3,8-trihydroxy-6-methylanthraquinone), is a natural anthraquinone that has recently entered the spotlight of natural compounds with potential anti-tumor and anti-inflammatory properties. Isolated from several Chinese herbs, including *Rheum palmatum, Polygonum cuspidatum,* and *Polygonum multiflorum,* emodin has been regularly used in traditional Chinese medicine. Multiple pre-clinical investigations have demonstrated emodin to contain a wide spectrum of pharmacological benefits, including; anti-viral, anti-bacterial, anti-allergic, anti-osteoporotic, anti-diabetic, anti-inflammatory, neuroprotective, hepatoprotective, and anti-tumorigenic properties. Utilizing these potential properties, our ultimate aim is to establish emodin as a safe compound to be used as potentially both a primary and complementary therapeutic.

The overall goal of this proposal is to determine the pre-clinical effectiveness of emodin in attenuating the toxicities associated with chemotherapy treatment and the potential for emodin to prevent the onset of colorectal cancer. Our *central hypothesis* is that emodin will reduce the inflammation associated with both chemotherapy toxicity and colorectal cancer burden through mechanisms involving the inactivation of macrophages leading to reduced inflammatory burden, better quality of life, and prolonged survival. This hypothesis will be tested in the following three aims:

Specific Aim #1 will evaluate the effect of 5 fluorouracil chemotherapy on inflammation, functional parameters, and gut microbiota.

Specific Aim #2 will determine the effects of dietary emodin on reducing toxicity of 5 fluorouracil chemotherapy.

Specific Aim #3 will determine the efficacy of dietary emodin on preventing colorectal cancer.

Working Model: Initially, this proposal will examine the overall toxic characteristics of 5FU chemotherapy both in the absence and presence of colorectal cancer (AIM 1). Next, this proposal will investigate the pharmacological properties of natural anthraquinone emodin and its ability to be used as a complementary therapeutic to reduce the toxic properties associated with 5-FU chemotherapy (AIM 2). Finally, this proposal will also evaluate the use emodin to prevent the onset of colorectal cancer (AIM 3). Overall, this proposal will provide a comprehensive understanding of 1) the toxicities associated with current cancer treatments, 2) the potential use of emodin to reduce toxicities associated with current cancer treatments, and 3) the potential for emodin to be used as a dietary therapeutic to prevent colorectal cancer. The results of the above described aims will serve as an important step for progression of emodin to human trials in addition to furthering our understanding of the role of natural anthraquinones in the prevention and treatment of colorectal cancer.

Specific Aim #1 will evaluate the effect of 5 fluorouracil chemotherapy on inflammation, functional parameters, and gut microbiota.

Rationale: It has been previously established that 5FU chemotherapy causes severe adverse reactions and non-selective toxicities in cancer patients. Side effects include fatigue, loss of appetite, and diarrhea among others, all of which can lead to a reduced quality of life and premature death. Identifying strategies to increase efficacy and reduce toxicity of chemotherapy are of significant public health importance. Further, 5FU has been reported to cause disturbances in the gut microbiome, which can further

influence the outcome of cancer therapy. Thus, the goal of this aim is to perform a comprehensive analysis of the physiological effects of 5FU therapy on inflammation, functional parameters, and gut microbiota.

Aim 1.1: We will observe the effects of 5FU on local and systemic inflammation in non-tumor burdened mice and in the AOM/DSS model of colorectal cancer. We will use a low dose regime of 5FU therapy (40 mg/kg) which is most comparable to the commonly prescribed dose in clinical medicine.

Aim 1.2: To observe the effects of 5FU on quality of life, we will employ a battery of functional tests to investigate fatigue, muscular strength, and peripheral nociception.

Aim 1.3: We will observe and characterize the changes in the gut microbiome-immune system using 16S rRNA sequencing and PICRUSt analysis. We will then utilize fecal microbial transplantation to characterize the changes in microbial composition and their effects on host physiology.

Specific Aim #2 will determine the effects of dietary emodin on reducing toxicity of 5 fluorouracil chemotherapy.

Rationale: Emodin is a natural anthraquinone derivative found in various Chinese medicinal herbs. Recent evidence has shown emodin to have many health benefits including anti-inflammatory, anti-viral, and anti-bacterial properties among others. In this aim we will first characterize the safety and pharmacodynamics of emodin and then use emodin as a complementary therapeutic to attenuate the toxicities of 5FU chemotherapy.

Aim 2.1: We will perform a standard pharmacokinetics study by giving emodin via IP and oral gavage to assay the clearance of emodin in the plasma over time.

Aim 2.2: To observe the potential long-term effects of emodin, we will feed male and female an emodin infused diet for three months.

Aim 2.3: Emodin will be given 3x/week at a dose of 40 mg/kg complementary to our 35 mg/kg 5FU regime and observed at an acute and chronic timepoint to observe the potential to ameliorate 5FU-associated toxicities.

Specific Aim #3 will determine the efficacy of dietary emodin on preventing colorectal cancer.

Rationale: There is emerging evidence that emodin may have anti-tumor properties. We will use the AOM/DSS and $Apc^{min/+}$ models of colorectal cancer to investigate the potential for emodin to be given as a preventative agent to patients at risk for developing colorectal cancer.

Aim 3.1: We will investigate the potential for emodin to reduce the tumor burden in both models of CRC when used as a preventative therapeutic.

Aim 3.2: We will investigate the ability for emodin to reduce the chronic inflammation associated with CRC.

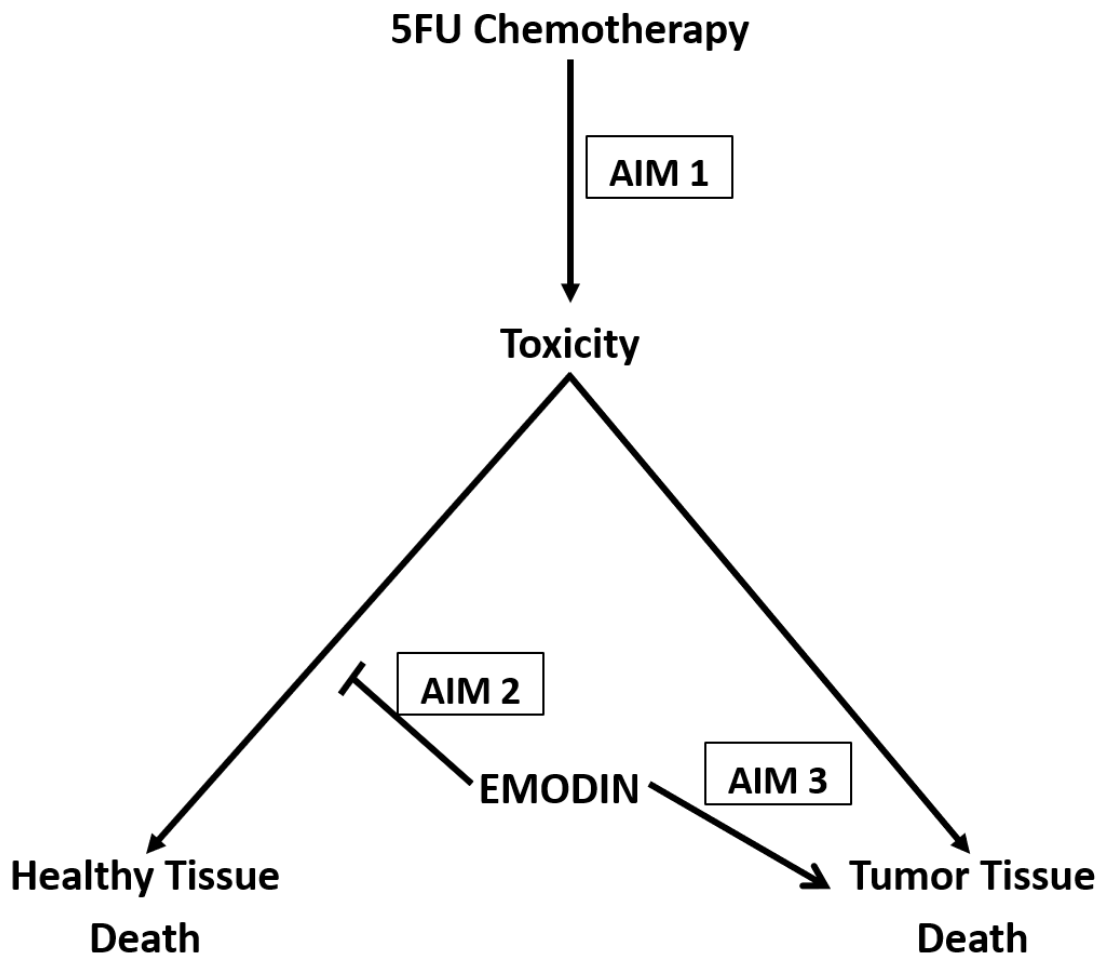

Figure 1.1 Research Model

CHAPTER 2

REVIEW OF LITERATURE

2.1 Colorectal Cancer

The WHO has reported cancer as the second leading cause of death, accounting for nearly 9.6 million deaths worldwide per year. The American Cancer Society estimated that in 2019 there were over 100 thousand new cases of colon cancer and over 40 thousand new cases of rectal cancer, while there were over 51 thousand deaths associated to colorectal cancer alone. It is estimated that the average American has a 5% lifetime risk of developing colorectal cancer (CRC) with men having a greater mortality rate of 59 per 100 thousand versus 44 per 100 thousand in women. The incidence of colorectal cancer increases with advancing age in both genders, with the highest risk occurring in those over 69 years of age. The financial burden of colorectal cancer has had a large impact on the current health care system. In 2010, the estimated direct cost of colorectal cancer was over $14 billion, with over $11 billion resulting from lost productivity and premature death. Thus, colorectal cancer has had, and is continuing, to have a major impact on both the population and economy of the United States.[1]

Clinical Symptoms of Colorectal Cancer

Colorectal cancer is a degenerative disease that takes years to develop in humans. The incidence of colorectal cancer is suggested to be onset by chronic stress and poor lifestyle management, the latter of which is typically a lack of physical activity and poor

diet. In the early stages of the disease, symptoms of colorectal cancer may be minimal or not present at all. The quantity and severity of symptoms associated with colorectal cancer typically accompany the progression of the disease.

In a clinical setting, symptoms of colorectal cancer are typically broken-down into two categories: local and systemic. Local symptoms are those which have a direct effect on the colon or rectum. These symptoms include changes in bowel habits, constipation, diarrhea, alternating diarrhea and constipation, rectal bleeding or bloody stools, abdominal bloating or cramping, incomplete bowel emptying, and narrower stools. Systemic symptoms are those that affect the entire body and are typically seen in the later stages of the disease. These symptoms typically include unexplained weight loss, unexplained loss of appetite, nausea or vomiting, anemia, jaundice, and weakness and fatigue. Due to the delayed onset of both local and systemic symptoms past the initial onset of the disease, the American Cancer Society recommends that the average American should start regular screening at age 45. Typical screening procedures can be done either with a sensitive stool-based test or with a physical exam consisting of a colonoscopy. Persons in good health are recommended to undergo a colonoscopy every 10 years or flexible sigmoidoscopy (FSIG) every 5 years.

The Two-Faced Future of Colorectal Cancer

The next 50 years will be challenged with a two-faced future of colorectal cancer. On the dark side of this face we see the frightening reality that Millennials and Gen Xers have twice the incidence of colorectal cancer. A study by Siegel et. al, 2017 reported the striking increase in colorectal cancer incidence rates among patients aged 20-39.[2] Although socially, this age group has been shown to be the most active and health

conscious group of Americans, the prevalence of preservatives and poor environmental health has been attributed to this increase of cancer incidence. This further provides rationale to develop a greater understanding of the etiology of colorectal cancer and to develop better preventative therapeutics to lower this increasing burden.

Whereas increased incidence will cause a heavy burden on the healthcare of the American people, improved screening and detection methods for colorectal cancer has been improving survival rates. This has included improved technological advancements in colonoscopy. Colonoscopy is the accepted gold standard for detecting and diagnosing colorectal adenomas and cancers. The Third Eye® Retroscope® and Third Eye® Panoramic™ are two recently developed colonoscopes that allow for a full 180^0 retroflex to provide a more complete view of the colonic folds and can improve polyp detection by up to 80%.[3] Another recent development, pioneered by Check Cap Ltd, has combined X-ray imaging with microtechnology to improve capture of gastrointestinal images. Check Cap's C-Scan® capsule utilizes a capsule size tablet taken with contrast agent. Over 24-72 hours the C-Scan capsule will pass through the gastrointestinal system and generate 3D images of the enteric system which can be assessed by physicians.

2.2 Models of Studying and Investigating Colorectal Cancer

There are many models of studying colorectal cancer that are being utilized to understand the development, progression, and potential therapies of the disease. Utilizing both sexes in multiple models is the gold standard to performing a comprehensive investigation of CRC. Cell culture methods have also been utilized, especially for drug development, to understand a direct impact of a compound on murine and human cells.

Human models are only used in later progressions of drug development, and therefore many investigators use rodent and *in-vitro* models to study colorectal cancer.

Non-rodent species

Canine use has become an attractive model for comparative oncology research. Similar to rodent models, there are many similarities between canine colorectal cancer and the human disease. One of the benefits to canine intestinal cancer models is the onset of tumors is more commonly found in the large intestine rather than the small intestine. This more closely mimics the descending colon/rectal cancers that are most frequently seen in human cases of colorectal cancer.[4] Evaluation of clinical cases of canine colorectal carcinomas have revelated cytoplasmic and nuclear accumulations of β-catenin, which further suggests a dysregulation of the WNT signaling pathway as an important driver in the onset of colorectal cancer in the canine species.[5] Despite the similarities between canine and human colorectal cancer, the prevalence in canines is less than 1% and therefore severely limits the effectiveness of using this model.[4,5]

Sheep are also an effective comparative pathological model of studying colorectal cancer due to the similarities of lesions and metastatic behavior with the human disease. Despite these similarities, it has been documented that 100% of intestinal adenocarcinomas developed in sheep are found in the small intestines. Along with this limitation, the unique physiological characteristics of the sheep ruminant fore-stomachs has been shown as a significant weakness of this model.[4,6]

Orthotopic Tumors

The transition from *in-vitro* experiments to *in-vivo* typically involves implanting a tumor in the flank of rodents. The most common models for colorectal cancer are the CT-

26 cell line, which are native to the BALB/c mouse strain, and the MC38 cell line which are native to the C57BL/6 moue strain. Palpable tumors typically develop within 14 days and the mice begin to show physiological perturbations associated with cancer. Tumors can grow to be large and can account for more than 15% of the animal's total body weight. These models typically mimic the symptoms of tumor burden which include increased circulating IL-6 and insulin resistance. These models are primarily used for rapid studies and are often incorporated into preliminary understandings of novel compounds. The accelerated development of tumors makes the tumor burden less like the human disease; but is still accepted as a model of studying colorectal cancer.[7] Further, in the development of colorectal cancer, it is important to understand that a colorectal tumor implanted in the flank of an animal is not in its native hypoxic environment and may develop and respond differently to treatments since the tumor is more available to the systemic circulation.[8,9]

Diet-Induced Rodent Neoplasia Models

Epidemiological evidence has shown diet as a key modulator to the incidence of colorectal cancer in humans.[10-12] Several rodent studies have been conducted to examine the influence of poor diet on the incidence of colorectal cancer. This diet typically is designed to mimic the poor "Western diet" that has become problematic to the current health of Americans. In rodent studies, the "Western diet" is designed to increase caloric fat intake from 5% to as much as 60%, decrease calcium intake from 0.5% to 0.05%, and decrease vitamin D intake to 100 IU/kg from 1,000 IU/kg.[4,13]

Feeding of the Western diet for as little as 12 weeks has been shown to induce hyperplasia of the colonic crypts in rats and mice.[13] Longevity studies have also shown

that after 2 years of being fed the Western diet, 70% of mice developed dysplastic crypts and small polypoid lesions, most of which were found in the distal colon.[14] Another study has also shown that a 2-year feeding of a Western diet low in fiber, choline, folate, and methionine lead to 25% of C57BL/6 mice to develop intestinal tumors and adenocarcinomas. Feeding the Western diet to mice has also been shown to induce a transcript profile in normal colonic mucosa that was similar to the pattern loss of the *Apc* allele in $Apc^{1638N/+}$ mice.[15] The Western diet model of spontaneous colorectal cancer is an attractive model to study the etiology of colorectal cancer, however, the severity of the dietary fat intake combined with the time necessary for tumor development do not reflect the etiology of human colorectal cancer.

Chemically Induced Models

A large variety of chemicals have been shown to have mutagenic properties and have been used to controllably induce cancer. 1,2-dimethylhydrazine (DMH) and its metabolite azoxymethane (AOM), are the two most commonly use carcinogens to induce colorectal cancer in rodents.[16] DMH and AOM are alkylating agents that are typically injected intraperitoneally or subcutaneously over several weeks to induce tumorigenesis. AOM is typically used to produce colorectal polyps and can cause mutations in the K-ras, Src/PI3K/Akt, β-catenin, TGF-β, and p53 signaling pathways to drive tumor development.[17,18] The AOM model can be used on its own or be paired with dietary DSS supplementation. DSS is used to induce colitis and systemic inflammation which further drives tumor development. This model is useful for studying the gene-gene and gene-environment interactions that influence the pathophysiology of colorectal cancer.

However, it is suggested that this model is not viable due to the little evidence supporting the etiology of human colorectal cancer resulting from exposure to alkylating agents.[4]

Apc$^{min/+}$

The Apc$^{min/+}$ mouse has been one of the leading models for preclinical colorectal and intestinal cancer research over the past 25 years. The phenotype of these mutant mice showed severe clinical symptoms of intestinal cancer from the onset of a usually fatal case of regenerative anemia attributed to multiple intestinal neoplasms, or "min." The min mouse has a naturally occurring T-to-A nonsense mutation at nucleotide 2,549 of the *Adenomatous polyposis coli (Apc)* gene that pares the Apc protein at the codon 850, this predisposes the mice to develop multiple intestinal adenomas.[19] The min mutation is autosomal dominant, and homozygosity for the mutant allele is embryonic lethal. Heterozygous Apc$^{min/+}$ typically become anemic by 60 days of age and progress through worsening clinical symptoms of intestinal cancer and usually die by 120 days of age.[4,19]

The use of the Apc$^{min/+}$ mouse model has been widely used to study carcinogenesis or to test novel treatments and delivery methods. The Apc$^{min/+}$ mouse has also been used to study genetic modifications of colorectal cancer risk or Modifiers of Min (MoM).[4,20] This model, however, leads to the development of polyps primarily in the small intestine with few polyps found in the colon. Therefore, it is commonly used as a model of cancer cachexia but is also effective as a preclinical model for drug development.

2.3 Treatments for Colorectal Cancer and Non-Specific Toxicities

The last 60 years has seen great strides for medical technology and has led to an improved ability to treat multiple cancers. Since the discovery of DNA replication blocking mechanisms of Aminopterin, the predecessor to current treatment methotrexate, research into blockading functions of cell growth have been the major focus for the development of anti-cancer therapies. As the incidence of different types of cancer evolved in the medical community, there was an increased demand of treatment methods. Present therapies have seen improved targetability of tumor subtypes and increased early detection. As various mechanisms of cancer development and treatment are discovered, so paralleled the evolution of chemotherapy treatments. This evolution of treatments has further led to treatments focused on drug combinations, delivery techniques, tissue specificity, and overcoming drug resistance by carcinomas.[21,22]

Common Treatment Regimes

Chemotherapy is the most widely used treatment of colorectal cancer. Specifically, 5 Fluorouracil has been the first-choice chemotherapy drug for CRC for many years. 5FU functions as a thymidylate synthase inhibitor and is typically injected intravenously (IV). The most common regimen used in clinical settings involves 4 consecutive days of 5FU treatment with daily monitoring of behavior and phenotypic changes in the patient. If the patient is described as well adapted and responsive to the treatment on day 5 another single injection will be delivered every other day for 6 days or until the patient starts to show symptoms of non-specific toxicity. This regimen is given at the discretion of the attending physician and can be prescribed either as an adjuvant therapy to a colon resection or as a sole method of treatment.[23,24]

The use of high energy radiation (such as x-rays) or particles to destroy cancer cells is more often used in rectal cancer than colon cancers. The use of radiation is commonly adjuvant to chemotherapy or surgical resection. When used with surgery, radiation is used to kill cancer cells that may have invaded through the colon, posing a risk for metastasis after surgery. Because of the risk for causing gut barrier dysfunction, radiation is seldomly used in cases where it can be avoided.

Immunotherapy

The introduction of immunotherapy has recently revolutionized the understanding of biology and medical science and has led to a vast array of targeted therapeutics.[25] Unfortunately, the realm of colorectal cancer has seen little benefits from the immunotherapy revolution. In a recent clinical trial, patients treated with Pembrolizumab (Keytruda) reported 0% response rate in primary CRC. However, Pembrolizumab did gain approval from the FDA in May 2017 for use in patients with unresectable or metastatic colon cancer that has tested positive for microsatellite instability-high (MSI-H) or deficient mismatch repair (dMMR) and have previously undergone chemotherapy. Currently, the use of immunotherapy in metastatic colorectal cancer has proven to be the most promising avenue. However, as stated above, the current technology has shown little to no promise in the treatment of primary colorectal cancers.[26]

Non-Specific Toxicities

Non-specific toxicities are the major burden associated with current treatments for colorectal cancer. As described above, 5FU is the most commonly used chemotherapeutic used in the treatment of colorectal cancer. However, its clinical utility remains hampered by acquired resistance and hematopoietic and gastrointestinal toxicities. Being the most

commonly prescribed chemotherapeutic for colorectal cancer, the majority of literature has focused on elucidating the non-specific toxicities associated with 5FU. 5FU functions as a thymidylate synthase inhibitor with a half-life of approximately 15 min when injected intravenously. When used in the treatment of CRC, it is estimated that approximately 1% of the injected compound will reach the colon to induce an anti-tumor effect. This translates to a 10-15% success rate in the clinic.[27]

As such, many side effects are associated with 5FU treatment, the most common including fatigue, loss of appetite, and diarrhea, all of which can lead to a reduced quality of life.[28] Furthermore, 7.5% of cancer patients treated with chemotherapy die as a result of non-selective chemotherapy toxicity rather than the cancer itself.[29] One of the most potent side effects of 5FU treatment is intestinal mucositis. Mucositis usually appears along the entire gastrointestinal tract from mouth to anus and causes general debility.[23,30-32] Mucositis of the intestine is characterized by increased crypt apoptosis and villus atrophy, leaving the mucosal tissue open to infection and ulceration.[33,34] Several factors or genes contributing to the 5FU-induced mucositis have been previously studied; the formation of reactive oxygen species (ROS) and the production of pro-inflammatory cytokines, such as interleukin-1β (IL-1β), IL-6, and tumor necrosis factor-α (TNFα) have been implicated in this process.[31,33,35] Furthermore, histological evaluation of the small intestine indicates obvious villus destruction and inflammation of the crypts.[35,36]

Another well-documented side-effect of 5FU is the incidence of cytopenia and anemia. Most patients present with severe cytopenia and anemia after treatment with 5FU. This directly translates to patients becoming immunocompromised and developing nosocomial infections which can worsen their condition. Further, anemia results in severe

fatigue and weakness which lowers quality of life and the ability to maintain tissue homeostasis during treatment periods.

Finally, many patients present with increased sensitivity to touch and complaints of pain. Where this mechanism of toxicity has remained elusive to medical research, recent efforts have utilized complementary and alternative therapeutics to blunt these responses to provide relief during intense bouts of pain.

The Future of Treatments in Colorectal Cancer

Recent advances in medical technology have improved the clinical efficacy of diagnosis and early-stage treatment of CRC. However, more needs to be done in the respect to treating and preventing colorectal cancer. The future of cancer treatment involves a bimodal approach through 1) prevention and 2) physiological engineering.[12,34,37-43] As our understanding of nature and biomolecular engineering improves, so will the ability to design personal therapies to prevent the onset and improve current therapeutic interventions. As with the focus of this dissertation, it is important to consider multiple aspects of physiology when designing experimental interventions and in clinical medicine.

Phases of Drug Development

The progression of drug testing requires many pre-clinical and clinical steps that are highly regulated by the FDA. The first step in drug development involves the use of pre-clinical animal and *in-vitro* based experiments that show effective and safe delivery methods of the proposed compound. After this extensive bout of investigations, the FDA can decide whether the drug is reasonably safe for progression to human trials, or to take the drug back to formulation. Once in clinical trials the drug is considered an

investigational new drug and must pass three phases of clinical testing. These phases are overseen by both medical research teams and non-research-based scientists and physicians.

Phase 1 testing is usually conducted in healthy volunteers in an effort to determine side effects and to perform necessary human pharmacokinetic analyses. The number of participants for this phase is typically between 20 and 80. Phase 2 studies begin once the drug has been determined safe for healthy humans. This phase tests a variety of patients with certain diseases or conditions and is compared in a controlled study against a placebo drug or current form of treatment. In Phase 2, the number of participants can be expanded to at most 300 and is usually determined based on the range of conditions being investigated. At the end of Phase 2, if a drug has shown evidence of effectiveness in a certain population, Phase 3 can begin. Phase 3 is typically aimed at a more targeted population and can be initiated as a follow-up study with larger participant populations. The number of participants in Phase 3 can be anywhere from a few hundred to three thousand. Phase 3 can also be expanded to multiple centers.

After passing all three phases of human clinical trials, post-market and commitment studies are required by a sponsor and are monitored by the FDA. This typically allows the drug to enter longevity studies in human participants to determine any long-term side effects that may arise from continuous use of the drug. Once passed by the FDA, the drug can be submitted as a new compound and within six months can be passed and distributed for use in clinical medicine.[44]

Many times, it has been necessary for a drug to undergo a Phase 4 trial. This involves recruiting greater numbers of participants to confirm certain findings that might have been contradictory or abnormal to previous investigation. Recently, companies such as Merk, have initiated Phase 0 studies of new drugs. This involves utilizing a small participant pool and performing microdosing of the drug. Microdosing allows for the drug to be delivered at a concentration 100X lower than the proposed therapeutic dose. Phase 0 also confirm bench-to-bedside translation of compounds to confirm mechanistic actions and deem the drug safe for use in greater populations of human participants.

2.4 Hallmarks of Immunology in Cancer and Cancer Treatments

The immune niche of a tumor

With the emergence of immune-based therapies, the immune microenvironment has become of significant interest as a primary regulatory mechanism that can determine the outcome of anti-cancer treatments. Tumor immune evasion and immune promoting factors are two primary hallmarks of cancer contributing to the maintenance of a tumor microenvironment.[45] Recently, the difference between a "Hot" and "Cold" tumor has been highlighted as significant to the prognosis and therapeutic outcome of anti-cancer treatments. "Hot" tumors are described as those that contain large amounts of immune cells and "cold" tumors are the opposite and do not contain large amounts of immune cells.

The "hot vs. cold" status has been shown to play a significant role in the outcome of therapies. A recent article by Newman et. al. 2020 injected unadjuvanted seasonal influenza vaccines into melanoma and breast cancer orthotopic tumors effectively

changing them into “hot” tumors[43]. This reduced tumor size by increasing CD8+ T-cells and decreasing regulatory B-cells within the tumor. This finding demonstrates that turning a tumor from “cold” to “hot” can promote anti-tumor effects and can be utilized to improve upon current therapies that may be ineffective.

Tumor associated macrophages

A major focus of this dissertation, specifically in Aim 3, will be on tumor associated macrophages or TAMs. The presence of TAMs has been shown to play a vital role in the outcome and prognosis of many cancers.[46] Macrophages are derived from monocyte precursors circulating in the blood and are recruited to the tumor by chemokines such as MCP-1 and TGFβ.[46] Once recruited to the tissue, monocytes will mature into macrophages. It is generally understood that the recruitment of macrophages to the tumor contribute to the maintenance of the tumor microenvironment and exert pro-tumoral functions. Pro-tumoral macrophages are characterized as M2-type macrophages, which are polarized from exposure to cytokines such as TGFβ and IL-10.[47,48] The presence of M2-type macrophages in the tumor microenvironment have been shown to promote proliferation, invasion and metastasis, angiogenesis, and tissue remodeling.[49,50] There is some evidence suggesting that recruitment of M1-type macrophages through increased TNFα, IL1β, and IFNγ might reverse this pro-tumoral environment and cause tumor remission. Therefore, therapeutic interventions targeting TAMs and reducing the M2-type phenotype within the tumor microenvironment might contribute to improved survival and subsequent success of further therapeutic outcome.[46,47,50,51]

It is important to establish that there is conflicting literature on macrophage phenotype, as defined by expression of cell-surface markers. This conflicting body of

literature is primarily derived from the discrepancy in what is defined as a 'mature macrophage' and the differences in these markers seen from tissue to tissue. For example, a review by Bain and Schridde 2018 describes mature macrophages as CD64+MHCII^{hi}CD206+CD163+ cells.[52] In addition, they define lamina propria macrophages as highly expressing CD11b, CD11c, CD14, and CX3CR1 cells. CD11b is widely accepted as a monocyte marker, but where Bain and Schridde do not follow some bodies of literature is with addressing the expression of F4/80 and CD68. F4/80 and CD68 are two of the most widely cited markers of macrophage expression and are commonly used to identify total mature macrophage populations.[53-55] Further, we and others have previously defined M1-type macrophages as CD11c-expressing cells and M2-type macrophages as CD206-expressing cells. CD80, CD86, TLR2, and TLR4 have also been suggested to be expressed on M1-type macrophages. Additionally, CD204 and CD163 have been suggested to be expressed on M2-type macrophages.

Whereas there is discrepancy in the expression of markers between tissues, there is a common consensus that macrophages are highly plastic cell types that exist on a transitionary spectrum that varies from tissue to tissue. In this dissertation, where we examine macrophages, we define total macrophages by flow cytometry as CD45+CD11b+Ly6C+F4/80+ cells which are then further gated against CD11c and CD206. From here where we define CD11c as M1-type and CD206 as M2-type macrophages. Where we use tissue gene analysis, we utilize expression of EMR1 (F4/80) to describe total macrophage populations and ITGAX (CD11c) and MRC1 (CD206) as M1-type and M2-type macrophages, respectively.

T-cells

T-cells function in both a direct and indirect manner in the response to cancer. Killer T-cells will attack and kill cancer cells directly and are identified as CD8 positive cells. Killer T-cells have been shown to first find cancer cells and can also be stimulated to kill cancer cells. Helper T-cells fight cancer indirectly and are identified as CD4 positive cells. Helper T-cells are known to assist in the communication between the T-cell receptor (TCR) and with antigen-presenting cells (APCs). The TCR complex and CD4 bind to distinct regions of the antigen-presenting MHC Class II molecule. T-Cells play a major role in what is known as the cancer-immunity cycle. As cancer cells are killed, tumor specific antigens are released and are taken up and presented by APCs. In the lymph, these APCs now activate CD4+ T-cells which allows them to specifically attack the tumor cells. CAR-T cells are engineered similarly to this process to specifically target cancer cells.[56-59]

In humans, the count of CD4+ and CD8+ cells have been shown to be directly related to clinical outcome and survival. In colon cancer patients, longer disease-free survival is correlated with higher CD8+ counts, lower CD4+/CD8+ ratio, and higher CD8+/FoxP3+ ratio. Immunoscoring (IS) is an index-based density of CD3+ and CD8+ tumor infiltrating lymphocytes (TILs). IS has been shown as a reproducible method from predicting survival of patients with advanced CRC. These values indicate that the presence of CD8+ cells, measured in the circulation or directly from tumors, is correlated to increased survival and anti-tumor responses.[58,60]

B-cells

Whereas T-cells physically attach to and attack cancer cells, B-cells target them indirectly through the production of antibodies. B-cells can play a critical role in cancer protection and anti-cancer response. B-cells present in the tumor microenvironment secrete antibodies that can directly inflame the tumor parenchyma and cytokines that can activate angiogenesis in the vasculature. These responses are capable of inhibiting effector cells such as CD8+ T-cells and NK cells. These B-cells are termed B-regulatory cells (B-regs) and exists as a heterogenous population that can directly or indirectly influence cancer outcome. The specific cytokine release can cause significant influence on the tumor microenvironment. For example, IL-10 producing B-regs can exacerbate inflammation and support cancer growth by promoting a pro-tumorigenic niche within and surrounding the tumor microenvironment.[61]

Solid tumors in humans often contain significant B-cell populations. The number of tumor-infiltrating B-cells were identified as the second-best predictor of positive disease outcome[51]. Antibodies directed against intracellular can be directly produced by B-cells. A study by Mizukami et. al. 2006 showed regression of human lung cancer tissue xenotransplanted into SCID mice was associated with higher levels of tumor-resident B-cell derived IgG in the serum of recipients[62]. Furthermore, B-cell derived antibodies have been shown to bind mouse tumors in an antigen-specific manner and mediate complement-dependent lysis[59].

Natural Killer (NK) cells

Natural Killer cells are lymphocytes that were first identified for their ability to attack tumor cells without deliberate immunization of activation. Furthermore, NK cells

have also been shown to kill cells that are infected with certain viruses and attack cells that lack expression of MHC class I antigens. Recently, the discovery of NK receptors and their ligands has uncovered the molecular mechanisms that regulate NK activation and function. One of the most documented mechanisms is through IL-12 dependent activation of NK cells. IL-12 release is part of a cytokine axis in which myeloid cell-derived IL-12 triggers lymphoid cell-derived IFNγ production and contributes to cytotoxic activation[63,64]. IL-23 and IL-27 are part of the IL-12 family of cytokines. As with IL-12, macrophages and DCs can produce IL-23 and IL-27 upon sensing pathogens or their products[64,65].

One of the original models of immunotherapy involved allogenic adoptive transfer of NK cells. Unlike T-cells, which can induce autoimmune reactions, NK cells appear to be safe when obtained from another person and then injected. Certain ligands such as NKG2D (CD314), DNAM1 (CD226), 2B4 (CD244), 4-1BB (CD137), PD1, and CTLA4 have been implicated in the activation of NK cells towards tumors. Of these ligands, CD314 has been shown to be removed by tumor cells which causes NK cell evasion. The most promising therapeutic intervention against this mutation has been the use of monoclonal antibodies against the proteolytic cleavage site on the MICA and MICB proteins. Preventing this cleavage, in-turn, prevents the shedding of CD314 and rendering tumors susceptible to NK attack[66].

Dendritic Cells (CDs)

Dendritic cells are a heterogenous population of antigen presenting cells that have been shown to infiltrate the tumor microenvironment. Where normally, DCs play a critical role in the priming and maintenance of local immunity; in the presence of cancer,

different subtypes of DCs are recruited to the tumor which can function to either enhance or suppress the anti-tumor immune response. There are four primary phenotypes of DCs which are associated with the tumor microenvironment: Plasmacytoid DCs (pDCs) which function in tolerance induction, Conventional DCs type 1 (cDC1) which function in MHC-I cross-presentation, Conventional DCs type 2 (cDC2) which function in MHC-II presentation, and Inflammatory DCs (Inf-DCs) or Monocyte-derived DCs (moDCs) which function in MHC-I cross-presentation and MHC-II presentation[67].

Death of tumor cells, especially from chemotherapy or radiation, have been shown to modulate tumor associated DCs and enhance anti-tumor immunity. Similarly, anti-PD1 therapy requires DC-T cell crosstalk and the initiation of anti-tumor CD8+ T cell responses by cross-presentation in DCs. DC modulating therapies are currently part of a large field of immunotherapy research. Flt3-L treatment has been one of the most promising strategies to elicit anti-tumor T-cell immunity. Flt3-L is highly expressed by cDC1. Pre-treatment of cDC1 cells with Flt3-L and then subsequent adoptive transfer has been shown to enhance efficacy of checkpoint therapy blockade in animal models of melanoma and glioblastoma.[68]

The actual understanding of the immunoregulatory functions of the tumor microenvironment expand past the scope of this review. However, it is well understood that certain changes in the tumor microenvironment can promote an anti-tumor niche and may be most efficiently achieved by directly or indirectly influencing one or more of the above described immune cells. Therefore, therapeutic interventions showing a mechanism directly influencing these cells is important in developing proper anti-cancer therapeutics.

Taken together, the immune system is well-known to regulate and directly impact the outcome of cancer onset and therapeutic intervention. Therefore, it is imperative to 1) understand the mechanisms of immune function during cancer and 2) to develop interventional and preventative therapeutics that can directly ameliorate the inflammatory consequences of cancer and the current debilitating therapeutics that are administered clinically.

2.5 Emodin: 1,3,8-trihydroxy-6-methylanthraquinone

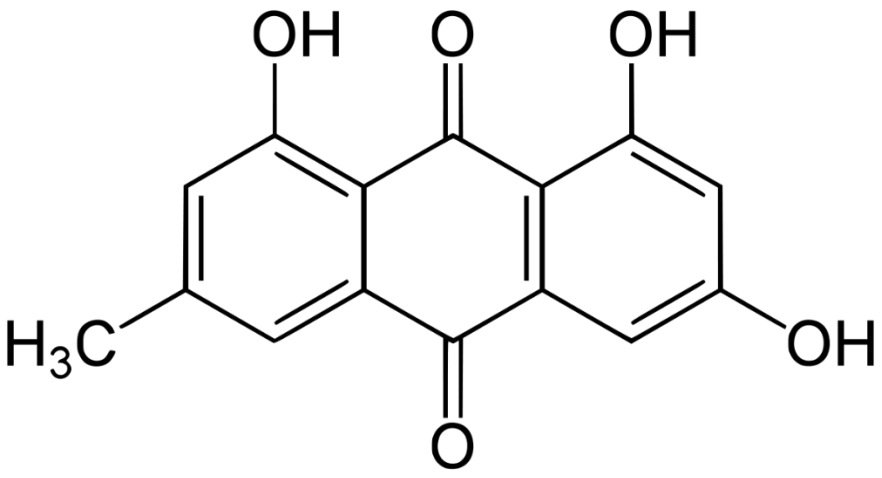

Fig 2.1 Emodin (1,3,8-trihydroxy-6-methylanthraquinone)

Emodin (1,3,8-tryhydroxyanthraquinone) (Fig 2.1) is a natural anthraquinone isolated from several Chinese herbs, including *Rheum palmatum, Polygonum cuspidatum*, and *Polygonum multiflorum*. Multiple pre-clinical investigations have demonstrated emodin to contain a wide spectrum of pharmacological benefits, including; antiviral[69], antibacterial[70], anti-allergic[71], anti-osteoporotic[72], anti-diabetic[73], anti-inflammatory[74,75], neuroprotective[76], hepatoprotective[77], and anti-tumorigenic[77-79] properties.

Evidence for anti-inflammatory properties

The primary goal of this proposal is to utilize emodin as a complementary therapeutic to attenuate the pro-inflammatory responses to 5FU chemotherapy and cancer. Recent evidence utilizing *in-vitro* investigations or orthotopic tumors have shown reduced NF-κB, STAT6, P38 signaling along with reduced IL-6, TNFα, and MCP1 secretion with emodin. In the presented investigations of this proposal, we will aim to 1) confirm these findings in models of 5FU toxicity and colorectal cancer and 2) to discover any further mechanisms of action that might contribute to associated benefits of Emodin as a primary or complementary therapeutic.

We will focus primarily, but not exclusively, on the polarization of macrophages in the gut. Iwanowycz et al 2016 showed evidence of M1 and M2 bi-directional depolarization of macrophages *in-vitro*.[80] A follow-up study by Iwanowycz et al 2016 confirmed this phenomenon and further showed increased cytotoxic T-cell activation leading to reduced orthotopic tumor burden in a model of breast cancer.[78] We will directly expand on this work utilizing two models of colorectal cancer to confirm the anti-tumor potential and build on the literature of immunoregulatory properties of emodin.

Tissue specific effects

As described above, the benefits of emodin have been extensively demonstrated *in-vitro*. However, these studies have revealed conflicting results about the mechanisms of emodin. For example, emodin has been shown to activate P38 MAP Kinase in human hepatoblastoma cells[81,82] and in osteoblasts[72] but has shown decreased activation in non-small cell lung carcinoma[83] and in hepatic stellate cells.[84] Further, activation of ERK1/2

MAP Kinase has been shown to be increased in non-small cell lung carcinoma[85] and colorectal cancer cells[86] but decreased activation in the amelioration of viral myocarditis.[69] These discrepancies overshadow the potential *in-vivo* benefits of emodin and provoke further investigations of this promising dietary agent.

P2X7 Receptor as potential mechanism of action

The mechanism of action of emodin has yet to be discovered. Recent investigations, however, show evidence *in-vitro* of a mechanism targeting the P2X7 receptor. The P2X7 receptor is found primarily in the central and peripheral nervous systems but also on the surface of microglia, macrophages, and the retina. There is evidence that has shown the P2X7 receptor as a pattern recognition receptor for the extracellular ATP-mediated apoptotic cell death, regulation of receptor trafficking, mast cell degranulation, and pro-inflammatory cascade. A study by Jelassi *et al.* 2013 demonstrated emodin was able to reduce breast and non-small cell lung carcinoma cell invasion by antagonizing P2X7 receptor mediated ATP-current.[79] Further, a study by Zhang *et al* 2019 showed emodin reduced ATP-dependent pancreatic duct cell injury by antagonizing the P2X7 receptor.[87]

Overall, emodin contains the potential to be used as a complementary and primary therapeutic in multiple aspects of cancer treatment. This dissertation will attempt to provide vital preclinical evidence in support of this hypothesis in an effort to promote the study of emodin in clinical trials.

CHAPTER 3

IMPACT OF 5 FLUOROURACIL CHEMOTHERAPY ON GUT INFLAMMATION, FUNCTIONAL PARAMETERS, AND GUT MICROBIOTA[1]

[1] Sougiannis AT, VanderVeen BN, Enos RT, et al. Impact of 5 fluorouracil chemotherapy on gut inflammation, functional parameters, and gut microbiota. *Brain Behav Immun*. 2019;80:44-55.

Reprinted here with permission of publisher.

3.1 Abstract

Emerging evidence suggests that gut microbiota may influence the response to chemotherapy. We sought to characterize the effects of 5 fluorouracil (5FU) chemotherapy on colon inflammation and functional measures in colorectal cancer (CRC) and to further determine whether gut microbiota can influence this response. 50 C57BL/6 were randomized into four groups; Control+Vehicle (n=10), Control+5FU (n=10), AOM/DSS+Vehicle (n=15), and AOM/DSS+5FU (n=15). CRC was induced chemically by a single 10 mg/kg injection of azoxymethane (AOM) followed by two cycles (2% and 1%) of dextran sodium sulfate (DSS). Mice were then treated with 3 cycles of vehicle or 5FU (cycle 1: 40 mg/kg, cycle 2+3: 20 mg/kg). Functional tests (grip strength and run-to-fatigue) were performed prior to 5FU treatment (baseline) and at the completion of the second cycle of 5FU. Following the third 5FU cycle, mice were euthanized, and the colon was evaluated for expression of inflammatory genes using RT-qPCR and stool samples were profiled using 16S rRNA sequencing. A second experiment used fecal microbiota transplantation from 5FU treated mice to control mice (n=10–15/group) to determine whether 5FU associated changes in the microbiota could influence functional measures and colon inflammation. 5FU reduced grip strength ($p < 0.05$) and caused a trending decrease in run-to-fatigue performance in cancer mice ($p=0.06$). Select intestinal inflammatory genes were significantly elevated with 5FU treatment and this was further exacerbated with cancer ($p < 0.05$). Microbiota analysis revealed increased dissimilarity and alterations in bacterial taxonomy in 5FU and AOM/DSS-treated mice ($p < 0.05$). Fecal transplant from 5FU treated mice reduced functional performance ($p < 0.05$) and altered select colon inflammatory markers ($p < 0.05$). This study provides evidence of an

effect of 5FU on inflammatory responses and functional measures in a mouse model of CRC and suggests that gut microbes may play a role in some, but not all, 5FU related perturbations.

3.2 Introduction

5 Fluorouracil (5FU) chemotherapy is widely used in the treatment of colorectal cancer (CRC), and has been the first-choice chemotherapy drug for CRC for many years[39,88]. However, its clinical utility remains hampered by acquired resistance and hematopoietic and gastrointestinal toxicities resulting from its non-selectivity[30,32]. 5FU functions as a thymidylate synthase inhibitor with a half-life of approximately 15 min when injected intravenously (I.V.)[30,89]. When used in the treatment of CRC, it is estimated that approximately 1% of the injected compound reaches the colon to induce a potential anti-tumor effect. This translates to a 10–15% success rate in the clinic[27]. Currently, the common regimen of 5FU therapy involves 4 consecutive days of 5FU treatment with daily monitoring of behavior and phenotypic changes in the patient. If the patient is described as well adapted and responsive to the treatment on day 5 another single injection will be delivered every other day for 6 days or until the patient starts to show symptoms of non-specific toxicity[23,24]. As such, many side effects are associated with 5FU treatment, the most common including fatigue, loss of appetite, and diarrhea, all of which can lead to a reduced quality of life[28]. Furthermore, 7.5% of cancer patients treated with chemotherapy die as a result of non-selective chemotherapy toxicity rather than the cancer itself[29]. Therefore, identifying methods to better evaluate the associated toxicity related to chemotherapy and the mechanisms involved is of great public health importance.

One of the most potent side effects of 5FU treatment is intestinal mucositis. Mucositis usually appears along the entire gastrointestinal tract from mouth to anus and causes general debility[23,30-32]. Mucositis of the intestine is characterized by increased crypt apoptosis and villus atrophy, leaving the mucosal tissue open to infection and ulceration[33,34]. Several factors or genes contributing to the 5FU-induced mucositis have been previously studied; the formation of reactive oxygen species (ROS) and the production of pro-inflammatory cytokines, such as interleukin-1β (IL-1β), IL-6, and tumor necrosis factor-α (TNFα) have been implicated in this process[31,33,35,90]. Furthermore, histological evaluation of the small intestine indicates obvious villus destruction and inflammation of the crypts[33,35,36]. However, the majority of literature explaining 5FU-induced intestinal mucositis fails to utilize a disease model limiting a complete understanding of the side effects of 5FU specifically in the context of CRC.

Gut microbiota have been implicated in 5FU associated toxicity[91,92]. 5FU leads to gut dysbiosis (i.e. an imbalance of gut microbes) and the ensuing inflammation leads to exacerbated intestinal mucositis[92]. Several preclinical studies have reported a drastic shift from commensal bacteria (i.e., Bifidobacterium and Lactobacillus spp.) to Escherichia, Clostridium, and Enterococcus spp. following even a single intraperitoneal dose of 5-FU[92]. Mechanistic support for this relationship is provided by the reduced intestinal mucositis and decreased cytokine levels in 5FU treated mice after antibiotic induced depletion of microbes[92]. Understanding the influence of gut microbes on 5FU related toxicity may lead to the dentification of targets (i.e. bacteria themselves or pathways that they mediate) to reduce side effects of chemotherapy.

Using the azoxymethane/dextran sodium sulfate (AOM/DSS) model of CRC, we sought to characterize the effects of 5FU on colon inflammation and functional measures in CRC and to further determine whether gut microbiota can influence this response. We detected a general anti-tumor effect of 5FU in AOM/DSS treated mice; however, side effects including mortality, adverse physiological outcomes, mucositis, and colon inflammation were evident. Further, we observed significant alterations in gut microbiota in the presence of 5FU. Fecal transplantation experiments also were conducted in control mice to investigate the potential causality between gut microbiota and 5FU toxicity. Our findings indicate that gut microbes may play a role in some, but not all, 5FU related perturbations.

3.3 Methods

3.3.1. Animals

Male C57BL/6 mice were purchased from Jackson Laboratories (Bar Harbor, ME) and were cared for in the animal facility at the University of South Carolina. Mice, randomized upon arrival to the animal facility to prevent litter biases in microbiome data, were housed five per cage and maintained on a 12:12-h light-dark cycle in a low-stress environment (22 °C, 50% humidity, low noise). Mice were kept in a room isolated from all other ongoing animal experiments and were handled only by the primary investigators. All mice were habituated to the AIN-76A diet prior to any interventions and were given food and water ad libitum through the course of the study. All methods were in accordance with the American Association for Laboratory Animal Science, and the Institutional Animal Care and Usage Committee of the University of South Carolina approved all experiments.

3.3.2. AOM/DSS protocol and 5FU treatment experiment 1

In experiment 1 (Fig. 1A), 50 mice were randomly divided into four groups: Control+Vehicle (n=10), Control+5FU (n=10), AOM/DSS+Vehicle (n=15), and AOM/DSS+5FU (n=15). At 12 wk of age (baseline week 0) mice received either an intraperitoneal injection of the carcinogen[93], AOM (10 mg/kg) (Sigma, St. Louis, MO), diluted in phosphate buffered saline (PBS) (AOM/DSS) or PBS alone (Control). Mice receiving the AOM injection were subjected to two cycles of DSS (36–50 kDa) (MP Biomedical, Solon, OH)-supplemented water at final concentrations of 2 and 1% at weeks 1 and 4, respectively. Each DSS cycle lasted for a 1-wk period. Body weights and symptom scores were determined semi-weekly along with food and water measurements. Calculation of symptom score was performed as previously described[94] , taking into account percent body weight loss, stool consistency, and rectal bleeding. Briefly, fresh colonic evacuates were smeared onto "Hemoccult" tape to assess severity of diarrhea and were tested with developer (Beckman Coulter, Brea, CA) to assess rectal bleeding. Bleeding was scored; no positive detection of blood (0), detection of blood but not grossly visible (2), and gross visibility of blood (4). Diarrhea was scored; solid cylinder (0), soft cylinder and easily spreadable (2), and non-cylindrical or runny (4). Body weight was calculated as percent body weight loss; 0–5% (0), 6–10% (1), 11–15% (2), 15–20% (3), 20–25% (4), and>25% (5). Scores of all three categories were summed to obtain an overall symptom score for each mouse.

5FU (Sigma Chemical Co., St. Louis, MO) was dissolved in sterile PBS, pH7.4 and then sterile filtered through a 0.2 μm syringe filter. 5FU was administered in 3 cycles; cycle 1: 40 mg/kg, cycle 2 and 3: 20 mg/kg via intraperitoneal injection. 5FU was

prepared fresh at the beginning of each cycle. Sterile filtered PBS alone was used as the vehicle control. Each cycle consisted of 5 consecutive days of injections followed by 9 days of recovery. The treatment period lasted for 5 weeks and mice were sacrificed 24 hr after the final injection of the third cycle.

3.3.3. Fecal transplantation experiment 2

For the fecal transplantation experiment (Fig. 1B), 35 mice were randomly divided into four groups: Donor Vehicle, Donor 5FU, Recipient Vehicle (Vehicle FMT), Recipient 5FU (5FU FMT) (n=5 per Donor group and n=10–15 per Recipient group). The Donor 5FU group was injected with 40 mg/kg 5FU for 5 consecutive days as described earlier. All Donor mice were sacrificed 9 days after initial injection and a mucosal scrape was performed of the distal enteric tract (cecum to anus) to harvest the microbiota for fecal transplantation. Fecal materials were suspended in sterile 10% glycerol/PBS, allowed to settle by gravity for 10 min, and aliquoted into daily requirements for Recipient groups. To perform the FMT study we adopted a protocol by Reikvam et al. 2011[95]. Recipient mice were pretreated with the following antibiotic cocktail every 12 h for 10 days prior to FMT: Vancomycin (50 mg/kg), Neomycin (100 mg/kg), Metronidazole (100 mg/kg), and Amphotericin-B (1 mg/kg) via oral gavage supplemented with Ampicillin (1 mg/ml) in the drinking water given ad libitum. All antibiotics were purchased from ACROS Organics, New Jersey. FMT was administered via oral gavage for 14 days with 150 µl respective fecal suspension from PBS or 5FU injected mice.

3.3.4. Grip strength assessment

All experimental mice were utilized to evaluate the effects of 5FU treatment on grip strength. Grip strength was measured prior to 5FU administration (week 8) and during the recovery period of the second cycle (week 11) in experiment 1 and following antibiotic treatment (week 0) and fecal transplantation (week 2) in experiment 2. Briefly, holding the mice by the tail, the front and back feet were allowed to grip the grate. Mice were then pulled from the grate, generating a force that was measured by the force transducer (Aurora Scientific, Ontario, Canada). Five measurements were taken consecutively, with 2 min rest between sets until a total of 15 measurements were taken for each mouse. The averages of the 15 measurements were used in the data analysis. Measurements were performed by the same investigator through the entirety of the study.

3.3.5. Run-to-fatigue assessment

To determine the effect of 5FU on fatigability, mice were subjected to a run-to-fatigue test prior to 5FU administration (week 8) and during the recovery period of the second cycle (week 11) in experiment 1 and following antibiotic treatment (week 0) and fecal transplantation (week 2) in experiment 2. After 3 consecutive days of habituation during the night cycle, mice were subjected to the following run-to fatigue protocol: 15-min warm-up, 20 m/min for 30 min, and 25 m/min thereafter until fatigue was reached. Fatigue was defined as the time at which mice were no longer able or willing to keep up with the treadmill despite hand prodding for at least 1 min. All treadmill tests were performed during the night cycle by the same two investigators (ATS, BNV) through the entirety of the study.

3.3.6. Tissue collection

Mice were euthanized by isoflurane overdose 24 h post final injection (cycle 3, day 6) in experiment 1 and on day 15 in experiment 2 (Fig. 1A, B). Blood was collected from the inferior vena cava and tissues were removed, weighed, and immediately snap-frozen in liquid nitrogen and stored at −80 °C or fixed in 10% formalin until further analysis. Briefly, the colon was carefully dissected distal to the cecum and proximal to the anus. Mesentery adipose tissue was removed with forceps. Colons were then flushed with PBS, opened longitudinally, and flattened with a cotton swab. In experiment 1, colonic polyps were counted under a dissecting microscope and were categorized according to size (> 2, 2-1, and<1). For both experiment 1 and 2, a 5-mm piece of the distal colon was cut and fixed in 10% buffered formalin (Fisher Scientific, Pittsburg, PA) for 24 h for immunohistochemical and morphological analysis. The remaining colon was cut in half and snap frozen for RNA analysis. The distal portion of the ileum also was cut and fixed in 10% buffered formalin for 24 h for morphological analysis. The liver was dissected, and a small portion was fixed in 10% buffered formalin for 24 h, for morphological analysis.

3.3.7. Blood profile

In both experiment 1 and 2, a complete blood count was performed using the VetScan HMT (Abaxis, Union City, CA) for determination of white blood cells (WBCs), lymphocytes (LYM), monocytes (MON), neutrophils (NEU), red blood cells (RBCs), Hemoglobin (HGB), Hematocrit (HCT), and platelets (PLT). Neutrophil/lymphocyte ratio (NLR) was calculated from obtained values. Briefly, whole blood removed from the

inferior vena cava was placed in an EDTA microtube and analyzed on the VetScan HMT according to the manufacturer's instructions.

3.3.8. Hematoxylin and eosin staining & histopathology

Hematoxylin and eosin staining of the colons, small intestines, and liver were performed as previously described[96]. Colon specimens were characterized according to the presence of epithelial neoplasia to: no adenomas/dysplasia (ND), adenomas with low grade dysplasia (LGD) adenomas with high-grade dysplasia (HGD) and adenocarcinomas. The presence of non-specific colitis also was evaluated in the small intestine and the colon (data not shown). Liver specimens were assessed and characterized according to the severity of hepatocellular injury: normal, early steatosis without inflammation, and acute hepatitis (AHI). All histological analyses were performed blindly by a certified pathologist (I.C.). All tissue morphological measurements were performed in triplicate and the coefficient of variance was determined to be less than 5%. Monocytes/macrophages were observed by positive staining of CD68+ (Abcam, ab125212) cells in the colon tissue.

3.3.9. Gene expression

Quantification of colonic expression of TNFα, MCP-1, NOS2, IL-6, IL-10, IL-1β, IL-4, EMR-1, Ly6G, IFN-γ, and FOXP3, were performed as previously described[96]. Briefly, RNA was extracted using TRIzol reagent (Life Technologies, GIBCO-BRL, Carlsbad, CA) and chloroform procedures. Because DSS has been shown to inhibit polymerase and reverse transcriptase activity, lithium chloride was used to purify the RNA as described in detail by Viennois et al. 2013[97]. RNA sample quality and quantities were verified using an Agilent Bioanalyzer and determined to be of good quality based

on A260/A280 values (> 1.8) prior to cDNA synthesis using QuantiTect Reverse Transcription kit (Qiagen 205313). Quantitative RT-PCR analysis was carried out as per the manufacturer's instructions (Applied Biosystems) using Taq-Man Gene Expression Assays. Data were normalized to vehicle treated controls and compared to two reference targets (TBP and H2AFV), which were evaluated for expression stability using GeNorm[98,99].

3.3.10. Microbiome analysis

All Microbiome analysis and sequencing was performed by the University of North Carolina Microbiome Core. Fecal evacuates were collected from each mouse at the conclusion of the study and were chosen at random for 16S rRNA sequencing, at least one sample from each cage was used to prevent a cage effect in the data. A final n=5/group was obtained and used for 16S rRNA sequencing. DNA was isolated from fecal evacuates homogenized with bead-beating using the Qiagen Qiamp Fast DNA Stool Mini Kit (Qiagen #51604) and was used for 16S rRNA gene targeted sequencing using the V4 region on an Illumina MiSeq sequencer[100,101]. Amplification of the 16S rRNA V4 hypervariable region was carried out using the 16S V4 515F forward (5′ TCGTCGGCAG CGTCAGATGTGTATAAGAGACAGGTGCCAGCMGCCGCGGTAA 3′) and V4 806R reverse primer (5′ GTCTCGTGGGCTCGGAGATGTGTATAAGAGACAGGGAC TACHVGGGTWTCTAAT 3′) with added Illumina adapter overhang nucleotide sequences. The PCR conditions used were initial denaturing step at 95 °C for 3 min, followed by a cycling of denaturing of 95 °C for 30 s, annealing at 55 °C for 30 s and a 30 s extension at 72 °C (25 cycles), a 5 min extension at 72 °C and a final hold at 4 °C. Each 16S amplicon was purified using the AMPure XP reagent (Beckman Coulter,

Indianapolis, IN). In the next step each sample was amplified using a limited cycle PCR program, adding Illumina sequencing adapters and dual index barcodes (index 1(i7) and index 2(i5)) (Illumina, San Diego, CA) to the amplicon target. The thermal profile for the amplification of each sample had an initial denaturing step at 95 °C for 3 min, followed by a denaturing cycle of 95 °C for 30 s, annealing at 55 °C for 30 s and a 30 s extension at 72 °C (8 cycles), a 5 min extension at 72 °C and a final hold at 4 °C. The final libraries were again purified using the AMPure XP reagent (Beckman Coulter), quantified and normalized prior to pooling. The DNA library pool was then denatured with NaOH, diluted with hybridization buffer and heat denatured before loading on the MiSeq reagent cartridge (Illumina) and on the MiSeq instrument (Illumina).

Automated cluster generation and paired–end sequencing with dual reads were performed according to the manufacturer's instructions. Multiplexed paired-end fastq files were produced from the sequencing results of the Illumina MiSeq using the Illumina software configure BclToFastq. The paired-end fastq files were joined into a single multiplexed, single-end fastq using the software tool fastq-join. Demultiplexing and quality filtering was performed on the joined results. Quality analysis reports were produced using the FastQC software. Bioinformatics analysis of bacterial 16S amplicon sequencing data was conducted using the Quantitative Insights Into Microbial Ecology (QIIME) software[102]. Operational taxonomic units (OTUs), an operational definition used to classify groups of closely related individuals[103], were picked from the quality filtered results using pick_de_novo_otus.py. Chimeric sequences were detected and removed using ChimeraSlayer. Alpha diversity and beta diversity analysis were performed on the data set using the QIIME routines: alpha_rarefaction.py and beta_diversity_-

through_plots.py, respectively. Summary reports of taxonomic assignment by sample and all categories were produced using QIIME summarize_taxa_through_plots.py and summarize_otu_by_cat.py[103]. Samples were rarefied at 10,000 reads/sample. FastTree2 (Price MN, Dehal PS, Arkin AP FastTree 2- approximately maximum-likelihood tress for large alignments) to build the phylogenetic tree. Finally, we used an open reference method for OTU picking. Phylogenetic Investigation of Communities by Reconstruction of Unobserved States (PICRUSt) was used to predict the functional gene content in the fecal microbiota based on taxonomy obtained from the Greengenes reference database. PICRUSt and LefSe were performed online in the Galaxy workflow framework.

3.3.11. Statistical analyses

All data were analyzed using commercial software (SigmaStat, SPSS, Chicago, IL). All outcomes were analyzed using a two-way ANOVA (disease×treatment), three-way ANOVA (disease×treatment×time) or by a Two-Tailed Student's T-Test where only two groups were compared. A Student-Newman-Keuls test was used for all post-hoc analyses. Survival curve analysis was conducted by Log-rank (Mantel-Cox) test. Pearson correlations were used to test the relationship between microbiota and colonic gene expression. Any data that were not normally distributed or did not display equal variance were logarithmically transformed so that those criteria were met. Statistical significance was set with an alpha value of $p < 0.05$. Data are presented as mean ± SEM.

3.4 Results

3.4.1. Experiment 1: 5FU causes adverse physiological effects, increases colon inflammation, and alters gut microbiome profile

3.4.1.1. 5FU reduces tumor burden but decreases survival in AOM/DSS mice

As expected, there was a main effect of AOM/DSS on body weight loss during the DSS administration (weeks 0–8) ($p < 0.05$) but not during the 5FU treatment period (weeks 8–13). Three cycles of 5FU (weeks 8–13) caused noticeable weight loss in both control and AOM/DSS mice but this did not reach statistical significance. However, there was a significant interaction detected beginning at week 9; within AOM/DSS, 5FU treated mice experienced greater weight loss than AOM/DSS alone (2A, B, $p < 0.05$). Consistent with this, a Mentel-Cox test indicated significant survival risk in AOM/DSS+5FU mice compared to all other groups (Fig. 2C, $p < 0.05$). As expected, a main effect of AOM/DSS on severity of symptoms was detected during DSS administration as well as during the duration of the 5FU treatment (Fig. 2D, $p < 0.05$). Similarly, at weeks 9–13 (beginning 1 week after 5FU treatment) a main effect of 5FU was detected for symptom score (Fig. 2D, $p < 0.05$). Further, there was a significant interaction at weeks 10–11; AOM/DSS+5FU exhibited greater symptom scores than AOM/DSS alone. At necropsy, there was no main effect of AOM/DSS or 5FU in liver weight; however, a significant interaction was detected within AOM/DSS mice where 5FU significantly increased liver weight compared to AOM/DSS alone (Fig. 2E, $p < 0.05$). As expected, a main effect of AOM/DSS was detected for spleen weight with AOM/DSS groups having significantly greater weight (Fig. 2F, $p < 0.05$) but there was no effect of 5FU and no interaction. Both AOM/DSS and 5FU reduced the total weight of

the epididymal fat pad (Fig. 2G, $p < 0.05$) but there was no significant interaction. Similarly, a main effect of 5FU was detected in mesenteric fat pad mass with 5FU resulting in overall lower weight (Fig. 2H, $p < 0.05$). A trending decrease in total polyp number (Fig. 2I, $p=0.18$) and a significant decrease in large polyp number (Fig. 2J) ($p < 0.05$) was recorded in AOM/DSS+5FU mice compared to AOM/DSS alone. Consistent with this, histological analysis of the colonic polyps in AOM/DSS mice treated with 5FU, revealed less adenomas with adenocarcinoma and more low-grade dysplasia (Fig. 2K,L) compared to AOM/DSS alone.

3.4.1.2. Nonspecific toxicity of 5FU destroys intestinal tissue morphology and induces hepatotoxicity

To observe some of the most commonly associated side effects of chemotherapy, we analyzed the small intestine and liver tissue. Histological analysis revealed a main effect of 5FU in shortening of the length/atrophy of the villi in small intestine (Fig. 3A, B, $p < 0.05$). Histology of the livers revealed acute hepatitis in 80% of the AOM/DSS mice treated with 5FU and in 90% of the cases the presence of necrosis accompanied by the formation of abscesses (Fig. 3C, D); findings compatible with liver toxicity.

3.4.1.3. 5FU alters blood profile differently in the presence of tumor burden

A main effect of both 5FU and AOM/DSS was detected in LYM, RBC, HGB, HCT, and PLT counts (Table 1, $p < 0.05$); 5FU treatment decreased LYM, RBC, HGB, HCT but increased PLT whereas AOM/DSS treated mice exhibited increased LYM but decreased RBC, HGB, HCT and PLT (Table 1, $p < 0.05$). Further, there was a significant interaction detected within AOM/DSS; 5FU treated mice presented with greater WBC, MON, NEU counts, and NLR (Table 1, $p < 0.05$) compared to AOM/DSS alone.

3.4.1.4. 5FU alters the immune profile of the colon.

There was a significant main effect of both 5FU and AOM/DSS in mRNA expression of inflammatory cytokines TNFα and NOS2 (Fig. 4, $p < 0.05$). Further, a main effect of AOM/DSS was detected in mRNA expression of inflammatory cytokine IFNγ and macrophage marker EMR1. Interestingly, a significant interaction was detected within AOM/DSS where AOM/DSS mice treated with 5FU showed increased mRNA expression of inflammatory cytokines and chemokines MCP-1, IL6, IL1β, IL10 and the regulatory T-cell marker FOXP3 (Fig. 4, $p < 0.05$) compared to AOM/DSS alone. There was no significant difference in IL4 expression between any groups (Fig. 4).

3.4.1.5. 5FU affects functional measures of fatigue

To evaluate the effects of 5FU on peripheral muscle fatigue we utilized grip strength testing (measured as absolute strength in N and relative N/Kg body weight). No significant differences between groups were detected in relative grip strength (N/Kg); however, analysis of absolute strength indicates a significant interaction within AOM/DSS treatment in which AOM/DSS mice treated with 5FU exhibited a significant decrease in strength (Fig. 5A, B, $p < 0.05$) compared to AOM/DSS alone. To measure the effect of 5FU on fatigability, mice were challenged with a run-to-fatigue test. Given that there were no differences in absolute values at baseline between any of the groups, the data is presented as percent performance change (Fig. 5C). No significant main effects were detected; however, AOM/DSS mice treated with 5FU showed a strong trend for a decreased overall performance compared to AOM/DSS alone with a majority (7/9) of mice recording negative changes in performance (Fig. 5C, $p=0.06$).

3.4.1.6. 5FU treatment alters gut microbiota and correlates with colonic gene expression

Recent investigations have indicated that 5FU significantly alters the gut microbiota in both the colon and small intestine. Further, alterations in gut microbiota composition may have detrimental effects on immune function in the gut. To focus our investigation on the colon microenvironment we performed 16S rRNA sequencing on fecal pellets collected during euthanasia (the full analysis will be available upon request to the corresponding author). A Shannon plot and total sequences per sample figures were generated to demonstrate differences in community richness and evenness to estimate within-community diversity (alpha-diversity) (Fig. 6A, B). Results of the alpha-diversity plots indicate that three cycles of 5FU did not necessarily alter microbiota diversity in control mice but did alter the richness and evenness in AOM/DSS mice (Fig. 6A, B). Unweighted UniFrac PCoA analysis demonstrated that there is a difference in beta-diversity across groups at the OTU level (Fig. 6C). A two-way ANOVA was performed to determine main effects and interactions among phyla and class. AOM/DSS increased the relative abundance of OTUs in Proteobacteria and Verrucomicrobia (Fig. 6D, $p < 0.05$) but decreased it in Actinobacteria, Bacteroidetes, and Tenericutes (Fig. 6D, $p < 0.05$) whereas 5FU increased the relative abundance of OTUs in the Actinobacteria and Verrucomicrobia phyla (Fig. 6D, $p < 0.05$). Surprisingly, there were no main effects in the relative abundance of OTUs of the Firmicutes phylum. Interactions were evident within AOM/DSS and 5FU; within AOM/DSS, 5FU decreased the relative abundance of OTUs in the Firmicutes phylum compared to AOM/DSS alone (Fig. 6D, $p < 0.05$) and within 5FU, AOM/DSS had significantly less relative abundance of OTUs of Actinobacteria compared to 5FU alone (Fig. 6D, $p < 0.05$). Interestingly, the

aforementioned differences were seen in a similar fashion at the class level. A main effect of AOM/DSS was detected for decreased relative abundance of Actinobacteria, Bacteroidia, Erysipelotrichi, Deltaproteobacteria, and Mollicutes and increased abundance of Betaproteobacteria and Verrucomicrobia classes (Fig. 6E, $p < 0.05$). Further, a main effect of 5FU was detected in which the relative abundance of OTUs were decreased in the classes Coriobacteria and Deltaproteobacteria and increased in the Actinobacteria, Bacilli, Betaproteobacteria, and Verrucomicrobia classes (Fig. 6E, $p < 0.05$). There was no significance differences detected in the class Clostridia. A significant interaction was found within 5FU in which AOM/DSS mice had significantly greater abundance of OTUs of Actinobacteria compared to 5FU alone whereas 5FU resulted in a decrease in Bacteroidia in the absence of AOM/DSS (Fig. 6E, $p < 0.05$).

To observe the potential relationship between gut microbiota changes and colon gene expression we performed Pearson correlations on three of the most influenced microbial phyla that relate to inflammation and cancer outcome; Bacteroidetes, Proteobacteria, and Verrucomicrobia. Six genes; TNFα ($r=0.788$, $p < 0.01$), MCP-1 ($r=0.588$, $p < 0.01$), NOS2 ($r=0.679$, $p < 0.001$), IL6 ($r=0.671$, $p < 0.01$), IL1b ($r=0.516p < 0.05$), and FOXP3 ($r=0.535$, $p < 0.05$) were positively correlated with Verrucomicrobia abundance (Fig. S1A–F). Similarly, eight genes; TNFα ($r=0.528$, $p < 0.05$), MCP-1 ($r=0.717$, $p < 0.01$), IL6 ($r=0.685$, $p < 0.01$), IFNγ ($r=0.582$, $p < 0.01$), IL1β ($r=0.742$, $p < 0.01$), IL10 ($r=0.647$, $p < 0.01$), FOXP3 ($r=0.717$, $p < 0.01$), and NOS2 ($r=0.624$, $p < 0.01$) were positively correlated with Proteobacteria abundance (Fig. S1G–N). Lastly, three genes; IL10 ($r=-0.616p < 0.01$), IL6 ($r=-0.476$, $p < 0.05$), and FOXP3 ($r=-0.680$, $p < 0.01$) were negatively correlated with Bacteroidetes abundance (Fig. S1O–Q).

3.4.1.7. Metagenomic PICRUSt analysis indicates functional consequences of altered microbiota.

To investigate the functional consequences of the taxonomic changes in gut microbial composition, we performed PICRUSt metagenomic analysis to generate a functional profile of the microbial communities investigated. The full analysis will be available upon request to the corresponding author. We present here the most interesting of the findings (Fig. S2A–D). We detected a main effect of 5FU and AOM/DSS in predicted expression of nitrate reductase subunits (alpha, beta, gamma, and delta), [citrate (pro-3S)-lyase] ligase and [protein-PII] uridylyltransferase (Fig. S2A, $p < 0.05$), and acylphosphatase (Fig. S2C, $p < 0.05$). Similarly, there is a main effect of AOM/DSS in predicted expression of 5′nucleotidase (Fig. S2A, $p < 0.05$) and a main effect of 5FU on fumarate hydratase expression (Fig. S2D, $p < 0.05$). There were no significant interactions for the aforementioned outcomes. However, a significant interaction was detected for beta-mannosidase within 5FU; 5FU alone increased beta-mannosidase but it was significantly decreased in AOM/DSS mice treated with 5FU (Fig. S2B, $p < 0.05$).

3.4.2. Experiment 2: fecal transplantation of 5FU-disturbed microbiota alters host physiology

3.4.2.1. Fecal transplantation affects functional measures of fatigue

To elucidate the role of the gut microbiota on the adverse side-effects associated with 5FU treatment we performed fecal transplantation studies in control mice (Fig. 1B). No body weight or organ weight difference was detected between the two groups (Vehicle FMT and 5FU FMT) (Fig. 7A–F). All mice were challenged to the same fatigue

tests used in experiment 1. A significant decrease in absolute grip strength (Fig. 7G, $p < 0.05$) and a trending decrease in relative grip strength (Fig. 7H, $p=0.06$) was detected in mice treated with 5FU FMT compared to vehicle control. In the run-to-fatigue test, a trending decrease (Fig. 7 I, $p=0.07$) in performance was recorded in 5FU mice compared to control. Similar to Experiment 1, we noticed a large number (6/15) of mice with negative performance changes following 5FU FMT.

3.4.2.2. Fecal transplantation manifests a unique blood profile

Upon analysis of the blood profile, we noticed a significant increase in WBC, MON, and LYM counts in 5FU FMT mice vs Vehicle FMT controls (Table 2, $p < 0.05$). However, no differences in NEU and RBC counts were detected (Table 2). The increase in lymphocyte count contributed to a trending decrease in NLR in 5FU FMT mice compared to Vehicle FMT controls (Table 2, $p=0.07$).

3.4.2.3. 5FU fecal microbial transplantation reduces macrophage populations in the colon

To further understand the potential contribution of gut microbiota on inflammatory responses following 5FU treatment, we performed gene expression analysis on the colon tissue. Contrary to our hypothesis, we found a decreased expression of MCP-1, IL10, and EMR1 in 5FU FMT mice compared to Vehicle FMT controls (Fig. 8A, $p < 0.05$). A trending decrease in IL1β ($p=0.08$) also was detected with no differences in TNFα, NOS2, IL4, and Ly6G expression (Fig. 8A). Investigating the morphology of the colon tissue, we did not notice any histological differences between Vehicle FMT and 5FU FMT mice (Fig. 8B). The gene expression data explained above indicate a decreased macrophage population in 5FU FMT mice relative to Vehicle FMT

controls. To confirm this finding, we performed immunohistochemical analysis of CD68+ cells present in the colons (Fig. 8C). Although we did not directly quantify, observation suggests fewer CD68+ positive cells in the lamina propria and epithelial layers in 5FU FMT mice.

3.5 Discussion

5FU chemotherapy is widely used in the treatment of CRC. However, side effects including fatigue, loss of appetite, and diarrhea, all of which can lead to a reduced quality of life, are common. Emerging evidence suggests that the gut microbiota may play a role in this response. In the current study, we sought to characterize the effects of 5FU on colon inflammation and functional measures in CRC and to further determine whether gut microbiota can influence this response. Despite a general anti-tumor effect of 5FU, we document findings of non-selective toxicity in intestinal and liver tissue that which are associated with reduced functional performance and decreased survival. Select intestinal inflammatory genes were significantly elevated with 5FU treatment and this was further exacerbated with cancer. Both 5FU and AOM/DSS treatment result in significant alterations in gut microbiota and predicted functional parameters. Finally, using fecal transplantation we demonstrate that a 5FU altered microbiome influences the systemic and colonic immune environment and can impact functional parameters.

Our findings indicate that a clinically relevant chemotherapy regimen has general anti-tumor effects in the AOM/DSS model of CRC. This is consistent with previous reports of a beneficial effect of 5FU in intestinal tumorigenesis in the $Apc^{min/+}$ mice model where a 60–80% reduction in polyps was reported[104]. Despite these benefits however, our data indicates that 5FU reduces body weight, exacerbates symptom severity

score, increases liver weight, and decreases epididymal fat mass, consistent with a decrease in survival. These results are not surprising given the well documented toxicities resulting from 5FU non-selectivity[30,32]. The manifestations of 5FU induced toxicity have been mainly attributed to 'mucositis' or the disruption of the mucosal barrier[35,105]. We confirm this damaging mechanism as we report a main effect of 5FU treatment on reducing villus length in the distal ilium. Further complications of chemotherapy in CRC include progressive liver failure leading to premature death[36,105,106]. Our results are consistent with this as the majority of AOM/DSS mic treated with 5FU presented with acute necrotizing inflammation with abscesses in the liver. These histological findings are indicative of an immune response against a bacterial infection[107,108], evidence that can be associated with the presence of leaky gut syndrome; however, further investigation would be needed to confirm this finding. Other studies have reported similar results using short, high-dosage treatment regimens (Chang et al., 2012; Li et al., 2017) but have utilized non-diseased mouse models[33,91]. Our findings suggest that the chemotherapy regimen administered in this experiment, using a mouse model of CRC, is effective in replicating the clinical outcome of 5FU treatment.

Given 5FU's well documented effects on blood parameters, we used a diverse blood panel analysis to specifically investigate its effects on circulating immune cells and factors contributing to chronic anemia in the context of CRC. Consistent with clinical and experimental literature, we observe decreased circulating immune cells and indications of severe anemia with 5FU treatment and in the presence of cancer.[35,37] As expected, the combined treatment of 5FU and AOM/DSS had worsening effects on anemia including RBCs, HCT and HGB. Interestingly, however, where 5FU seemingly causes significant

immune cell death in a healthy physiological state, it appears that the already altered physiology caused by the AOM/DSS model of tumor burden increased the systemic immune response when combined with 5FU. This specifically caused an increase in neutrophils and monocytes, but not lymphocytes. The mechanism for this increase in circulating innate immune cells is unclear and warrants further investigation.

ROS produced following initiation of 5FU-related mucositis induces tissue injury and triggers a cascade of inflammatory pathways including nuclear factor kappa-B (NF-κB) activation. Once activated by 5FU, NF-κB induces gene expression and production of pro-inflammatory cytokines, which, in turn, lead to tissue injury and apoptosis.[109] In addition, CRC itself leads to significant colon inflammation as we have previously reported.[110] Therefore, it is possible that colon-specific inflammation may be exacerbated following treatment of 5FU in CRC leading to worsening symptoms and poor prognosis. Thus, we next examined the effects of 5FU on colon inflammation in the context of CRC. As hypothesized, both 5FU and AOM/DSS lead to an increase in select inflammatory mediators with a greater degree of inflammation noted in AOM/DSS mice treated with 5FU. As such, it is possible that this 'inflammatory cytokine storm' may explain, at least in part, the increased mortality in AOM/DSS mice treated with 5FU.

To establish the functional deficits associated with chronic 5FU treatment, we performed a grip strength and run-to-fatigue test. AOM/DSS mice treated with three cycles of 5FU significantly reduced absolute grip strength and there was a strong trend towards a decreased run-to-fatigue time. This was consistent with findings of a previous study by our group that characterized the chronic fatigue of 5FU treatment.[111] The mechanisms responsible for 5FU-related fatigue in cancer patients have not yet been fully

elucidated. However, several hypotheses have been postulated and include: central serotonin dysregulation, hypothalamus-pituitary-adrenal axis dysfunction, circadian disruption, depression, anemia, and central and peripheral inflammation.[112,113] Arguably, the strongest of these are inflammation and anemia. Our data supports these hypotheses given the increase in anemia related outcomes and inflammation in AOM/DSS mice treated with 5FU – mice with the greatest performance deficits.

Recent investigations have implicated a direct role of gut microbiota in the development and treatment of CRC. Therefore, we next examined the effects of 5FU on the gut microbiota profile. Others have reported differences in gut microbiota following 5FU treatment in non-cancer mice.[91] However, to our knowledge this is the first report of a change in microbiota profile when 5FU is administered in the presence of CRC in an experimental mouse model; specifically, we note a decrease in alpha diversity. We focus our discussion on the most important and novel findings of the post-hoc analysis of bacterial phyla. We saw a decrease in abundance of Firmicutes phylum in AOM/DSS mice treated with 5FU but not in AOM/DSS alone. The Firmicutes represent one of the most abundant phyla of the gut microbiota and are important for short-chain fatty acid production and maintenance of gut homeostasis.[91,114] In-fact decreases in Firmicutes have previously been associated with inflammatory bowel disease and CRC.[114,115] This suggests a possible role of chemotherapeutics in altering the gut microbiota in the presence of CRC in a manner that exacerbates gut dysbiosis and may contribute to a worse prognosis following chemotherapy treatments. Further, both 5FU treatment and AOM/DSS treatment increased relative abundance of Verrucomicrobia. This is not surprising given that the Verrucomicrobia phylum is suggested to be directly related to

inflammation in the colon.[40,116,117] The increase in Proteobacteria phylum with AOM/DSS appeared to result from increased Betaproteobacteria. This is consistent with findings in human fecal samples in which Betaproteobacteria were found to be increased in patients with CRC.[118] Our findings of a decrease in Bacteroidetes in AOM/DSS treated mice are consistent with some reports of lower levels of Bacteroidetes being linked to increased cancer risk.[115] The strong correlations detected between the above-mentioned phyla and colon inflammatory mediators suggest a potential link between gut microbes and the exacerbated inflammation in AOM/DSS mice treated with 5FU. If Verrucomicrobia and Proteobacteria are indeed playing a role in the creation of an 'inflammatory cytokine storm,' selected targeting of these phyla may help lower the adverse toxicities common to 5FU treatment. Further, PICRUSt analysis of OTUs indicates significant changes in predicted genes involved in environmental processing and cellular processes. From these predicted changes it can be suggested that alterations in the gut microbiota may affect key processes outside the gut that may be contributing to the exacerbated disease state in AOM/DSS mice treated with 5FU.

While our gut microbiota findings are consistent with some of the previously reported literature for both 5FU and CRC, it is important to note that inconsistencies also exist. For example, a recent study by Li et al. (2017), reported decreased Firmicutes and Proteobacteria, increased Bacteroidetes, and no significant change in Verrucomicrobia following 5FU treatment in a cancer-free model[91], whereas we saw increases in Verrucomicrobia and Actinobacteria with no changes in the other phyla. However, only 3 consecutive injections of 5FU (50 mg/kg) were used by Li et al. (2017), whereas we employed a cycled regime with the aim of investigating chronic effects of 5FU treatment.

These differences in treatment regime likely contributed to the disparities in findings across studies. Further, some of these differences may stem from our utilization of the AIN-76A purified diet instead of standard chow and randomization of the mice upon arrival to the facility to prevent maternal bias in fecal analysis.[116] Similarly, while we report here a decrease in Bacteroidetes with AOM/DSS, it should be noted that reports of increases also have been reported in CRC[119] indicating inconsistencies in the literature.

Culminating from the differences in the gut microenvironment of 5FU treated mice, we next sought to determine whether gut microbes may be responsible for some of the side effects associated with 5FU. Thus, we designed an experiment utilizing gut microbiota depletion followed by subsequent engraftment by either Vehicle FMT or 5FU FMT (Fig. 1B).[95] An absence of body weight and organ weight changes from fecal transplantation was contrary to our hypothesis and the findings of Li et al. (2017), which showed a significant decrease in body weight following transplantation of feces from 5FU treated mice.[91] As noted above, differences in the study design may have contributed to the disparities among findings. Interestingly, however, we did find a decrease in muscle strength and run-to-fatigue times following engraftment of 5FU FMT that is consistent with the findings in Experiment 1. To our knowledge this is the first report of a direct relationship between 5FU, gut microbes, and performance deficits and probes the determination of the exact microbes that may be contributing to this response.

We next examined the effects of engraftment by either Vehicle FMT or 5FU FMT on circulating and colonic immune responses. Performing the same diverse blood panel as Experiment 1, we observe an increased number of circulating immune cells (WBC, LYM, MON) in 5FU FMT mice engrafted with 5FU treated feces, a finding contrary to

the results of direct 5FU treatment in Experiment 1. Others have reported effects of gut bacteria on circulating immune cells.[57] However, to our knowledge this is the first report of a 5FU influenced gut microbiome on circulating immune cells. Fecal Microbial Transplantation of microbes from mice treated with 5FU (5FU FMT) to non-diseased (Control) mice specifically reduced the MCP-1 and EMR1 gene expression in the colon but Ly6G was unaltered. This indicates that the engrafted microbiome may be causing a reduction specifically in the macrophage population in the colon but not in neutrophils. This was consistent with a notable reduction in CD68+ cells in the colon. This finding was further supported by a decreased expression of IL-10 and a trending decrease in IL-1β, cytokines that are known to be released from macrophages.[111] This suggests that the altered microbial composition resulting from 5FU treatment may, in-itself, be eliciting an anti-inflammatory response independent of 5FU, where cellular damage from 5FU is most likely contributing to the proinflammatory response reported in Experiment 1. Although requiring further investigation, this would explain the correlations of certain bacteria to both pro- and anti-inflammatory markers in the colon tissue in Experiment 1. Taken together, these data suggest that transfer of 5FU treated feces leads to an increased production of circulating immune cells including monocytes; yet appears to reduce macrophages in the colon. However, the exact microbes that are driving this response cannot be determined from the current study.

The novel findings from this study implicate that 1) the immune response to cancer therapy may be regulated by gut microbiota and 2) gut microbiota may influence functional outcomes following cancer therapy. This suggests that gut microbiota may serve as a potential therapeutic target for manipulating immune responses and improving

quality of life outcomes during cancer therapy. It is certainly possible, and even likely, that some microbes may confer beneficial effects in this model whereas others may have detrimental effects. Thus, future preclinical studies should determine the exact microbes that are responsible for the aforementioned effects so that therapeutics can be developed. Administration of antibiotics and FMT are viable options for manipulating gut microbiota during cancer therapy and could be implemented in the clinic.

In summary, this study examined the functional and physiological effects of 5FU in the context of CRC. Despite a general anti-tumor effect of 5FU, we report findings of non-selective toxicity in intestinal and liver tissue that are associated with reduced functional performance and decreased survival. The side effects of 5FU in CRC were associated with alterations in gut bacteria and functional pathways. Finally, using fecal transplantation we demonstrate that a 5FU altered microbiome can influence the systemic and colonic immune environment and can impact functional parameters. However, further studies are necessary to determine the exact bacterial populations that are responsible for these effects and whether gut bacteria can be targeted for reducing side effects associated with chemotherapy.

3.6 Acknowledgements

This work was funded by a Center of Biomedical Research Excellence (COBRE) grant (P30GM103336045) from the NIGMS to the Center for Colon Cancer Research and an F31 grant from NCCIH to ATS (F31AT009820).

3.7 Figures & Legends

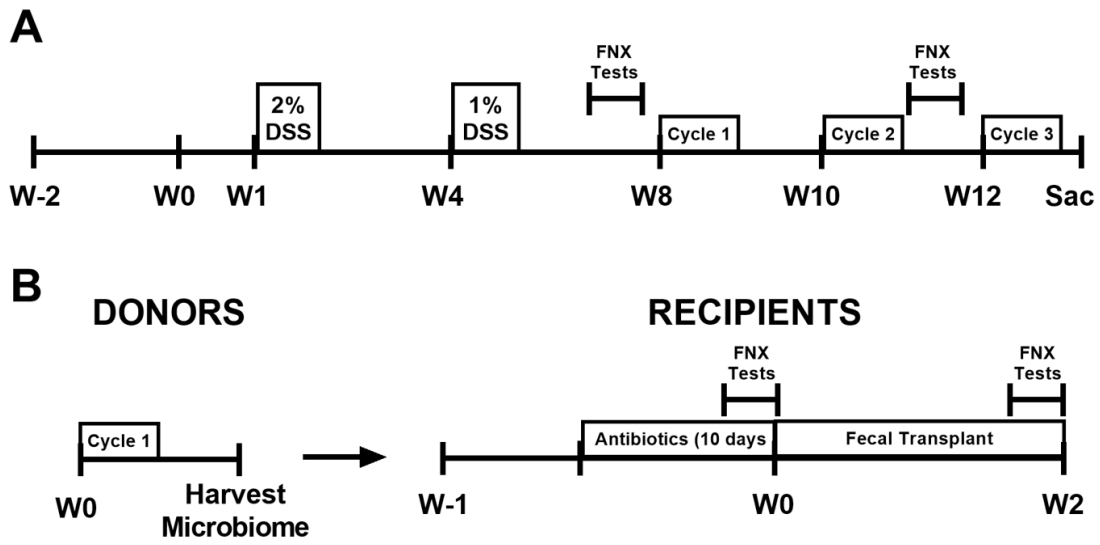

Figure 3.1. Study Design for experiment 1 and experiment 2. A. Experiment 1 design and 5FU treatment regimen. **B.** Experiment 2 design, antibiotics treatment regimen and fecal transplantation.

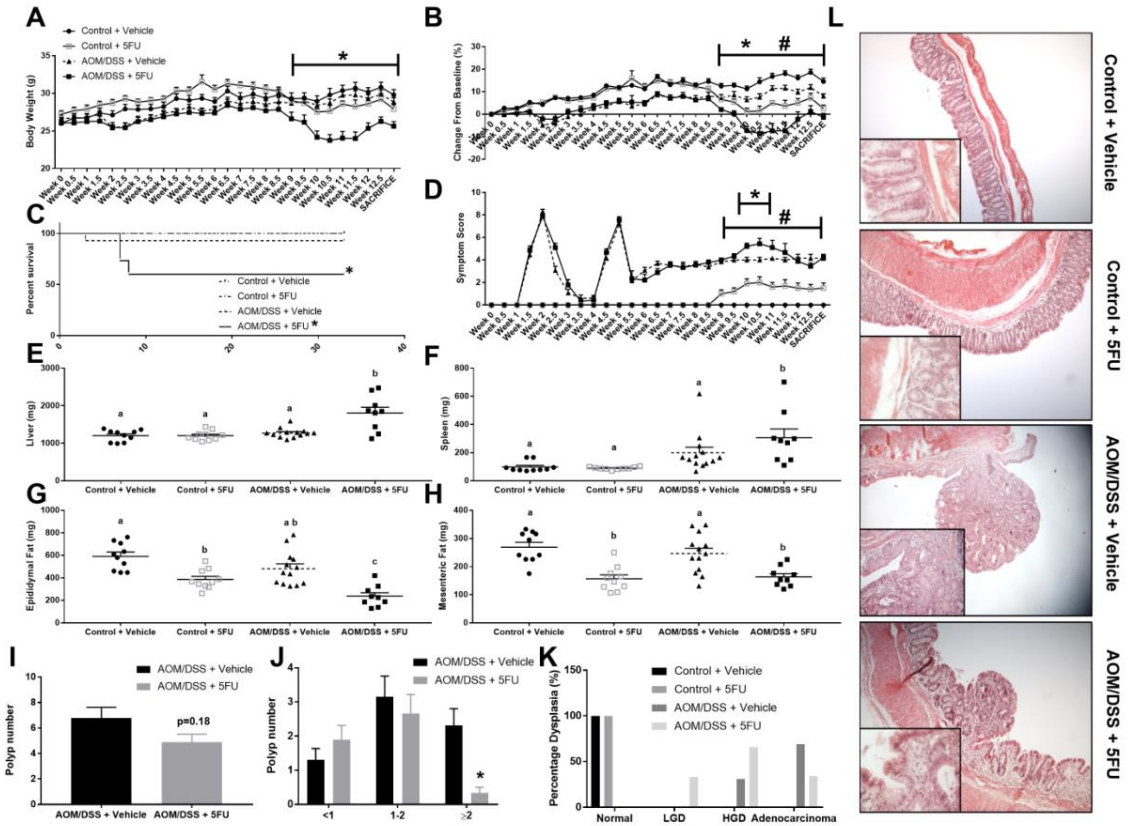

Figure 3.2. 5FU reduces tumor burden but decreases survival in AOM/DSS mice. A. Gross body weight. **B.** Percent body weight change. **C.** Survival curve. **D.** Symptom score. * Indicates statistical significance ($p < 0.05$) for AOM/DSS+5FU group vs. all groups, # indicates statistical significance ($p < 0.05$) for Control+5FU vs. Control+Vehicle from 3-way ANOVA. **E-H.** Liver, spleen, epididymal fat, and mesenteric fat, weights at euthanization. Groups not containing the same letters (a, b, ab) indicate statistical significance between groups ($p < 0.05$) from two-way ANOVA, n=9–13/group. **I.** Total Polyp count. **J.** Polyp size. **K.** Dysplasia characterization. **L.** Representative H&E staining of distal colon specimens at 4X, insets are 20X. * Indicates statistical significance ($p < 0.05$) from students t-test, n=9–13/group.

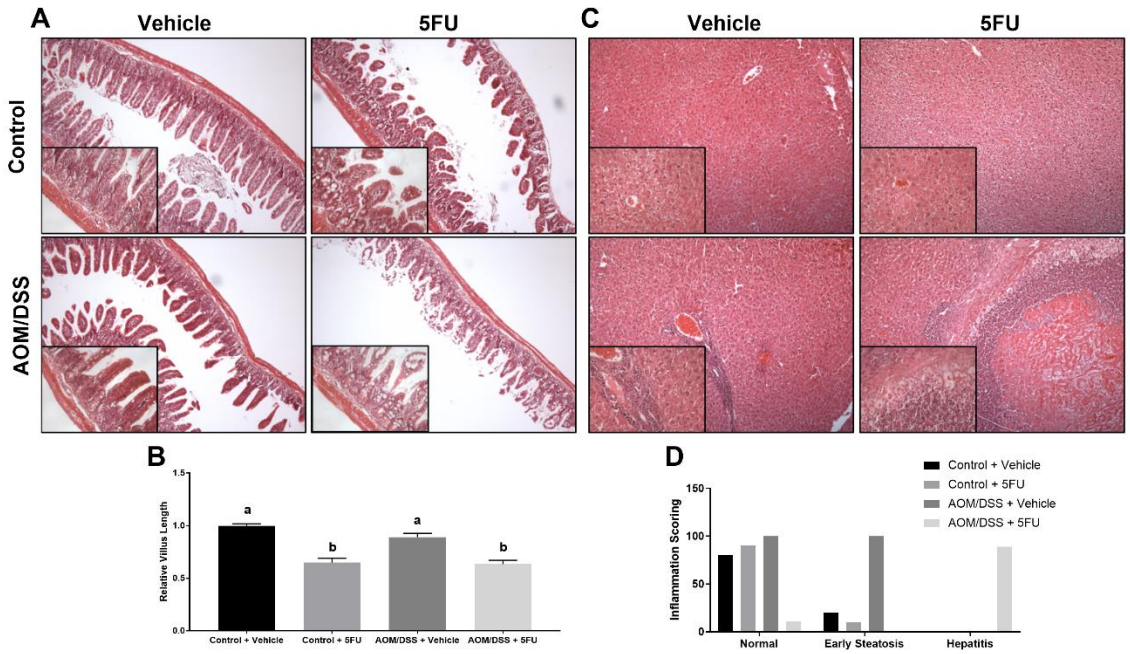

Figure 3.3. Nonspecific toxicity of 5FU in distal ileum and liver tissue. A. Representative H&E staining of distal ileum specimens at 4X, insets are 20X. **B.** Measurement of villus length in small intestine. Groups not containing the same letters (a, b) indicate statistical significance between groups ($p < 0.05$) from two-way ANOVA. **C.** Representative H&E staining of liver tissue specimens at 4X, insets are 20X. **D.** Histopathological analysis of liver inflammation. n=9–13/group.

Table 3.1. 5FU alters blood profile in AOM/DSS mice different from control. White blood cells (WBC), Lymphocytes (LYM), Monocytes (MON), Neutrophils (NEU), Neutrophil:Lymphocyte Ratio (NLR), Red Blood Cells (RBC), Hemoglobin (HGB), and Hematocrit (HCT). Groups not containing the same letters (a,b,c,d) indicate statistical significance between groups ($p < 0.05$) from two-way ANOVA, n=9–13/group.

Group	WBC (10^9/l)	LYM (10^9/l)	MON (10^9/l)	NEU (10^9/l)	NLR	RBC (10^12/l)	HGB (g/dl)	HCT (%)	PLT (10^9/l)
Control + Vehicle	4.19 ± 0.39 [a]	2.58 ± 0.25 [a]	0.20 ± 0.06 [a]	1.40 ± 0.29 [a]	0.61 ± 0.12 [a]	9.62 ± 0.48 [a]	14.80 ± 0.22 [a]	38.65 ± 1.52 [a]	881.50 ± 69.44 [a]
Control + 5FU	2.16 ± 0.12 [b]	1.52 ± 0.11 [b]	0.06 ± 0.01 [b]	0.58 ± 0.05 [b]	0.40 ± 0.04 [b]	7.45 ± 0.25 [b]	11.28 ± 0.13 [b]	30.51 ± 0.98 [b]	1851.00 ± 115.22 [b]
AOM/DSS + Vehicle	3.65 ± 0.3 [a]	2.70 ± 0.27 [a]	0.17 ± 0.04 [a]	0.78 ± 0.08 [a]	0.33 ± 0.05 [b]	7.63 ± 0.48 [b]	11.38 ± 0.62 [b]	32.49 ± 1.76 [b]	532.69 ± 48.35 [c]
AOM/DSS + 5FU	7.21 ± 1.50 [c]	2.43 ± 0.26 [a]	0.53 ± 0.17 [c]	4.25 ± 1.33 [c]	2.04 ± 0.67 [c]	6.85 ± 0.21 [c]	8.80 ± 0.43 [c]	25.47 ± 1.08 [c]	1381.00 ± 101.99 [d]

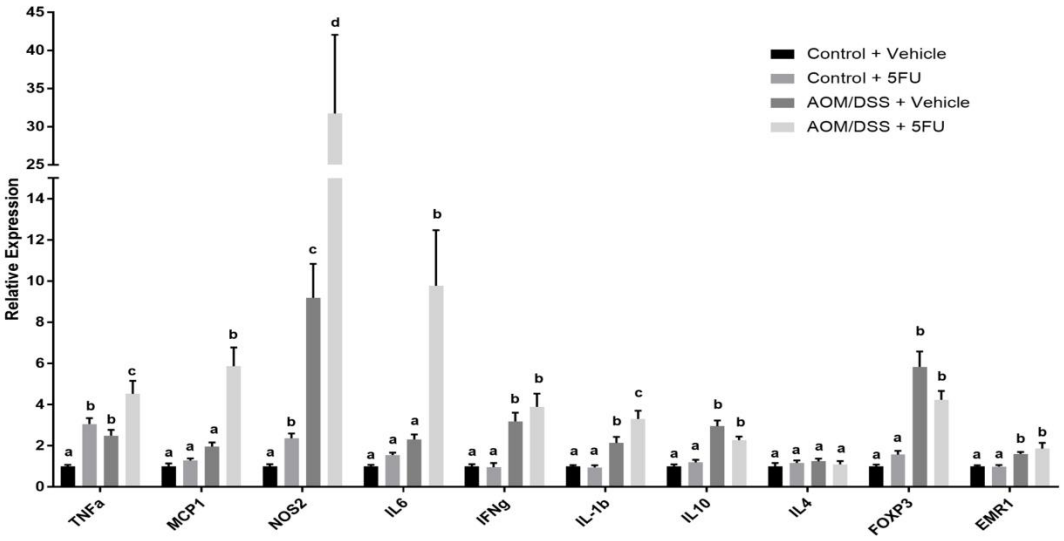

Figure 3.4. 5FU alters the immune profile of the colon. A. qPCR analysis of TNFα, MCP-1, NOS2, IL6, IFNg, IL1b, IL10, IL4, FOXP3 genes. Data were normalized to vehicle treated controls and compared to two reference targets (TBP and H2AFV), which were evaluated for expression stability using GeNorm. Groups not containing the same letters (a–d) indicates statistical significance between groups ($p < 0.05$) from two-way ANOVA, n=9–13/group.

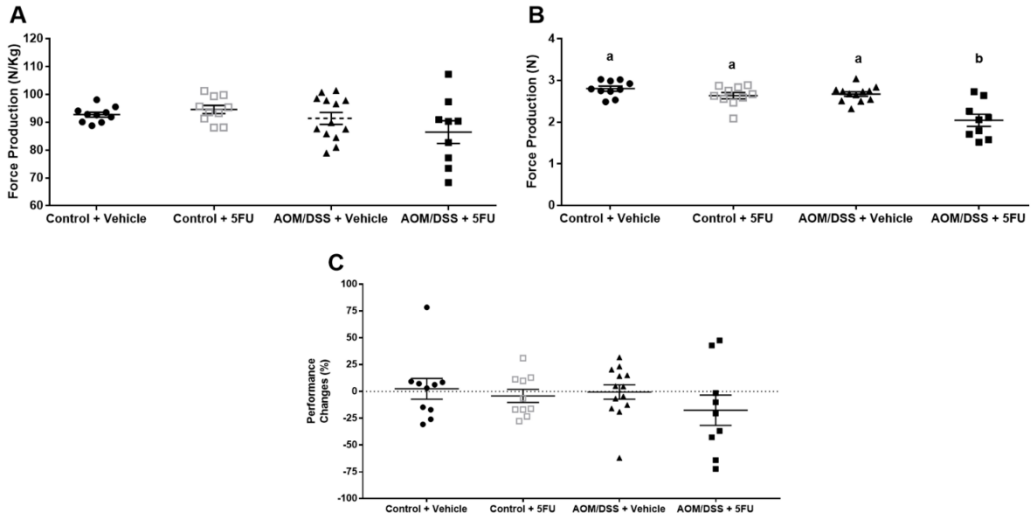

Figure 3.5. 5FU affects functional measures of fatigue. A. Relative grip strength measured in newtons/kilogram (N/kg). **B.** Absolute grip strength measured in newtons (N). **C.** Percent performance change in run-to-fatigue test from pre-5FU treatment to post-5FU treatment. Groups not containing the same letters (a, b) indicates statistical significance between groups ($p < 0.05$) from two-way ANOVA, n=9–13/group.

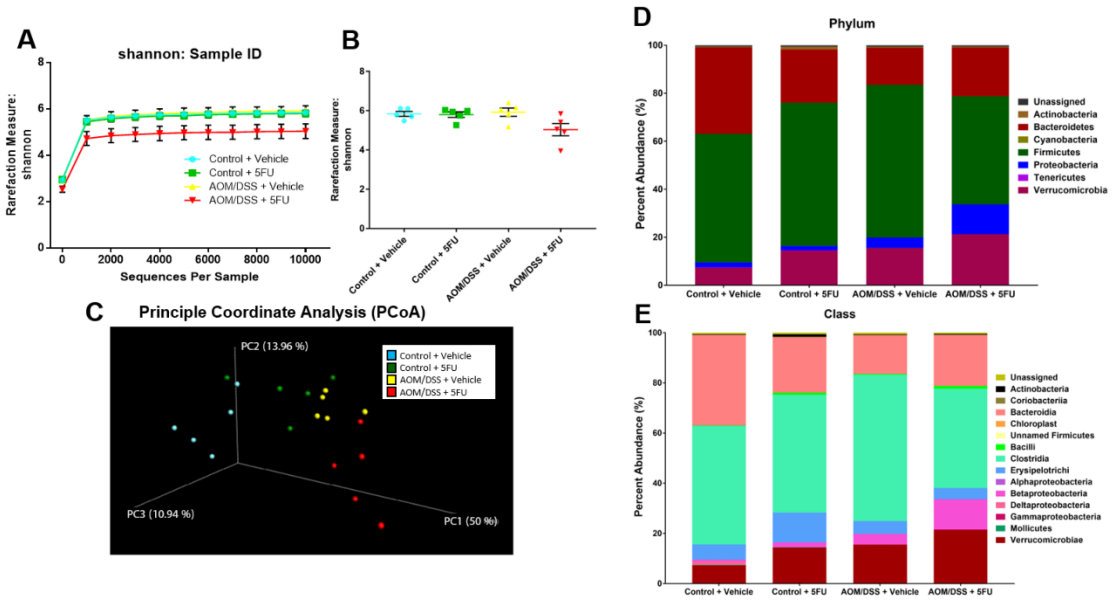

Figure 3.6. 5FU alters gut microbial profile. A. Shannon plot of alpha-diversity in microbial communities. **B.** Total sequences per sample by Shannon rarefaction. **C.** Unweighted UniFrac Principle Coordinate Analysis (PCoA) of beta-diversity in microbial communities. **D.** Percent abundance of microbial phyla. E. Percent abundance of microbial class, n=5/group.

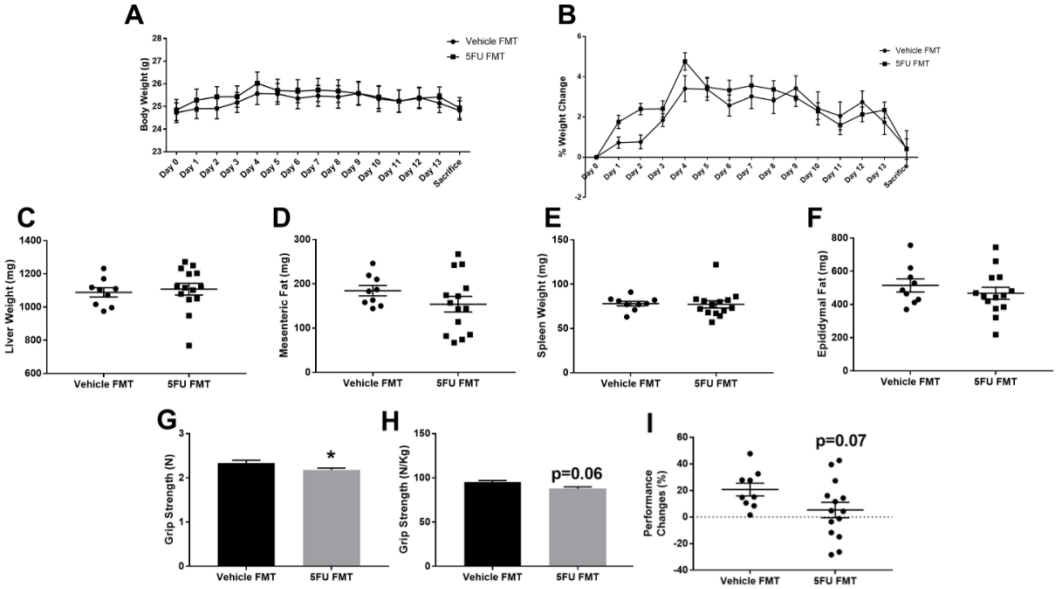

Figure 3.7. Fecal Transplantation of 5FU altered microbiome does not alter body weight but does affect functional measures of fatigue. A. Gross body weight. **B.** Percent body weight change. **C-F.** Liver, spleen, epididymal fat, and mesenteric fat, weights at euthanization. **G.** Relative grip strength measured in newtons/kilogram (N/kg). **H.** Absolute grip strength measured in newtons (N). **I.** Characterization of performance changes in run-to-fatigue test. **J.** Percent performance change in run-to-fatigue test from pre-5FU treatment to post-5FU treatment. * Indicates statistical significance between groups ($p < 0.05$) from students t-test n=10–15/group.

Table 3.2 5FU FMT manifests a unique blood profile. White blood cells (WBC), Lymphocytes (LYM), Monocytes (MON), Neutrophils (NEU), Neutrophil:Lymphocyte Ratio (NLR), Red Blood Cells (RBC), Hemoglobin (HGB), and Hematocrit (HCT). * Indicates statistical significance between groups ($p < 0.05$) from students t-test, n=10–15/group.

Group	WBC (10^9/l)	LYM (10^9/l)	MON (10^9/l)	NEU (10^9/l)	NLR	RBC (10^12/l)	HGB (g/dl)	HCT (%)	PLT (10^9/l)
Vehicle FMT	4.84 ± 0.40	3.76 ± 0.20	0.12 ± 0.00	0.97 ± 0.20	0.25 ± 0.00	9.79 ± 0.20	14.61 ± 0.30	38.41 ± 0.80	864.11 ± 64.30
5FU FMT	6.34 ± 0.39 *	5.12 ± 0.31 *	0.34 ± 0.06 *	0.89 ± 0.10	0.18 ± 0.02	10.28 ± 0.24	14.27 ± 0.25	40.78 ± 0.83	808.23 ± 35.46

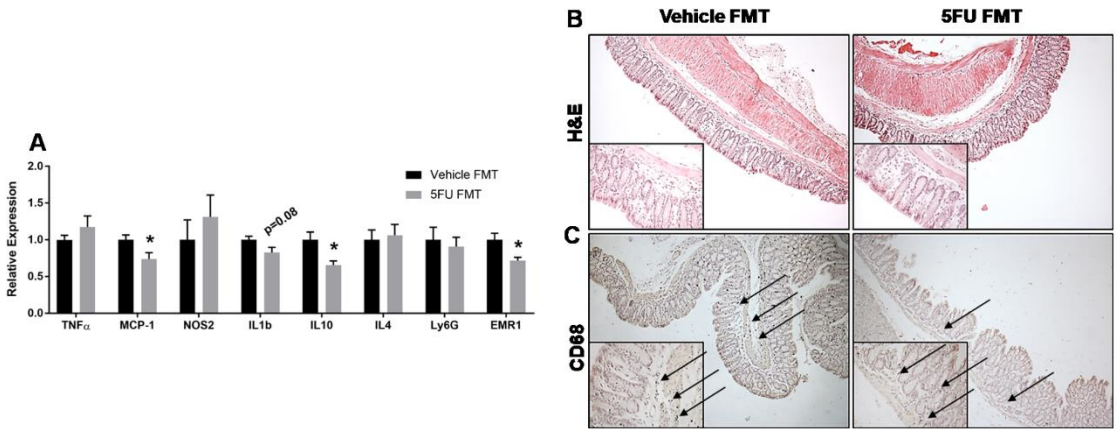

Figure 3.8. 5FU alters macrophage population in the colon lamina propria and is replicated with fecal transplantation. A. qPCR analysis of TNFα, MCP-1, NOS2, IL1b, IL10, IL4, Ly6G, and EMR1 genes in fecal transplantation mice. **B, C.** Representative H&E staining and CD68+ staining, respectively, in distal colons of fecal transplantation mice. Arrows indicate examples of positive staining. * Indicates statistical significance between groups ($p < 0.05$) from students t-test, n=10–15/ group.

3.8 Supplemental Material

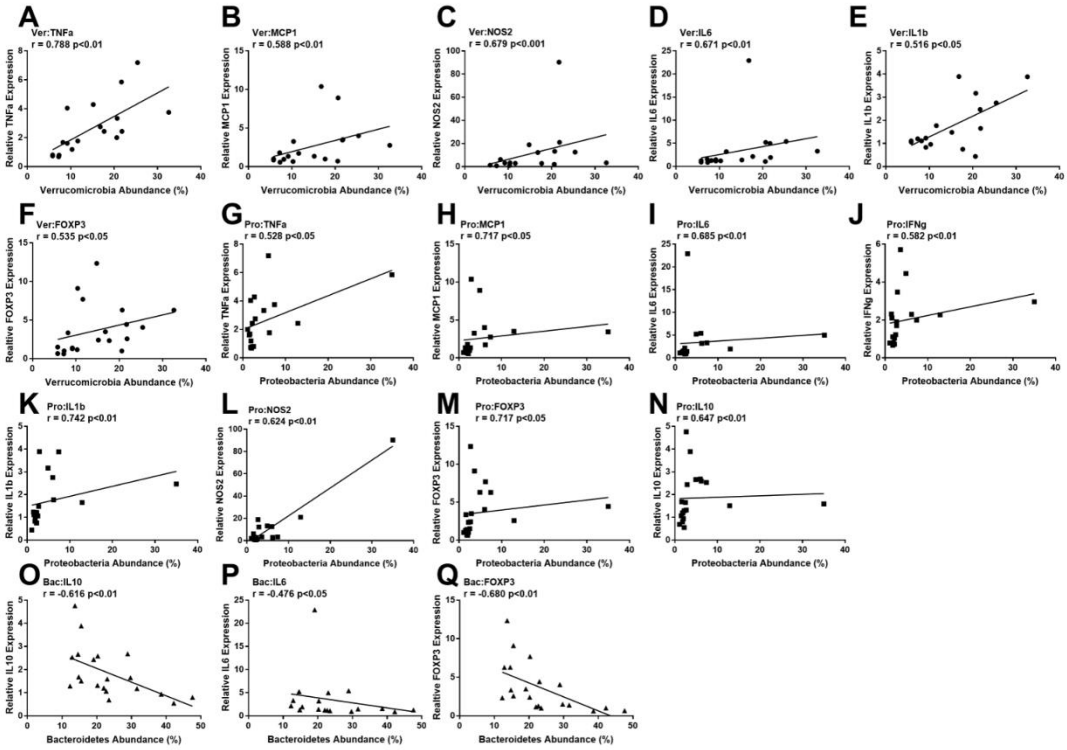

Supplementary Figure S3.1. ***Verrucomicrobia, Proteobacteria,*** **and** ***Bacteroidetes*** **phyla correlate with key markers of inflammation in the colon.** Pearson correlation coefficients (r) are shown for *Verrucomicrobia* to colon gene expression of **A.** TNFα **B.** MCP1 **C.** NOS2 **D.** IL6 **E.** IL1b and **F.** FOXP3 with the associated p-values. Pearson correlation coefficients (r) are shown for *Proteobacteria* to colon gene expression of **G.** TNFα **H.** MCP1 **I.** IL6 **J.** IFNg **K.** IL1b **L.** NOS2 **M.** FOXP3 and **N.** IL10 with the associated p-values. Pearson correlation coefficients (r) are shown for *Bacteroidetes* to colon gene expression of **O.** IL10 **P.** IL6 and **Q.** FOXP3 with the associted p-values.

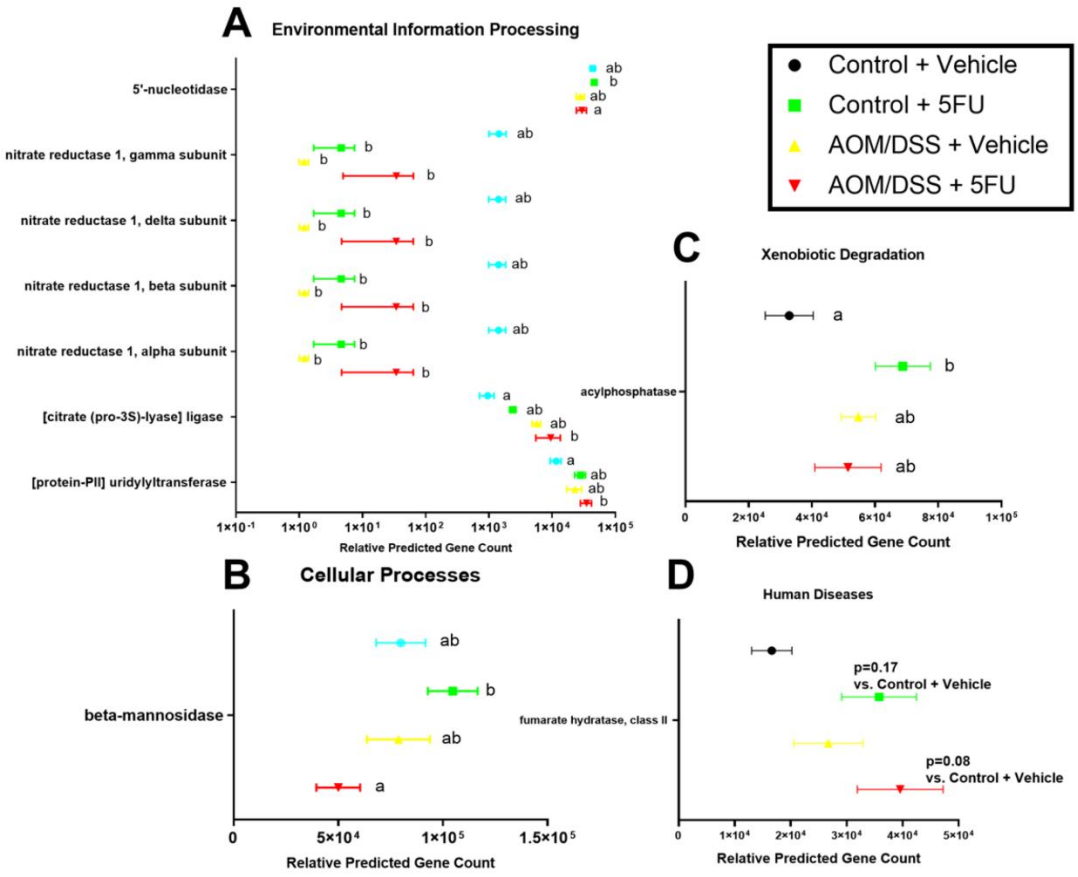

Supplementary Figure S3.2. Select PICRUSt analysis results indicating altered functional consequences of 5FU treatment. A. Select markers of environmental information processing. **B.** Select marker of cellular processes. **C.** Select marker of xenobiotic degradation. **D.** Select marker involved in development of human diseases. Different letters indicates statistical significance ($p<0.05$) from two-way ANOVA n=5.

CHAPTER 4

SAFETY OF NATURAL ANTHRAQUINONE EMODIN: AN ASSESSMENT IN MICE[2]

[2] Sougiannis AT et. al. Submitted to *BMC Pharmacology and Toxicology,* 4/10/2020.

4.1 Abstract

Background: Emodin, a natural anthraquinone, has shown potential as an effective therapeutic agent in the treatment of many diseases including cancer. However, its clinical development is hindered by uncertainties surrounding its potential toxicity. The primary purpose of this study was to uncover any potential toxic properties of emodin in mice at doses that have been shown to have efficacy in our cancer studies. In addition, we sought to assess the time course of emodin clearance when administered both intraperitoneally (I.P.) and orally (P.O.) in order to begin to establish effective dosing intervals. **Methods:** We performed a subchronic (12 week) toxicity study using 3 different doses of emodin (~20 mg/kg, 40 mg/kg, and 80 mg/kg) infused into the AIN-76A diet of male and female mice (n=5/group/sex). Body weight and composition were assessed following the 12-week feeding regime. Tissues were harvested and assessed for gross pathological changes and blood was collected for a complete blood count and evaluation of ALT and creatinine. For the pharmacokinetic study, emodin was delivered intraperitoneally I.P. or P.O. at 20 mg/kg or 40 mg/kg doses to male and female mice (n=4/group/sex/time-point) and circulating levels of emodin were determined at 1, 4 and 12 hrs following administration via LC-MS/MS analysis. **Results:** We found that 12 weeks of low (20 mg/kg), medium (40 mg/kg), or high (80 mg/kg) emodin feeding did not cause pathophysiological perturbations in major organs. We also found that glucuronidated emodin peaks at 1hr for both I.P. and P.O. administered emodin and is eliminated by 12 hr. Interestingly, female mice appear to metabolize emodin at a faster rate than male mice as evidenced by greater levels of glucuronidated emodin at the 1hr time-point (40 mg/kg for both I.P. and P.O. and 20 mg/kg I.P.) and the 4-hour time-point

(20 mg/kg I.P.). **Conclusions:** In summary, our studies establish that 1) emodin is safe for use in both male and female mice when given at 20, 40, and 80 mg/kg doses for 12 weeks and 2) sex differences should be considered when establishing dosing intervals for emodin treatment.

4.2 Background

Emodin (1,3,8-trihydroxy-6-methylanthraquinone) (Fig 1A) is a natural anthraquinone isolated from several Chinese herbs, including *Rheum palmatum*, *Polygonum cuspidatum,* and *Polygonum multiflorum*. Pre-clinical investigations have demonstrated emodin to contain a wide spectrum of pharmacological benefits, including; anti-viral[69], anti-bacterial[70], anti-allergic[71], anti-osteoporotic[72], anti-diabetic[73,85], anti-inflammatory[74,75,80,120], neuroprotective[76], hepatoprotective[77], and anti-tumorigenic[78,79,86,121-123] properties (Supplemental Table 1). In fact, studies by our group have shown that emodin is effective at reducing mammary tumorigenesis given its actions on macrophages.[78,122] Both the National Cancer Institute (NCI) and the National Center for Complementary and Integrative Health (NCCIH) recognize the importance of evidence-based complementary medicine modalities that may be integrated as part of standard cancer care for all patients across the cancer continuum. However, further development of emodin as an effective anti-cancer agent is hindered by uncertainties surrounding its potential toxicity.

Evaluation of the safety of dietary compounds is paramount to their clinical development. Several studies have reported side effects of emodin that may preclude its development beyond pre-clinical studies. For instance, it has been suggested that emodin may have mutagenic properties given the documented reports of genotoxicity and

mutagenicity in certain strains of bacteria.[124,125] There also are reports of hepatotoxic effects of emodin depending on the dose. [126-130] Further, at very high doses (1-3 g/kg/d for mice), emodin has been shown to have laxative effects leading to melanosis.[125,131] While the number of negative reports is arguably balanced by the number of studies reporting no side-effects, uncertainties remain and have hampered enthusiasm for further development of this promising dietary agent.

Given the potential toxicity associated with emodin along with our efforts in the development of emodin as a complementary cancer therapy, we performed a sub-chronic toxicity study of emodin as a first step to clinical translation. We subjected mice to an emodin infused diet of three different concentrations (~20 mg/kg, 40 mg/kg and 80 mg/kg) – similar doses that we have used in our efficacy studies – for 12 weeks to monitor any potential toxic effects that emodin may have. In addition, we performed a pharmacokinetic study to evaluate the time course of emodin clearance from the circulation when given via two different routes of administration, intraperitoneally (I.P.) and orally (P.O.). To ensure that we are not limiting translational relevance, both male and female mice were used in both the toxicity and pharmacokinetic studies.

4.3 Methods

4.3.1 Animals

Male and female *C57BL/6J* mice were purchased from Jackson Laboratories (Bar Harbor, ME) and were cared for in the animal facility at the University of South Carolina School of Medicine. Mice (n=4-5/group/sex/experiment) were randomized upon arrival to the animal facility to prevent litter biases and were housed 4-5 per cage and maintained on a 12:12-h light-dark cycle in a low-stress environment (22^0C, 50% humidity, low

noise). Mice were handled only by the primary investigator (ATS). All mice were habituated for 6 weeks to the AIN-76A diet prior to any interventions and were given food and water *ad libitum* through the course of the study. All methods were performed in accordance with the American Association for Laboratory Animal Science and the Institutional Animal Care and Usage Committee at the University of South Carolina.

4.3.2 Emodin

Emodin was purchased from Nanjing Zelang Medical Technology Co., Ltd, (Nanjing, China). Emodin was independently analyzed by the Mass Spectrometry Center at the University of South Carolina prior to the initiation of the experimental study. Liquid Chromatography -Ultraviolet-Mass Spectrometry (LC-UV-MS) and Nuclear Magnetic Resonance (NMR) was performed to confirm the purity and molecular structure of emodin (Fig 1A).

4.3.3 Emodin dosing and time course analysis for pharmacokinetic studies

Emodin was delivered intraperitoneally (I.P.) or by oral gavage (P.O.) at 20 mg/kg or 40 mg/kg doses. For the I.P. study, emodin, dissolved in DMSO was made in a large batch, aliquoted, and stored at -20^{0}C until used for injections. It was subsequently diluted in PBS (1% DMSO) and administered to mice I.P. at doses of 20 mg/kg (0.5 mg/mL) or 40 mg/kg (1 mg/mL). To deliver emodin P.O., we utilized a 20G 30-mm flexible plastic tubal oral gavage needle (Instech, #FTP-20). To prevent aspiration of the emodin bolus, mice were briefly anesthetized with 2% isoflurane prior to gavage and held upright until consciousness was regained. Emodin was prepared fresh on the day of administration. Briefly, emodin was mixed in pure propylene glycol (VWR, #97061) for 6-8 hours at room temperature while protected from light. The emodin solution was

delivered to mice at 20 mg/kg (6mg/mL) and 40 mg/kg (12mg/mL) doses. We used 1% DMSO in PBS (I.P.) or pure propylene glycol (P.O.) for vehicle controls.

Plasma emodin content was analyzed at three specific time points (t=1hr, 4hr, and 12hr) after treating male and female WT *C57BL/6J* mice I.P. or P.O. Emodin was given at 20 mg/kg or 40 mg/kg; n=4 mice were used per dosage, per timepoint, and per sex. Vehicle treated mice were used to analyze empty plasma extracts.

4.3.4 Solid Phase Extraction and LC-MS/MS Analysis

Whole blood was collected in EDTA coated tubes from the inferior vena cava and centrifuged at 4,000 RPM for 10 min. Plasma was aliquoted and stored at -20^{0}C until solid phase extractions. For free emodin quantification, 50 µl plasma was mixed with equal 0.2M sodium acetate buffer with 1% ascorbic acid (pH 5.0). For emodin glucuronide quantification, 50 µl plasma was mixed with half volume of 0.2M sodium acetate buffer with 1% ascorbic acid and 1000 units of β-glucuronidase (Millipore Sigma #G2174). D4-emodin (1 ng/µl) was used as an internal standard (Santa Cruz #218302). Both tubes were then incubated at 37^{0}C for 2hr. After incubation, the mixture was extracted with 600 µl ethyl acetate three times. The ethyl acetate layer was evaporated under N_2 gas to dryness and reconstituted in 5% ammonia water. Solid phase extraction was performed using a vacuum manifold (Supelco #SU57250-U) with Oasis MCX cartridges (Fisher #186000254) and was eluted with 3 mL 5% formic acid-methanol. After elution, the eluent was evaporated under N_2 gas to dryness and reconstituted in 400 µl 5% ammonia methanol.

Emodin samples were analyzed and quantified by LC-MS/MS using electrospray ionization in negative ion mode. Chromatorgraphic separation was performed on a Waters Acquity UPLC system using a binary solvent gradient. Solvent A was water containing 0.1% formic acid and solvent B was methanol. The LC column was a Waters XBridge C18 reversed phase column (2.1mm X 100mm containing 3.5um particles) running at a flow rate of 0.2 mL/min. The solvent gradient started at 50%B, ramped to 95%B over 10 minutes and was maintained at 95%B until 14 minutes. The gradient then returned to initial conditions. The mass spectrometer was a Waters Premier XE triple quadrupole instrument. Data was collected in multiple reaction monitoring (MRM) mode. Two precursor/product ion pairs were monitored; one pair for emodin (269 daltons > 225 daltons) and one pair for the internal standard deuterium labeled emodin (273 daltons > 229 daltons). According to the standard curve of emodin in 5% ammonia methanol, the concentration of emodin was calculated relative to the D4-emodin internal standard. Total emodin was measured from the tube containing the β-glucuronidase, free emodin was measured from the tube without β-glucuronidase, and glucuronidated emodin was calculated as the difference between total emodin and free emodin.

4.3.5 Emodin diets for sub-chronic toxicity study

We analyzed the effect of emodin feeding over a 12-week period. Emodin was infused into the AIN-76A diet at three different concentrations; 170 mg/kg, 340 mg/kg, and 680 mg/kg (BioServ, Frenchtown, NJ). These concentrations were based on our established average food intake of C57BL/6 mice and translate to a daily ingested dose per body weight of ~20 mg/kg, 40 mg/kg, and 80 mg/kg, respectively. Therefore, we separated mice into 4 groups consisting of n=5 sex/diet; Control (AIN), 20 mg/kg, 40

mg/kg, and 80 mg/kg. Mice were purchased at 4 weeks of age, kept on AIN-76A diet until 10 weeks of age, and then separated into experimental groups and started on their respective diets. Mice were maintained on their treatment diets for 12 weeks and were given food and water *ad libitum*.

4.3.6 Body weights and body composition

Body weight, food, and water consumption were monitored on a weekly basis throughout the study. Body composition was assessed after 12 weeks of emodin diet using dual-energy X-ray absorptiometry (DEXA) (Lunar PIXImus, Madison, WI). Briefly, mice were placed under gas anesthesia (isoflurane, 2%) and were assessed for bone mineral density (BMD), lean mass, fat mass, and body fat percentage. Lean mass (%) was calculated as percent lean weight and bone mineral content (BMC) of total body weight.

4.3.7 Tissue Collection

After 12 weeks of dietary treatment, mice were euthanized by isoflurane overdose following a 4 hour fast, blood was collected from the inferior vena cava and placed in EDTA coated lavender top tubes for plasma collection and blood panel analysis. The following tissues were harvested and fixed overnight in 10% neutral buffered formalin and subsequently embedded in paraffin; spleen, liver, kidney, heart, colon, and ileum. Colon and ileum were cleaned with PBS and swiss rolled prior to fixation. Liver, epididymal fat, mesenteric fat, and spleen weight were determined from freshly excised tissue prior to fixation. Colon, entire small intestine, and tibial length were also measured using calipers during tissue collection.

4.3.8 Blood Panel Analysis

A complete blood panel analysis was performed using the VetScan HMT (Abaxis, Union City, CA) for determination of white blood cells (WBC), lymphocytes (LYM), monocytes (MON), neutrophils (NEU), platelets (PLT), red blood cells (RBC), hematocrit (HCT), and hemoglobin (Hb). Neutrophil/lymphocyte ratio (NLR) was calculated from obtained values.

4.3.9 Plasma Markers of Toxicity

Plasma was analyzed for common markers of major organ toxicity/physiological impairment including ALT (Cayman Chemical, 700260) and creatinine (Cayman Chemical, 700460) and according to manufacturer's instructions.

4.3.10 Histopathology Analysis

All tissues collected were stained with hematoxylin and eosin (H&E) as previously described.[132] To analyze the presence of fibrosis, trichrome staining was performed in heart, liver, kidney, and spleen as previously described.[133] Goblet cells were identified in the colon and small intestine by Alcian blue staining and counterstained by nuclear fast red as previously described.[94] All histopathological analyses were performed by a board-certified pathologist blinded to the experimental conditions (I.C.).

4.4 Results

4.4.1 There is no difference in bioavailability of emodin when given I.P. vs P.O. but it is more bioavailable in female mice.

We measured the concentrations of free emodin and glucuronidated emodin in plasma of mice given emodin via I.P. or P.O. at 20 or 40 mg/kg doses and at t=1, 4, or 12 hrs (n=4/timepoint/sex; Fig 4.1B-E). The majority of emodin detected in each sample was glucuronidated while free emodin was scarcely found at all time points following both I.P. and P.O. routes of administration. The highest point of emodin detection was at the t=1hr time point and was at approximately 50% concentration at t=4hr and was completely eliminated at t=12hrs. Interestingly, we found that female mice had greater concentrations of glucuronidated emodin at t=1hr in all doses and routes except for the 20 mg/kg dose given P.O. (Fig 4.1B-E, $p<0.05$) and at t=4hr only in mice given the 20 mg/kg dose by I.P. (Fig 4.1B, $p<0.05$). Overall, there was no difference between I.P. and P.O. administration at any of the timepoints tested.

4.4.2 12-week emodin feeding does not present phenotypic toxicities in mice.

We fed male (n=5/group) and female (n=5/group) mice a purified diet (AIN-76A) infused with three different concentrations of emodin. In statistical analysis, male and female mice were combined. After 12 weeks of feeding, emodin dose did not affect body weight compared to control mice (AIN-76A fed) (Fig 4.2A). Similarly, body composition analysis did not show any differences in lean mass (%) or body fat (%) (Table 4.1) for any of the emodin doses versus the control group. Further, there was no difference in organ weight (liver, spleen, mesenteric fat, epididymal fat) or length (colon length, small intestine length, or tibial length) with emodin dose (Table 4.1).

4.4.3 Spleen and blood analyses do not indicate inflammatory responses to emodin feeding.

To assess the sub-chronic effect of emodin on circulating immune cells we performed a comprehensive blood panel analysis. Table 4.2 indicates that there was no effect of emodin at any dose on circulating immune cells. To further investigate the potential toxicity of emodin on the immune system, we performed H&E staining on spleen biopsies. There were no histological changes of red or white pulp and there appears to be no indication of blood flow blockage or fibrosis (Fig 4.3A).

4.4.4 Liver, Kidney, and Heart do not present with any noticeable toxicities after 12-wk emodin feeding.

4.4.4.1 Emodin feeding does not cause liver toxicity

To investigate the potential toxicity of emodin to the liver we performed H&E and trichrome staining. There were no indications of fibrosis or NASH in any of the mice fed emodin diets (Fig 4.4A,B). To confirm our findings, we measured ALT levels in plasma. We found that there were no elevated plasma ALT levels following any dose of emodin (Fig 4.4C).

4.4.4.2 Emodin feeding does not cause kidney toxicity

To investigate the potential toxicity of emodin to the kidneys we performed H&E and trichrome staining. There were very few indications (<5%) of isolated tubular ectasia and sloughed cells in tubular lumens in addition to an absence of inflammation (Fig 4.5A). To test the function of the kidneys we measured creatinine levels in plasma. Plasma creatinine levels were in normal range, lower that 5mg/dl in any of the mice indicating the normal renal function (Fig 4.5B).

4.4.4.3 Emodin feeding does not cause noticeable toxicity to the cardiovascular system.

To investigate the potential toxicity of emodin to the cardiovascular system, we performed H&E and trichrome staining on heart muscle (Fig 4.6A,B). There was no indication of architectural change of the tissue or fibrosis in cardiac tissue. Further, we did not observe any indications of atrial or ventricular hypertrophy.

4.4.5 Small intestine and colon analysis do not indicate GI toxicity after 12-wks of emodin feeding.

To assess potential gastrointestinal toxicities of sub-chronic emodin feeding, we performed histopathological analysis on small intestine (Fig 4.7A) and colon tissue (Fig 4.7B,C). H&E staining did not indicate any significant dysplasia in either the small intestine (Fig 4.7A) or colon (Fig 4.7B). We furthered stained colon biopsies with Alcian blue to assess goblet cell integrity. Alcian blue staining did not show any significant differences in goblet cell count or morphology in the colon (Fig 4.7C).

4.5 Discussion

Emodin (Fig 4.1A), a natural anthraquinone, has shown many potential health benefits in pre-clinical models. In fact, we have reported that emodin is effective at reducing tumorigenesis given its actions on macrophages.[78,122] However, further development of emodin as an effective anti-cancer agent is hindered by uncertainties surrounding its potential toxicity. The primary purpose of this study was to uncover any potential toxic properties of emodin in mice using doses that we have found to have efficacy in our cancer studies.[78,122] In addition, we sought to assess the time course of emodin clearance when administered both I.P. and P.O. in order to begin to establish effective dosing intervals. We found that 12 wks of low (20 mg/kg), medium (40 mg/kg),

or high (80 mg/kg) emodin feeding does not cause pathophysiological perturbations in major organ systems. We also found that glucuronidated emodin peaks at 1hr for both I.P. and P.O. administered emodin and is eliminated by 12 hr.

Despite inconsistencies in the literature, previous investigations have shown that emodin is typically cleared by 12 hr after injection/ingestion.[77,122,134] We show in the present study that emodin is rapidly metabolized to its glucuronidated form, peaking at 1 hr, and is completely cleared by 12 hr when given both I.P. and P.O. Further, we confirm that the parent free emodin is undetectable after 1 hr, even at higher doses. Some of the inconsistences in the literature are likely due to the varying vehicles used. It is important to note that emodin is not soluble solely in PBS or water and must have an alcohol-based solvent to dissolve. Several previous studies have reported using saline or PBS only as a vehicle,[70,73,121,135] which is likely to result in delivery of a non-homogenous solution, and presumably inconsistent pharmacokinetic data. We aimed to deliver a homogenous solution of emodin to improve our consistency of plasma analysis. Thus, emodin was dissolved in pure DMSO for the I.P. study and in propylene glycol for the P.O. study. Our findings are supported by previously published work.[77,122,134,136] For example, a study by Shia et al., 2010 utilized a similar solvent to propylene glycol (PEG 400) and showed comparable results using male Sprague-Dawley rats.[136] While we report peak levels of emodin at 1 hr post administration for both the I.P. and P.O. studies, it is important to note that our assessment was limited to 1 hr, 4 hr and 12 hr time-points. Thus, it is certainly possible that emodin may have peaked prior to, or following, the 1 hr time-point. Evaluation of additional time-points is necessary to fully determine the timing of peak levels of emodin.

Of further interest with the pharmacokinetic findings is the indication that females have almost double the amount of glucuronidated emodin in the circulation at 1 hr following injection/gavage. When given I.P., this difference remains at the 4 hr time-point (only significant in the 20 mg/kg dose), but not in mice given emodin via P.O. This finding is consistent with Liu et al., (2010) that showed in an *ex vivo* experiment that emodin is absorbed and metabolized at a faster rate in females vs. males.[75] Although the clearance of emodin is comparable between males and females, it is important to note this difference in pharmacokinetics between males and females so that appropriate dosing can be implemented during the transition to clinical investigations.

Given the potential toxicity associated with emodin along with our efforts in the development of emodin as a complementary cancer therapy we performed a sub-chronic toxicity study of emodin as a first-step to clinical translation. We subjected mice to an emodin infused diet of three different concentrations (~20 mg/kg, 40 mg/kg and 80 mg/kg) – similar doses that we have used in our efficacy studies - for 12 wks to observe any potential toxic effects that emodin may have. Emodin did not impact body weight or body composition in the current study. Further, there was no effect of emodin on major organs. It should be noted that others have reported beneficial effects of emodin on metabolic disorders including a reduction in body weight; however, unlike the current study, these effects were documented in the settings of diet-induced obesity. [137,138]

There is some suggestion that emodin may have mutagenic properties given the documented reports of genotoxicity and mutagenicity in certain strains of bacteria.[124,125] However, a two-year genetic toxicology and carcinogenesis study conducted by the National Toxicology Program (NTP) of the NCI showed no evidence of carcinogenic

activity for emodin in female mice and equivocal evidence in male mice given a low incidence of renal tubule adenoma and carcinoma (1 mouse in each of 35 mg/kg and 70 mg/kg groups of 10) following a two year feeding study.[139] Only in doses of 170 mg/kg and higher were significant toxicities noticed in this study.[139] Together with other assessments of emodin from carcinogenicity studies, evidence does not support a genotoxic risk of emodin to humans.[124,125,131] In fact, there are a number of recent reports that indicate anti-tumor effects of emodin including studies by our group.[78,122] This is further supported by the current study; we show that emodin, when given at doses of 20, 40, and 80 mg/kg for 12 wks, does not appear to have mutagenic properties.

There also are some reports of hepatotoxic effects of emodin while other studies report hepatoprotection.[126-130] Based on a review of the literature it is likely that emodin has bidirectional potential, both liver protection[126,127] and hepatoxicity[126-130] depending on the dose. In our study, we found no hepatoxicity with daily emodin treatment for 12 wks and this was supported by no elevation in plasma ALT levels. Similarly, there are some indications that emodin, or foods containing emodin, may cause kidney toxicity[140] while other reports document that emodin may actually serve as a therapeutic for kidney injury.[141] We found no evidence of nephrotoxicity in the current study nor did we see elevated plasma creatinine levels following emodin treatment. Further, emodin has been shown to have laxative effects leading to melanosis, but only at very high doses, for example, 1-3 g/kg/d for mice.[125,131] Thus, it is not surprising that we did not find any laxative effects following administration of emodin in the 20-80 mg/kg dose range. Nor did we document any dysplasia in the small intestine or the colon. While toxic effects of

emodin have not been documented in the spleen or heart, at least to our knowledge, we assessed these tissues and report no toxic effects.

4.6 Conclusion

In summary, we show that the pharmacokinetics of emodin does not differ significantly between the peritoneal and oral routes of administration. However, there are sex differences in the pharmacokinetics of emodin with female mice having higher levels of metabolized emodin that should be considered during the transition to clinical investigations. Further, we confirm that emodin is a safe compound to be used in both male and female mice when given at 20, 40, and 80 mg/kg doses for 12 wks.

4.7 Figures & Legends

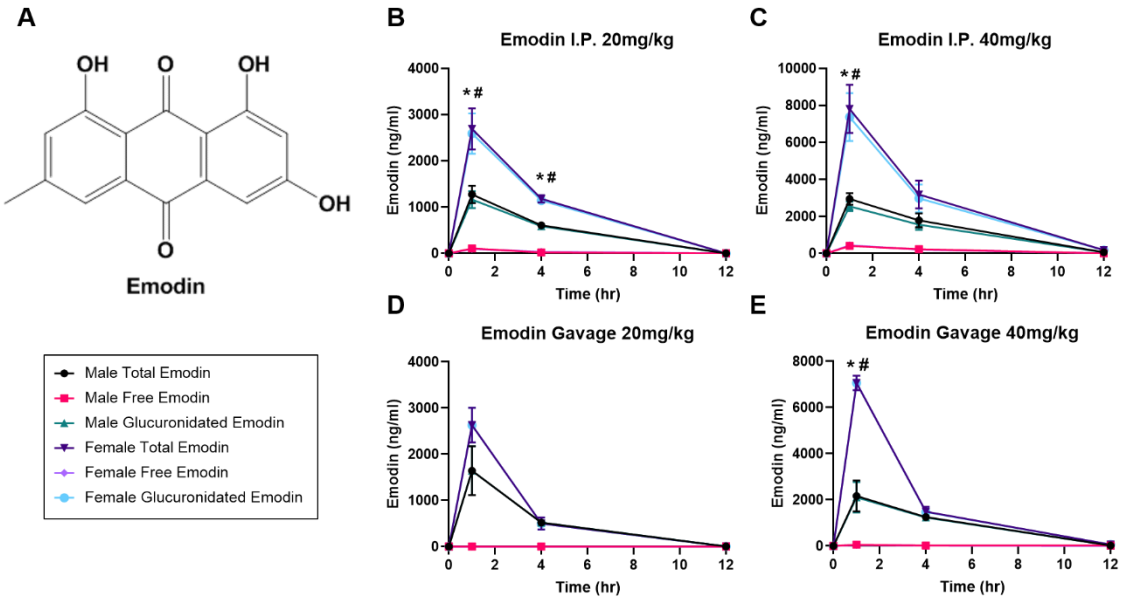

Figure 4.1. Emodin is rapidly glucuronidated when given I.P. and P.O. and is more bioavailable in females. A. Chemical structure of emodin (PubChem CID: 3220). **B-E.** Total, glucuronidated, and free emdoin bioavailability in male and female mice 1hr, 4hr, and 12hr after given I.P at **B)** 20 mg/kg and **C)** 40 mg/kg and P.O. at **D)** 20 mg/kg and **E)** 40 mg/kg. n=3-4/dose/timepoint/sex. * indicates statistical significance ($p<0.05$) between sexes of total emodin. # indicates statistical significance ($p<0.05$) between sexes of glucuronidated emodin.

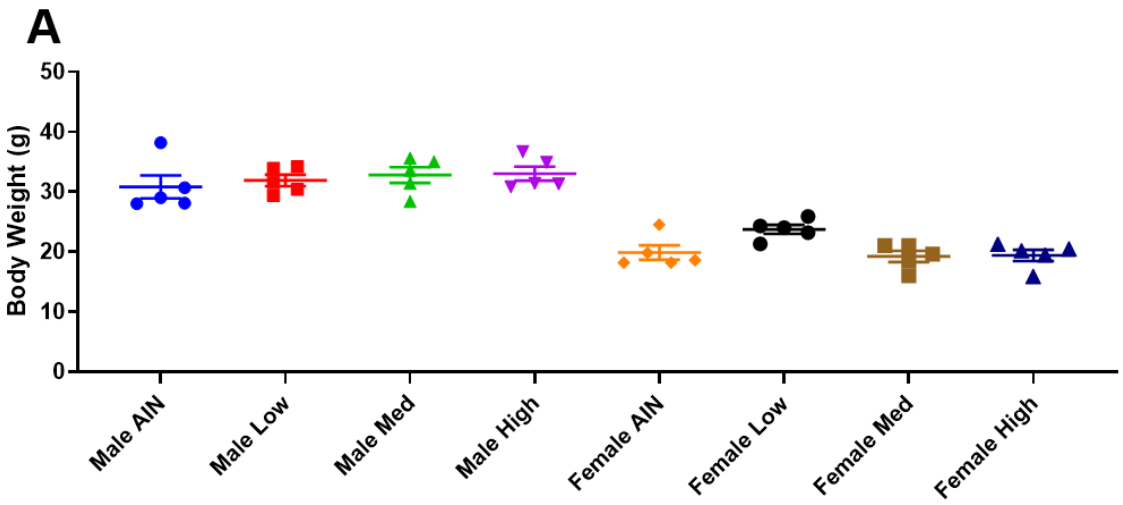

Figure 4.2. 12-week emodin feeding does not present phenotypic changes in male and female mice. **A.** Body weight at end of 12-week feeding for male and female mice. n=5/group.

Table 4.1. Male and female mice fed emodin for 12-weeks do not show differences in body composition and major organ weight. Lean mass and body fat percentage (%) were measured using DEXA scan. Liver, spleen, mesenteric fat, and epididymal fat were measured in milligrams (mg). Tibial length was measured in millimeters (mm). Colon length and small intestine (SI) length were measured in centimeters (cm). n=5/group.

Group	Lean Mass (%)	Body Fat (%)	Liver (mg)	Spleen (mg)	Mesenteric Fat (mg)	Epididymal Fat (mg)	Tibial Length (mm)	Colon Length (cm)	SI Length (cm)
Control (AIN)	72.5 ± 1.11	18.4 ± 1.65	1162.0 ± 90.66	110.1 ± 9.72	281.8 ± 41.55	464 ± 118.45	16.57 ± 0.15	8.0 ± 0.21	32.7 ± 0.58
Low Emodin (20mg/kg)	72.8 ± 1.19	19.6 ± 1.21	1225.4 ± 67.54	110.1 ± 7.52	333.8 ± 39.18	6098.1 ± 86.46	16.65 ± 0.14	7.95 ± 0.17	32.35 ± 0.50
Medium Emodin (40 mg/kg)	73.7 ± 1.49	18.6 ± 1.77	1272.9 ± 65.02	98.8 ± 5.78	328 ± 57.04	569 ± 141.06	16.62 ± 0.17	7.78 ± 0.14	31.33 ± 0.37
High Emodin (80 mg/kg)	73.5 ± 1.28	18.3 ± 0.97	1268.7 ± 69.63	89.4 ± 4.04	332.3 ± 60.85	504.9 ± 102.89	16.67 ± 0.16	8.03 ± 0.20	32.1 ± 0.48

Table 4.2. Male and female mice fed emodin for 12-weeks do not show changes in CBC counts. White blood cells (WBC), lymphocytes (LYM), monocytes (MON), neutrophils (NEU), neutrophil:lymphoctye ration (NLR), red blood cells (RBC), hemoglobin (HGB), hematocrit (HCT), and platelets (PLT) were measured using a VetScan HMT (Abaxis, Union City, CA). n=5/group.

Group	WBC (10^9/l)	LYM (10^9/l)	MON (10^9/l)	NEU (10^9/l)	NLR	RBC (10^12/l)	HGB (g/dl)	HCT (%)	PLT (10^9/l)
Control (AIN)	5.39 ± 0.63	4.03 ± 0.38	0.21 ± 0.06	1.15 ± 0.31	0.27 ± 0.06	10.41 ± 0.54	15.97 ± 0.15	42.06 ± 1.86	717.78 ± 62.73
Low Emodin (20mg/kg)	4.99 ± 0.32	3.97 ± 0.26	0.17 ± 0.04	0.85 ± 0.10	0.21 ± 0.02	10.82 ± 0.10	16.39 ± 0.15	42.88 ± 0.43	716.90 ± 22.33
Medium Emodin (40 mg/kg)	5.30 ± 0.43	4.31 ± 0.29	0.14 ± 0.04	0.85 ± 0.16	0.19 ± 0.02	10.49 ± 0.14	16.39 ± 0.25	41.86 ± 0.59	680.20 ± 32.56
High Emodin (80 mg/kg)	5.58 ± 0.38	4.48 ± 0.31	0.18 ± 0.04	0.91 ± 0.12	0.21 ± 0.03	10.23 ± 0.17	16.03 ± 0.25	40.32 ± 0.67	693.60 ± 26.30

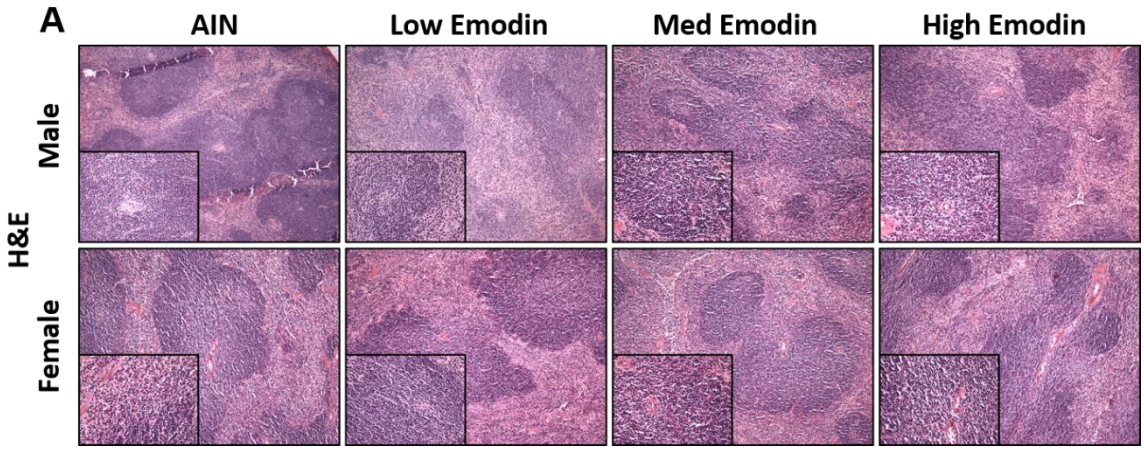

Figure 4.3. 12-week emodin feeding does not present histological changes in spleen. **A.** Representative 10X and 40X (insets) images of male and female spleens stained with H&E. n=5/group.

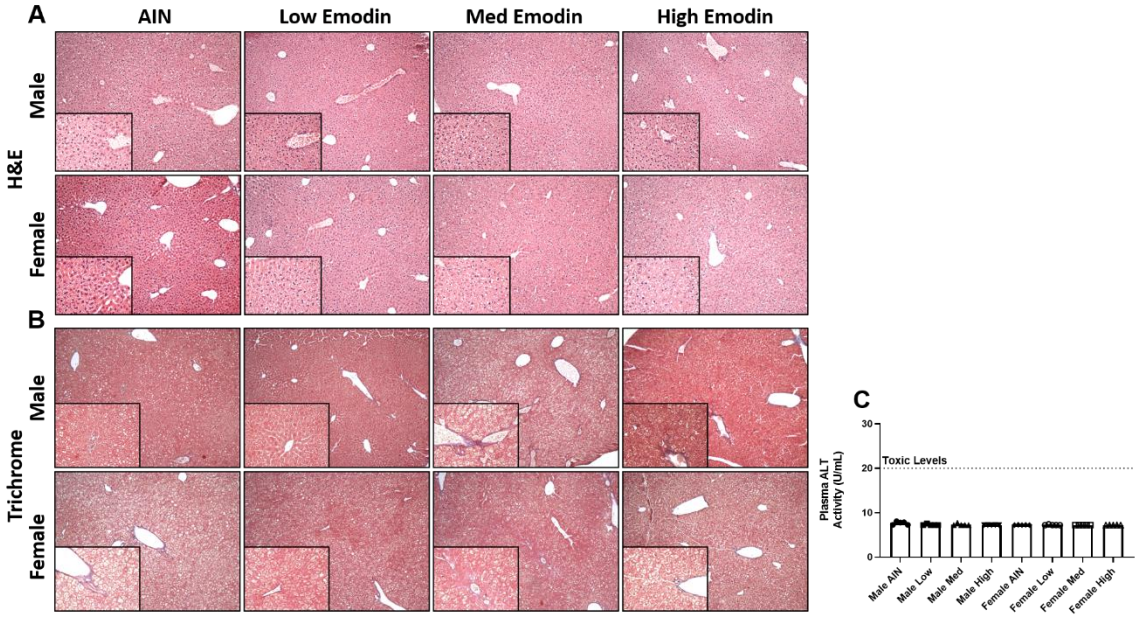

Figure 4.4. 12-week emodin feeding does not cause liver toxicity. A. Representative H&E stains of livers imaged at 10X and 40X (insets). **B.** Representative trichrome stains of livers imaged at 10X and 40X (insets). **C.** Plasma ALT activity measured in units/mL (U/mL) plasma. Dashed line indicates critical toxic levels (20 U/mL). n=5/group.

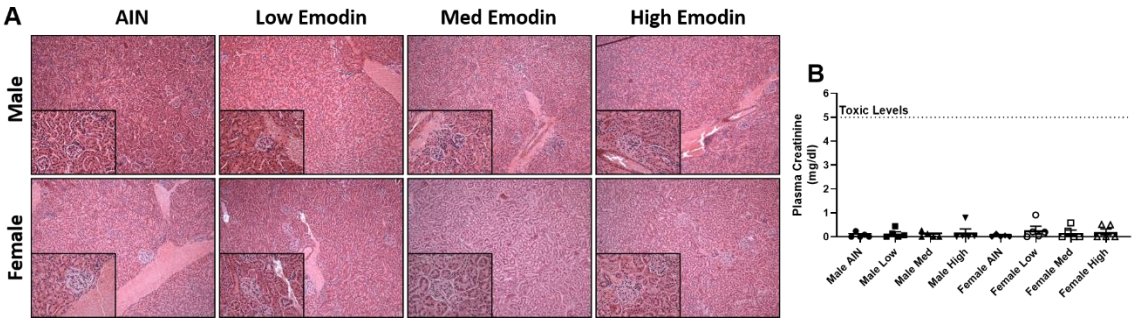

Figure 4.5. 12-week emodin feeding does not cause kidney toxicity. A. Representative H&E stains of kidneys imaged at 10X and 40X (insets). **B.** Plasma creatinine measured in milligrams/deciliters (mg/dl) of plasma. Dashed line indeicates critical toxic levels (5mg/dl). n=5/group.

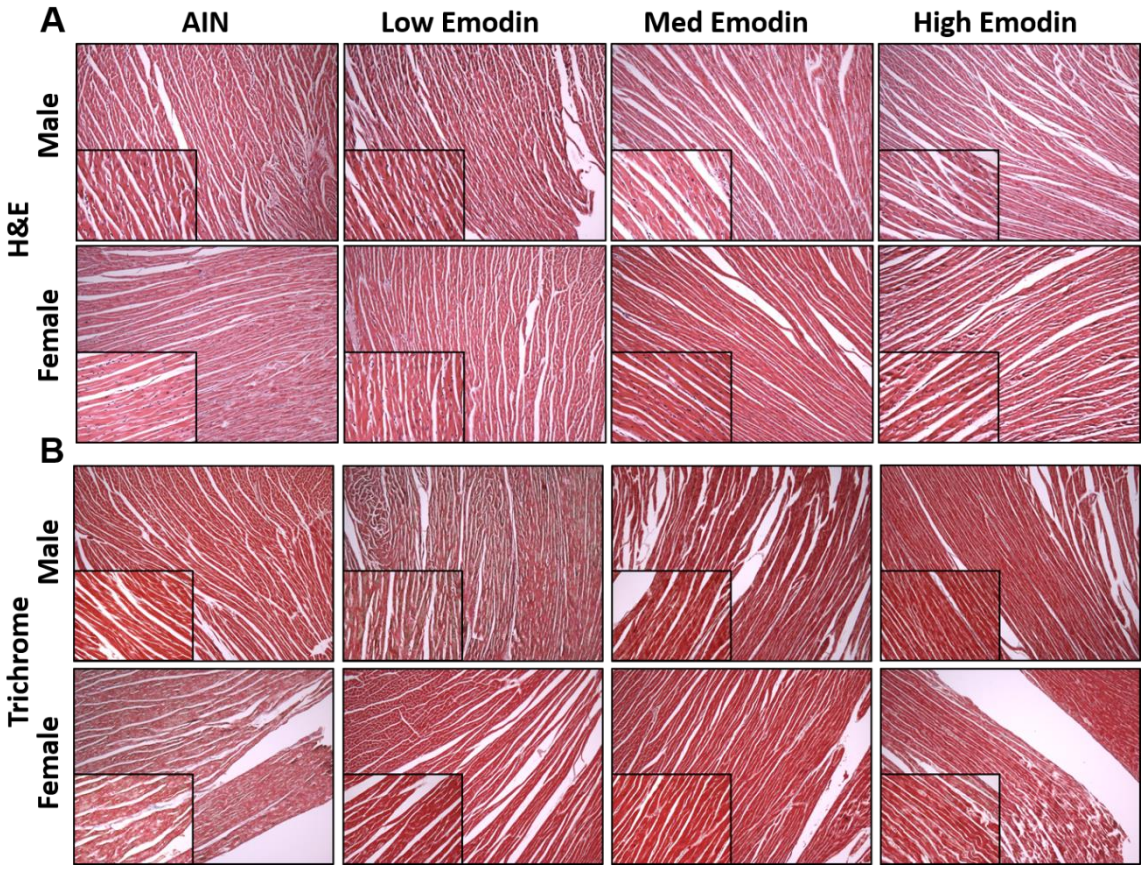

Figure 4.6. 12-week emodin feeding does not cause cardiotoxicity. A. Representative H&E stains of cardiac tissue imaged at 10X and 40X (insets). **B.** Representative trichrome stains of cardiac tissue imaged at 10X and 40X (insets).

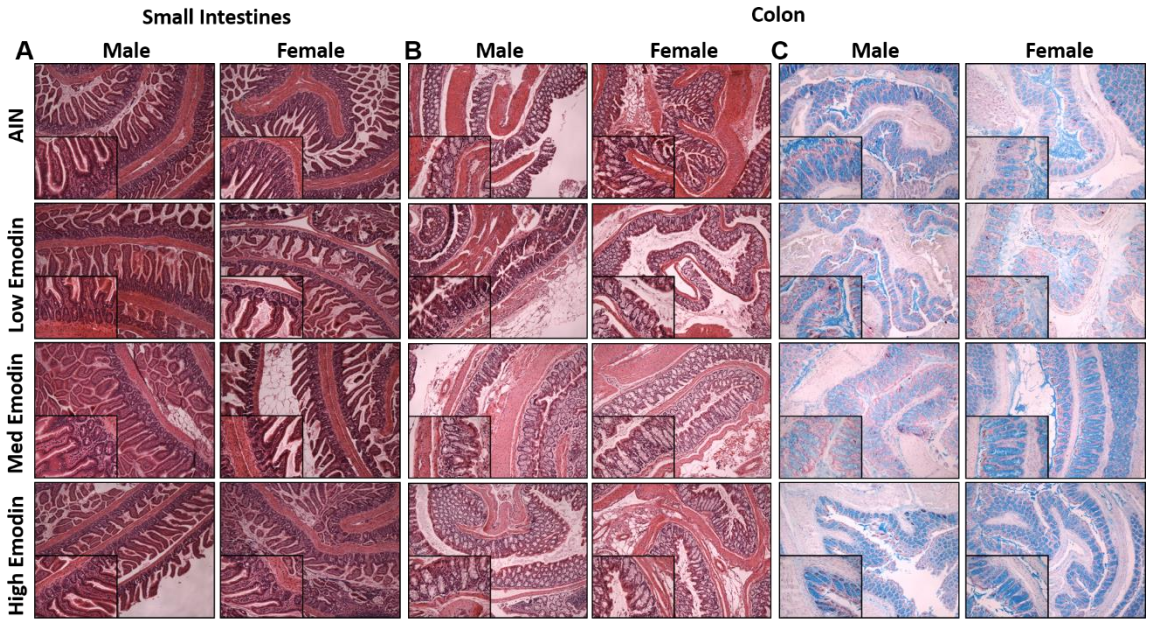

Figure 4.7 12-week emodin feeding does not cause GI toxicity. A. Representative H&E stains of swiss rolled small intestines imaged at 10X and 40X (insets). **B.** Representative H&E stains of swiss rolled colons imaged at 10X and 40X (insets). **C.** Representative alcian blue stains of swiss rolled colons imaged at 10X and 40X (insets). n=5/group.

4.8 Supplemental Material

Supplementary Table 4.1. Emodin Review. Assessment of studies examining the potential therapeutic properties of emodin in various models of pathology. Studies that examined more than one dose of emodin or time point were treated as separate experiments when totaling each respective outcome. ↔ = No Change, ↓ = Decrease, ↑ = Increase, N/A = Not Assessed, HFD = High Fat Diet.

Author	Pathology	Model	Method	Dose	Route	Outcomes					
						Overall Outcome	**BW**	**Inflammation/ Pathology**	**Signaling**	**PK/PD**	**Gut Microbiota**
Bai *et al*. (1)	Liver Cancer	BALB/cnu/nu mice (Male)	HepG2 Implantation	1 mg/kg or 10 mg/kg	Hypodermic Injection	Inhibition of tumorigenesis and reduced mortality	N/A	10 mg/kg dose showed no mortality and reduced metastasis	SMAD 2: ↓ SMAD 4: ↓ miR-34a: ↑ VEGFR: ↓ AKT: ↓ ERK1/2: ↓	Peak: 1hr Cleared: 12 hr $t_{1/2}$: 2hr	N/A
Feng *et al*. (2)	Obesity and Metabolic Syndrome	C57BL/6J mice (Male)	HFD (60 kcal% fat, 20 kcal% protein, 20 kcal%	50 mg/kg or 100 mg/kg or 200 mg/k	Daily Oral Gavage (Distilled H_2O)	Improves body weight and reduces metabolic dysfunction	↓	Reduced blood glucose with Prednisone Improved insulin sensitivity Reduced cholesterol and	11βHSD1: ↓ PEPCK: ↓ G6Pase: ↓	N/A	N/A

			carbohydrates)	g				triglycerides			
Guo *et al*. (3)	Pancreatic Cancer	BALB/cnu/nu mice (Male)	PANC-1 Implantation	40 mg/kg and 80 mg/kg	I.P. (0.9% Sodium Chloride)	Improves Gemcitabine Efficacy	↑ compared to Gemcitabine Alone	Reduced NF-κB but no specific inflammatory markers were assayed	p-NF-κB: ↓ Survivin: ↓ XIAP: ↓ Caspase-9: ↑ Caspase-3: ↑	N/A	N/A
Höhn *et al*. (4)	Colon Cancer	WAG/Rjj Rats (Male)	CC-531	2.5 mg/kg or 5 mg/kg	I.V. or I.P. (Saline) Daily	Anti-tumor effects when given in low doses	↓	N/A	N/A	Both routes had similar efficacies	N/A
Iwanowycz *et al*. (5)	Inflammation	*In-vitro* peritoneal MΦs	IL4, LPS, and IFNγ	10 mg/ml	*In vitro* (DMSO)	Modulation of MΦ activity	N/A	Suppress M1 and M2 activity	Inhibited H3K27 trimethylation removal	N/A	N/A
Iwanowycz *et al*. (6)	Breast Cancer	C57BL/6 and BALB/c mice (Female	EO771 and 4T1 Implantation	40 mg/kg	I.P. (2% DMSO) daily	Attenuated tumor growth	N/A	Inhibited MΦ infiltration Increased T-cell activation	IRF4: ↓ p-STAT6: ↓	N/A	N/A

		)							p-C/EBPβ: ↓ MCP1: ↓ CSF1: ↓ Thy-1: ↓		
Jelassi *et al.* (7)	Breast and non-small cell lung carcinomas	*In vitro* carcinoma	<u>Breast</u> MCA-10A MDA-MB-435 MDA-MB-468 <u>Lung</u> A549	0.001 μM – 10 μM	*In vitro* (DMSO)	Inhibits cell invasion by antagonizing P2X7 receptors	N/A	N/A	Reduced P2X7 Receptor-mediated ATP current	N/A	N/A
Jia *et al.* (8)	Obesity and Metabolic Syndrome	LDLR$^{-/-}$ Mice (Female)	Western-type Diet	40 mg/kg	I.P. with LPS once daily (up to 70 days)	Reduced NAFLD pathology	↔	Reduction of systemic and liver immune cell infiltration	p-Erk1/2: ↓ p-P38: ↓	Peak: 1hr Cleared: 24hr	N/A
Jia *et al.* (9)	Breast Cancer Metastasis	BALB/c and C57BL/6 mice (Female	4T1 and E0771 Implantation	40 mg/kg	I.P. (2% DMSO) daily	Reduced breast tumor metastasis and	N/A	Reduced metastasis to lungs Reduced MΦ migration	p-STAT6: ↓ p-C/EBP	Peak: 1hr Cleared: 24hr	N/A

		)				macrophage polarization		Suppressed M2 MΦ polarization	β: ↓		
Kuo *et al.* (10)	Glioma	*In vitro* carcinoma	C6 Glioma	10-50 μM	*In vitro* (DMSO)	Attenuated cellular growth but induced drug resistance	N/A	N/A	ROS: ↓ Cellular Ca^{2+}: ↓ p-NF-κB (24hr): ↓ p-NF-κB (48hr): ↑ Mdr1a: ↑	N/A	N/A
Lee *et al*. (11)	Bone remodeling	*In vitro* osteoclasts	MC3T3-E1 mouse osteoblasts	1 μM – 40μM	*In vitro* (DMSO)	Improve bone health and prevent osteoporosis	N/A	N/A	BMP-2: ↑ AP-1: ↑ p-PI3K: ↑ p-Akt: ↑ p-NF-κB: ↑ p-JNK: ↑	Toxic at 20 μM and above	N/A

									p-p38: ↑		
Lee *et al*. (12)	Colorectal Cancer Tumorigenesis	*In vitro* carcinoma	HCT116, SW480, SNU-C2A, and SNU-C5	10 μM - 50 μM	*In vitro* (DMSO)	Reduced cell proliferation and increased protein ubiquitination	N/A	Reduced tumor cell growth and fatty acid synthase activity	FASN: ↓ LC3-II: ↓ Ubiquitin: ↑ p-Akt: ↓ p-PI3K: ↓ p-ERK1/2: ↑	N/A	N/A
Liu *et al*. (13)	Chronic Inflammation	*In vitro* peritoneal MΦ (Wistar Rats) and HEK293	ATP	0.1 μM – 10 μM	*In vitro* (DMSO)	Inhibition of ATP-induced MΦ death	N/A	Expression of $P2X_7$ receptor is essential	N/A	N/A	N/A
Liu *et al*. (14)	Pancreatic Cancer	*In vitro* carcinoma and BALB/c nu/nu	SW1990 (*In vitro* and implantation)	*In vitro:* 10-40 μM	*In vitro* (DMSO) *In*	Attenuated cellular growth and increased apoptosis	N/A	Reduced metastasis by 50%	p-NF-κB: ↓ Survivin: ↓ MMP-	N/A	N/A

		mice (Male)		*In vivo:* 20 mg/kg and 40 mg/kg	*vivo*: Intragastric intubation (DMSO)				9: ↓ Cleaved Caspase-3: ↑		
Lu *et al*. (15)	Anaphylaxis	*In vitro*: Bone marrow-derived mast cells (Balb/cJ) and HMC-1 cells *In vivo*: ICR mice	*In vitro* and *In vivo*: DNP IgE and human serum albumin	*In vitro:* 10-20 μM *In vivo:* 5-40 mg/kg orally	*In vitro* (DMSO) *In vivo*: Orally (DMSO)	Attenuation from mast cell-dependent anaphylactic reaction	N/A	Reduced mast cell degranulation	COX-2: ↓ IL-6: ↓ TNFα: ↓ p-Akt: ↓ p-Iκκα/β: ↓ p-p65: ↓ Syk: ↓ LAT: ↓ PLCγ1: ↓	N/A	N/A
Ma *et al.* (16)	Nasopharyngeal Carcinoma	*In vitro* carcinoma	CNE-2Z	6.25 μM – 100 μM	*In vitro* (DMSO)	Attenuated cellular growth	N/A	N/A	Chloride channel blocker and tamoxi	N/A	N/A

									fen block anti-tumor effect		
Meng *et al*. (17)	Atherosclerosis	*In vitro* Sprague-Dawley primary RASMC	TNFα (10 ng/ml)	0.1 μM – 10 μM	*In vitro* (DMSO)	Inhibited MMPs and Inflammatory Responses and improved cell viability	N/A	Improved cell migration and reduced inflammatory cytokines	MMP-2: ↓ MMP-9: ↓ IL1β: ↓ IL-6: ↓ ICAM-1: ↓ VCAM-1: ↓ MCP-1: ↓ CINC-2β: ↓ NF-κB: ↓	N/A	N/A
Song *et al.* (18)	Autoimmune Myocarditis	Lewis Rats (Male)	Porcine cardiac myosin with Freund's complete adjuvant and *Mycoba*	50 mg/kg	Intragastric intubation (DMSO) for 3 weeks	Improved ventricular function and reduced myocarditis	↑	Myocarditis: ↓ Heart Weight: ↓	p-NF-κB: ↓ IL-1β: ↓ TNFα: ↓	N/A	N/A

			cterium tuberculosis H37Ra								
Tang *et al*. (19)	Non-small cell lung carcinoma	*In vitro* carcinoma *In vivo*: BALB/cnu/nu mice (female)	A549 and H1975	*In vitro:* 25, 50, and 75 μM *In vivo:* 25 mg/kg and 50 mg/kg	*In vitro* (DMSO) *In vivo* (DMSO) every other day	Reduced proliferation and invasion *in vitro* and at high dose reduced tumor size *in vivo*	N/A	Invasion: ↓ Inhibition of cell cycle arrest	PPARγ: ↓ p-ERK1/2: ↑ p-AMPKα: ↑	N/A	N/A
Tzeng *et al*. (20)	Obesity	Wistar Rats (Male)	HFD (45% kcal% fat)	40 mg/kg and 80 mg/kg	Daily Oral gavage (Distilled H_2O) for 8 weeks	Reduced body weight and lipid profile	↓	Reduced hepatic lipid content and lipogenesis	p-AMPK: ↑ ACO: ↑ p-SREBP-1: ↑ FAS: ↑ CPT-1:	N/A	N/A

									↑		
Wang *et al*. (21)	Gamma Radiation Toxicity	C57BL/6 Mice (Male)	7Gy Radiation	30 mg/kg daily	Not specified	Improved survival of mice undergoing gamma radiation	N/A	Increased villus height, crypt number, and goblet cell count in proximal jejunum	p53: ↓	N/A	N/A
Wang *et al.* (22)	Allergic Rhinitis	C57BL/6 Mice (Female)	Ovalbumin-induced sensitivity	10 mg/kg and 20 mg/kg	DMSO diluted to 0.1%	Reduced inflammatory reaction and inflammatory mediators	N/A	Reduced cellular infiltration to lungs and reduced IgE levels	IL-4: ↓ IL-5: ↓ IL-13: ↓ Eotaxin: ↓ MMP-9: ↓ HO-1: ↑	N/A	N/A
Yang *et al*. (23)	Virus Transmission	Mosquito Species: *A. aegypti, A. togoi, and C. pipens pallens*	Blood from live mouse	1 mg/L – 25 mg/L	Dissolved in blood	Caused death of 3 mosquito species	N/A	Will kill mosquitos before transmission of diseases	N/A	N/A	N/A
Yang *et al*. (24)	Liver Cancer	*In vitro* carcinoma	Bel-7402 HCC cell line	100 μM	*In vitro* (DMSO)	Induced apoptosis in cell cultures	N/A	Reduced lipid metabolism in cell cultures	Caspase-3: ↑ Caspase-9: ↑	N/A	N/A

									Cytochrome-C: ↑ AIF: ↑ Bax: ↑ Bcl-2: ↓		
Zeng *et al*. (25)	Chronic Kidney Disease	Sprague-Dawley rats (Male)	Chronic renal failure via nephrectomy	1 mg/day	5 ml colonic irrigation (0.4% CMC-Na)	Mitigation of renal injury and reduction of toxic bacteria	↔	Urea: ↓ Indoxyl sulfate: ↓ Creatinine: ↓	N/A	N/A	Total Bacteria: ↔ Clostridium spp.: ↓ Lactobacillus spp.: ↑ Bifidbacteria spp.: ↑ Enteroco

											ccus spp.: ↓ C. perf ring ens: ↓ E. coli: ↓
Zhang *et al*. (26)	Viral Myocarditis	*In vitro*: HL-1 and Human Cardiomyocytes *In vivo*: A/J Mice (Male)	CVB3 Viral Infection	*In vitro*: 5 - 20 μM *In vivo*: 40 mg/kg	*In vitro*: DMSO 30 min before infection *In vivo*: I.P. (2% DMSO) 1hr before infection	Improved cell viability and survival	N/A	VP1: ↓ and reduced pfu count in heart	eEF2 (K366): ↓ eEF2 (T56): ↑ p-Akt: ↓ p70S6K: ↓ p-ERK1/2: ↓ p-p60RSK: ↑ p-mTORC1: ↓ p-	N/A	N/A

									4EBP1 : ↓ L32: ↓		
Zhang *et al*. (27)	Acute Pancreatitis	HPDE6-C7	ATP	5.625 μM - 180 μM	*In vitro* (DMSO)	Reduced cell injury	N/A	Reduces the inflammatory response to ATP	P2X7: ↓ NLRP3 : ↓ ASC: ↓ Caspase-1: ↓ IL-1β: ↓ IL-18: ↓	N/A	N/A

1. Bai J, Wu J, Tang R, Sun C, Ji J, Yin Z, et al. Emodin, a natural anthraquinone, suppresses liver cancer in vitro and in vivo by regulating VEGFR. Invest New Drugs. 2019 Apr. PubMed PMID: 30976957. Epub 2019/04/11. eng.
2. Feng Y, Huang SL, Dou W, Zhang S, Chen JH, Shen Y, et al. Emodin, a natural product, selectively inhibits 11beta-hydroxysteroid dehydrogenase type 1 and ameliorates metabolic disorder in diet-induced obese mice. Br J Pharmacol. 2010 Sep;161(1):113-26. PubMed PMID: 20718744. PMCID: PMC2962821. eng.
3. Guo HC, Bu HQ, Luo J, Wei WT, Liu DL, Chen H, et al. Emodin potentiates the antitumor effects of gemcitabine in PANC-1 pancreatic cancer xenograft model in vivo via inhibition of inhibitors of apoptosis. Int J Oncol. 2012 Jun;40(6):1849-57. PubMed PMID: 22378302. Epub 2012/02/29. eng.
4. Höhn P, Braumann C, Freiburger M, Koplin G, Dubiel W, Luu AM. Anti-tumorigenic Effects of Emodin and Its' Homologue BTB14431 on Vascularized Colonic Cancer in a Rat Model. Asian Pac J Cancer Prev. 2020 Jan;21(1):205-10. PubMed PMID: 31983185. Epub 2020/01/01. eng.
5. Iwanowycz S, Wang J, Altomare D, Hui Y, Fan D. Emodin Bidirectionally Modulates Macrophage Polarization and Epigenetically Regulates Macrophage Memory. J Biol Chem. 2016 May;291(22):11491-503. PubMed PMID: 27008857. PMCID: PMC4882421. Epub 2016/03/23. eng.

6. Iwanowycz S, Wang J, Hodge J, Wang Y, Yu F, Fan D. Emodin Inhibits Breast Cancer Growth by Blocking the Tumor-Promoting Feedforward Loop between Cancer Cells and Macrophages. Mol Cancer Ther. 2016 08;15(8):1931-42. PubMed PMID: 27196773. PMCID: PMC4975665. Epub 2016/05/18. eng.
7. Jelassi B, Anchelin M, Chamouton J, Cayuela ML, Clarysse L, Li J, et al. Anthraquinone emodin inhibits human cancer cell invasiveness by antagonizing P2X7 receptors. Carcinogenesis. 2013 Jul;34(7):1487-96. PubMed PMID: 23524196. Epub 2013/03/23. eng.
8. Jia X, Iwanowycz S, Wang J, Saaoud F, Yu F, Wang Y, et al. Emodin attenuates systemic and liver inflammation in hyperlipidemic mice administrated with lipopolysaccharides. Exp Biol Med (Maywood). 2014 Aug;239(8):1025-35. PubMed PMID: 24740873. PMCID: PMC4988953. Epub 2014/04/16. eng.
9. Jia X, Yu F, Wang J, Iwanowycz S, Saaoud F, Wang Y, et al. Emodin suppresses pulmonary metastasis of breast cancer accompanied with decreased macrophage recruitment and M2 polarization in the lungs. Breast Cancer Res Treat. 2014 Nov;148(2):291-302. PubMed PMID: 25311112. PMCID: PMC4224983. Epub 2014/10/14. eng.
10. Kuo TC, Yang JS, Lin MW, Hsu SC, Lin JJ, Lin HJ, et al. Emodin has cytotoxic and protective effects in rat C6 glioma cells: roles of Mdr1a and nuclear factor kappaB in cell survival. J Pharmacol Exp Ther. 2009 Sep;330(3):736-44. PubMed PMID: 19549930. Epub 2009/06/23. eng.
11. Lee SU, Shin HK, Min YK, Kim SH. Emodin accelerates osteoblast differentiation through phosphatidylinositol 3-kinase activation and bone morphogenetic protein-2 gene expression. Int Immunopharmacol. 2008 May;8(5):741-7. PubMed PMID: 18387517. Epub 2008/02/22. eng.
12. Lee KH, Lee MS, Cha EY, Sul JY, Lee JS, Kim JS, et al. Inhibitory effect of emodin on fatty acid synthase, colon cancer proliferation and apoptosis. Mol Med Rep. 2017 Apr;15(4):2163-73. PubMed PMID: 28260110. PMCID: PMC5364834. Epub 2017/02/28. eng.
13. Liu L, Zou J, Liu X, Jiang LH, Li J. Inhibition of ATP-induced macrophage death by emodin via antagonizing P2X7 receptor. Eur J Pharmacol. 2010 Aug;640(1-3):15-9. PubMed PMID: 20452342. Epub 2010/05/07. eng.
14. Liu A, Chen H, Wei W, Ye S, Liao W, Gong J, et al. Antiproliferative and antimetastatic effects of emodin on human pancreatic cancer. Oncol Rep. 2011 Jul;26(1):81-9. PubMed PMID: 21491088. Epub 2011/04/12. eng.
15. Lu Y, Yang JH, Li X, Hwangbo K, Hwang SL, Taketomi Y, et al. Emodin, a naturally occurring anthraquinone derivative, suppresses IgE-mediated anaphylactic reaction and mast cell activation. Biochem Pharmacol. 2011 Dec;82(11):1700-8. PubMed PMID: 21907188. Epub 2011/09/03. eng.
16. Ma L, Yang Y, Yin Z, Liu M, Wang L, Chen L, et al. Emodin suppresses the nasopharyngeal carcinoma cells by targeting the chloride channels. Biomed Pharmacother. 2017 Jun;90:615-25. PubMed PMID: 28411554. Epub 2017/04/12. eng.

17. Meng L, Yan D, Xu W, Ma J, Chen B, Feng H. Emodin inhibits tumor necrosis factor-α-induced migration and inflammatory responses in rat aortic smooth muscle cells. Int J Mol Med. 2012 Jun;29(6):999-1006. PubMed PMID: 22426603. Epub 2012/03/15. eng.
18. Song ZC, Wang ZS, Bai JH, Li Z, Hu J. Emodin, a naturally occurring anthraquinone, ameliorates experimental autoimmune myocarditis in rats. Tohoku J Exp Med. 2012 07;227(3):225-30. PubMed PMID: 22791134. eng.
19. Tang Q, Wu J, Zheng F, Hann SS, Chen Y. Emodin Increases Expression of Insulin-Like Growth Factor Binding Protein 1 through Activation of MEK/ERK/AMPKα and Interaction of PPARγ and Sp1 in Lung Cancer. Cell Physiol Biochem. 2017;41(1):339-57. PubMed PMID: 28214826. Epub 2017/01/26. eng.
20. Tzeng TF, Lu HJ, Liou SS, Chang CJ, Liu IM. Emodin, a Naturally Occurring Anthraquinone Derivative, Ameliorates Dyslipidemia by Activating AMP-Activated Protein Kinase in High-Fat-Diet-Fed Rats. Evid Based Complement Alternat Med. 2012;2012:781812. PubMed PMID: 22649478. PMCID: PMC3357974. Epub 2012/05/10. eng.
21. Wang J, Zhang Y, Zhu Q, Liu Y, Cheng H, Li T. Data on the radioprotective effect of emodin. Data Brief. 2017 Apr;11:290-5. PubMed PMID: 28275662. PMCID: PMC5328685. Epub 2016/12/30. eng.
22. Wang T, Zhong XG, Li YH, Jia X, Zhang SJ, Gao YS, et al. Protective effect of emodin against airway inflammation in the ovalbumin-induced mouse model. Chin J Integr Med. 2015 Jun;21(6):431-7. PubMed PMID: 25519442. Epub 2014/12/18. eng.
23. Yang YC, Lim MY, Lee HS. Emodin isolated from Cassia obtusifolia (Leguminosae) seed shows larvicidal activity against three mosquito species. J Agric Food Chem. 2003 Dec;51(26):7629-31. PubMed PMID: 14664519. eng.
24. Yang N, Li C, Li H, Liu M, Cai X, Cao F, et al. Emodin Induced SREBP1-Dependent and SREBP1-Independent Apoptosis in Hepatocellular Carcinoma Cells. Front Pharmacol. 2019;10:709. PubMed PMID: 31297058. PMCID: PMC6607744. Epub 2019/06/25. eng.
25. Zeng YQ, Dai Z, Lu F, Lu Z, Liu X, Chen C, et al. Emodin via colonic irrigation modulates gut microbiota and reduces uremic toxins in rats with chronic kidney disease. Oncotarget. 2016 Apr;7(14):17468-78. PubMed PMID: 27003359. PMCID: PMC4951226. eng.
26. Zhang HM, Wang F, Qiu Y, Ye X, Hanson P, Shen H, et al. Emodin inhibits coxsackievirus B3 replication via multiple signalling cascades leading to suppression of translation. Biochem J. 2016 Feb;473(4):473-85. PubMed PMID: 26621875. Epub 2015/11/30. eng.
27. Zhang Q, Hu F, Guo F, Zhou Q, Xiang H, Shang D. Emodin attenuates adenosine triphosphate-induced pancreatic ductal cell injury in vitro via the inhibition of the P2X7/NLRP3 signaling pathway. Oncol Rep. 2019 Aug. PubMed PMID: 31524270. Epub 2019/08/08. eng.

CHAPTER 5

THE EFFECT OF ANTHRAQUINONE EMODIN ON SURVIVAL, LYMPHOCYTOPENIA, AND GUT HEALTH DURING 5FU CHEMOTHERAPY[3]

[3] Sougiannis AT et. al. To be submitted to *AJP Gastrointestinal and Liver Physiology.*

5.1 Abstract

Emodin, a natural anthraquinone, has been shown to have anti-inflammatory properties and may be effective to ameliorate off-target toxicities of 5FU chemotherapy. We evaluated chronic (n=5-20/group) and acute (n=20/group/sex) interventions to 5FU. Emodin improved run-to-fatigue time both acutely and chronically but only improved grip strength and peripheral nociception sensitivity chronically. Acutely, emodin reduced small intestine IL10, Mrc1, and Ly6G while reducing NOS2, TNFα, and Ly6G and increasing Mrc1 chronically. In the colon, emodin did not cause significant alterations in inflammatory gene expression but reduced NOS2 and Muc5ac chronically. Acutely, male mice retained circulating lymphocytes with increased emodin dosage. Further, emodin improved cell cycling in bone marrow increasing S and G2/M phase cells. Utilizing 16S rRNA FISH, 5FU caused pockets of mucus disruption, gut barrier damage, and alterations in bacterial spatial arrangement, which were mitigated with emodin. Taken together, emodin treatment may contribute to improved hematopoietic integrity and GI health by reducing damaging inflammation, which may improve overall quality of life.

5.2 Introduction

Synthetic chemotherapeutics such as antimetabolites, anthracyclines, and taxanes have improved the overall efficacy of cancer treatment regimens but present significant risk to the patient both during and after treatment[29,88,142]. Chemotherapy treatment has approximately a 12% success rate clinically. However, nearly 10% of patients receiving chemotherapy die during the first 30 days of treatment. Further, it is estimated that 70% of surviving patients will develop non-specific toxicities as a result of chemotherapy treatment[29]. Therefore, it is of great importance to develop safe and effective

complementary treatments to attenuate the toxicity of chemotherapeutics giving the patient a better quality of life during treatment. We, and others, have previously characterized hallmark characteristics of 5FU toxicity[32,35,111,132,142]. Most notably the presence of intestinal mucositis and lymphocytopenia contributes to the reduced survival and quality of life associated with 5FU[23,33,91,142]. These characteristics are closely monitored clinically and can be limiting to the success of interventional therapies[39,143]. Therefore, amelioration of these symptoms might improve 5FU outcome.

There has been a recent upsurge in the clinical utilization of herb-derived compounds due to evidence of multiple health benefits attributed to continual use with these compounds. A compound that could attenuate the multiple non-selective toxicities associated with chemotherapy could have great clinical potential. Emodin is a trihydroxy-anthraquinone found in several Chinese herbs, including *Rheum palmatum* and *Polygonum multiflorum*[144,145]. Emodin has been shown to attenuate the severity of multiple experimental disease models including arthritis, liver damage, atherosclerosis, myocardial ischemia, and cancer by reducing the inflammatory cascades associated with these conditions[73,77,79,80,121,134,144,146,147]. Recent investigations have indicated emodin can reduce activation of pro-inflammatory signaling NF-κB, STAT6, Erk1/2, and P38[72,77,122,148]. However, the direct mechanism of action of emodin has yet to be discovered. Emodin may have a potential target in the P2X7 receptor[75,79,87,145,149]. The P2X7 receptor is found the central and peripheral nervous systems, in microglia, macrophages, and the retina[75,149]. The P2X7 receptor has also been shown to serve as a pattern recognition receptor for extracellular ATP-mediated apoptotic cell death,

regulation of receptor trafficking, mast cell degranulation, and inflammation[145,149] and is therefore of interest as a therapeutic target.

In the present study, we aimed to establish the efficacy of emodin as a complementary therapeutic to attenuate the non-selective toxicity of 5FU chemotherapy. We utilized a previously established protocol of 5FU treatment which was paired with complementary emodin treatment given three-times per week. We performed chronic and acute studies of 5FU toxicity investigating the benefits of complementary emodin. Investigating the chronic effects, we observed a 100% survival rate in mice treated with 5FU + Emodin. This was complemented by reduced pain sensitivity, improved grip strength, and reduced fatigability. We observed increased M2-type macrophages (MRC1) and reduced neutrophils (Ly6g) in the small intestine but not in the colon. However, we did report a decrease in dysplasia inducing Muc5ac in the colon. Acutely, we observed improved body weight in 5FU + Emodin treated mice and a maintained peripheral lymphocyte count. Utilizing 16S rRNA FISH we observed a dose dependent response of maintained structural integrity of the proximal and distal colon in emodin treated mice. We saw increased macrophages in the bone marrow and expression of the proinflammatory markers which was paralleled by drastic cell death and cell cycle arrest with 5FU. Interestingly, we observed increased cells inG2/M phase in the bone marrow and decreased CD11c expression of Emodin treated mice. Overall, we believe that emodin may be protecting the hematopoietic system during 5FU treatment, leading to a more regulated inflammatory response and protection of the gastrointestinal system.

5.3 Methods

5.3.1 Animals

Male and female C57BL/6 mice were purchased from Jackson Laboratories (Bar Harbor, ME) and were cared for in the animal facility at the University of South Carolina. Mice were randomized upon arrival to the animal facility to prevent litter biases in microbiome data and were housed five per cage, maintained on a 12:12-h light-dark cycle in a low-stress environment (22^0C, 50% humidity, low noise). Mice were kept in a room isolated from all other ongoing animal experiments and were only handled by the primary investigators. All mice were habituated to the AIN-76A diet prior to any interventions and were given food and water *ad libitum* through the course of the study. All methods were in accordance with the American Association for Laboratory Animal Science, and the Institutional Animal Care and Usage Committee of the University of South Carolina approved all experiments.

5.3.2 Experimental Design

Mice were acclimated to the animal facility at the University of South Carolina for 6 weeks prior to the start of experiments. In the chronic study (Fig 5.1A), N=50 mice were randomly assigned into 4 groups: Control (n=5), Emodin (n=5), 5FU + Vehicle (n=20), and 5FU + 40 mg/kg Emodin (n=20). In the acute study (Fig 5.4A): N=80/sex mice were randomly assigned into 4 groups; 5FU + Vehicle (n=20/sex), 5FU + 20 mg/kg Emodin (n=20/sex), 5FU + 40 mg/kg Emodin (n=20/sex), and 5FU + 80 mg/kg Emodin (n=20/sex).

5.3.3 Emodin Preparation

Emodin was purchased from Nanjing Zelang Medical Technology Co., Ltd, (Nanjing, China). Emodin was independently analyzed by the Mass Spectrometry Center at the University of South Carolina prior to the initiation of the experimental study. LC-UV-MS and NMR was performed to confirm the purity of Emodin and the molecular structure (Fig S1A). Emodin was delivered via oral gavage to mice using 20ga 30mm flexible plastic tubing oral gavage needles (Instech, #FTP-20). Emodin was prepared fresh, daily, in a 24mg/mL stock solution using pure propylene glycol (VWR) and mixed for 6-8 hours at room temperature protected from light prior to gavage. The 24mg/mL solution was used for 80 mg/kg dosing; 12mg/mL and 6mg/mL dilutions were also prepared for 40 mg/kg and 20 mg/kg doses, respectively. Pure propylene glycol was used as a vehicle control in all experiments.

5.3.4 5FU and Emodin treatment regime

5FU (Sigma Chemical Co., St. Louis, MO) was dissolved in sterile phosphate buffered saline (PBS), pH7.4 and then sterile filtered through a 0.2μm syringe filter. 5FU was administered in 3 (chronic, Fig 5.1A) or 1 (acute, Fig 5.4A) cycles of a 35 mg/kg dosage and was administered via intraperitoneal injection. Each cycle consisted of 5 consecutive days of injections followed by 9 days of recovery. 5FU was prepared fresh at the beginning of each cycle. Sterile filtered PBS alone was used as the vehicle control. To avoid potential drug interactions Emodin and 5FU were administered separately. 5FU was given in the AM time slot of the light cycle and Emodin was given in the PM time slot of the light cycle. The $t_{1/2}$ of 5FU is 15 minutes and we have previously determined that emodin is cleared from the circulation 12 hr after oral gavage.

5.3.5 Peripheral Neuropathic Nociception

All experimental mice were utilized to evaluate the effects of 5FU treatment on peripheral neuropathic nociception. After a brief habituation to the testing apparatus, right hind-paws were tested for neuropathic nociception by a single experimenter blinded to experimental conditions using Von Frey filaments (North Coast Medical, Morgan Hill, CA). Each Von Frey filament was tested for 5 consecutive measurements, data was calculated as the paw withdrawal threshold in grams of force. Threshold was determined by 3 consecutive reactions to the stimulus. Measurements were performed by the same investigators through the entirety of the study (ATS). Total stimuli were also summed to interpret total sensitivity to the touch test.

5.3.6 Grip strength assessment

All experimental mice were utilized to evaluate the effects of 5FU treatment on grip strength. Grip strength was measured prior to 5FU administration and during the recovery period of the second cycle. Briefly, holding the mice by the tail, the front and back feet were allowed to grip the grate. Mice were then pulled from the grate, generating a force that was measured by the force transducer. Five measurements were taken consecutively, with 2 min rest between sets until a total of 15 measurements were taken for each mouse. The averages of the 15 measurements were used in the data analysis. Measurements were performed by the same investigator through the entirety of the study (ATS).

5.3.7 Run-to-fatigue assessment

To determine the effect of 5FU on fatigability, all experimental mice were subjected to a run-to-fatigue test prior to 5FU administration and during the recovery

period of the second cycle (chronic) or in the night cycle after the final 5FU administration (acute). After 3 consecutive days of habituation during the night cycle, mice were subjected to the following run-to fatigue protocol: 20 m/min for 30 min and 25 m/min following a 15-min warm-up. Fatigue was defined as the time at which mice were no longer able or willing to keep up with the treadmill despite hand prodding for at least 1 minute. All treadmill performances were performed during the night cycle by the same investigators through the entirety of the study (ATS and BNV). Data were analyzed as percent performance change from baseline (*week -1*) to post treatment (*week 1 – acute, week 4 – chronic*).

5.3.8 Tissue collection

Mice were euthanized by isoflurane overdose and blood was collected from the inferior vena cava. Tissues were removed, weighted and immediately snap-frozen in liquid nitrogen and stored at -80^{0}C or fixed in 10% formalin until further analysis. The colon was carefully dissected distal to the cecum and proximal to the anus. Mesentery adipose tissue was removed with forceps. The colon was flushed with PBS, opened longitudinally, and flattened with a cotton swab. Colon length was measured using calipers. A 5-mm piece of the distal portion of the colon was cut and fixed in 10% buffered formalin (Fisher Scientific, Pittsburg, PA) for morphological analysis. The remaining colon was hemi-sectioned longitudinally and snap-frozen for further analysis. The distal portion of the ileum was cut and fixed in 10% buffered formalin for immunohistochemical and morphological analysis, the remining distal-middle portion of the small intestine was cut in half and snap-frozen for further analysis.

5.3.9 Anemia markers

A complete blood panel analysis was performed using the VetScan HMT (Abaxis, Union City, CA) for determination of WBCs, LYM, MON, NEU, PLT, RBCs, Hct, and Hb. Neutrophil/Lymphocyte ratio (NLR) was calculated from obtained values.

5.3.10 Histopathology

Hematoxylin and eosin (H&E) staining of the colon and small intestines were performed as previously described[132]. All images were obtained using a Nikon E600. Intestinal mucositis was assessed via measurement of the epithelial architecture of the villi (small intestine) using ImageJ. Goblet cells were identified by Alcian blue staining and counterstained with nuclear fast red as previously described[94]. All histopathological analyses were performed by a board-certified pathologist blinded to the experimental conditions (I.C.). All tissue morphological measurements were performed in triplicate and the coefficient of variance was determined to be less than 5%.

5.3.11 Gene expression

Quantification of colonic expression of EMR-1, MRC1, ITGAX, Ly6G, IL10, NOS2, TNFα, MCP1, OCLN, MUC2, and MUC5ac were performed as previously described[132]. Briefly, RNA was extracted using TRIzol reagent (Life Technologies, GIBCO-BRL, Carlsbad, CA) and chloroform procedures. RNA sample quality and quantities were verified using an Agilent Bioanalyzer and determined to be of good quality based on A260/A280 values (>1. 8) prior to cDNA synthesis using QuantiTect Reverse Transcription kit (Qiagen 205313). Quantitative RT-PCR analysis was carried out as per the manufacturer's instructions (Applied Biosystems) using Taq-Man Gene Expression Assays. Data were normalized to vehicle treated controls and compared to

five reference targets (B2M, TBP, HPRT, HMBS, and H2AFV), which were evaluated for expression stability using GeNorm algorithm.[98,99]

5.3.12 Bone Marrow Flow Cytometry and Cell Cycle Analysis

Bone marrow was taken from both femoral shafts by flushing with saline and passing the resulting extracts through a 70μm filter. Red blood cell lysis was performed with 20 second hypotonic solution (0.2% NaCl) treatment followed by hypertonic (1.6% NaCl) cessation. Bone marrow isolates were blocked with FC block and stained with CD11b – APC, F4/80 – FITC, and CD45 – PE/Cy7 (Biolegend, San Diego, CA) antibodies for 1hr at 4^0C. Lymphocytes were identified by gating for CD45+ cells. Macrophages were determined to be CD11b+F4/80+ cells. Aliquots of bone marrow isolates were also fixed in 70% ethanol for 24h at -20^0C before staining with Ki67 – APC and propidium iodide – PE-Texas Red (Biolegend San Diego, CA) according to standard protocols. Data were acquired using a BD FACS Aria II cell sorter and analyzed by FlowJo v10.6.2.

5.3.13 Western Blotting

Briefly, bone marrow extracts were homogenized in Mueller Buffer containing protease inhibitor cocktail (Sigma Aldrich, St. Louis, MO). Total protein concentrations were determined by the Bradford method. Equal amounts of crude protein homogenates (10ug) were separated on hand-casted SDS-polyacrylamide gels and electrophoretically transferred to a PVDF membrane using a Royal Genie Blotter (IDEA Scientific, Minneapolis, MN). Membranes were blocked for 1hr at room temperature with 5% non-fat milk in tris-buffered saline with 0.1% tween (TBST). Western blots were performed using primary antibodies $P2X_7$ (Alomone Labs #APR-004), TNFα (Proteintech #60291-

1-Ig), and CD11c (Cell Signaling #97585). An anti-rabbit (Cell signaling: #7047) IgG horseradish peroxidase conjugated secondary antibody was diluted 1:2000 in 5% milk-TBST and incubated for one hour at room temperature. An enhanced chemiluminescent substrate for detection of horseradish peroxidase (Thermo Scientific, Watham, MA) was used to visualize the antibody-antigen interaction. Autoradiography films were scanned, and blots were quantified using scientific imaging software ImageJ (NIH Bethesda, MD). After completion of the western blot, all membranes were stained with Amido black (VWR #AAJ66798-14) and the densitometry of each lane was calculated using ImageJ allowing for total protein normalization as previously described[150].

5.3.14 16S rRNA FISH

A subset of mice (n=3) were used to observe the bacterial spatial organization present in the colon. Briefly, colons were excised whole from the rectum to the anus, opened longitudinally without disturbing opened tissue, and fixed for 24hrs in Carnoy's solution (6:6:1 – Ethanol:Acetic Acid:Chloroform) then processed and embedded into paraffin blocks by standard techniques. 5μm section were placed on SuperFrost slides for FISH studies. The oligonucleotide probe (EUB338: 5'-GCTGCCTCCCGTAGGAGT-3') was purchased from EuroFins synthesized with carbocyanite dye (Cy3) added to the 5'-end. *In-Situ Hybridizations* were performed according to previously published protocols[117,151,152]. Fluorescent images were taken using a Leica DM2500 fluorescent microscope.

5.3.15 Statistical analyses

All data were analyzed using commercial software (SigmaStat V3.5, SPSS, Chicago, IL). All outcomes were analyzed using a two-way ANOVA (disease x

treatment) for the chronic treatment investigation and a one-way ANOVA for the acute investigation. A Student-Newman-Keuls test was used for all post-hoc analyses. A student's t-test was used to analyze Ly6G expression during the chronic study due to only two groups (of four total) have detectable levels of expression. Survival curve analysis was conducted by Log-rank (Mantel-Cox) test. Any data that were not normally distributed or did not display equal variance were logarithmically transformed so that those criteria were met. Statistical significance was set with an alpha value of $p<0.05$. Data are presented as mean ± SEM.

5.4 Results

5.4.1 Complementary emodin delays weight loss and improves survival and quality of life during chronic 5FU.

A 3-cycle 5FU regimen caused significant body weight loss through the entire duration of the treatment period (Fig 5.1A,B; $p<0.05$). A main effect of 5FU and emodin therapy exists at various points through the course of treatment (Day 2, 4, 6, 8, 10, 28, 30, 32, and 34); within control mice there was no effect of emodin therapy throughout the treatment period. However, there was a significant interaction detected within 5FU, in which emodin treated mice had significantly greater body weight at days 7, 8, 10, 11, 12, 13, and 14 (Fig 5.1B; $p<0.05$). n=3/20 mice in the 5FU+Vehicle group did not survive the first cycle of 5FU chemotherapy, a Mantel-Cox test indicated that there was no significant risk for this group; regardless, no other experimental groups had decreased survival (Fig 5.1C). At necropsy, there were no significant differences detected for liver and spleen weight (Table 1). A main effect of 5FU was detected for decreasing epididymal and mesenteric fat pads; but no significant interaction of emodin treatment

was found. Interestingly, a main effect of emodin treatment was detected in increasing colon length; however, there was no interaction detected with 5FU (Table 5.1).

5.4.2 Complementary emodin improves functional measures of fatigue associated with chronic 5FU.

We have previously established a battery of functional tests that can detect differences in performance associated with 5FU toxicity[132]. We find a main effect of 5FU on increasing touch sensitivity ($p<0.05$), a trending effect of emodin treatment ($p=0.051$), and a trending interaction ($p=0.051$) between 5FU and emodin treatment (Fig 5.1D). Despite these results, two-way ANOVA indicated a difference between treatment groups within 5FU in which emodin treated mice showed reduced pain sensitivity ($p<0.05$). This result is likely from the ceiling effect inherent of this assay which does not allow for main effects to be elucidated from the data collection. To further our analysis of peripheral neuropathy, we summed the total responses of each mouse throughout the peripheral neuropathy assay (see methods). Two-way ANOVA of these summed responses indicated a main effect of both 5FU and emodin treatment (Fig 1E; $p<0.05$). Again, we report a trending interaction ($p=0.058$) between emodin and vehicle treated groups within 5FU mice. Despite this, emodin treated 5FU mice showed significantly reduced total responses during the peripheral neuropathy assay compared to 5FU alone (Fig 5.1E; $p<0.05$).

A grip strength test was used to measure absolute (N) and relative (N/kg) front limb strength. We found no main effects of 5FU or emodin treatment in absolute grip strength (Fig 5.1F); however, vehicle treated 5FU mice showed significantly lower absolute force production compared to control mice (Fig 5.1F; $p<0.05$). Further, there

was a significant interaction (Fig 5.1F; $p<0.05$) within 5FU in which emodin treated mice showed increased absolute grip strength compared to 5FU alone, however, were still lower than control mice. Relative grip strength showed no significant main effects of either 5FU or emodin treatment; further, there was no significant interaction detected (Fig 5.1G).

To investigate the fatiguability induced by 5FU treatment we analyzed run-to-fatigue data as a percent performance change from baseline (see methods). We report a main effect of both 5FU and emodin treatment on percent performance change (Fig 5.1H; $p<0.05$). 5FU mice treated with vehicle had significantly lower performance compared to control mice. Interestingly, 5FU mice treated with emodin showed significantly less performance deficits compared to 5FU alone, however, were still lower than control mice (Fig 5.1H; $p<0.05$).

5.4.3 Complementary emodin does not rescue 5FU-induced anemia and lymphocytopenia.

We have previously reported that 5FU treatment causes significant cytopenia.[132] As expected, we observe a main effect of 5FU on decreasing WBC, LYM, NEU, RBC, HGB, and HCT; however, we do not detect an interaction of 5FU with emodin treatment (Table 5.2; $p<0.05$). Further, we find a main effect of 5FU for increasing PLT counts; however, we also do not find a significant interaction of 5FU with emodin treatment (Table 5.2; $p<0.05$). Interestingly we do not report any significant effects of 5FU or emodin treatment on MON counts and the NLR (Table 5.2).

5.4.4 Complementary emodin reduces inflammation and protects small intestine tissue during chronic 5FU treatment.

One of the most significant effects of 5FU is non-selective toxicity targeted towards the small intestine tissue. Measuring the villus length of small intestine tissue, we find a significant main effect of 5FU treatment in decreasing villus length (Fig 5.2A,B; $p<0.05$); further, we find a significant interaction with emodin treatment within the 5FU group which had greater villus length compared to 5FU treatment alone, but lower length compared to control mice (Fig 5.2A,B; $p<0.05$). We performed gene expression analysis to observe any differences select pro-inflammatory cytokines in addition to macrophage (F4/80) and neutrophil (Ly6g) populations. Interestingly, mice treated with 5FU had decreased NOS2 expression in the small intestine but increased TNFα and MCP-1 (Fig 5.2C; $p<0.05$). Emodin treatment only seemed to interact significantly with TNFα leading to reduced levels compared to mice treated with 5FU alone (Fig 5.2C; $p<0.05$). We further report no difference in total macrophages (EMR1) or M1-like macrophages (Itgax) but increased M2-like macrophages (Mrc1) in mice treated with 5FU+Emodin compared to 5FU alone (Fig 5.2D; $p<0.05$). Neutrophils are minimally expressed in the small intestine and are not usually detected with conventional qPCR. Within 5FU treated mice, however, we detect Ly6g expression in the small intestine which was trending ($p=0.12$) decrease in emodin treated mice when normalized back to 5FU+Vehicle treated mice and analyzed via a student's t-test (Fig 5.2E).

5.4.5 Emodin improves colon health during chronic 5FU treatment.

We performed a similar analysis in the colon as reported above. Interestingly, we find a significant increase in NOS2, TNFα, and MCP1 in mice treated with 5FU alone compared to vehicle treated controls (Fig 5.3A; $p<0.05$). Further, however, we find a

significant interaction with emodin only in NOS2 expression ($p<0.05$) but not in TNFα or MCP1 (Fig 5.3A) We assessed macrophage markers EMR1, Itgax, and Mrc1 but found no changes across all groups (Fig 3B). We found a main effect of neutrophil marker Ly6g in 5FU treated mice but no interaction between 5FU and emodin (Fig 5.3C). To assess gut health, we measured OCLN expression and report a main effect of 5FU to decrease OCLN expression but there was no significant interaction with emodin (Fig 5.3D). Interestingly, we show an increase in Muc5ac expression in 5FU treated mice with a trending decrease ($p=0.05$) in 5FU+Emodin mice. Despite this, we report no difference in Muc2 expression across all groups. We stained distal colon biopsies with hematoxylin and eosin and Alcian blue but found no significant histopathological differences between all groups (Fig 5.3E).

5.4.6 Complementary emodin delays weight loss during an acute bout of 5FU in male and female mice and reduces fatigability.

To study the acute benefits of emodin on reducing 5FU toxicity, we investigated male and female mice treated with 5 consecutive days of 5FU and complementary emodin given at 20 mg/kg, 40 mg/kg, or 80 mg/kg (Fig 5.4A). All three dosing groups of emodin lost significantly less weight compared to mice treated with 5FU alone (Fig 5.4B,C; $p<0.05$). Specifically, male mice treated with 20 mg/kg, 40 mg/kg, and 80 mg/kg had significantly lower weight loss compared to vehicle treated controls on days 3, 4, 5, 6, and 7 (Fig 5.4B; $p<0.05$). Female mice treated with 20 mg/kg had significantly lower weight loss compared to vehicle treated controls on days 5, 6, and 7, female mice treated with 40 mg/kg had significantly lower weight loss compared to vehicle treated controls on day 7 only, and female mice treated with 80 mg/kg had significantly lower weight loss compared to vehicle treated controls on days 5 and 7 only (Fig 5.4C; $p<0.05$).

A subset of mice (n=10) were utilized to assess the same functional tests used in the chronic phase of the study. Male and female mice functional test performances were pooled for analysis. We saw no noticeable differences between or within all groups in peripheral nociception (Fig 5.4D,E) or grip strength (Fig 5.4F,G) tests. Interestingly, we found a dose dependent response to improvement in run-to-fatigue performance change (Fig 5.4G; $p<0.05$), with the benefits beginning to show in the 40mg/kg dose and improving in the 80 mg/kg dose.

Weighing the major organs, we found no significant differences between groups (Table 5.3). Interestingly, male mice treated with 5FU + 20 mg/kg emodin had a significantly greater (Table 5.3; $p<0.05$) spleen weights compared to all other groups. However, this weight was not indicative of significant pathology and is expected to be a type I error.

5.4.7 Increasing dosage of emodin rescues peripheral blood lymphocytopenia associated with acute 5FU treatment in males only.

In both male and female mice, 5FU decreases total WBC count, of which is mostly attributed to loss in circulating LYM. In male mice only, we found a dose dependent increase in total WBC with increasing emodin dosage which was attributed primarily to increased total LYM counts (Table 5.4; $p<0.05$). There was no difference in MON, NEU, RBC, HGB, HCT, or PLT measures between sex or treatment dosage. Interestingly, we found a significant decrease in NLR in male mice treated with 80 mg/kg emodin. This was also seen in female mice treated with both 40 mg/kg and 80 mg/kg emodin (Table 5.4; $p<0.05$).

5.4.8 Emodin reduces inflammation to small intestines and benefits gut architecture.

To investigate the acute benefits of emodin on small intestine health, we performed villus measurements on male mice as described in our chronic experiment. Interestingly, each treatment group had significantly different measurements compared to all other groups with mice treated with 80mg/kg emodin recording the greatest relative villus length compared to mice treated with 5FU alone (Fig 5.5 A,B; $p<0.05$). Gene expression analysis indicates no significant differences in pro-inflammatory cytokines NOS2, TNFα, or MCP1 (Fig 5.5C). However, we do show a significant decrease in IL10 expression in mice treated with 40 mg/kg and 80 mg/kg emodin compared to mice treated with 5FU alone (Fig 5.5C; $p<0.05$). This trend was paralleled by a significant decrease in M2-like macrophages (MRC1) ($p<0.05$) but no decrease in total macrophages (EMR1) and M1-like macrophages (Itgax) (Fig 5.5D). Interestingly, we also show a decrease in neutrophil marker Ly6G expression in mice treated with 40 mg/kg and 80 mg/kg emodin compared to mice treated with 5FU alone (Fig 5.5E; $p<0.05$).

5.4.9 Emodin does not alter immune status of the colon acutely but, may benefit bacterial spatial arrangement and gut integrity.

We performed an immune cell panel analysis on the colon tissue of male mice treated acutely with 5FU + emodin. Analyzing NOS2, TNFα, MCP1, and IL10 expression we only report a significant increase in NOS2 in mice treated with 40 mg/kg (Fig 5.6A;$p<0.05$), however we believe this to be a type-I error and not attributed to pathology associated with emodin treatment at 40 mg/kg. We analyzed macrophage markers EMR1, MRC1, and ITGAX in addition to neutrophil marker Ly6g, however, we found no significant differences between groups (Fig 5.6B,C). Interestingly, upon

performing markers for gut integrity, as in out chronic investigation, we did not notice any difference in OCLN, Muc5ac, and Muc2 between groups (Fig 5.6D).

To further our analysis of the colon, we used a subset of male mice to assess gut bacterial spatial arrangement using 16S rRNA FISH. Because of the landscape differences between the distal and proximal portions of the colon we separated our analysis to include each region. Within the proximal colon, we notice a thin mucous layer separating the bacteria (yellow) and epithelial cells (blue). When assessing 5FU treated mice, we noticed significant disposition of the mucosal layer and bacterial organization (arrow). We also observed invasion of bacteria within the crypts (arrow). We saw reduction of this phenotype when emodin is introduced into the treatment regime. In the 20mg/kg emodin treated mice we observed a reduced incidence of crypt invading bacteria and a complete elimination of this phenotype in the 40 mg/kg and 80 mg/kg doses (Fig 6A). Interestingly, we see that mice treated with 5FU + Vehicle also have significant bacterial invasion in the distal portion of the colon. As seen in the proximal portion of the colon, the 20 mg/kg emodin treated mice have a slight reduction of this characteristic and a complete elimination of this exists in the 40 mg/kg and 80 mg/kg emodin treated mice (Fig 5.6B).

5.4.10 Emodin reduces bone marrow inflammation and may work to maintain actively cycling cells.

In a separate cohort of male mice, we performed an acute analysis of 5FU + 40 mg/kg emodin treatment to analyze bone marrow health. We isolated bone marrow and assessed the macrophage content using flow cytometry. Interestingly, we found a significant increase in percentage of CD11b+ F4/80+ cells in 5FU treated mice ($p<0.05$),

however this was not decreased with emodin treatment (Fig 5.7A,B). The severity of cytopenia caused discrepancies on whether more inflammation was present in 5FU mice. Therefore, we isolated protein content of bone marrow and assessed protein expression of the CD11c, $P2X_7$ receptor, and TNFα. Paralleling the trends seen in macrophage content, we see that 5FU treated mice had a significantly increased CD11c ($p<0.05$), $P2X_7$ receptor ($p<0.05$), and TNFα ($p<0.05$) expression but only CD11c was significantly lower ($p<0.05$) in emodin treated mice compared to 5FU alone (Fig 5.7C-E). Interestingly, when normalizing to total protein content using amido black staining, we observed a significant banding difference between control and 5FU treated mice. Although total protein content was the same according to Bradford assay, this finding indicates that there are substantial perturbations to the cellular environment of the bone marrow in 5FU treated mice.

We performed a cell cycle analysis of the bone marrow content and observed that 5FU treated mice have fewer total cells compared to controls (Fig 5.8A). Further, we found that emodin treated mice have a lower percentage of cells in G1/G0 phase compared to control and 5FU+Vehicle treated mice. Interestingly, there was a greater percentage of cells in S phase in emodin treated mice compared to 5FU alone (Fig 5.8A,B; $p<0.05$). Following this pattern, emodin treated mice had a trending increase in G2/M phase cells (Fig 5.8A,B; $p=0.07$). Although total cell content is lower in 5FU treated mice compared to controls, this finding indicates more cells are proliferating in mice receiving complementary emodin compared to 5FU alone.

5.5 Discussion

5FU chemotherapy is widely used in the treatment of CRC. However, common side effects including fatigue, peripheral neuropathy, and diarrhea can lead to a reduced quality of life[24,31,153]. Emerging evidence has shown that natural anthraquinone emodin can be used as a safe and effective anti-inflammatory compound to reduce such physiological perturbations[77,78,121]. Therefore, in the current study, we aimed to investigate the ability for emodin to reduce the common side effects and inflammation associated with 5FU treatment. Despite significant weight loss, complementary emodin treatment improved survival in cancer-free mice and reduced severity of sensitive peripheral nociception, muscular weakness, and fatigability. Select intestinal markers of inflammatory cells indicate cite specific benefits of emodin and a reduction of pathological perturbations to the small intestine and colon barrier. Further, bone marrow analysis indicated a mitigation of the toxic effects of 5FU to the bone marrow and an attenuation of associated lymphocytopenia.

We report here an important first step in establishing emodin as a safe and effective complementary therapeutic in clinical oncology. In the chronic study, we observe 100% survival in mice treated with emodin compared to 84% survival in mice treated with 5FU alone during a 3-cycle regimen. Previous investigations by our lab have shown that 5FU can cause significant toxicities in the presence of cancer[132]. However, this previous investigation utilized a different dosing regimen (40, 20, 20 mg/kg) compared to the present study. In the present study, we utilized a consistent 35 mg/kg dosing regimen which caused significant physiological perturbations in a cancer-free model. Our data indicate that emodin can effectively reduce the functional deficits

associated with chronic 5FU treatment. We report here that chronic 5FU given at 35 mg/kg can increase peripheral nociception sensitivity, reduce muscular strength, and cause significant fatiguability; each of which can be rescued with complementary emodin treatment. The mechanisms of these 5FU-associated perturbations have not yet been fully elucidated. However, several hypotheses have been proposed including serotonin dysregulations, HPA dysfunction, circadian disruptions, depression, anemia/cytopenia, and central/local inflammation.[27,88,154] Arguably, the strongest of these are inflammation and anemia. In our acute phase investigation, in male mice only, we observe significant increases in WBC and LYM counts with complementary emodin compared to 5FU alone. In our chronic phase investigation, however, we do not see significant recovery of systemic anemia and cytopenia with complementary emodin. However, we do report increased hemoglobin and reduced platelet count in mice treated with emodin compared to 5FU alone. This indicating that preventing the drastic lymphocytopenic effects early in 5FU treatment might be sufficient to prolong survival and improve quality of life. Incidentally, where these mitigated effects may contribute to performance and quality of life improvements, it does not explain the full benefits of emodin.

One of the most documented 5FU-induced toxicities involves inflammatory damage to the gastrointestinal barrier or 'mucositis.' We report here that the characteristic shortening of the villi in the small intestine typically seen with 5FU can be ameliorated with complementary emodin treatment both acutely and chronically. Where the mechanisms of mucositis remain elusive, our findings here indicate that 5FU causes an increase in neutrophil marker Ly6g which is attenuated with complementary emodin. Further, we report that there is no increase in total macrophages, according to EMR1

(F4/80) expression with 5FU but an increase in M2-type macrophage marker MRC1 (CD206) in mice receiving complementary emodin. M2-type macrophages are more anti-inflammatory type macrophages and are characterized as resident 'repair' cells[53]. Interestingly, we see that M2-type macrophages are reduced acutely with complementary emodin. It is likely that this response is indicative of gut resilience during 5FU. Acutely, emodin may be working to reduce tissue damaging neutrophil infiltration to the gut and, in result, reduces the severity of mucositis leading to less activation of M2-type macrophages. Chronically, however, emodin may be benefiting the homeostatic balance that exists in the gut leading to an improved immune response through activation of M2-type macrophages. This, in turn, would lead to maintained turnover of tissue and repair of 5FU-induced damage to the intestinal villi. Interestingly, when we assay the colon for the same markers, we do not find increased MRC1 expression or reduced Ly6g expression with complementary emodin treatment. This indicates that despite an overall benefit to gastrointestinal physiology, it appears that emodin might be playing a site-specific role in the small intestine leading to the observed overall benefits to quality of life.

The degree of mucositis varies through the GI system, we have previously shown that low dose 5FU can disrupt immune homeostasis and cause severe small intestine and colon inflammation[132]. In the present study, we show that there is no increase in colon macrophages with both acute and chronic 5FU treatment, but there is a pathological response causing increased Muc5ac expression. Muc5ac is transiently expressed in the colon and is increased in situations of dysplasia and colon dysfunction[155]. Here we show that chronic 5FU increases Muc5ac expression 7-fold and that emodin can reduce this expression of Muc5ac despite not rescuing the increased Ly6g or reduced OCLN

expression. Interestingly, we did not see any increased inflammation or alterations in Muc5ac or OCLN in our acute phase analysis but a decrease in NOS2 expression when mice are treated chronically with 5FU and emodin. To our knowledge, there is no body of literature linking NOS2 expression with Muc5ac perturbations. However, we believe that 5FU-induced overexpression of Muc5ac may be increasing tissue/location dependent increases in NOS2 which would cause gut barrier dysfunction and reduced gut integrity during 5FU treatment. This further suggests that initial exposure to 5FU might not elucidate these toxic mechanisms and that repeated 5FU exposure might be contributing to the chronic toxicities associated with chemotherapy. Where these findings require further investigation, we believe we have uncovered a significant mechanism of intestinal mucositis in the colon which can be attenuated with complementary emodin at a dose of 40 mg/kg.

The role of the microbiome has been implicated in many pathologies[40,94,116-118,150]. We have previously shown that 5FU can cause significant perturbations to the gut microbiota which might be exacerbating associated non-specific toxicities[132]. In the present study, we aimed to investigate the spatial arrangement and homeostatic environment of the colon. Swidsinski et. al. 2016[152], describes the colon as a bacterial bioreactor that has evolutionarily been developed to house the commensal relationship between bacteria and humans. In taking with these ideals, we examined the spatial arrangement of bacteria within the colon using 16S rRNA FISH. We observe that 5FU, when given acutely, can cause significant perturbations to the bacterial environment. We observe pockets of significant invasion of bacteria to the mucous layer and the epithelia in the distal colon and disruption of gut morphology in 5FU treated mice. Interestingly,

we observe a dose dependent reduction of this phenotype with emodin and a re-established mucous barrier. Where emodin may not be altering the immune environment of the colon, we show here that significant alteration in bacterial spatial arrangement may have implications on the gut-immune system axis and may be contributing to the overall benefit to quality of life seen with our functional testing.

We further aimed to investigate the hematopoietic benefits of emodin when given acutely. As a thymidylate synthase inhibitor, 5FU will target any actively proliferating tissue. It has been well established that 5FU causes significant lymphocytopenia and anemia when given acutely and chronically[27,30,36]. We investigated the inflammatory status of the bone marrow via flow cytometry and found that despite systemic cytopenia, there was an increase in total macrophages counts in the bone marrow. This indicating that local inflammation might be present in the bone marrow leading to exacerbated effects of 5FU toxicity. Interestingly, we show that a 40 mg/kg dose of emodin does not ameliorate the total macrophage count in the bone marrow but may reduce CD11c expressing M1-type macrophages. This reduction in M1-type macrophages may signify the mechanism of emodin in ameliorating the toxicities associated with 5FU. Previous investigations have shown macrophages specific 'depolarizing' effects of emodin *in-vitro*[80], a mechanism that may be occurring in the bone marrow with 5FU treatment *in-vivo*. To further investigate the mechanism of emodin, we assayed the expression of the P2X7 receptor in the bone marrow. Interestingly, we did not find similar trends to CD11c expression. However, it is important to note that despite no difference in protein expression, emodin might be reducing activity of this Ca^{2+} ATPase receptor. Further experimentation would be needed to confirm this mechanism, however. Complementary

to these findings, we also show that 40 mg/kg emodin is sufficient to cause increased percentage of S phase and G2/M phase cells according to Ki67/PI staining. This provides further evidence that emodin may be acting directly on the hematopoietic system to ameliorate 5FU-induced cytopenia. Further investigations on specific types of myeloid precursor cells would be needed to find specific mechanisms associated with the benefits of complementary emodin.

In summary, we show here that natural anthraquinone emodin is a safe and effective complementary therapeutic which can be used to ameliorate the toxic side-effects of 5FU both acutely and chronically. We report improved quality of life measures through reduced pain sensitivity, improved grip strength, and reduced fatigability. We show improved gut resilience to 5FU-induced mucositis through reduced Ly6g expression and a M2-type macrophage dependent maintenance of gut homeostasis. This was complemented by a reduction of perturbations to gut bacterial spatial arrangement and bacterial invasion to crypts within the proximal and distal colon. Finally, we report a potential mechanism of emodin which might reduce bone marrow inflammation and reduce systemic lymphocytopenia. Despite the benefits described here, further studies are necessary to determine the exact mechanisms of emodin before moving to clinically based investigations.

5.6 Figures & Legends

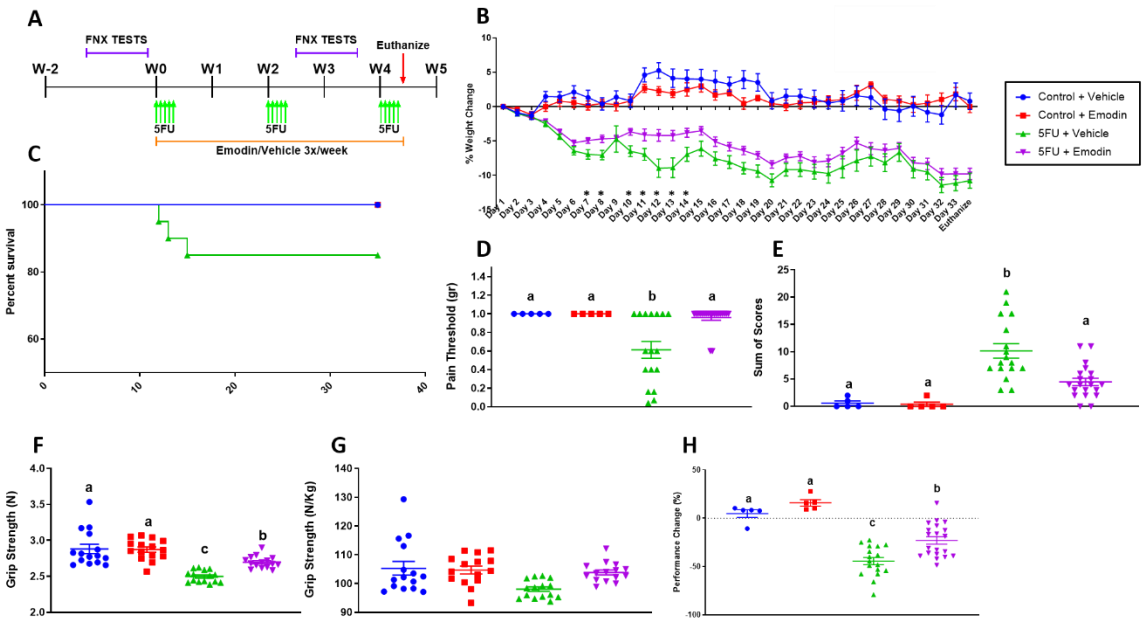

Figure 5.1. Complementary emodin improves survival and quality of life during a 3-cycle regimen of 5FU. A. Study design. **B.** Relative change in body weight measured as percent (%) from baseline. * indicates statistical significance at indicated time point from two-way ANOVA between 5FU + Emodin and 5FU alone. **C.** Percent survival. **D.** Pain threshold measured in grams (gr). 1 gr was maximal pressure tested using VonFrey Filaments. **E.** Pain threshold measured as a sum of scores during VonFrey filament test. **F.** Absolute grip strength measured in Newtons (N). **G.** Relative grip strength measured as Newtons per kilogram (N/Kg) **H.** Percent (%) performance change in run-to-fatigue test from pre-5FU treatment to post-5FU treatment. Groups not containing the same letters (a-c) indicates statistical significance between groups ($p < 0.05$) from two-way ANOVA, n = 5–20/group.

Table 5.1. The effect of chronic 5FU and emodin on major organs. Liver, spleen, epididymal fat, mesenteric fat, and colon length weights at euthanization. Groups not containing the same letters (a, b, ab) indicate statistical significance between groups ($p < 0.05$) from two-way ANOVA, n = 5–20/group.

Group	Liver (mg)	Spleen (mg)	Mesenteric Fat (mg)	Epididymal Fat (mg)	Colon Length (mm)
Control + Vehicle	1143 ± 87.47	91.80 ± 13.86	165.0 ± 11.70 [a]	672.0 ± 99.77 [a]	72.75 ± 4.15
Control + Emodin	1166 ± 39.86	74.80 ± 7.42	146.2 ± 33.61 [a]	619.6 ± 86.16 [a]	79.20 ± 3.33
5FU + Vehicle	1216 ± 29.04	81.41 ± 5.94	123.1 ± 10.88 [b]	398.6 ± 17.77 [b]	78.12 ± 1.34
5FU + Emodin	1207 ± 23.77	80.05 ± 2.826	120.1 ± 9.75 [b]	465.6 ± 25.16 [b]	81.21 ± 1.41

Table 5.2. The effect of chronic 5FU and emodin on blood profile in mice. White blood cells (WBC), Lymphocytes (LYM), Monocytes (MON), Neutrophils (NEU), Neutrophil:Lymphocyte Ratio (NLR), Red Blood Cells (RBC), Hemoglobin (HGB), Hematocrit (HCT), and Platelets (PLT). Groups not containing the same letters (a-c) indicate statistical significance between groups ($p<0.05$) from two-way ANOVA, n=5-20/group.

Group	WBC (10^9/l)	LYM (10^9/l)	MON (10^9/l)	NEU (10^9/l)	NLR (A.U.)	RBC (10^12/l)	HGB (g/dl)	HCT (%)	PLT (10^9/l)
Control + Vehicle	4.37 ± 0.21[a]	3.31 ± 0.21 [a]	0.186 ± 0.10	0.88 ± 0.10 [ab]	0.27 ± 0.05	10.22 ± 0.14 [a]	15.07 ± 0.40 [a]	40.37 ± 0.57 [a]	734.0 ± 21.59 [a]
Control + Emodin	5.24 ± 0.38 [a]	3.95 ± 0.32 [a]	0.13 ± 0.02	1.14 ± 0.05 [a]	0.29 ± 0.01	9.9 ± 0.25 [a]	14.70 ± 0.32 [a]	38.98 ± 1.21 [a]	728.3 ± 38.36 [a]
5FU + Vehicle	2.55 ± 0.16 [b]	1.80 ± 0.15 [b]	0.11 ± 0.02	0.64 ± 0.04 [ab]	0.88 ± 0.55	6.23 ± 0.19 [b]	9.28 ± 0.26 [b]	25.25 ± 0.74 [b]	2350.0 ± 159.6 [b]
5FU + Emodin	2.93 ± 0.17 [b]	2.16 ± 0.17 [b]	0.13 ± 0.02	0.63 ± 0.05 [b]	0.35 ± 0.05	6.37 ± 0.14 [b]	9.99 ± 0.09 [c]	26.16 ± 0.61 [b]	1856.0 ± 109.2 [c]

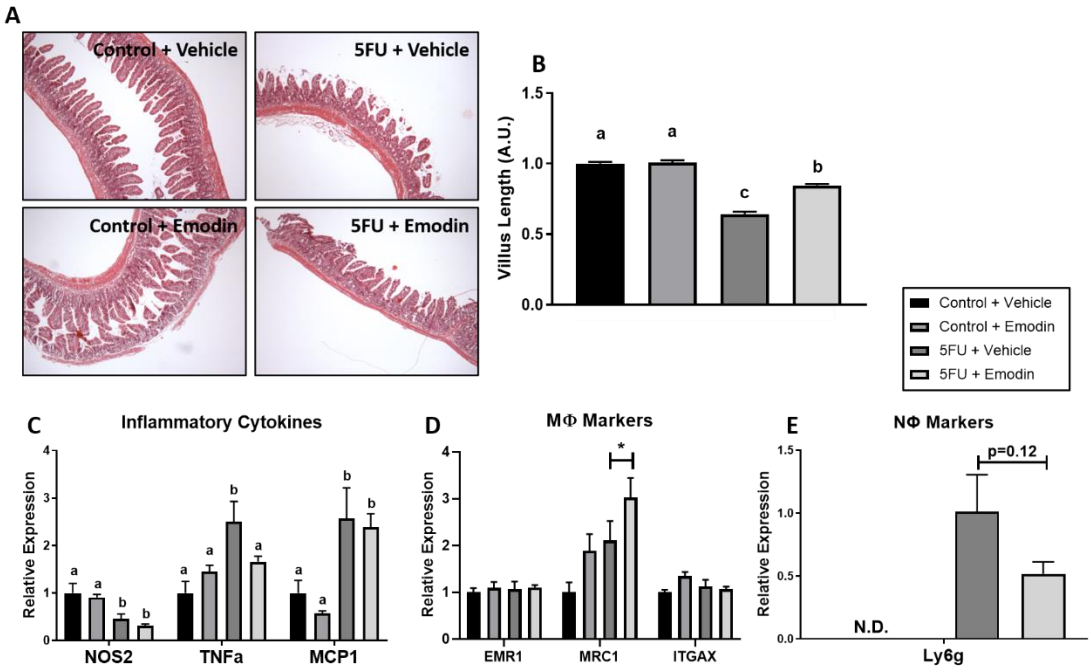

Figure 5.2. Emodin improves small intestine morphology and promotes M2-macrphage polarization during 5FU treatment. A. Representative H&E images of small intestine biopsies at 4X. **B.** Measurement of villus length in small intestine, measurements are normalized to vehicle treated controls and represented as arbitrary units (A.U.). **C.** qPCR analysis of NOS2, TNFα, and MCP1 inflammatory cytokines. **D.** qPCR analysis of macrophage markers EMR1, MRC1, and ITGAX. **E.** qPCR analysis of neutrophil marker Ly6G. Data were normalized to vehicle treated controls and compared to five reference targets (B2M, TBP, HPRT, HMBS, and H2AFV), which were evaluated for expression stability using GeNorm. Groups not containing the same letters (a-c) indicates statistical significance between groups ($p<0.05$) from two-way ANOVA, n=5-20/group.

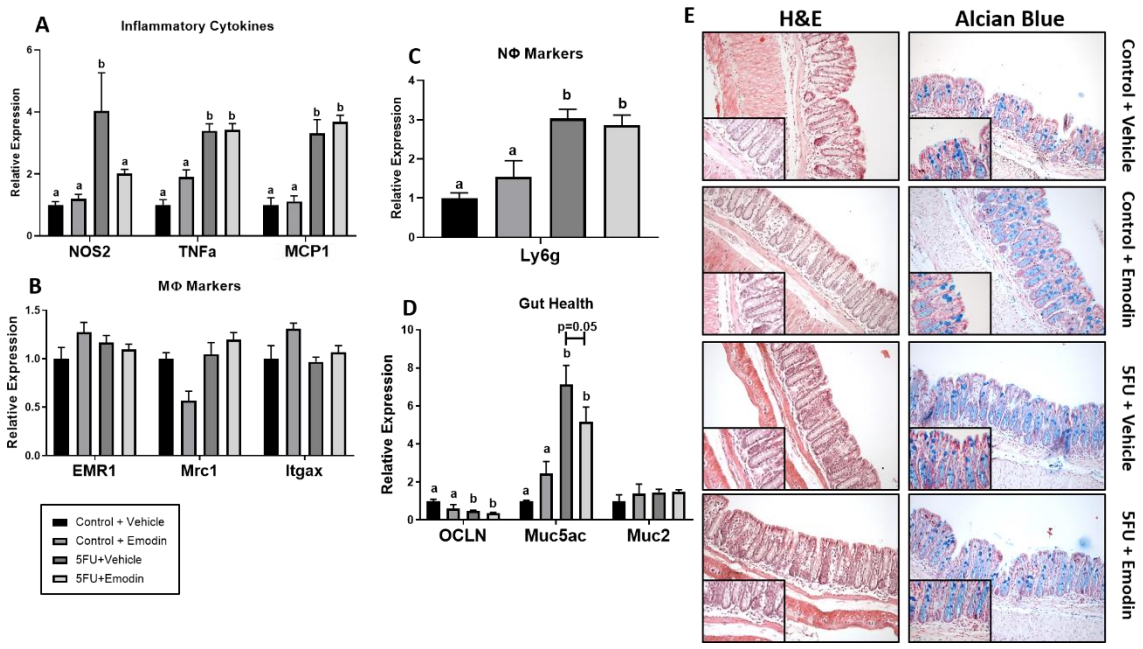

Figure 5.3. Emodin does not reduce colon inflammation but may improve gut resilience during 5FU treatment. A. qPCR analysis of NOS2, TNFα, and MCP1 inflammatory cytokines. **B.** qPCR analysis of macrophage markers EMR1, MRC1, and ITGAX. **C.** qPCR analysis of neutrophil marker Ly6G. **D.** qPCR analysis of gut health markers OCLN, Muc5ac, and Muc2. **E.** Representative H&E and Alcian Blue images of colon biopsies at 4X, insets are 20X. Data were normalized to vehicle treated controls and compared to five reference targets (B2M, TBP, HPRT, HMBS, and H2AFV), which were evaluated for expression stability using GeNorm. Groups not containing the same letters (a-c) indicates statistical significance between groups ($p<0.05$) from two-way ANOVA, n=5-20/group.

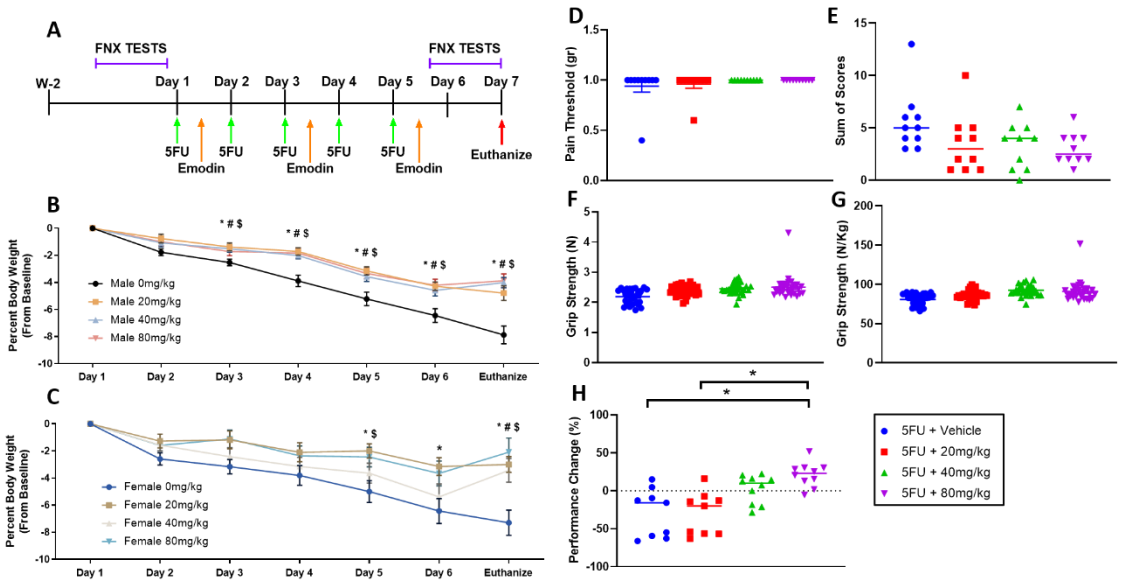

Figure 5.4. Emodin benefits quality of life during a single cycle 5FU treatment. A. Study design. **B.** Relative change in body weight measured as percent (%) from baseline in male mice. **C.** Relative change in body weight measured as percent (%) from baseline in male mice. *,#, and $ indicate statistical significance ($p<0.05$) between 20 mg/kg, 40 mg/kg, and 80 mg/kg groups, respectively, compared to vehicle treated controls from one-way ANOVA at each time point, n=25/group. **D.** Pain threshold measured in grams (gr). 1 gr was maximal pressure tested using VonFrey Filaments. **E.** Pain threshold measured as a sum of scores during VonFrey filament test. **F.** Absolute grip strength measured in Newtons (N). **G.** Relative grip strength measured as Newtons per kilogram (N/Kg) **H.** Percent (%) performance change in run-to-fatigue test from pre-5FU treatment to post-5FU treatment. * indicates statistical significance between groups ($p < 0.05$) from one-way ANOVA, $n = 10$/group.

Table 5.3. The effect of acute 5FU and emodin on major organs. Liver, spleen, epididymal fat, mesenteric fat, and colon length weights at euthanization. Groups not containing the same letters (a, b, ab) indicate statistical significance between groups ($p < 0.05$) from one-way ANOVA, n = 5–20/group.

Group	Liver (mg)	Spleen (mg)	Mesenteric Fat (mg)	Epididymal Fat (mg)	Colon Length (cm)
Male 5FU+Vehicle	1148 ± 29.30	59.5 ± 1.34 [a]	229 ± 17.20	396 ± 27.80	7.50 ± 0.10
Male 5FU+20mg/kg	1140 ± 47.20	66.2 ± 1.64 [b]	201 ± 12.20	368 ± 21.10	7.75 ± 0.10
Male 5FU+40mg/kg	1253 ± 32.00	62.6 ± 1.36 [a]	235 ± 19.40	403 ± 27.00	7.94 ± 0.09
Male 5FU+80mg/kg	1177 ± 46.40	62.3 ± 1.75 [a]	202 ± 11.80	355 ± 20.90	7.79 ± 0.11
Female 5FU+Vehicle	1105 ± 39.50	60.6 ± 1.49	202 ± 21.60	221 ± 26.20	7.63 ± 0.12
Female 5FU+20mg/kg	1101 ± 39.90	60.9 ± 1.24	180 ± 17.60	266 ± 28.8	7.59 ± 0.13
Female 5FU+40mg/kg	1147 ± 50.60	63.1 ± 2.54	200 ± 22.00	234 ± 21.40	7.66 ± 0.10
Female 5FU+80mg/kg	1058 ± 45.50	61.1 ± 1.98	178 ± 15.80	225 ± 21.90	7.49 ± 0.12

Table 5.4. The effect of acute 5FU and emodin on blood profile in male and female mice. White blood cells (WBC), Lymphocytes (LYM), Monocytes (MON), Neutrophils (NEU), Neutrophil:Lymphocyte Ratio (NLR), Red Blood Cells (RBC), Hemoglobin (HGB), Hematocrit (HCT), and Platelets (PLT). Groups not containing the same letters (a-c) indicate statistical significance between groups ($p<0.05$) from one-way ANOVA, n=20/group.

Group	WBC (10^9/l)	LYM (10^9/l)	MON (10^9/l)	NEU (10^9/l)	NLR	RBC (10^12/l)	HGB (g/dl)	HCT (%)	PLT (10^9/l)
Male 5FU+Vehicle	1.87 ± 0.11 [a]	1.61 ± 0.12 [a]	0.10 ± 0.01	0.15 ± 0.02	0.12 ± 0.02 [a]	8.40 ± 0.11	11.84 ± 0.16	33.25 ± 0.46	280.00 ± 18.19
Male 5FU+20mg/kg	2.52 ± 0.12 [b]	2.23 ± 0.11 [b]	0.12 ± 0.01	0.17 ± 0.02	0.08 ± 0.01 [a]	8.48 ± 0.14	12.01 ± 0.15	33.56 ± 0.48	285.40 ± 21.14
Male 5FU+40mg/kg	2.63 ± 0.13 [b]	2.36 ± 0.13 [b]	0.10 ± 0.01	0.17 ± 0.02	0.08 ± 0.01 [a]	8.31 ± 0.14	12.08 ± 0.13	33.22 ± 0.58	308.4 ± 14.04
Male 5FU+80mg/kg	3.14 ± 0.18 [c]	2.86 ± 0.18 [c]	0.14 ± 0.02	0.14 ± 0.03	0.05 ± 0.01 [b]	8.59 ± 0.17	11.92 ± 0.16	34.09 ± 0.60	283.30 ± 20.13
Female 5FU+Vehicle	2.50 ± 0.41	2.05 ± 0.35	0.13 ± 0.04	0.33 ± 0.06	0.20 ± 0.03 [a]	8.03 ± 0.22	11.80 ± 0.19	32.90 ± 0.82	332.00 ± 32.90
Female 5FU+20mg/kg	2.33 ± 0.15	1.87 ± 0.16	0.12 ± 0.02	0.34 ± 0.04	0.20 ± 0.02 [a]	8.26 ± 0.21	12.20 ± 0.23	33.40 ± 0.90	340.00 ± 25.70
Female 5FU+40mg/kg	2.91 ± 0.28	2.59 ± 0.28	0.11 ± 0.02	0.21 ± 0.03	0.09 ± 0.01 [b]	8.48 ± 0.22	12.2 ± 0.28	34.20 ± 0.86	293.00 ± 33.50
Female 5FU+80mg/kg	2.41 ± 0.10	2.07 ± 0.10	0.11 ± 0.01	0.22 ± 0.02	0.11 ± 0.01 [b]	8.12 ± 0.21	12.1 ± 0.24	32.80 ± 0.82	320.00 ± 24.30

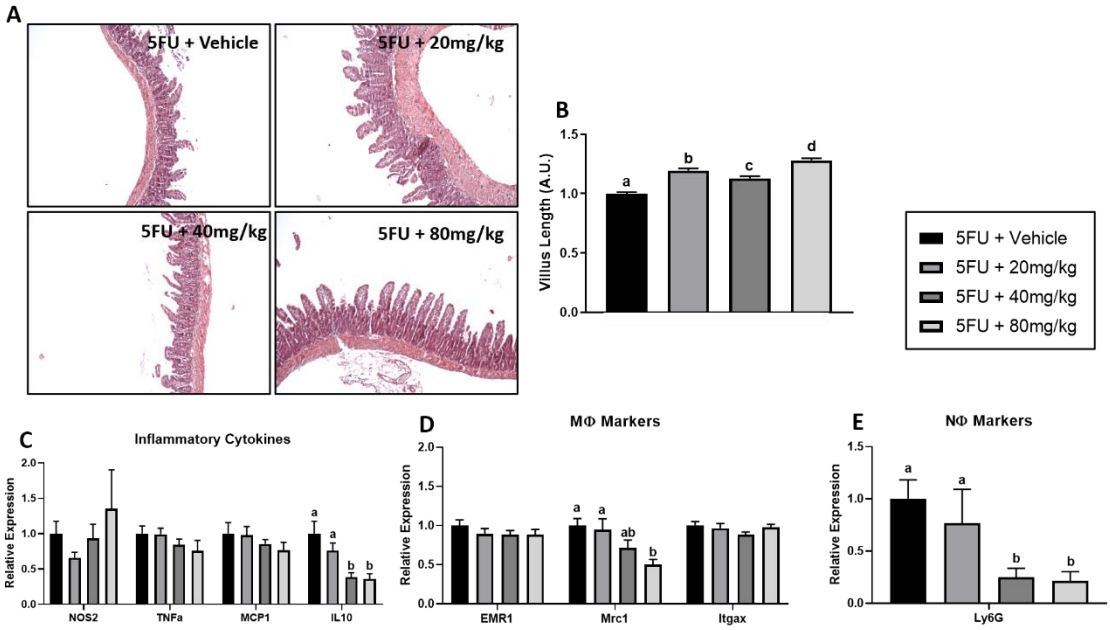

Figure 5.5. Emodin protects small intestine morphology and reduces neutrophil and M2-macrphage expression during 5FU treatment. A. Representative H&E images of small intestine biopsies at 4X. **B.** Measurement of villus length in small intestine, measurements are normalized to vehicle treated controls and represented as arbitrary units (A.U.). **C.** qPCR analysis of NOS2, TNFα, MCP1, and IL10 inflammatory cytokines. **D.** qPCR analysis of macrophage markers EMR1, MRC1, and ITGAX. **E.** qPCR analysis of neutrophil marker Ly6G. Data were normalized to vehicle treated controls and compared to five reference targets (B2M, TBP, HPRT, HMBS, and H2AFV), which were evaluated for expression stability using GeNorm. Groups not containing the same letters (a-c) indicates statistical significance between groups ($p<0.05$) from one-way ANOVA, n=15/group.

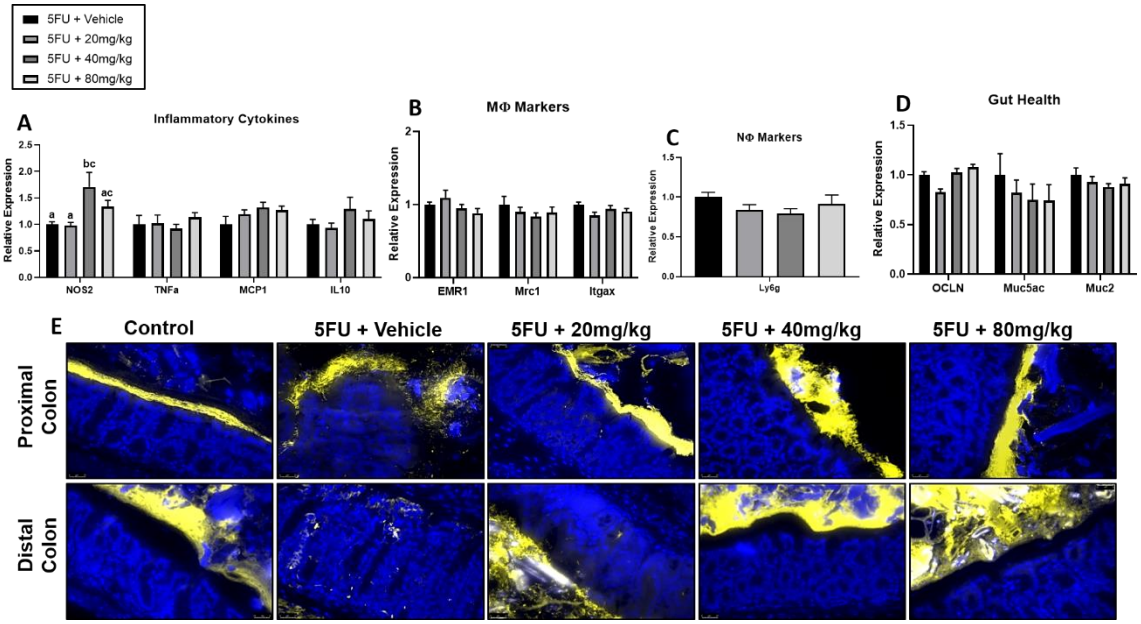

Figure 5.6. Emodin does not reduce colon inflammation acutely but may improve gut microbial spatial arrangement during 5FU treatment. A. qPCR analysis of NOS2, TNFα, MCP1, and IL10 inflammatory cytokines. **B.** qPCR analysis of macrophage markers EMR1, MRC1, and ITGAX. **C.** qPCR analysis of neutrophil marker Ly6G. **D.** qPCR analysis of gut health markers OCLN, Muc5ac, and Muc2. **E.** Representative 16S rRNA FISH images hybridized with EUB338 probe in proximal and distal colons. Images are at 20X. Arrows indicate invasion of bacteria to crypts and mucus layer. Data were normalized to vehicle treated controls and compared to five reference targets (B2M, TBP, HPRT, HMBS, and H2AFV), which were evaluated for expression stability using GeNorm. Groups not containing the same letters (a-c) indicates statistical significance between groups ($p<0.05$) from one-way ANOVA, n=15/group.

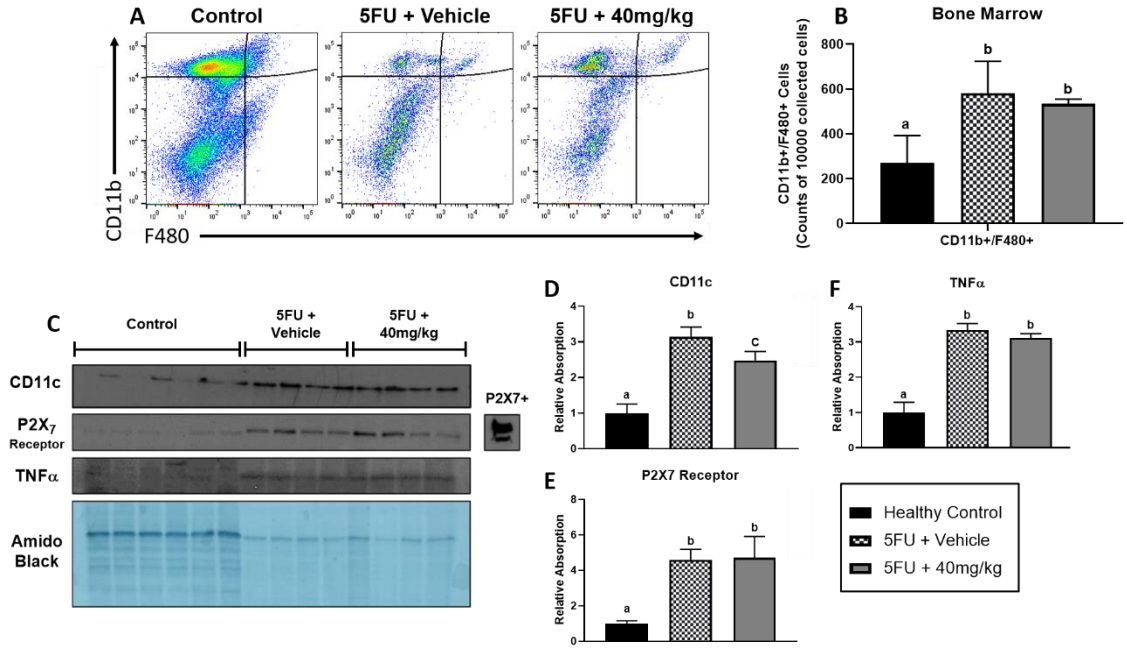

Figure 5.7. 5FU causes local bone marrow inflammation which may be ameliorated acutely with emodin. A. Representative flow plots of bone marrow isolates indicating relative macrophage content (CD11b+F4/80+). **B.** Counted events of total macrophages per 10000 events collected. **C.** Representative western blots of CD11c, P2X7, and TNFα and amido black staining of bone marrow protein extracts. 10 μg of protein was added to each well. Healthy whole mouse brain was used to identify P2X7+ control. **D-F.** Quantification of western blots for **(D)** CD11c, **(E)** P2X7 Receptor, and **(F)** TNFα. Data were normalized to vehicle treated controls. All western blots were normalized to amido black (total protein) content. Groups not containing the same letter (a-c) indicates statistical significance between groups ($p<0.05$) from one-way ANOVA, n=4-6/group.

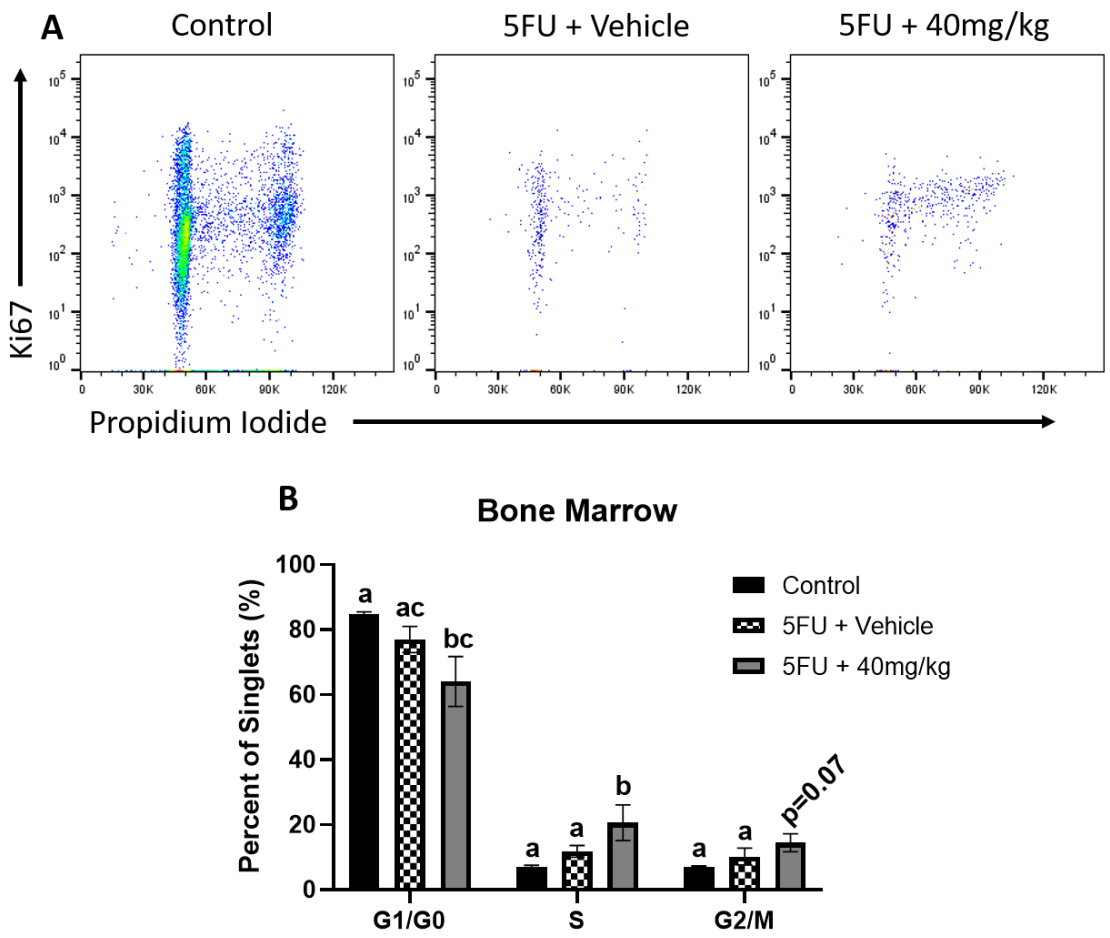

Figure 5.8. Emodin increases S phase cells during 5FU treatment. A. Representative flow plots of bone marrow isolates stained with Ki67 and Propidium Iodide. **B.** Quantification of G1/G0, S, and G2/M phase cells as percent of 100,000 cells collected. Groups not containing the same letter (a-c) indicates statistical significance between groups ($p<0.05$) from one-way ANOVA, n=4-6/group.

CHAPTER 6

ANTHRAQUINONE EMODIN REDUCES TUMOR BURDEN AND DECREASES PRO-TUMORIGENIC M2-TYPE MACROPHAGES IN THE AOM/DSS MODEL OF CRC[4]

[4] Sougiannis AT et. al. To be submitted to *Journal of Experimental Medicine.*

6.1 Abstract

Emodin, a natural anthraquinone, has shown potential as an effective therapeutic agent in the treatment of many diseases including cancer. We sought to investigate the utility of emodin as a dietary agent used in the prevention of intestinal/colorectal cancer using the $Apc^{min/+}$ and AOM/DSS mouse models. Emodin was given 3x/week orally in both studies dissolved in pure propylene glycol. 16 $Apc^{min/+}$ mice were randomized into two groups; $Apc^{min/+}$ + Vehicle and $Apc^{min/+}$ + 80 mg/kg emodin. 60 C57BL/6 were randomized into three groups; Control (n=5), AOM/DSS+Vehicle (n=20), AOM/DSS+40 mg/kg (n=20), AOM/DSS+80 mg/kg (n=20). CRC was induced chemically by a single 10 mg/kg injection of azoxymethane (AOM) followed by two cycles (2% and 1%) of dextran sodium sulfate (DSS). Oral emodin treatment began at the initiation of DSS (Week 2). At the conclusion of both studies, emodin reduced total polyp count in $Apc^{min/+}$ mice treated with 80 mg/kg ($p<0.05$) and in both 40 mg/kg ($p<0.05$) and 80 mg/kg ($p<0.05$) AOM/DSS mice. We found that emodin reduces M2-type macrophages in the colonic lamina propria of AOM/DSS mice at both 40 mg/kg ($p<0.05$) and 80mg/kg ($p<0.05$) doses. Further we see that emodin reduces the pro-inflammatory environment of the bone marrow in AOM/DSS mice by reducing the number of M1-type macrophages ($p<0.05$). In evaluating bone protein expression; we observe that emodin reduces the expression of the P2X7 Receptor and the phosphorylation of STAT3 at Y705 with both 40 mg/kg and 80 mg/kg doses. Taken together, we provide vital evidence of anti-tumorigenic and anti-inflammatory potential for emodin to be used as an effective therapeutic in the prevention of intestinal/colorectal cancer.

6.2 Introduction

Colorectal cancer (CRC) is the third most common malignancy for men or women. Preventative interventions, such as exercise and improving dietary patterns has been shown to improve outcome. However, as CRC progresses, treatment options become more limited and some patients select a no treatment option. Therefore, there is a critical need to develop new preventative strategies that improve outcome and can be administered safely.

There has been a recent increase in the clinical utility of herb-derived compounds due to evidence of the anti-inflammatory properties of many of these compounds. Emodin is a trihydroxy-anthraquinone that is found in several Chinese herbs, including *Rheum palmatum* and *Polygonum multiflorum*. Emodin has been shown to attenuate the severity of multiple experimental disease models including arthritis, liver damage, atherosclerosis, myocardial ischemia, and cancer by reducing the inflammatory cascades associated with these conditions. The mechanism of action of emodin has yet to be discovered. However, an investigation by Jelassi *et al* 2013 suggested the P2X7 receptor as a potential target of emodin[79]. The P2X7 receptor is a Ca^{2+} channel receptor that it is found the central and peripheral nervous systems, in microglia, macrophages, and the retina.[75] The P2X7 receptor has also been shown to serve as a pattern recognition receptor for extracellular ATP-mediated apoptotic cell death, regulation of receptor trafficking, mast cell degranulation, and inflammation.[145,149]

Macrophages have been demonstrated to represent the majority of immune cells in the tumor microenvironment. They are derived from monocyte precursors circulating

in the blood and are recruited to the tumor by chemokines such as MCP-1 and TGFβ. Once recruited to the tissue, monocytes will mature into macrophages. It is generally understood that the recruitment of macrophages to the tumor contribute to the maintenance of the tumor microenvironment and exert pro-tumoral functions. Pro-tumoral macrophages are characterized as M2-type macrophages, which are polarized from exposure to cytokines such as TGFβ and IL-10. The presence of M2-type macrophages in the tumor microenvironment have been shown to promote proliferation, invasion and metastasis, angiogenesis, and tissue remodeling. Further, high counts of tumor associated macrophages (TAMs) have been associated with poor prognosis and therapeutic outcome in CRC. Therefore, therapeutic interventions targeting TAMs and reducing the M2-type/M1-type ratio within the tumor microenvironment might contribute to improved survival and subsequent success of further therapeutic outcome.

In the present study, we aimed to establish the efficacy of emodin as a preventative therapeutic in two models of colorectal/intestinal cancer. Giving emodin as a preventative therapeutic to at-risk patients might contribute to prolonged survival and improved immune-based therapeutic outcome. We utilized a chemically induced model of CRC (AOM/DSS) and a genetic model of intestinal cancer ($Apc^{min/+}$). In both models, mice develop tumors and present with chronic inflammation and anemia with increasing tumor burden. We utilized oral emodin administration at a dose of 40 mg/kg and 80 mg/kg given orally 3x/week to observe the preventative effects in both these models. Our data indicate that emodin is able to reduce total polyp count and size in both models. Within the polyps of AOM/DSS mice, emodin reduced the presence of M2-type macrophages and increase the production of NOS2.

6.3 Methods

6.3.1 Animals

Male WT C57BL/6 and male $Apc^{min/+}$ mice were purchased from Jackson Laboratories (Bar Harbor, ME) and were cared for in the animal facility at the University of South Carolina. Mice were randomized upon arrival to the animal facility to prevent litter biases in microbiome data and were housed four-five per cage, maintained on a 12:12-h light-dark cycle in a low-stress environment (22^0C, 50% humidity, low noise). Mice were kept in a room isolated from all other ongoing animal experiments and were only handled by the primary investigators. All mice were habituated to the AIN-76A diet prior to any interventions and were given food and water *ad libitum* through the course of the study. All methods were in accordance with the American Association for Laboratory Animal Science, and the Institutional Animal Care and Usage Committee of the University of South Carolina approved all experiments.

6.3.2 $Apc^{min/+}$ protocol

Fig 1A illustrates the protocol used to treat $Apc^{min/+}$ mice with emodin. Briefly, 16 male $Apc^{min/+}$ mice randomly divided into 2 groups: $Apc^{min/+}$ + Vehicle (n=8) and $Apc^{min/+}$ + 80 mg/kg emodin (n=8). Mice arrived at the animal facility at the University of South Carolina at 4 weeks of age and were immediately placed n=4/cage and given AIN-76A diet and drinking water *ad libitum*. After one week of habituation, mice were started on either Vehicle or emodin intervention.

6.3.3 AOM/DSS protocol

Fig 2A illustrates the protocol used to chemically induce colorectal cancer with the AOM/DSS protocol and concurrent treatment with emodin. Briefly, 65 mice were

randomly divided into four groups: Control + Vehicle (n=5), AOM/DSS + Vehicle (n=20), AOM/DSS + 40 mg/kg emodin (n=20), and AOM/DSS + 80 mg/kg emodin (n=20). At 12 wk of age (*baseline week 0*) mice received either an intraperitoneal injection of the carcinogen[156], AOM (10 mg/kg) (Sigma, St. Louis, MO), diluted in PBS (AOM/DSS) or PBS alone (Control). Mice receiving the AOM injection were subjected to two cycles of DSS (36-50 kDa) (MP Biomedical, Solon, OH)-supplemented water at final concentrations of 2% and 1% at weeks 1 and 4, respectively. Each DSS cycle lasted for a 1-wk period.

6.3.4 Symptom monitoring and score calculation

Both $Apc^{min/+}$ and AOM/DSS mice underwent the same symptom monitoring and score calculation. Body weights and symptom scores were determined semi-weekly along with food and water measurements. Calculation of symptom score was performed as previously described[94], taking into account percent body weight loss, stool consistency, and rectal bleeding. Briefly, fresh colonic evacuates were smeared onto "Hemoccult" tape to assess severity of diarrhea and were tested with developer (Beckman Coulter, Brea, CA) to assess rectal bleeding. Bleeding was scored; no positive detection of blood (0), detection of blood but not grossly visible (2), and gross visibility of blood (4). Diarrhea was scored; solid cylinder (0), soft cylinder and easily spreadable (2), and non-cylindrical or runny (4). Body weight was calculated as percent body weight loss; 0-5% (0), 6-10% (1), 11-15% (2), 15-20% (3), 20-25% (4), and >25% (5). Scores of all three categories were summed to obtain an overall symptom score for each mouse.

6.3.5 Emodin Preparation

Emodin was purchased from Nanjing Zelang Medical Technology Co., Ltd, (Nanjing, China). Emodin was independently analyzed by the Mass Spectrometry Center at the University of South Carolina prior to the initiation of the experimental study. LC-UV-MS and NMR was performed to confirm the purity of Emodin and the molecular structure. Emodin was delivered via oral gavage to mice using flexible plastic tubing oral gavage needles (Instech, #FTP-20). Emodin was prepared fresh in a 24mg/mL stock solution using pure propylene glycol (VWR) and mixed for 6-8 hours at room temperature protected from light prior to gavage. The 24mg/mL solution was used for 80 mg/kg dosing and was used to prepare a 12mg/mL dilution for delivering the 40 mg/kg dose. Pure propylene glycol was used as a vehicle control in all experiments.

6.3.6 Tissue collection

Mice were euthanized 24 hr post final treatment with emodin and blood was collected from the inferior vena cava. Tissues were removed, weighted and immediately snap-frozen in liquid nitrogen and stored at -80^{0}C or fixed in 10% formalin until further analysis. The colon was carefully dissected distal to the cecum and proximal to the anus. Mesentery adipose tissue was removed with forceps. The colon was opened longitudinally, and polyps were counted and measured using a dissecting microscope. Colon length was measured using calipers. A subset of mice (n=4) was used for flow cytometry analysis in which the colon was placed in ice cold PBS until digestion. The remaining mice were used for qPCR analysis, polyps were removed from normal appearing tissue and both were snap frozen until further analysis. In a subset of mice, femurs were decalcified for 48 hr and then fixed in 10% formalin for 24 hr before being

embedded in paraffin blocks. Within the same subset of mice, contralateral femurs and both tibias and fibulas were snap frozen in liquid nitrogen and stored at -80^{0}C until further analysis.

6.3.7 Polyp counting and measurements

At the conclusion of each study polyps were counted and measured using a dissecting microscope. For Apc$^{min/+}$ mice, whole colons and small intestines were opened longitudinally, laid flat on filter paper, and fixed in 10% formalin overnight. Tissues were then stained in 0.1% methylene blue to visualize polyps. Polyps were counted by the same investigator who was blinded to the treatments. Polyps were counted under a dissecting microscope, using forceps to pick through the intestinal villi and identify polyps. Polyps were categorized as small (< 1 mm), medium (1-2 mm), or large (> 2 mm). After polyps were counted, intestinal sections were washed with 70% ethanol and embedded in paraffin for further analysis.

For AOM/DSS mice, freshly dissected colons were opened longitudinally, and polyps were counted and measured under a dissecting microscope. Polyps were counted to obtain total numbers and were also categorized as small (< 1 mm), medium (1-2 mm), or large (> 2 mm) as in Apc$^{min/+}$ mice. Further, colons were segmented into proximal, middle, and distal regions to record location of polyps. After polyps were counted, mice that were not used for flow cytometry had polyps removed from healthy appearing tissue and flash frozen in liquid nitrogen and stored at -80^{o}C until further analysis.

6.3.8 Blood Panel Analysis

A complete blood panel analysis was performed using the VetScan HMT (Abaxis, Union City, CA) for determination of WBCs, LYM, MON, NEU, PLT, RBCs, Hct, and

Hb. Neutrophil/lymphocyte ratio (NLR) was calculated from obtained values. Briefly, whole blood was placed in an EDTA coated microtube and analyzed on the VetScan HMT according to the manufacturer's instructions.

6.3.9 Lymphocyte Isolation and Flow Cytometry

Colons were removed and digested to obtain single cell suspensions using the Miltenyi Biotech Lamina Propria Dissociation Kit (#130-097-410). Bone marrow was taken from both femoral shafts by flushing with saline. Red blood cell lysis was performed with 20 second hypotonic solution (0.2% NaCl) treatment followed by hypertonic (1.6% NaCl) cessation. All isolates were passed through a 70 μm filter prior to antibody staining. Bone marrow and lamina propria isolates were stained with macrophage panel (CD11b – FITC, F4/80 – PE, CD206 - APC, CD11c – APC/Cy7, Ly6c – PerCP/Cy5.5, and CD45 – PE/Cy7). All antibodies were purchased from Biolegend (San Diego, CA). Cell suspensions were blocked with CD16/32 FC Block and staining was performed for 1hr at 4^0C. Lymphocytes were identified by gating for CD45+ cells. Active monocytes were identified as Ly6C+ cells. Data were acquired using a BD FACS Aria II cell sorter and analyzed by FlowJo v10.6.2.

6.3.10 Gene expression

Quantification of colonic expression of IFN-γ, TNFα, MCP-1, IL4, IL-6, IL-10, IL-1β, and P2RX7 were performed as previously described[132]. Briefly, RNA was extracted using TRIzol reagent (Life Technologies, GIBCO-BRL, Carlsbad, CA) and chloroform procedures. Because DSS has been shown to inhibit polymerase and reverse transcriptase activity, lithium chloride was used to purify the RNA as described in detail by Viennois et al. 2013.[97] RNA sample quality and quantities were verified using an

Agilent Bioanalyzer and determined to be of good quality based on A260/A280 values (>1. 8) prior to cDNA synthesis using QuantiTect Reverse Transcription kit (Qiagen 205313). Quantitative RT-PCR analysis was carried out as per the manufacturer's instructions (Applied Biosystems) using Taq-Man Gene Expression Assays. Data were normalized to vehicle treated controls and compared to five reference targets (B2M, TBP, HPRT, HMBS, and H2AFV), which were evaluated for expression stability using the GeNorm algorithm.[98,99]

6.3.11 Histopathology

Hematoxylin and eosin (H&E) staining of the bone tissue was performed as previously described[132]. All images were obtained using a Nikon E600. All histopathological analyses were performed by a board-certified pathologist blinded to the experimental conditions (I.C.).

6.3.12 Bone Protein Isolation and Western Blot

Frozen bone femurs, tibias, and fibulas were pulverized using a mortar and pestle while kept frozen at liquid nitrogen. Protein was purified by further homogenizing pulverized products in Mueller buffer containing protease inhibitor cocktail (Sigma Aldrich, St. Louis, MO). Total protein concentrations were determined by the Bradford method. Equal amounts of crude protein homogenates (20ug) were separated on hand-casted SDS-polyacrylamide gels and electrophoretically transferred to a PVDF membrane using a Royal Genie Blotter (IDEA Scientific, Minneapolis, MN). Membranes were blocked for 1hr at room temperature with 5% non-fat milk in tris-buffered saline with 0.1% tween (TBST). Western blots were performed using primary antibodies $P2X_7$ (Alomone Labs #APR-004), p-P38 (Cell Signaling #9211), and t-P38 (Cell Signaling

#8690). An anti-rabbit (Cell signaling: #7047) IgG horseradish peroxidase conjugated secondary antibody was diluted 1:2000 in 5% milk-TBST and incubated for one hour at room temperature. An enhanced chemiluminescent substrate for detection of horseradish peroxidase (Thermo Scientific, Watham, MA) was used to visualize the antibody-antigen interaction. Autoradiography films were scanned, and blots were quantified using scientific imaging software ImageJ (NIH Bethesda, MD). After completion of the western blot, all membranes were stained with Amido black (VWR #AAJ66798-14) and the densitometry of each lane was calculated using ImageJ allowing for total protein normalization as previously described[150].

6.3.13 Statistical analyses

All data were analyzed using commercial software (SigmaStat V3.5, SPSS, Chicago, IL). All outcomes were analyzed using a one-way ANOVA. A Student-Newman-Keuls test was used for all post-hoc analyses. Survival curve analysis was conducted by Log-rank (Mantel-Cox) test. Any data that were not normally distributed or did not display equal variance were logarithmically transformed so that those criteria were met. Statistical significance was set with an alpha value of $p<0.05$. Data are presented as mean ± SEM.

6.4 Results

6.4.1 Emodin reduces polyp load in $Apc^{min/+}$ mice.

There was no difference in body weight or calculated symptom score between $Apc^{min/+}$ mice treated with vehicle or 80 mg/kg emodin (Fig 6.1B,C). After 11 weeks of treatment, mice were euthanized, and the entire small intestines were stained with methylene blue and polyps were counted. We found that 11 weeks of emodin treatment

reduced total polyps in $Apc^{min/+}$ mice (Fig 6.1D; $p<0.05$). Further, emodin reduced the number of large (>2mm) and medium (1-2mm) sized polyps in the small intestine compared to vehicle treated controls (Fig 6.1E; $p<0.05$). There was no difference in small polyp count (<1mm) with emodin treatment (Fig 6.1E).

6.4.2 Emodin does not alter organ weight but might improve immune health in $Apc^{min/+}$ mice.

Splenomegaly, anemia/cytopenia, and cachexia are hallmarks of advanced colorectal/intestinal cancer; therefore, reduced spleen size/weight, maintenance of healthy major organ weight, and improved circulating blood cell counts can indicate improved prognosis and a successful therapy. At the conclusion of the study, there was no detectable difference in liver, spleen, epididymal fat, or mesenteric fat pad weight (Table 6.1) between vehicle and emodin treated mice. However, it is important to note that splenomegaly was achieved at this stage with both groups having average spleen weights greater than 200mg (Splenomegaly in mice is described as spleen weight >100mg). We also observe no difference small intestine or colon length (Table 6.1). We performed a comprehensive blood panel analysis at the conclusion of the study. Although not statistically significant, we detected trending increases in total WBC count ($p=0.149$) and MON count ($p=0.137$) and a trending decrease in NLR ($p=0.081$) with emodin treatment (Table 2). Supplemental to these findings, there were no differences in LYM, NEU, RBC, HGB, HCT, or PLT counts with emodin treatment.

6.4.3 Emodin reduces polyp load in AOM/DSS mice.

All mice injected with AOM had significantly lower body weight loss compared to control mice for the remainder of the study. Compared to AOM/DSS mice treated with

vehicle only; 40 mg/kg of emodin yielded a smaller change in body weight at Week 4.5, and 80 mg/kg of emodin yielded a smaller change in body weight at Week 2, Week 4.5, and Week 5 (Fig 6.2AB; $p<0.05$). Within AOM/DSS mice treated with emodin there was a significantly smaller difference in body weight change between 40m/kg treatment and 80 mg/kg treatment at Week 2 (Fig 6.2AB; $p<0.05$). There was a significantly lower symptom score calculation in 40 mg/kg and 80 mg/kg mice compared to vehicle treated mice at Week 5, Week 8, Week 9, and Week 10 (Fig 6.2AC; $p<0.05$). Survival was monitored through the course of the study. No mice expired due to complications from oral gavage treatment. Mice that were found dead in cage (FDIC) were counted as part of survival measurements. Although not statistically significant, through the course of study there were three deaths in the AOM/DSS + Vehicle group (17/20 survival), two deaths in the AOM/DSS + 40 mg/kg group (18/20 survival), and no deaths in the AOM/DSS + 80 mg/kg group (20/20 survival) (Fig 6.2A,D).

At the conclusion of the study colons were excised and polyps were counted under a dissecting microscope. There was a statistically significant difference between vehicle treated mice and mice treated with 40 mg/kg and 80 mg/kg (Fig 6.2E; $p<0.05$). Similar to our $Apc^{min/+}$ study, we categorized polyp counts by size. This revealed that both 40 mg/kg and 80 mg/kg emodin treatment significantly reduced medium sized (1-2mm) ($p<0.05$) polyps but not small (<1mm) and large (>2mm) polyps (Fig 2F). The location of polyps within the colon has been shown to be important in the prognosis of colorectal cancer with more distal polyps indicating worse outcome. With this understanding we analyzed colon polyps in distal, middle, and proximal sections of the colon. We found that both 40 mg/kg and 80 mg/kg emodin does not change the presence

of distal or proximal polyps but does significantly reduce the presence of polyps in the middle portion of the colon (Fig 6.2G; $p<0.05$).

6.4.4 Emodin improves liver weight in AOM/DSS mice but does associate with other organ weight changes.

As described in the $Apc^{min/+}$ section; splenomegaly, anemia/cytopenia, and cachexia are hallmarks of advanced colorectal/intestinal cancer. We observed splenomegaly in all AOM/DSS mice ($p<0.05$) but this was not changed with emodin treatment (Table 6.3). Advanced CRC causes organ wasting which is observed experimentally through decreased major organ weight. We observe decreased epididymal fat and mesenteric fat weight in all AOM/DSS mice (Table 6.3; $p<0.05$). Interestingly we found that mice treated with 80 mg/kg emodin had lower epididymal fat pad weight compared to mice treated with 40 mg/kg emodin ($p<0.05$) but not vehicle treated controls (Table 6.3). There was no difference in mesenteric fat pad weight with emodin treatment (Table 6.3). Liver weight has also been shown to decrease with progressed CRC. We show that vehicle treated AOM/DSS mice had significantly lower liver weights on average (Table 6.3; $p<0.05$). Interestingly, although not statistically significant from vehicle treated AOM/DSS mice, we found that both 40 mg/kg and 80 mg/kg had increased liver weight compared to vehicle treated AOM/DSS mice which yielded a non-statistically significant difference between emodin treated mice and healthy controls (Table 6.3).

6.4.5 Emodin reduces pro-tumoral M2-macrophage count in colon lamina propria of AOM/DSS mice.

Tumor associated macrophages are understood to play an essential role in the prognosis and treatment outcome of colorectal cancer. Using flow cytometry, we show

here that colon cancer increases total lamina propria macrophages (Gated from: CD45+/CD11b+/Ly6C+/F480+ cells). Compared to healthy controls, total macrophages were significantly greater in AOM/DSS mice treated with vehicle (Fig 6.3A,B; $p<0.05$). However, both 40 mg/kg and 80 mg/kg emodin treated mice did not have different total macrophages compared to vehicle treated AOM/DSS mice or healthy controls (Fig 6.3A,B).

We characterize CD11c expressing macrophages as M1-type macrophages and CD206 expressing macrophages as M2-type macrophages. Double expressing CD11c and CD206 macrophages are characterized as cells undergoing transition and not completely polarized M1- or M2-type macrophages. Further, cells not expressing CD11c or CD206 are characterized as M0-type macrophages. As expected, we observed a significant increase in M2-type macrophages in the lamina propria of AOM/DSS mice treated with vehicle (Fig 6.3C,D; $p<0.05$). Both 40 mg/kg and 80 mg/kg emodin treatment decreased the abundance of CD206+ M2-type macrophages in the lamina propria (Fig 6.3C,D; $p<0.05$). There was a similar trend in CD11c-/CD206- M0-type macrophages (Fig 6.3C,D; $p<0.05$), however, emodin treated mice did not have significantly lower M0-type macrophages compared to mice treated with vehicle (Fig 6.3C,D). There was no significant difference between groups in the presence of M1-type or transitioning macrophages (Fig 6.3C,D).

M1-type macrophages are described as having anti-tumor properties and M2-type macrophages are described as having pro-tumor properties. To observe the general pro- vs. anti-tumor niche we show the ratio of M2 vs. M1 macrophages within the lamina propria. We confirm the presence of a more pro-tumoral niche by reporting an increase in

the ratio of M2/M1 macrophages which is ameliorated with 40 mg/kg and 80 mg/kg emodin treatment (Fig 6.3E; $p<0.05$).

6.4.6 High dose emodin increases intra-polyp NOS2 expression.

Polyps were removed from normal appearing tissue and RNA was extracted for inflammatory cytokine analysis via RT-PCR. Interestingly, despite reduced polyp load, mice treated with 40 mg/kg and 80 mg/kg emodin do not have differences in MCP1, IL6, TNFα, IL1β, IFNγ, IL10, IL4, or Tgfb1 (Fig 6.4). However, there was a significant increase in NOS2 expression of mice treated with 80 mg/kg emodin compared to vehicle treated controls and mice treated with 40 mg/kg emodin (Fig 6.4; $p<0.05$).

6.4.7 Emodin does not ameliorate cancer associated anemia but does reduce bone marrow associated inflammation.

Hematological perturbations are a significant hallmark of advanced CRC. We find here that all AOM/DSS mice had significantly greater monocyte counts compared to healthy controls (Table 6.4; $p<0.05$). Although not statistically significant, there was a trending decrease in monocyte counts ($p=0.121$) in 80 mg/kg mice compared to vehicle treated mice. Further, there was a significant decrease in RBC counts, HGB, and HCT in all AOM/DSS mice ($p<0.05$), but no difference was detected in mice treated with emodin (Table 6.4). In parallel, there was a significant decrease in PLT counts in AOM/DSS mice treated with vehicle and 40 mg/kg emodin (Table 6.4; $p<0.05$). Interestingly, AOM/DSS mice treated with 80 mg/kg emodin had increased PLT counts but was not statistically different from AOM/DSS mice treated with vehicle and 40 mg/kg or healthy controls (Table 6.4). There were no significant differences detected in WBC, LYM, NEU, or NLR detected in any experimental groups (Table 6.4).

Bone marrow macrophages were analyzed by flow cytometry from a subset of mice (n=2-4). Interestingly, mice treated with both 40 mg/kg and 80 mg/kg had significantly lower total macrophages (CD45+/CD11b+/Ly6C+/F480+ cells) compared to control and AOM/DSS alone (Fig 6.5A,B; $p<0.05$). Upon further analysis, we found that AOM/DSS mice had increased M1-type macrophages (CD11c+ cells) compared to control mice (Fig 6.5C,D; $p<0.05$). Interestingly, 40 mg/kg and 80 mg/kg emodin treatment reduced M1-type macrophage counts to similar values as control mice (Fig 6.5C,D; $p<0.05$). In all AOM/DSS groups there was a significant decrease in M2-type (CD206+ cells) and M0 (CD11c-/CD206- cells) compared to controls (Fig 6.5C,D; $p<0.05$). There was no difference in CD11c+/CD206+ cells between all groups. We confirm this increase in M1-type macrophages by reporting a significant increase in the M1/M2 ratio of AOM/DSS mice compared to controls (Fig 6.5E; $p<0.05$). Interestingly, we show a dose response decrease in this ratio with increasing emodin treatment in which 40 mg/kg emodin is not different from control or AOM/DSS alone but 80 mg/kg emodin is significantly lower ($p<0.05$) than AOM/DSS alone but not different than control (Fig 6.5E).

6.4.8 Emodin reduces expression of P2X7 and STAT3 signaling in bone tissue of AOM/DSS mice.

To further observe the effects of emodin on bone and bone marrow health, we performed western blot analysis on frozen distal limb bones (femur, tibia, fibula). We observe a significant increase in P2X7 expression in AOM/DSS mice which was reduced with 40 mg/kg and 80 mg/kg emodin treatment (Fig 6.6A,B; $p<0.05$). STAT3 activation by phosphorylation at Y705 was significantly increased in AOM/DSS mice treated with vehicle and was decreased with both 40 mg/kg and 80 mg/kg emodin treatment (Fig

6.6A,C; $p<0.05$). Interestingly, there was a significant increase in total STAT3 protein expression in all AOM/DSS mice which was not changed with emodin treatment but caused a significant decrease in the ratio of phospho/total STAT3 protein expression (Fig 6.6A,C; $p<0.05$). We found a significant increase in phospho-ERK1/2 (T202/Y204) in all AOM/DSS mice ($p<0.05$) which was not changed with emodin treatment (Fig 6.6A,D; $p<0.05$). Further, we found no increase in total ERK1/2 expression which caused the phospho/total ERK1/2 ratio to have the same trends as the phospho-ERK1/2 expression (Fig 6.6A,D; $p<0.05$). We also detected a significant increase in phospho-P38 in AOM/DSS mice which trended towards a decrease in mice treated with 80mg/kg emodin (Fig 6.6A,E; $p=0.117$). There was no difference in the expression of total P38 which caused a similar trend in the phospho/total P38 ratio to have the same trends as the phospho-P38 expression (Fig 6.6A,E; $p<0.05$).

6.5 Discussion

There is overwhelming evidence supporting the use of natural compounds as preventative therapeutics in the treatment and prevention of colorectal cancer. We utilize two models ($Apc^{min/+}$ and AOM/DSS) of intestinal/colorectal cancer to examine the ability for dietary emodin to reduce tumor burden. In both models, we observe a significant decrease in colon polyps. Mice treated with emodin exhibited lower pro-tumorigenic M2-type macrophages and had reduced the ratio of M2/M1 macrophages within the colon. Despite this decrease in M2-type macrophages, we did not observe any change in M2 associated cytokines IL10, IL4, and Tgfb1 within excised polyps. Further, we did not see changes in M1 associated cytokines IL6, TNFα, IL1β, and IFNγ, but we did observe a significant increase in NOS2 expression in mice treated with 80 mg/kg

emodin. Emodin treatment also decreased total macrophage content within the bone marrow and reduced activation of M1-type macrophages compared to vehicle treated controls. Further analysis showed decreased P2X7 receptor expression in whole bone homogenates compared to vehicle treated AOM/DSS mice which presented with increased P2X7 expression compared to healthy controls. Taken together, these data suggest that emodin reduces pro-tumorigenic macrophages in the colon in the presence of colon cancer and can ameliorate the pro-inflammatory consequences of colorectal cancer by potentially targeting the P2X7 receptor.

The tumor microenvironment consists of a heterogenous population of immune cells that can act to reduce or promote tumor growth. TAMS are conditioned by the tumor microenvironment and exert pro-tumoral properties. Cytokines such as TGF-β, IL-10, and IL-4 polarize monocytes recruited to the tumor microenvironment into M2-type macrophages which act to promote proliferation, invasion and metastasis, angiogenesis, and matrix deposition and remodeling. [157] TAMs have been shown to be directly associated with poor prognosis and therapeutic outcome in CRC.[46,158] Emodin has been shown to act as a macrophage deactivator *in-vitro,* but has never been tested *in-vivo*. We show that emodin treatment decreases polyp count and size in both $Apc^{min/+}$ and AOM/DSS models of intestinal/colorectal cancer. This was partially explained by the reduced M2-type macrophage (CD206+) counts within the colons of AOM/DSS mice treated with emodin which resulted in a more balanced M2/M1 ratio of macrophages. Interestingly, this was not elicited by reduced expression of M2-promoting cytokines TGF-β, IL-10, and IL-4. The only change in cytokine expression detected was an increase in NOS2 expression in mice treated with 80 mg/kg emodin only. NOS2 is known to

promote M1-type macrophage polarization, but in the case of emodin, might be promoting depolarization of M2-type macrophages. A study by Iwanowycz *et al* 2016 demonstrated that emodin promotes TNFα release from IL-4 induced M2-type macrophages *in-vitro* and depolarized M2-type macrophages. Although not the same mechanism, this suggests that emodin may be promoting M2-type macrophage depolarization by increasing M1-promoting cytokines in a tissue dependent manner. It is important to note that flow cytometry was performed in whole colons and not specifically polyps; therefore, this altered macrophage phenotype may not completely represent the tumor microenvironment.

Systemic inflammation is a hallmark characteristic of advanced colorectal cancer. Where wo do not see alterations in the blood profile of $Apc^{min/+}$ mice, we do see a trending decrease in circulating monocyte counts of AOM/DSS mice treated with 80 mg/kg emodin, a value which is increased with advanced CRC as indicated by AOM/DSS mice treated with vehicle. This finding was complemented by reduced total macrophage counts and M1-type (CD11c+) macrophages in the bone marrow of mice treated with emodin. We identified that there were no gross histological indications of metastasis to the bone in AOM/DSS mice (Fig 6.7), and therefore the increase of M1-type macrophages in the bone marrow is likely attributed to extraneous factors from CRC burden. However, this finding does not explain the complete benefits of emodin. The physiological effects of this change in macrophage count needs to also be considered. We observe a drastic decrease in total macrophage count in 40 mg/kg and 80 mg/kg emodin treated mice that falls well below healthy control mice (2,490 and 2,380 cells vs. 9,031 cells, respectively). Considering our characterization of macrophage phenotyping, we see

this loss in macrophage count solely attributed to the reduction of CD11c+ (M1-type) macrophages. Beyond this finding, AOM/DSS mice presented with a drastic decrease in CD206+ (M2-type) macrophages and CD11c-/CD206- (M0-type) macrophages compared to healthy controls, which was not altered with emodin treatment. Therefore, it is imperative to provide further investigations into the physiological consequences of this drastic macrophage reduction in the bone marrow to understand the benefits associated with emodin treatment.

The mechanism of action of emodin has yet to be discovered; however, it has been suggested that emodin may inhibit the activity and expression of the P2X7 receptor. The P2X7 receptor is found the central and peripheral nervous systems, in microglia, macrophages, and the retina[75,149]. The P2X7 receptor has also been shown to serve as a pattern recognition receptor for extracellular ATP-mediated apoptotic cell death, regulation of receptor trafficking, mast cell degranulation, and inflammation.[145,149] We demonstrate in the present study that the expression of P2X7 receptor is increased in mice receiving AOM/DSS mice alone and decreased with increasing emodin dosage. Previous investigations have also showed that emodin can change the expression of P38 and ERK1/2 MAP Kinases, however these findings have been inconsistent.[72,81-84] Interestingly, although we see increased activation of P38 and ERK1/2 in the bone tissue of AOM/DSS mice, there is no change associated with emodin treatment. Emodin has also been shown to antagonize STAT3 signaling *in-vitro*. We confirm this mechanism in the bone marrow environment where we see that AOM/DSS mice treated with vehicle have increased STAT3 signaling, which was decreased with both 40 mg/kg and 80 mg/kg emodin treatment. The culmination of previous investigations and the role of the P2X7

receptor would suggest that emodin is working to antagonize the P2X7 receptor, which is present on activated pro-inflammatory immune cells, and therefore contributes to the decreased expression of STAT3 signaling. However, this mechanism needs further investigation.

Overall, our findings indicate the efficacy of emodin as a primary therapeutic to be used in the prevention of intestinal/colon-based cancers. The *in-vivo* mechanisms of emodin have proven to be elusive and have not been explored in the presence of CRC. We provide evidence that emodin can decrease pro-tumorigenic M2-type macrophages in the colon of AOM/DSS by increasing NOS2 expression within the polyp environment. We further demonstrate that emodin ameliorates the increased systemic monocyte counts and bone marrow M1-type macrophages likely by inhibiting the activity of the P2X7 receptor. Although these findings do not definitively indicate the mechanism of action of emodin, we are the first to show evidence of anti-cancer and anti-inflammatory mechanisms of emodin *in-vivo*. These findings indicate that the benefit of emodin is highly tissue specific and warrants further investigation to confirm the mechanisms discussed here.

In conclusion, the present study confirms that emodin is an effective primary therapeutic against the onset of genetic and chemically induced sporadic intestinal/colorectal cancer. We established that emodin reduces the M2-type pro-tumorigenic macrophages within the colon of AOM/DSS mice. Further, we provide evidence that emodin may be acting to antagonize the P2X7 receptor within the bone tissue of with advanced CRC and decrease the activation of macrophages within the bone marrow. Our data support the continuing investigation of emodin as an effective anti-

inflammatory and anti-cancer therapeutic and provide insight into the tissue specific mechanisms in which this novel drug might benefit longevity of patients at risk for chronic diseases.

6.5 Figures and Legends

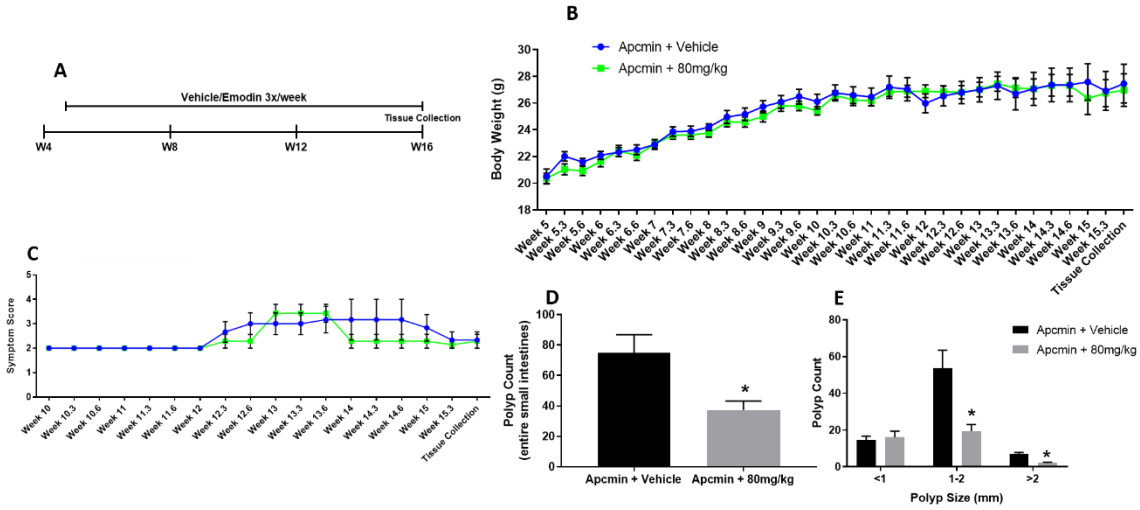

Figure 6.1. 80 mg/kg emodin reduces polyp count in Apc$^{min/+}$ mice. A. Experimental design. **B.** Absolute body weight measurements during the experiment. **C.** Symptom score calculation during the experiment. **D.** Total polyp count in the entire small intestine. **E.** Polyp size. * Indicates statistical significance ($p < 0.05$) from students t-test, n=6–7/group.

Table 6.1. Emodin does not alter organ weight in $Apc^{min/+}$ mice. Liver, spleen, epididymal fat, mesenteric fat, small intestine, and colon length weights at the conclusion of the study. Milligrams (mg), centimeters (cm).

Group	Liver (mg)	Spleen (mg)	Epididymal Fat (mg)	Mesenteric Fat (mg)	Small Intestine (cm)	Colon (cm)
Apcmin + Vehicle	1237.5 ± 115.1	233.0 ± 44.4	625.8 ± 80.6	224.0 ± 36.9	32.4 ± 0.5	8.2 ± 0.2
Apcmin + 80mg/kg	1328.0 ± 47.1	277.1 ± 65.6	613.7 ± 106.5	201.2 ± 20.7	32.9 ± 0.9	8.2 ± 0.1

Table 6.2. Emodin does not alter hematological perturbations in $Apc^{min/+}$ mice. White blood cells (WBC), lymphocytes (LYM), monocytes (MON), neutrophils (NEU), neutrophil:lymphoctye ration (NLR), red blood cells (RBC), hemoglobin (HGB), hematocrit (HCT), and platelets (PLT) were measured using a VetScan HMT (Abaxis, Union City, CA). n=6-7/group.

Group	WBC (10^9)	LYM (10^9)	MON (10^9)	NEU (10^9)	NLR (A.U.)	RBC (10^12)	HGB (g/dl)	HCT (%)	PLT (10^9)
Apcmin + Vehicle	3.83 ± 0.71	2.27 ± 0.65	0.120 ± 0.048	1.46 ± 0.19	0.779 ± 0.204	6.32 ± 1.12	9.75 ± 1.59	27.26 ± 4.60	950.50 ± 41.97
Apcmin + 80mg/kg	5.42 ± 0.64	3.63 ± 0.64	0.301 ± 0.078	1.48 ± 0.17	0.642 ± 0.265	5.52 ± 0.95	9.00 ± 1.21	24.60 ± 3.68	957.14 ± 94.73

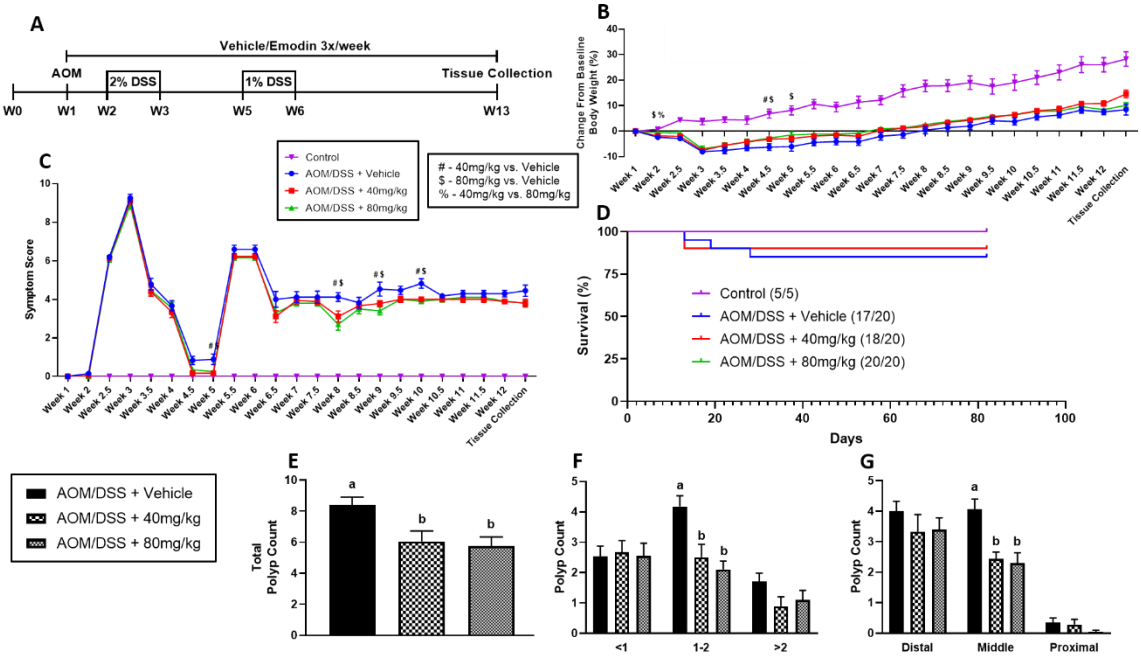

Figures 6.2. Emodin reduces polyp count in AOM/DSS mice. A. Experimental design. **B.** Percent (%) change in body weight from start of experiment (W1). **C.** Symptom score calculation. **D.** Survival curve. **E.** Total polyp count. **F.** Polyp size. **G.** Polyp location. # indicates statistical significance ($p<0.05$) between 40 mg/kg and vehicle treated mice, $ indicates statistical significance ($p<0.05$) between 80 mg/kg and vehicle treated mice, % indicates statistical significance ($p<0.05$) between 40 mg/kg and 80 mg/kg treated mice from one-way ANOVA, n=5=20/group.

Table 6.3. Emodin treatment does not alter organ weight in AOM/DSS mice. Liver, spleen, epididymal fat, mesenteric fat, small intestine, and colon length weights at the conclusion of the study. Milligrams (mg), centimeters (cm), millimeters (mm).

Group	Liver (mg)	Spleen (mg)	Epididymal Fat (mg)	Mesenteric Fat (mg)	Tibia (mm)	Small Intestine (cm)	Colon (cm)
Control	1478.2 ± 43.1[a]	82.2 ± 1.4	1426.0 ± 127.0[a]	586.0 ± 52.3[a]	18.6 ± 0.2	32.6 ± 0.4	8.0 ± 0.2
Vehicle	1245.2 ± 46.7[bc]	152.5 ± 20.0	714.8 ± 77.4[bc]	310.9 ± 28.5[b]	18.3 ± 0.1	32.3 ± 0.3	7.5 ± 0.1
40mg/kg	1336.3 ± 41.8[ac]	139.7 ± 12.6	844.8 ± 59.4[b]	347.3 ± 25.0[b]	18.0 ± 0.1	32.6 ± 0.4	7.6 ± 0.1
80mg/kg	1314.6 ± 25.1[ac]	144.7 ± 13.4	626.9 ± 35.0[c]	317.2 ± 13.8[b]	18.3 ± 0.1	33.8 ± 0.6	7.6 ± 0.1

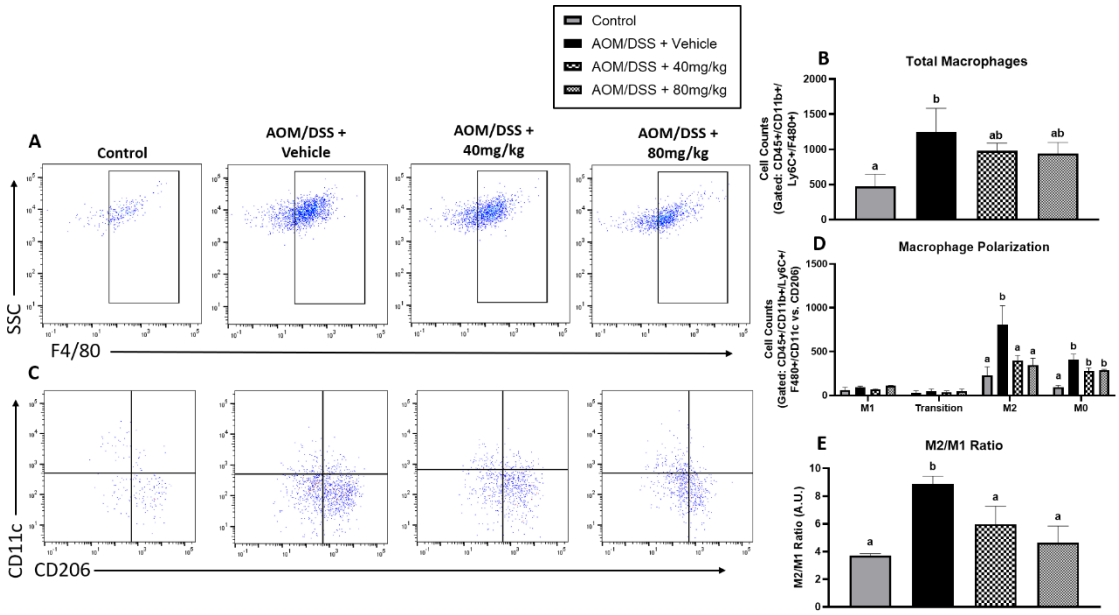

Figure 6.3. Emodin reduces pro-tumorigenic M2-type Macrophages within the AOM/DSS mouse colon lamina propria. A. Flow plots identifying mature macrophages (CD45+/CD11b+/Ly6C+/F480+ cells). **B.** Quantification of mature macrophages. **C.** Flow plots identifying M1-type (CD11c+) vs. M2-type (CD206+) macrophages. CD11c/CD206+ cells are considered transitioning cells and CD11c-/CD206- cells are considered M0-type macrophages. **D.** Quantification of M1, transition, M2, and M0 macrophages. **E.** Ratio of M2/M1 macrophage counts. Groups not containing the same letter (a-c) indicates statistical significance between groups ($p<0.05$) from one-way ANOVA, n=2(control)-4(AOM/DSS)/group.

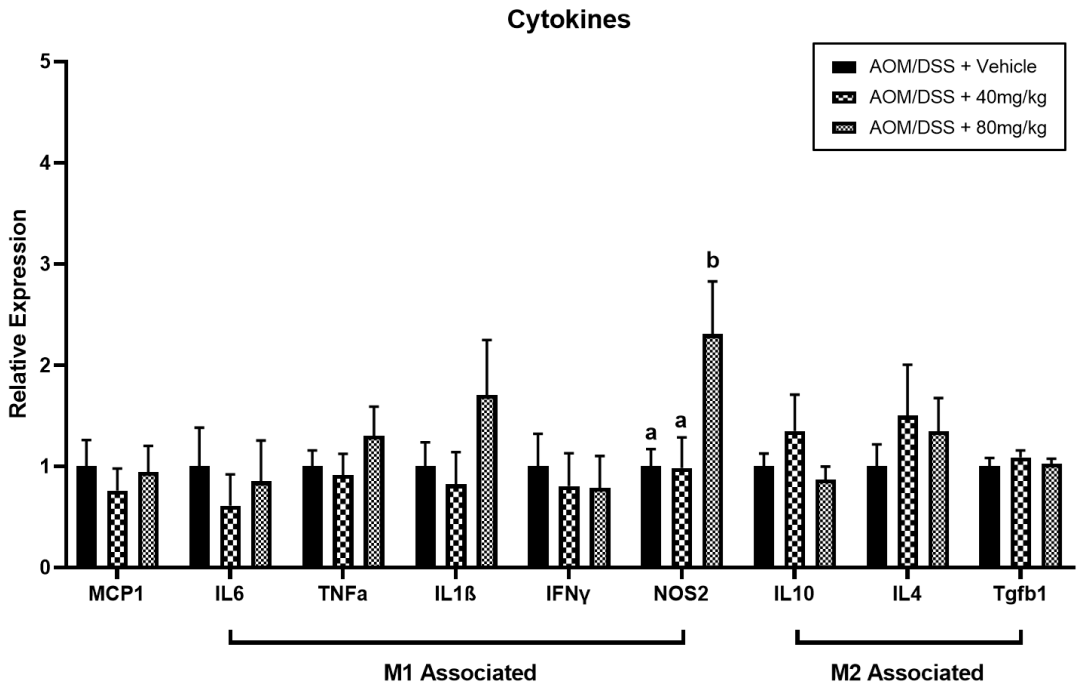

Figure 6.4. 80 mg/kg emodin increases NOS2 expression within polyps of AOM/DSS mice. qPCR analysis of MCP-1, IL6, TNFα, IL1b, IFNg, NOS2, IL10, IL4, and Tgfb1 genes. Data were normalized to vehicle treated controls and compared to five reference targets (B2M, TBP, HPRT, HMBS, and H2AFV), which were evaluated for expression stability using GeNorm. Groups not containing the same letters (a,b) indicates statistical significance between groups ($p < 0.05$) from one-way ANOVA, n=12–15/group.

Table 6.4. Emodin does not significantly alter hematological parameters within AOM/DSS mice. White blood cells (WBC), lymphocytes (LYM), monocytes (MON), neutrophils (NEU), neutrophil:lymphoctye ration (NLR), red blood cells (RBC), hemoglobin (HGB), hematocrit (HCT), and platelets (PLT) were measured using a VetScan HMT (Abaxis, Union City, CA). n=5(control)-20(AOM/DSS)/group**.**

Group	WBC (10^9)	LYM (10^9)	MON (10^9)	NEU (10^9)	NLR (A.U.)	RBC (10^12)	HGB (g/dl)	HCT (%)	PLT (10^9)
Control	5.38 ± 0.48	4.27 ± 0.40	0.040 ± 0.004 [a]	1.04 ± 0.11	0.24 ± 0.01	10.28 ± 0.27 [a]	16.00 ± 0.26 [a]	41.96 ± 1.18 [a]	781.60 ± 62.84
Vehicle	4.57 ± 0.27	3.22 ± 0.26	0.215 ± 0.029 [b]	1.13 ± 0.12	0.43 ± 0.09	8.19 ± 0.32 [b]	13.11 ± 0.46 [b]	33.86 ± 1.19 [b]	481.18 ± 66.84
40mg/kg	4.83 ± 0.43	3.48 ± 0.36	0.194 ± 0.038 [b]	1.16 ± 0.09	0.36 ± 0.02	8.77 ± 0.29 [b]	13.76 ± 0.31[b]	35.75 ± 1.00 [b]	520.28 ± 59.99
80mg/kg	5.73 ± 0.26	4.15 ± 0.23	0.166 ± 0.031 [b]	1.41 ± 0.11	0.36 ± 0.38	8.38 ± 0.24 [b]	21.88 ± 0.29 [b]	34.90 ± 0.68 [b]	615.25 ± 32.46

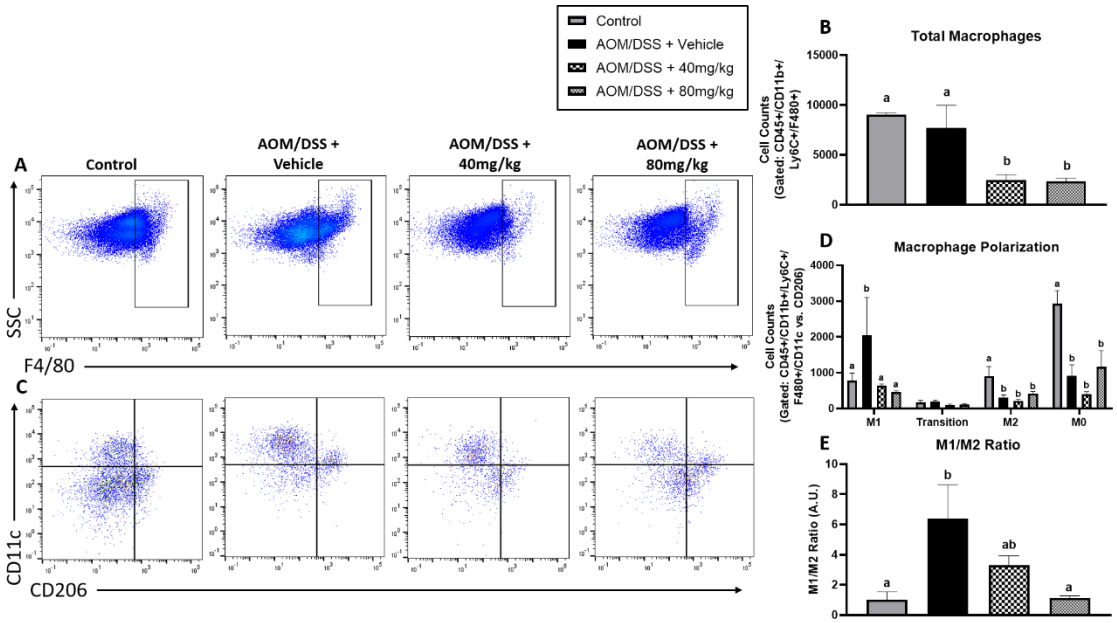

Figure 6.5. Increasing dose of emodin reduces pro-inflammatory macrophage environment within the bone marrow of AOM/DSS mice. A. Flow plots identifying mature macrophages (CD45+/CD11b+/Ly6C+/F480+ cells). **B.** Quantification of mature macrophages. **C.** Flow plots identifying M1-type (CD11c+) vs. M2-type (CD206+) macrophages. CD11c/CD206+ cells are considered transitioning cells and CD11c-/CD206- cells are considered M0-type macrophages. **D.** Quantification of M1, transition, M2, and M0 macrophages. **E.** Ratio of M1/M2 macrophage counts. Groups not containing the same letter (a-c) indicates statistical significance between groups ($p<0.05$) from one-way ANOVA, n=2(control)-4(AOM/DSS)/group.

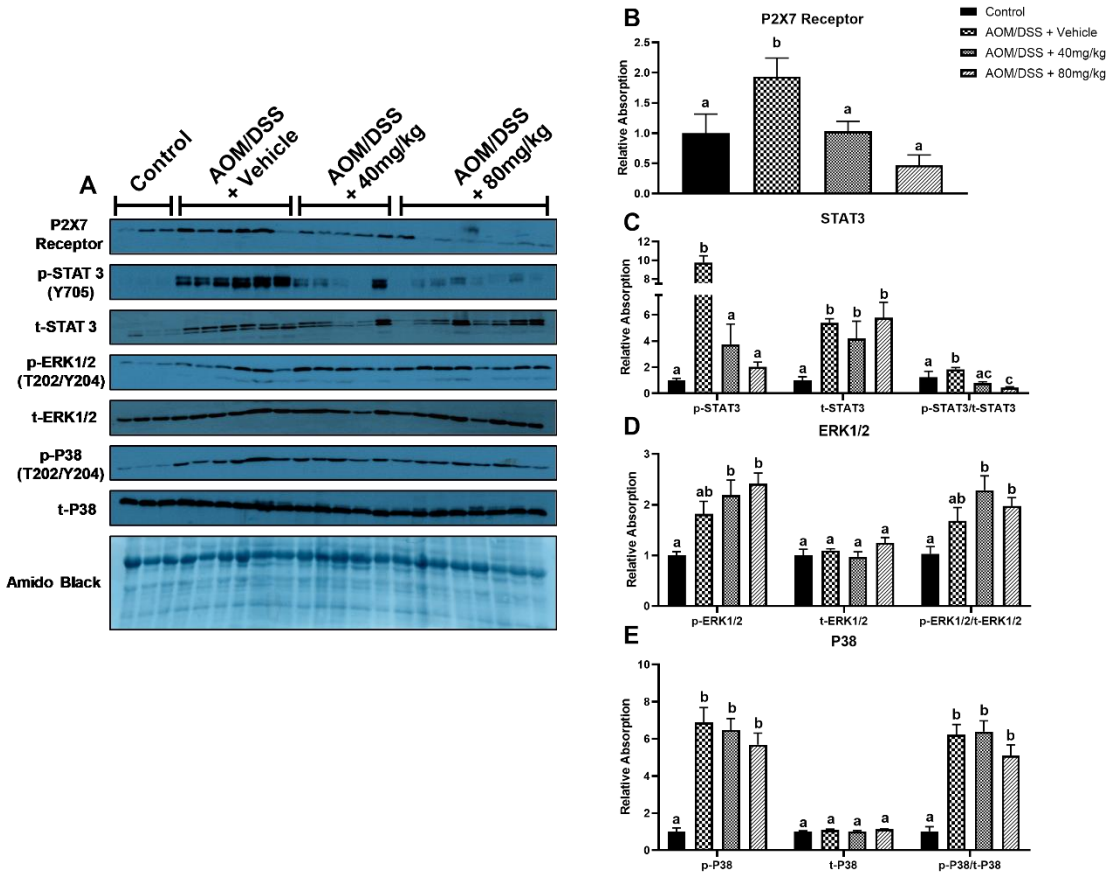

Figure 6.6. Increasing dose of emodin reduces P2X7 receptor expression and STAT3 phosphorylation/activation within the bone tissue of AOM/DSS mice. A. Representative western blots of P2X7, p-STAT3 (Y705), t-STAT3, p-ERK1/2 (), t-ERK1/2, p-P38 (), t-P38, and amido black stain. **B-E.** Quantification of relative expression of **B)** P2X7 receptor, **C)** STAT3, **D)** ERK1/2, **E)** P38. Groups not containing the same letter (a-b) indicates statistical significance between groups ($p<0.05$) from one-way ANOVA, n=2(control)-4(AOM/DSS)/group.

6.6 Supplemental Material

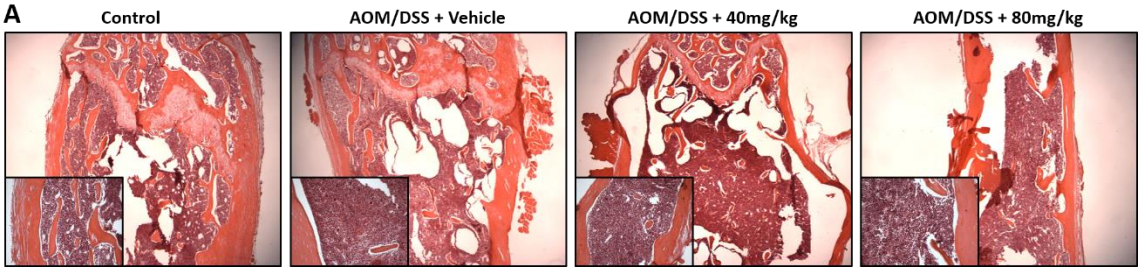

Figure 6.7. No histological evidence of metastasis to bone in AOM/DSS mice. A. Representative H&E images of bone tissue at 4X, insets are at 20X.

CHAPTER 7

SUMMARY AND CONCLUSIONS

When used in the treatment of colorectal cancer, it is reported that 5 Fluorouracil has a 10-15% success rate. However, many patients present with multiple side effects associated with 5FU treatment, the most common including fatigue, loss of appetite, diarrhea, increased pain sensitivity, and anemia, all of which can lead to a reduced quality of life. Furthermore, 7.5% of cancer patients treated with chemotherapy die prematurely as a result of non-selective chemotherapy toxicity rather than the cancer itself. Natural anthraquinone emodin, found in several Chinese herbs, has been shown to attenuate the severity of multiple disease models including, arthritis, liver damage, atherosclerosis, and cancer and thus presents an excellent subject for use as a complementary therapeutic against 5FU toxicity and colorectal cancer. In the present document, I describe the pro-inflammatory consequences of 5FU treatment and identify the gut microbiome as a potential target for amelioration of these symptoms. I further demonstrate the safety of emodin and show its efficacy as a complementary therapeutic to ameliorate the toxicities associated with 5FU. Finally, I show that emodin can be given as a preventative therapeutic against colorectal cancer and demonstrate *in-vivo* evidence for a potential mechanism of action of emodin to ameliorate inflammation and cancer cell survival.

In Chapter 3 I present my first study describing the mechanisms of 5FU toxicity. In this study, I provide evidence showing 5FU causes significant perturbations to the hematopoietic and gastrointestinal systems which correlate to reduced quality of life, as demonstrated by reduced muscular strength and fatigability, all of which may be associated with perturbations in the gut microbiota. In cancer-free mice we show that 5FU causes significant anemia and systemic lymphocytopenia and reduces the presence of colon macrophages. I utilize fecal microbial transplantation to illustrate that this

phenotype is likely controlled, in part, by alterations in the gut microbial microenvironment and may be a targetable system against 5FU-induced toxicities.

Chapter 4 introduces the natural anthraquinone emodin (1,3,8-trihydroxy-6-methylanthraquinone). It was imperative to establish the safety and pharmacodynamics of emodin in mice prior to initiating any interventional investigations. In Chapter 4 I show that emodin is poorly absorbed through the gut when given orally and when given systemically. I further demonstrate that emodin is rapidly metabolized to its active form (glucuronidated-emodin) within one hour of dosing and is cleared from the plasma within 12 hours; but does not differ between peritoneal and oral routes of administration. However, I did uncover a significant difference in the bioavailability of emodin between male and female mice, in which female mice have significantly higher plasma emodin concentrations 1 hour after dosing. We also show that emodin does not cause any noticeable pathological indications in major organ systems when given through the diet continuously for 12 weeks at relative doses of 20 mg/kg, 40 mg/kg, and 80 mg/kg. This culminated into an understanding that emodin is a safe compound to be used in both male and female mice.

The pairing of emodin with 5FU was the major focus of the novelty of this dissertation. In Chapter 5 I demonstrate that emodin improves survival and quality of life in mice both after an acute and chronic regime of 5FU. This primarily involved amelioration of pro-inflammatory cytokines TNFα and NOS2 within the gastrointestinal system leading us to suggest that emodin, while not well absorbed, is able to improve gut resilience during 5FU therapy. Where the cytokine profile of the colon did not mirror the phenotypic benefits of emodin, I utilize 16S rRNA FISH to illustrate a dose dependent

preservation of colon integrity and reduced infiltration of bacteria to the crypts. This finding further illustrating the likelihood that the benefits of emodin are partially due to mechanisms involving benefits to the gut microbial environment. Taken together, we show that emodin treatment improves gut resilience during 5FU treatment. I further demonstrate that acutely, emodin reduces the severity of lymphocytopenia caused by 5FU and improves cell cycling in the bone marrow at a moderate dose (40 mg/kg). This finding was also complemented with evidence showing that 5FU causes infiltration of pro-inflammatory macrophages to the bone marrow which is partially ameliorated with a 40 mg/kg dose of emodin. Together, Chapter 4 and 5 demonstrate the safety and efficacy of emodin as a complementary therapeutic and provide vital evidence for further investigation of emodin in models of chemotherapy toxicity.

My final aim was to demonstrate that emodin can be used as primary therapeutic against the onset of colorectal cancer. In Chapter 6, I utilize two models of sporadic intestinal/colorectal cancer development ($Apc^{min/+}$ and AOM/DSS) to show that emodin reduces tumor burden by up to 50% when given as a dietary supplement. I focused my mechanistic investigations on the AOM/DSS mouse because it is a more translatable model to the development of colorectal cancers in humans. I show using flow cytometry that emodin diminishes the pro-tumorigenic niche in the colon by reducing the presence of M2-type macrophages. This was complemented by an increase in NOS2 expression within the polyps which is known to induce differentiation of anti-tumor M1-type macrophages. Stemming from my findings in Chapter 5, I analyzed the bone marrow inflammatory environment. I show that emodin significantly reduces the presence of total macrophages primarily by reducing the presence of M1-proinflammatory macrophages.

This was complemented by whole bone tissue reductions in the expression of the P2X7 receptor and decreased activation of STAT3, giving further evidence to a specific mechanism of action of emodin.

Taken together, the evidence presented in this document illustrate the utility of emodin as both a safe and effective complementary and primary therapeutic. Our data specifically shows essential evidence for the use of emodin as a complementary therapeutic to reduce 5FU induced toxicities. Additionally, we show evidence that emodin is an effective preventative therapeutic which can reduce tumor associated pro-tumorigenic macrophages. Due to the increasing prevalence of CRC and the hampered clinical utility of 5FU chemotherapy, any potential complementary and alternative therapeutic that shows promise is important to the field of biomedicine. Although further studies are needed, the data presented here provide an essential first step towards bringing emodin to clinical trials.

CHAPTER 8

FUTURE DIRECTIONS

The data presented in this document pave the way for the next step in the progression of emodin to clinical trials. Where I have provided evidence on the efficacy of emodin, there is still much to learn mechanistically before the next steps are taken.

In Chapter 3, we uncovered a significant role of the microbiome-immune axis involved in the non-specific toxicities associated with chemotherapy treatment. I am confident in this data but urge the expansion of these research designs into a cancer model. Utilizing FMT from 5FU treated AOM/DSS mice to observe the direct role of the microbiome in the presence of cancer will provide vital evidence towards the understanding the role of the microbiome-immune axis in the treatment and progression of colorectal cancer.

In Chapters 4 and 5 I revealed promising evidence towards the clinical utility for emodin to be used as a complementary therapeutic to reduce the toxicities associated with 5FU. However, as stated above, now these investigations need to be performed in cancer burdened mice in order to fully appreciate the clinical utility of emodin as a complementary therapeutic to ameliorate 5FU-induced toxicity.

Finally, I am excited for the continuation of data gathering from the studies presented in Chapter 6. Our results indicate emodin is a safe and effective drug that can be used to prevent the onset of CRC in at-risk populations. I hope this *in-vivo* evidence provided can be utilized to return to *in-vitro* mechanistic investigations to further our understanding of the P2X7 receptor and its role in the benefits provided from emodin treatment.

REFERENCES

1. Färkkilä N, Torvinen S, Sintonen H, et al. Costs of colorectal cancer in different states of the disease. Acta Oncol 2015;54(4):454-62. (In eng). DOI: 10.3109/0284186X.2014.985797.
2. Siegel RL, Fedewa SA, Anderson WF, et al. Colorectal Cancer Incidence Patterns in the United States, 1974-2013. J Natl Cancer Inst 2017;109(8) (In eng). DOI: 10.1093/jnci/djw322.
3. Gralnek IM. Emerging technological advancements in colonoscopy: Third Eye® Retroscope® and Third Eye® Panoramic(TM) , Fuse® Full Spectrum Endoscopy® colonoscopy platform, Extra-Wide-Angle-View colonoscope, and NaviAid(TM) G-EYE(TM) balloon colonoscope. Dig Endosc 2015;27(2):223-31. (In eng). DOI: 10.1111/den.12382.
4. Johnson RL, Fleet JC. Animal models of colorectal cancer. Cancer Metastasis Rev 2013;32(1-2):39-61. (In eng). DOI: 10.1007/s10555-012-9404-6.
5. McEntee MF, Brenneman KA. Dysregulation of beta-catenin is common in canine sporadic colorectal tumors. Vet Pathol 1999;36(3):228-36. (In eng). DOI: 10.1354/vp.36-3-228.
6. Munday JS, Brennan MM, Jaber AM, Kiupel M. Ovine intestinal adenocarcinomas: histologic and phenotypic comparison with human colon cancer. Comp Med 2006;56(2):136-41. (In eng).
7. Bonetto A, Aydogdu T, Jin X, et al. JAK/STAT3 pathway inhibition blocks skeletal muscle wasting downstream of IL-6 and in experimental cancer cachexia. Am J Physiol Endocrinol Metab 2012;303(3):E410-21. (In eng). DOI: 10.1152/ajpendo.00039.2012.
8. Sahami-Fard MH, Yazd EF, Khazaei Z. The Relationship of CXCR1, IκBα and HIF-1α Expression Levels with Clinicopathological Parameters in Colorectal Cancer. Clin Lab 2019;65(5) (In eng). DOI: 10.7754/Clin.Lab.2018.181004.
9. Zhao FL, Qin CF. EGF promotes HIF-1α expression in colorectal cancer cells and tumor metastasis by regulating phosphorylation of STAT3. Eur Rev Med Pharmacol Sci 2019;23(3):1055-1062. (In eng). DOI: 10.26355/eurrev_201902_16993.
10. Lee IM, Shiroma EJ, Lobelo F, et al. Effect of physical inactivity on major non-communicable diseases worldwide: an analysis of burden of disease and life expectancy. Lancet 2012;380(9838):219-29. (In eng). DOI: 10.1016/S0140-6736(12)61031-9.
11. Shivappa N, Prizment AE, Blair CK, Jacobs DR, Steck SE, Hébert JR. Dietary inflammatory index and risk of colorectal cancer in the Iowa Women's Health Study. Cancer Epidemiol Biomarkers Prev 2014;23(11):2383-92. (In eng). DOI: 10.1158/1055-9965.EPI-14-0537.

12. Steck SE, Murphy EA. Dietary patterns and cancer risk. Nat Rev Cancer 2020;20(2):125-138. (In eng). DOI: 10.1038/s41568-019-0227-4.
13. Newmark HL, Yang K, Kurihara N, Fan K, Augenlicht LH, Lipkin M. Western-style diet-induced colonic tumors and their modulation by calcium and vitamin D in C57Bl/6 mice: a preclinical model for human sporadic colon cancer. Carcinogenesis 2009;30(1):88-92. (In eng). DOI: 10.1093/carcin/bgn229.
14. Risio M, Lipkin M, Newmark H, et al. Apoptosis, cell replication, and Western-style diet-induced tumorigenesis in mouse colon. Cancer Res 1996;56(21):4910-6. (In eng).
15. Yang K, Kurihara N, Fan K, et al. Dietary induction of colonic tumors in a mouse model of sporadic colon cancer. Cancer Res 2008;68(19):7803-10. (In eng). DOI: 10.1158/0008-5472.CAN-08-1209.
16. Bissahoyo A, Pearsall RS, Hanlon K, et al. Azoxymethane is a genetic background-dependent colorectal tumor initiator and promoter in mice: effects of dose, route, and diet. Toxicol Sci 2005;88(2):340-5. (In eng). DOI: 10.1093/toxsci/kfi313.
17. Bienz M, Clevers H. Linking colorectal cancer to Wnt signaling. Cell 2000;103(2):311-20. (In eng). DOI: 10.1016/s0092-8674(00)00122-7.
18. Nayak L, Bhattacharyya NP, De RK. Wnt signal transduction pathways: modules, development and evolution. BMC Syst Biol 2016;10 Suppl 2:44. (In eng). DOI: 10.1186/s12918-016-0299-7.
19. Moser AR, Pitot HC, Dove WF. A dominant mutation that predisposes to multiple intestinal neoplasia in the mouse. Science 1990;247(4940):322-4. (In eng). DOI: 10.1126/science.2296722.
20. Balmain A, Gray J, Ponder B. The genetics and genomics of cancer. Nat Genet 2003;33 Suppl:238-44. (In eng). DOI: 10.1038/ng1107.
21. Silvestris N, Gnoni A, Brunetti AE, et al. Target therapies in pancreatic carcinoma. Curr Med Chem 2014;21(8):948-65. (In eng). DOI: 10.2174/09298673113209990238.
22. McKeown SR, Cowen RL, Williams KJ. Bioreductive drugs: from concept to clinic. Clin Oncol (R Coll Radiol) 2007;19(6):427-42. (In eng). DOI: 10.1016/j.clon.2007.03.006.
23. Phillips E, France A, Thatvihane G, Nnaemeka U, Zaidi S. Mucositis and Cardiotoxicity Due to 5-Fluorouracil. Am J Ther 2018 (In eng). DOI: 10.1097/MJT.0000000000000725.
24. Zorzi D, Laurent A, Pawlik TM, Lauwers GY, Vauthey JN, Abdalla EK. Chemotherapy-associated hepatotoxicity and surgery for colorectal liver metastases. Br J Surg 2007;94(3):274-86. (In eng). DOI: 10.1002/bjs.5719.
25. Markman JL, Shiao SL. Impact of the immune system and immunotherapy in colorectal cancer. J Gastrointest Oncol 2015;6(2):208-23. (In eng). DOI: 10.3978/j.issn.2078-6891.2014.077.
26. Picard E, Verschoor CP, Ma GW, Pawelec G. Relationships Between Immune Landscapes, Genetic Subtypes and Responses to Immunotherapy in Colorectal Cancer. Front Immunol 2020;11:369. (In eng). DOI: 10.3389/fimmu.2020.00369.

27. Longley DB, Harkin DP, Johnston PG. 5-fluorouracil: mechanisms of action and clinical strategies. Nat Rev Cancer 2003;3(5):330-8. (In eng). DOI: 10.1038/nrc1074.
28. Iacovelli R, Pietrantonio F, Maggi C, de Braud F, Di Bartolomeo M. Combination or single-agent chemotherapy as adjuvant treatment of gastric cancer: A systematic review and meta-analysis of published trials. Crit Rev Oncol Hematol 2016;98:24-8. (In eng). DOI: 10.1016/j.critrevonc.2015.09.002.
29. O'Brien ME, Borthwick A, Rigg A, et al. Mortality within 30 days of chemotherapy: a clinical governance benchmarking issue for oncology patients. Br J Cancer 2006;95(12):1632-6. (In eng). DOI: 10.1038/sj.bjc.6603498.
30. Lee CS, Ryan EJ, Doherty GA. Gastro-intestinal toxicity of chemotherapeutics in colorectal cancer: the role of inflammation. World J Gastroenterol 2014;20(14):3751-61. (In eng). DOI: 10.3748/wjg.v20.i14.3751.
31. Pereira VB, Melo AT, Assis-Júnior EM, et al. A new animal model of intestinal mucositis induced by the combination of irinotecan and 5-fluorouracil in mice. Cancer Chemother Pharmacol 2016;77(2):323-32. (In eng). DOI: 10.1007/s00280-015-2938-x.
32. Ribeiro RA, Wanderley CW, Wong DV, et al. Irinotecan- and 5-fluorouracil-induced intestinal mucositis: insights into pathogenesis and therapeutic perspectives. Cancer Chemother Pharmacol 2016;78(5):881-893. (In eng). DOI: 10.1007/s00280-016-3139-y.
33. Chang CT, Ho TY, Lin H, et al. 5-Fluorouracil induced intestinal mucositis via nuclear factor-κB activation by transcriptomic analysis and in vivo bioluminescence imaging. PLoS One 2012;7(3):e31808. (In eng). DOI: 10.1371/journal.pone.0031808.
34. Taieb J, Tabernero J, Mini E, et al. Oxaliplatin, fluorouracil, and leucovorin with or without cetuximab in patients with resected stage III colon cancer (PETACC-8): an open-label, randomised phase 3 trial. Lancet Oncol 2014;15(8):862-73. (In eng). DOI: 10.1016/S1470-2045(14)70227-X.
35. Ferreira TM, Leonel AJ, Melo MA, et al. Oral supplementation of butyrate reduces mucositis and intestinal permeability associated with 5-Fluorouracil administration. Lipids 2012;47(7):669-78. (In eng). DOI: 10.1007/s11745-012-3680-3.
36. Gelen V, Şengül E, Yıldırım S, Atila G. The protective effects of naringin against 5-fluorouracil-induced hepatotoxicity and nephrotoxicity in rats. Iran J Basic Med Sci 2018;21(4):404-410. (In eng). DOI: 10.22038/IJBMS.2018.27510.6714.
37. Atreya CE, Yaeger R, Chu E. Systemic Therapy for Metastatic Colorectal Cancer: From Current Standards to Future Molecular Targeted Approaches. Am Soc Clin Oncol Educ Book 2017;37:246-256. (In eng). DOI: 10.14694/EDBK_175679.
38. Martínez-Lostao L, Anel A, Pardo J. How Do Cytotoxic Lymphocytes Kill Cancer Cells? Clin Cancer Res 2015;21(22):5047-56. (In eng). DOI: 10.1158/1078-0432.CCR-15-0685.
39. McQuade RM, Stojanovska V, Bornstein JC, Nurgali K. Colorectal Cancer Chemotherapy: The Evolution of Treatment and New Approaches. Curr Med Chem 2017;24(15):1537-1557. (In eng). DOI: 10.2174/0929867324666170111152436.

40. Vétizou M, Pitt JM, Daillère R, et al. Anticancer immunotherapy by CTLA-4 blockade relies on the gut microbiota. Science 2015;350(6264):1079-84. (In eng). DOI: 10.1126/science.aad1329.
41. Wu J, Lanier LL. Natural killer cells and cancer. Adv Cancer Res 2003;90:127-56. (In eng). DOI: 10.1016/s0065-230x(03)90004-2.
42. Iida N, Dzutsev A, Stewart CA, et al. Commensal bacteria control cancer response to therapy by modulating the tumor microenvironment. Science 2013;342(6161):967-70. (In eng). DOI: 10.1126/science.1240527.
43. Newman JH, Chesson CB, Herzog NL, et al. Intratumoral injection of the seasonal flu shot converts immunologically cold tumors to hot and serves as an immunotherapy for cancer. Proc Natl Acad Sci U S A 2020;117(2):1119-1128. (In eng). DOI: 10.1073/pnas.1904022116.
44. Kinch MS. An overview of FDA-approved biologics medicines. Drug Discov Today 2015;20(4):393-8. (In eng). DOI: 10.1016/j.drudis.2014.09.003.
45. Hanahan D, Weinberg RA. Hallmarks of cancer: the next generation. Cell 2011;144(5):646-74. (In eng). DOI: 10.1016/j.cell.2011.02.013.
46. Kang JC, Chen JS, Lee CH, Chang JJ, Shieh YS. Intratumoral macrophage counts correlate with tumor progression in colorectal cancer. J Surg Oncol 2010;102(3):242-8. (In eng). DOI: 10.1002/jso.21617.
47. Dandekar RC, Kingaonkar AV, Dhabekar GS. Role of macrophages in malignancy. Ann Maxillofac Surg 2011;1(2):150-4. (In eng). DOI: 10.4103/2231-0746.92782.
48. Li J, Li L, Li Y, et al. Tumor-associated macrophage infiltration and prognosis in colorectal cancer: systematic review and meta-analysis. Int J Colorectal Dis 2020 (In eng). DOI: 10.1007/s00384-020-03593-z.
49. Sui H, Tan H, Fu J, et al. The active fraction of Garcinia yunnanensis suppresses the progression of colorectal carcinoma by interfering with tumorassociated macrophage-associated M2 macrophage polarization in vivo and in vitro. FASEB J 2020 (In eng). DOI: 10.1096/fj.201903011R.
50. Zhang X, Quan F, Xu J, Xiao Y, Li X, Li Y. Combination of multiple tumor-infiltrating immune cells predicts clinical outcome in colon cancer. Clin Immunol 2020;215:108412. (In eng). DOI: 10.1016/j.clim.2020.108412.
51. Erdag G, Schaefer JT, Smolkin ME, et al. Immunotype and immunohistologic characteristics of tumor-infiltrating immune cells are associated with clinical outcome in metastatic melanoma. Cancer Res 2012;72(5):1070-80. (In eng). DOI: 10.1158/0008-5472.CAN-11-3218.
52. Bain CC, Schridde A. Origin, Differentiation, and Function of Intestinal Macrophages. Front Immunol 2018;9:2733. (In eng). DOI: 10.3389/fimmu.2018.02733.
53. Denning TL, Wang YC, Patel SR, Williams IR, Pulendran B. Lamina propria macrophages and dendritic cells differentially induce regulatory and interleukin 17-producing T cell responses. Nat Immunol 2007;8(10):1086-94. (In eng). DOI: 10.1038/ni1511.
54. Orecchioni M, Ghosheh Y, Pramod AB, Ley K. Macrophage Polarization: Different Gene Signatures in M1(LPS+) vs. Classically and M2(LPS-) vs.

Alternatively Activated Macrophages. Front Immunol 2019;10:1084. (In eng). DOI: 10.3389/fimmu.2019.01084.
55. Sica A, Mantovani A. Macrophage plasticity and polarization: in vivo veritas. J Clin Invest 2012;122(3):787-95. (In eng). DOI: 10.1172/JCI59643.
56. Deng X, Terunuma H, Terunuma A, Takane T, Nieda M. Ex vivo-expanded natural killer cells kill cancer cells more effectively than ex vivo-expanded γδ T cells or αβ T cells. Int Immunopharmacol 2014;22(2):486-91. (In eng). DOI: 10.1016/j.intimp.2014.07.036.
57. Hegazy AN, West NR, Stubbington MJT, et al. Circulating and Tissue-Resident CD4. Gastroenterology 2017;153(5):1320-1337.e16. (In eng). DOI: 10.1053/j.gastro.2017.07.047.
58. Kwak Y, Koh J, Kim DW, Kang SB, Kim WH, Lee HS. Immunoscore encompassing CD3+ and CD8+ T cell densities in distant metastasis is a robust prognostic marker for advanced colorectal cancer. Oncotarget 2016;7(49):81778-81790. (In eng). DOI: 10.18632/oncotarget.13207.
59. Li Q, Grover AC, Donald EJ, et al. Simultaneous targeting of CD3 on T cells and CD40 on B or dendritic cells augments the antitumor reactivity of tumor-primed lymph node cells. J Immunol 2005;175(3):1424-32. (In eng). DOI: 10.4049/jimmunol.175.3.1424.
60. Lavotshkin S, Jalas JR, Torisu-Itakura H, et al. Immunoprofiling for prognostic assessment of colon cancer: a novel complement to ultrastaging. J Gastrointest Surg 2015;19(6):999-1006. (In eng). DOI: 10.1007/s11605-015-2759-6.
61. Ammirante M, Luo JL, Grivennikov S, Nedospasov S, Karin M. B-cell-derived lymphotoxin promotes castration-resistant prostate cancer. Nature 2010;464(7286):302-5. (In eng). DOI: 10.1038/nature08782.
62. Mizukami M, Hanagiri T, Shigematsu Y, et al. Effect of IgG produced by tumor-infiltrating B lymphocytes on lung tumor growth. Anticancer Res 2006;26(3A):1827-31. (In eng).
63. Gazzinelli RT, Hieny S, Wynn TA, Wolf S, Sher A. Interleukin 12 is required for the T-lymphocyte-independent induction of interferon gamma by an intracellular parasite and induces resistance in T-cell-deficient hosts. Proc Natl Acad Sci U S A 1993;90(13):6115-9. (In eng). DOI: 10.1073/pnas.90.13.6115.
64. Zwirner NW, Ziblat A. Regulation of NK Cell Activation and Effector Functions by the IL-12 Family of Cytokines: The Case of IL-27. Front Immunol 2017;8:25. (In eng). DOI: 10.3389/fimmu.2017.00025.
65. Molle C, Nguyen M, Flamand V, et al. IL-27 synthesis induced by TLR ligation critically depends on IFN regulatory factor 3. J Immunol 2007;178(12):7607-15. (In eng). DOI: 10.4049/jimmunol.178.12.7607.
66. Pomeroy EJ, Hunzeker JT, Kluesner MG, et al. A Genetically Engineered Primary Human Natural Killer Cell Platform for Cancer Immunotherapy. Mol Ther 2020;28(1):52-63. (In eng). DOI: 10.1016/j.ymthe.2019.10.009.
67. Wylie B, Macri C, Mintern JD, Waithman J. Dendritic Cells and Cancer: From Biology to Therapeutic Intervention. Cancers (Basel) 2019;11(4) (In eng). DOI: 10.3390/cancers11040521.
68. O'Keeffe M, Hochrein H, Vremec D, et al. Effects of administration of progenipoietin 1, Flt-3 ligand, granulocyte colony-stimulating factor, and

pegylated granulocyte-macrophage colony-stimulating factor on dendritic cell subsets in mice. Blood 2002;99(6):2122-30. (In eng). DOI: 10.1182/blood.v99.6.2122.
69. Zhang HM, Wang F, Qiu Y, et al. Emodin inhibits coxsackievirus B3 replication via multiple signalling cascades leading to suppression of translation. Biochem J 2016;473(4):473-85. (In eng). DOI: 10.1042/BJ20150419.
70. Zeng YQ, Dai Z, Lu F, et al. Emodin via colonic irrigation modulates gut microbiota and reduces uremic toxins in rats with chronic kidney disease. Oncotarget 2016;7(14):17468-78. DOI: 10.18632/oncotarget.8160.
71. Lu Y, Yang JH, Li X, et al. Emodin, a naturally occurring anthraquinone derivative, suppresses IgE-mediated anaphylactic reaction and mast cell activation. Biochem Pharmacol 2011;82(11):1700-8. (In eng). DOI: 10.1016/j.bcp.2011.08.022.
72. Lee SU, Shin HK, Min YK, Kim SH. Emodin accelerates osteoblast differentiation through phosphatidylinositol 3-kinase activation and bone morphogenetic protein-2 gene expression. Int Immunopharmacol 2008;8(5):741-7. (In eng). DOI: 10.1016/j.intimp.2008.01.027.
73. Feng Y, Huang SL, Dou W, et al. Emodin, a natural product, selectively inhibits 11beta-hydroxysteroid dehydrogenase type 1 and ameliorates metabolic disorder in diet-induced obese mice. Br J Pharmacol 2010;161(1):113-26. (In eng). DOI: 10.1111/j.1476-5381.2010.00826.x.
74. Li HL, Chen HL, Li H, et al. Regulatory effects of emodin on NF-kappaB activation and inflammatory cytokine expression in RAW 264.7 macrophages. Int J Mol Med 2005;16(1):41-7. (In eng).
75. Liu L, Zou J, Liu X, Jiang LH, Li J. Inhibition of ATP-induced macrophage death by emodin via antagonizing P2X7 receptor. Eur J Pharmacol 2010;640(1-3):15-9. (In eng). DOI: 10.1016/j.ejphar.2010.04.036.
76. Wang J, Zhang Y, Zhu Q, Liu Y, Cheng H, Li T. Data on the radioprotective effect of emodin. Data Brief 2017;11:290-295. (In eng). DOI: 10.1016/j.dib.2016.12.038.
77. Jia X, Iwanowycz S, Wang J, et al. Emodin attenuates systemic and liver inflammation in hyperlipidemic mice administrated with lipopolysaccharides. Experimental biology and medicine 2014;239(8):1025-1035. DOI: 10.1177/1535370214530247.
78. Iwanowycz S, Wang J, Hodge J, Wang Y, Yu F, Fan D. Emodin Inhibits Breast Cancer Growth by Blocking the Tumor-Promoting Feedforward Loop between Cancer Cells and Macrophages. Molecular cancer therapeutics 2016;15(8):1931-42. DOI: 10.1158/1535-7163.MCT-15-0987.
79. Jelassi B, Anchelin M, Chamouton J, et al. Anthraquinone emodin inhibits human cancer cell invasiveness by antagonizing P2X7 receptors. Carcinogenesis 2013;34(7):1487-96. (In eng). DOI: 10.1093/carcin/bgt099.
80. Iwanowycz S, Wang J, Altomare D, Hui Y, Fan D. Emodin Bidirectionally Modulates Macrophage Polarization and Epigenetically Regulates Macrophage Memory. J Biol Chem 2016;291(22):11491-503. (In eng). DOI: 10.1074/jbc.M115.702092.

81. Cui Y, Lu P, Song G, Liu Q, Zhu D, Liu X. Involvement of PI3K/Akt, ERK and p38 signaling pathways in emodin-mediated extrinsic and intrinsic human hepatoblastoma cell apoptosis. Food Chem Toxicol 2016;92:26-37. (In eng). DOI: 10.1016/j.fct.2016.03.013.
82. Lin W, Zhong M, Yin H, et al. Emodin induces hepatocellular carcinoma cell apoptosis through MAPK and PI3K/AKT signaling pathways in vitro and in vivo. Oncol Rep 2016;36(2):961-7. (In eng). DOI: 10.3892/or.2016.4861.
83. Yeh FT, Wu CH, Lee HZ. Signaling pathway for aloe-emodin-induced apoptosis in human H460 lung nonsmall carcinoma cell. Int J Cancer 2003;106(1):26-33. (In eng). DOI: 10.1002/ijc.11185.
84. Wang X, Niu C, Zhang X, Dong M. Emodin suppresses activation of hepatic stellate cells through p38 mitogen-activated protein kinase and Smad signaling pathways in vitro. Phytother Res 2018;32(12):2436-2446. (In eng). DOI: 10.1002/ptr.6182.
85. Tang Q, Wu J, Zheng F, Hann SS, Chen Y. Emodin Increases Expression of Insulin-Like Growth Factor Binding Protein 1 through Activation of MEK/ERK/AMPKα and Interaction of PPARγ and Sp1 in Lung Cancer. Cell Physiol Biochem 2017;41(1):339-357. (In eng). DOI: 10.1159/000456281.
86. Lee KH, Lee MS, Cha EY, et al. Inhibitory effect of emodin on fatty acid synthase, colon cancer proliferation and apoptosis. Mol Med Rep 2017;15(4):2163-2173. (In eng). DOI: 10.3892/mmr.2017.6254.
87. Zhang Q, Hu F, Guo F, Zhou Q, Xiang H, Shang D. Emodin attenuates adenosine triphosphate-induced pancreatic ductal cell injury in vitro via the inhibition of the P2X7/NLRP3 signaling pathway. Oncol Rep 2019 (In eng). DOI: 10.3892/or.2019.7270.
88. Lee JJ, Beumer JH, Chu E. Therapeutic drug monitoring of 5-fluorouracil. Cancer Chemother Pharmacol 2016;78(3):447-64. (In eng). DOI: 10.1007/s00280-016-3054-2.
89. Zhang N, Yin Y, Xu SJ, Chen WS. 5-Fluorouracil: mechanisms of resistance and reversal strategies. Molecules 2008;13(8):1551-69. (In eng).
90. Nijhuis A, Thompson H, Adam J, et al. Remodelling of microRNAs in colorectal cancer by hypoxia alters metabolism profiles and 5-fluorouracil resistance. Hum Mol Genet 2017;26(8):1552-1564. (In eng). DOI: 10.1093/hmg/ddx059.
91. Li HL, Lu L, Wang XS, et al. Alteration of Gut Microbiota and Inflammatory Cytokine/Chemokine Profiles in 5-Fluorouracil Induced Intestinal Mucositis. Front Cell Infect Microbiol 2017;7:455. (In eng). DOI: 10.3389/fcimb.2017.00455.
92. Hamouda N, Sano T, Oikawa Y, et al. Apoptosis, Dysbiosis and Expression of Inflammatory Cytokines are Sequential Events in the Development of 5-Fluorouracil-Induced Intestinal Mucositis in Mice. Basic Clin Pharmacol Toxicol 2017;121(3):159-168. (In eng). DOI: 10.1111/bcpt.12793.
93. Enos RT, Velázquez KT, McClellan JL, et al. High-fat diets rich in saturated fat protect against azoxymethane/dextran sulfate sodium-induced colon cancer. Am J Physiol Gastrointest Liver Physiol 2016;310(11):G906-19. (In eng). DOI: 10.1152/ajpgi.00345.2015.

94. Kaur K, Saxena A, Debnath I, et al. Antibiotic-mediated bacteriome depletion in Apc. Cancer Med 2018;7(5):2003-2012. (In eng). DOI: 10.1002/cam4.1460.
95. Reikvam DH, Erofeev A, Sandvik A, et al. Depletion of murine intestinal microbiota: effects on gut mucosa and epithelial gene expression. PLoS One 2011;6(3):e17996. (In eng). DOI: 10.1371/journal.pone.0017996.
96. Velázquez KT, Enos RT, Carson MS, et al. miR155 deficiency aggravates high-fat diet-induced adipose tissue fibrosis in male mice. Physiol Rep 2017;5(18) (In eng). DOI: 10.14814/phy2.13412.
97. Viennois E, Chen F, Laroui H, Baker MT, Merlin D. Dextran sodium sulfate inhibits the activities of both polymerase and reverse transcriptase: lithium chloride purification, a rapid and efficient technique to purify RNA. BMC Res Notes 2013;6:360. (In eng). DOI: 10.1186/1756-0500-6-360.
98. Selvarajah GT, Bonestroo FAS, Timmermans Sprang EPM, Kirpensteijn J, Mol JA. Reference gene validation for gene expression normalization in canine osteosarcoma: a geNorm algorithm approach. BMC Vet Res 2017;13(1):354. (In eng). DOI: 10.1186/s12917-017-1281-3.
99. St-Pierre J, Grégoire JC, Vaillancourt C. A simple method to assess group difference in RT-qPCR reference gene selection using GeNorm: The case of the placental sex. Sci Rep 2017;7(1):16923. (In eng). DOI: 10.1038/s41598-017-16916-y.
100. Caporaso JG, Lauber CL, Walters WA, et al. Ultra-high-throughput microbial community analysis on the Illumina HiSeq and MiSeq platforms. ISME J 2012;6(8):1621-4. (In eng). DOI: 10.1038/ismej.2012.8.
101. Kozich JJ, Westcott SL, Baxter NT, Highlander SK, Schloss PD. Development of a dual-index sequencing strategy and curation pipeline for analyzing amplicon sequence data on the MiSeq Illumina sequencing platform. Appl Environ Microbiol 2013;79(17):5112-20. (In eng). DOI: 10.1128/AEM.01043-13.
102. Caporaso JG, Kuczynski J, Stombaugh J, et al. QIIME allows analysis of high-throughput community sequencing data. Nat Methods 2010;7(5):335-6. (In eng). DOI: 10.1038/nmeth.f.303.
103. Lozupone C, Knight R. UniFrac: a new phylogenetic method for comparing microbial communities. Appl Environ Microbiol 2005;71(12):8228-35. (In eng). DOI: 10.1128/AEM.71.12.8228-8235.2005.
104. Tucker JM, Davis C, Kitchens ME, et al. Response to 5-fluorouracil chemotherapy is modified by dietary folic acid deficiency in Apc(Min/+) mice. Cancer Lett 2002;187(1-2):153-62. (In eng). DOI: 10.1016/s0304-3835(02)00402-0.
105. Cai Z, Yang J, Shu X, Xiong X. Chemotherapy-associated hepatotoxicity in colorectal cancer. J BUON 2014;19(2):350-6. (In eng).
106. Grigorian A, O'Brien CB. Hepatotoxicity Secondary to Chemotherapy. J Clin Transl Hepatol 2014;2(2):95-102. (In eng). DOI: 10.14218/JCTH.2014.00011.
107. Diao L, Mei Q, Xu JM, et al. Rebamipide suppresses diclofenac-induced intestinal permeability via mitochondrial protection in mice. World J Gastroenterol 2012;18(10):1059-66. (In eng). DOI: 10.3748/wjg.v18.i10.1059.
108. Pozzoli C, Menozzi A, Grandi D, et al. Protective effects of proton pump inhibitors against indomethacin-induced lesions in the rat small intestine. Naunyn

Schmiedebergs Arch Pharmacol 2007;374(4):283-91. (In eng). DOI: 10.1007/s00210-006-0121-y.
109. Sonis ST, Elting LS, Keefe D, et al. Perspectives on cancer therapy-induced mucosal injury: pathogenesis, measurement, epidemiology, and consequences for patients. Cancer 2004;100(9 Suppl):1995-2025. (In eng). DOI: 10.1002/cncr.20162.
110. Velázquez KT, Enos RT, Carson MS, et al. Weight loss following diet-induced obesity does not alter colon tumorigenesis in the AOM mouse model. Am J Physiol Gastrointest Liver Physiol 2016;311(4):G699-G712. (In eng). DOI: 10.1152/ajpgi.00207.2016.
111. Mahoney SE, Davis JM, Murphy EA, McClellan JL, Gordon B, Pena MM. Effects of 5-fluorouracil chemotherapy on fatigue: role of MCP-1. Brain Behav Immun 2013;27(1):155-61. (In eng). DOI: 10.1016/j.bbi.2012.10.012.
112. Dantzer R, Meagher MW, Cleeland CS. Translational approaches to treatment-induced symptoms in cancer patients. Nat Rev Clin Oncol 2012;9(7):414-26. (In eng). DOI: 10.1038/nrclinonc.2012.88.
113. Jager A, Sleijfer S, van der Rijt CC. The pathogenesis of cancer related fatigue: could increased activity of pro-inflammatory cytokines be the common denominator? Eur J Cancer 2008;44(2):175-81. (In eng). DOI: 10.1016/j.ejca.2007.11.023.
114. Bader JE, Enos RT, Velázquez KT, et al. Macrophage depletion using clodronate liposomes decreases tumorigenesis and alters gut microbiota in the AOM/DSS mouse model of colon cancer. Am J Physiol Gastrointest Liver Physiol 2018;314(1):G22-G31. (In eng). DOI: 10.1152/ajpgi.00229.2017.
115. Shen XJ, Rawls JF, Randall T, et al. Molecular characterization of mucosal adherent bacteria and associations with colorectal adenomas. Gut Microbes 2010;1(3):138-47. (In eng). DOI: 10.4161/gmic.1.3.12360.
116. Kubinak JL, Petersen C, Stephens WZ, et al. MyD88 signaling in T cells directs IgA-mediated control of the microbiota to promote health. Cell Host Microbe 2015;17(2):153-63. (In eng). DOI: 10.1016/j.chom.2014.12.009.
117. Swidsinski A, Dörffel Y, Loening-Baucke V, et al. Reduced Mass and Diversity of the Colonic Microbiome in Patients with Multiple Sclerosis and Their Improvement with Ketogenic Diet. Front Microbiol 2017;8:1141. (In eng). DOI: 10.3389/fmicb.2017.01141.
118. Peters BA, Dominianni C, Shapiro JA, et al. The gut microbiota in conventional and serrated precursors of colorectal cancer. Microbiome 2016;4(1):69. (In eng). DOI: 10.1186/s40168-016-0218-6.
119. O'Keefe SJ, Li JV, Lahti L, et al. Fat, fibre and cancer risk in African Americans and rural Africans. Nat Commun 2015;6:6342. (In eng). DOI: 10.1038/ncomms7342.
120. Song ZC, Wang ZS, Bai JH, Li Z, Hu J. Emodin, a naturally occurring anthraquinone, ameliorates experimental autoimmune myocarditis in rats. Tohoku J Exp Med 2012;227(3):225-30. (In eng). DOI: 10.1620/tjem.227.225.
121. Guo HC, Bu HQ, Luo J, et al. Emodin potentiates the antitumor effects of gemcitabine in PANC-1 pancreatic cancer xenograft model in vivo via

inhibition of inhibitors of apoptosis. Int J Oncol 2012;40(6):1849-57. (In eng). DOI: 10.3892/ijo.2012.1389.
122. Jia X, Yu F, Wang J, et al. Emodin suppresses pulmonary metastasis of breast cancer accompanied with decreased macrophage recruitment and M2 polarization in the lungs. Breast cancer research and treatment 2014;148(2):291-302. DOI: 10.1007/s10549-014-3164-7.
123. Kuo TC, Yang JS, Lin MW, et al. Emodin has cytotoxic and protective effects in rat C6 glioma cells: roles of Mdr1a and nuclear factor kappaB in cell survival. J Pharmacol Exp Ther 2009;330(3):736-44. (In eng). DOI: 10.1124/jpet.109.153007.
124. Muller SO, Eckert I, Lutz WK, Stopper H. Genotoxicity of the laxative drug components emodin, aloe-emodin and danthron in mammalian cells: topoisomerase II mediated? Mutation research 1996;371(3-4):165-73.
125. Srinivas G, Babykutty S, Sathiadevan PP, Srinivas P. Molecular mechanism of emodin action: transition from laxative ingredient to an antitumor agent. Medicinal research reviews 2007;27(5):591-608. DOI: 10.1002/med.20095.
126. Wang J, Zhao Y, Xiao X, et al. Assessment of the renal protection and hepatotoxicity of rhubarb extract in rats. Journal of ethnopharmacology 2009;124(1):18-25. DOI: 10.1016/j.jep.2009.04.018.
127. Wang JB, Zhao HP, Zhao YL, et al. Hepatotoxicity or hepatoprotection? Pattern recognition for the paradoxical effect of the Chinese herb Rheum palmatum L. in treating rat liver injury. PloS one 2011;6(9):e24498. DOI: 10.1371/journal.pone.0024498.
128. Jiang LL, Zhao DS, Fan YX, Yu Q, Li P, Li HJ. Detection of Emodin Derived Glutathione Adduct in Normal Rats Administered with Large Dosage of Polygoni Multiflori Radix. Frontiers in pharmacology 2017;8:446. DOI: 10.3389/fphar.2017.00446.
129. Dong X, Fu J, Yin X, et al. Emodin: A Review of its Pharmacology, Toxicity and Pharmacokinetics. Phytotherapy research : PTR 2016;30(8):1207-18. DOI: 10.1002/ptr.5631.
130. Ma J, Zheng L, He YS, Li HJ. Hepatotoxic assessment of Polygoni Multiflori Radix extract and toxicokinetic study of stilbene glucoside and anthraquinones in rats. Journal of ethnopharmacology 2015;162:61-8. DOI: 10.1016/j.jep.2014.12.045.
131. Zheng YF, Liu CF, Lai WF, et al. The laxative effect of emodin is attributable to increased aquaporin 3 expression in the colon of mice and HT-29 cells. Fitoterapia 2014;96:25-32. (Research Support, Non-U.S. Gov't) (In eng). DOI: 10.1016/j.fitote.2014.04.002.
132. Sougiannis AT, VanderVeen BN, Enos RT, et al. Impact of 5 fluorouracil chemotherapy on gut inflammation, functional parameters, and gut microbiota. Brain Behav Immun 2019;80:44-55. (In eng). DOI: 10.1016/j.bbi.2019.02.020.
133. Cranford TL, Enos RT, Velazquez KT, et al. Role of MCP-1 on inflammatory processes and metabolic dysfunction following high-fat feedings in the FVB/N strain. International journal of obesity 2016;40(5):844-51. DOI: 10.1038/ijo.2015.244.

134. Bai J, Wu J, Tang R, et al. Emodin, a natural anthraquinone, suppresses liver cancer in vitro and in vivo by regulating VEGFR. Invest New Drugs 2019 (In eng). DOI: 10.1007/s10637-019-00777-5.
135. Tzeng TF, Lu HJ, Liou SS, Chang CJ, Liu IM. Emodin, a Naturally Occurring Anthraquinone Derivative, Ameliorates Dyslipidemia by Activating AMP-Activated Protein Kinase in High-Fat-Diet-Fed Rats. Evid Based Complement Alternat Med 2012;2012:781812. (In eng). DOI: 10.1155/2012/781812.
136. Shia CS, Hou YC, Tsai SY, Huieh PH, Leu YL, Chao PD. Differences in pharmacokinetics and ex vivo antioxidant activity following intravenous and oral administrations of emodin to rats. J Pharm Sci 2010;99(4):2185-95. (In eng). DOI: 10.1002/jps.21978.
137. Dong H, Lu FE, Gao ZQ, Xu LJ, Wang KF, Zou X. Effects of emodin on treating murine nonalcoholic fatty liver induced by high caloric laboratory chaw. World J Gastroenterol 2005;11(9):1339-44. (In eng). DOI: 10.3748/wjg.v11.i9.1339.
138. Li J, Ding L, Song B, et al. Emodin improves lipid and glucose metabolism in high fat diet-induced obese mice through regulating SREBP pathway. Eur J Pharmacol 2016;770:99-109. (In eng). DOI: 10.1016/j.ejphar.2015.11.045.
139. Program NT. NTP Toxicology and Carcinogenesis Studies of EMODIN (CAS NO. 518-82-1) Feed Studies in F344/N Rats and B6C3F1 Mice. Natl Toxicol Program Tech Rep Ser 2001;493:1-278. (In eng).
140. Wang JB, Ma YG, Zhang P, et al. [Effect of processing on the chemical contents and hepatic and renal toxicity of rhubarb studied by canonical correlation analysis]. Yao xue xue bao = Acta pharmaceutica Sinica 2009;44(8):885-90.
141. Li Y, Xiong W, Yang J, et al. Attenuation of Inflammation by Emodin in Lipopolysaccharide-induced Acute Kidney Injury via Inhibition of Toll-like Receptor 2 Signal Pathway. Iranian journal of kidney diseases 2015;9(3):202-8.
142. Stringer AM, Gibson RJ, Bowen JM, Logan RM, Yeoh AS, Keefe DM. Chemotherapy-induced mucositis: the role of gastrointestinal microflora and mucins in the luminal environment. J Support Oncol 2007;5(6):259-67. (In eng).
143. Walker EA, Foley JJ, Clark-Vetri R, Raffa RB. Effects of repeated administration of chemotherapeutic agents tamoxifen, methotrexate, and 5-fluorouracil on the acquisition and retention of a learned response in mice. Psychopharmacology (Berl) 2011;217(4):539-48. (In eng). DOI: 10.1007/s00213-011-2310-8.
144. Jin JH, Ngoc TM, Bae K, Kim YS, Kim HP. Inhibition of experimental atopic dermatitis by rhubarb (rhizomes of Rheum tanguticum) and 5-lipoxygenase inhibition of its major constituent, emodin. Phytother Res 2011;25(5):755-9. (In eng). DOI: 10.1002/ptr.3480.
145. Zhang Q, Tao X, Xia S, et al. Emodin attenuated severe acute pancreatitis via the P2X ligand-gated ion channel 7/NOD-like receptor protein 3 signaling pathway. Oncol Rep 2019;41(1):270-278. (In eng). DOI: 10.3892/or.2018.6844.
146. Meng L, Yan D, Xu W, Ma J, Chen B, Feng H. Emodin inhibits tumor necrosis factor-α-induced migration and inflammatory responses in rat aortic smooth muscle cells. Int J Mol Med 2012;29(6):999-1006. (In eng). DOI: 10.3892/ijmm.2012.940.

147. Wang T, Zhong XG, Li YH, et al. Protective effect of emodin against airway inflammation in the ovalbumin-induced mouse model. Chin J Integr Med 2015;21(6):431-7. (In eng). DOI: 10.1007/s11655-014-1898-z.
148. Liu A, Chen H, Wei W, et al. Antiproliferative and antimetastatic effects of emodin on human pancreatic cancer. Oncol Rep 2011;26(1):81-9. (In eng). DOI: 10.3892/or.2011.1257.
149. Zhu S, Wang Y, Wang X, Li J, Hu F. Emodin inhibits ATP-induced IL-1β secretion, ROS production and phagocytosis attenuation in rat peritoneal macrophages via antagonizing $P2X_7$ receptor. Pharm Biol 2014;52(1):51-7. (In eng). DOI: 10.3109/13880209.2013.810648.
150. Velázquez KT, Enos RT, Bader JE, et al. Prolonged high-fat-diet feeding promotes non-alcoholic fatty liver disease and alters gut microbiota in mice. World J Hepatol 2019;11(8):619-637. (In eng). DOI: 10.4254/wjh.v11.i8.619.
151. Swidsinski A, Weber J, Loening-Baucke V, Hale LP, Lochs H. Spatial organization and composition of the mucosal flora in patients with inflammatory bowel disease. J Clin Microbiol 2005;43(7):3380-9. (In eng). DOI: 10.1128/JCM.43.7.3380-3389.2005.
152. Swidsinski A, Loening-Baucke V, Schulz S, Manowsky J, Verstraelen H, Swidsinski S. Functional anatomy of the colonic bioreactor: Impact of antibiotics and Saccharomyces boulardii on bacterial composition in human fecal cylinders. Syst Appl Microbiol 2016;39(1):67-75. (In eng). DOI: 10.1016/j.syapm.2015.11.002.
153. Polk A, Vistisen K, Vaage-Nilsen M, Nielsen DL. A systematic review of the pathophysiology of 5-fluorouracil-induced cardiotoxicity. BMC Pharmacol Toxicol 2014;15:47. (In eng). DOI: 10.1186/2050-6511-15-47.
154. Miura K, Kinouchi M, Ishida K, et al. 5-fu metabolism in cancer and orally-administrable 5-fu drugs. Cancers (Basel) 2010;2(3):1717-30. (In eng). DOI: 10.3390/cancers2031717.
155. Buisine MP, Desreumaux P, Leteurtre E, et al. Mucin gene expression in intestinal epithelial cells in Crohn's disease. Gut 2001;49(4):544-51. (In eng). DOI: 10.1136/gut.49.4.544.
156. Enos RT, Velazquez KT, McClellan JL, et al. High-fat diets rich in saturated fat protect against azoxymethane/dextran sulfate sodium-induced colon cancer. American journal of physiology Gastrointestinal and liver physiology 2016;310(11):G906-19. DOI: 10.1152/ajpgi.00345.2015.
157. Ono M. Molecular links between tumor angiogenesis and inflammation: inflammatory stimuli of macrophages and cancer cells as targets for therapeutic strategy. Cancer Sci 2008;99(8):1501-6. (In eng). DOI: 10.1111/j.1349-7006.2008.00853.x.
158. Jedinak A, Dudhgaonkar S, Sliva D. Activated macrophages induce metastatic behavior of colon cancer cells. Immunobiology 2010;215(3):242-9. (In eng). DOI: 10.1016/j.imbio.2009.03.004.

APPENDIX A

DETAILED AIMS AND METHODOLOGY

Specific Aim #1 will evaluate the effect of 5 fluorouracil chemotherapy on inflammation, functional parameters, and gut microbiota.

Rationale: It has been previously established that 5FU chemotherapy causes severe adverse reactions and non-selective toxicities in cancer patients. Side effects include fatigue, loss of appetite, and diarrhea among others, all of which can lead to a reduced quality of life and premature death. Identifying strategies to increase efficacy and reduce toxicity of chemotherapy are of significant public health importance. Further, 5FU has been reported to cause disturbances in the gut microbiome, which can further influence the outcome of cancer therapy. Thus, the goal of this aim is to perform a comprehensive analysis of the physiological effects of 5FU therapy on inflammation, functional parameters, and gut microbiota.

Experimental design for specific aim #1. Experiment 1 will contain two separate animal experiments to test the effect of 5FU on inflammation, functional parameters and gut microbiota.

Primary Outcomes

Functional Testing: Functional tests will be employed to evaluate the effect of 5FU on quality of life measures associated with non-specific toxicities attributed to 5FU toxicity.

Inflammation: The inflammatory response to 5FU will be evaluated systemically and in major organs.

Microbiome: The effect of 5FU on the gut microbiome and microbial ecosystem will be evaluated by 16S rRNA sequencing.

Secondary outcomes:

Polyp count and size: To confirm the anti-tumor response to 5FU we will evaluate colon polyp count and size after 5FU treatment.

Specific Methodology Aim #1:

Animals: At approximately 12 weeks of age, *C57BL/6J* mice were randomized into four groups: Control + Vehicle (n=10), Control + 5FU (n=10), AOM/DSS + Vehicle (n=15), and AOM/DSS + 5FU (n=15). Control mice received a 200µl dose of sterile PBS and AOM/DSS mice received a 10 mg/kg dose of AOM prepared in sterile PBS. After one week, AOM/DSS mice received 2% DSS drinking water *ad libitum* for one week followed by two weeks of recovery. After two weeks of recovery, AOM/DSS mice received 1% DSS drinking water *ad libitum* for one week followed by 2 weeks of recovery. After two weeks of recovery all groups were subjected to a battery of functional tests (peripheral nociception, grip strength, and run-to-fatigue) over the course of one week. After recovery from functional tests, all mice commenced a three-cycle regime of PBS or 5FU treatment; cycle 1: 40 mg/kg, cycle 2 and 3: 20 mg/kg via intraperitoneal injection. Each cycle consisted of 5 consecutive days of injection followed by 9 days of recovery. The treatment period lasted for 5 weeks and mice were sacrificed 24 hr after the final injection of the third cycle.

The second animal study contained two phases; a donor phase and a recipient phase. The donor phase contained two groups of *C57BL/6J* mice that received either Vehicle (n=5) or 40 mg/kg 5FU (n=5). Treatments lasted for five consecutive days and then mice were sacrifice four days after the final injection. Fecal matter was collected

from mice via mucosal scrape and pellet collection from the anus to the cecum. Fecal matter was suspended in sterile 10% glycerol/PBS, allowed to settle by gravity for 10 min, and aliquoted into daily requirements for delivery as fecal microbial transplants to their respective recipient groups. Recipient mice were separated into two groups; Vehicle FMT (n=10) and 5FU FMT (n=15). Prior to receiving fecal microbial transplantation, recipient mice initially received an antibiotic cocktail which consisted of: Vancomycin (50 mg/kg), Neomycin (100 mg/kg), Metronidazole (100 mg/kg), and Amphotericin-B (1 mg/kg) via oral gavage and was supplemented with Ampicillin (1 mg/kg) in the drinking water given *ad libitum*. Antibiotic treatment lasted 10 days and mice were treated every 12 hours with gavage boluses. A few days prior to cessation of antibiotic treatment, all mice were subjected to functional tests (grip strength and run-to-fatigue). 12 hours after final antibiotic treatment all mice began a 14-day FMT protocol which involved 150 µl of fecal aliquot every 24 hrs. All mice were sacrifice 24 hours after the final FMT.

Table A.1 Animal treatment groups for experiment #1.

Strain	Treatment	Age (Weeks)	N
C57BL/6J	Control + Vehicle	12	10
C57BL/6J	Control + 5FU	12	10
C57BL/6J	AOM/DSS + Vehicle	12	15
C57BL/6J	AOM/DSS + 5FU	12	15
C57BL/6J	Donor Vehicle	10	5
C57BL/6J	Donor 5FU	10	5
C57BL/6J	Recipient Vehicle	12	10
C57BL/6J	Recipient 5FU	12	15

Table A.2 Animal clinical score guidelines.

Body Weight Loss	Fecal Hemoccult	Diarrhea
5% = 0	No blood = 0	Hard stool
6-10% = 1	Positive test = 2	Soft stool = 2
11-15% = 2	Visible blood = 4	Runny stool = 4
16-20% = 3		
>20% = 4		

Functional Testing:

Grip strength assessment

All experimental mice were utilized to evaluate the effects of 5FU treatment on grip strength. Grip strength was measured prior to 5FU administration (week 8) and during the recovery period of the second cycle (week 11) in experiment 1 and following

antibiotic treatment (week 0) and fecal transplantation (week 2) in experiment 2. The assay was performed as follows: Holding the mice by the tail, the front and back feet were allowed to grip a grate attached to a force transducer (Aurora Scientific, Ontario, Canada). Mice were then pulled from the grate, generating a force that was measured by the force transducer. Five measurements were taken consecutively, with at least 2 min rest between sets until a total of 15 measurements were taken for each mouse. The averages of the 15 measurements were used in the data analysis. Measurements were performed by the same investigator through the entirety of the study. Body weight was measured immediately prior to the administration of the grip strength test and used to calculate relative (N/kg) grip strength.

Run-to-fatigue assessment

To determine the effect of 5FU on fatigability, mice were subjected to a run-to-fatigue test prior to 5FU administration (week 8) and during the recovery period of the second cycle (week 11) in experiment 1 and following antibiotic treatment (week 0) and fecal transplantation (week 2) in experiment 2. After 3 consecutive days of habituation during the night cycle, mice were subjected to the following run-to fatigue protocol: 15-min warm-up, 20 m/min for 30 min, and 25 m/min thereafter until fatigue was reached. Fatigue was defined as the time at which mice were no longer able or willing to keep up with the treadmill despite hand prodding for at least 1 min. All treadmill tests were performed during the night cycle by the same investigators through the entirety of the study.

Blood Panel Analysis: Blood panel analysis was performed using the VetScan HMT (Abaxis, Union City, CA). Blood was collected in EDTA-coated lavender top tubes from

the inferior vena cava of mice that were overdosed with isoflurane. Tubes were mixed by inverting multiple times and stored on ice until transported to the School of Medicine for analysis. Tubes were places in the VetScan HMT apparatus, and the following counts were obtained: WBC, LYM, MON, NEU, PLT, RBC, Hct, and Hb. Neutrophil/Lymphocyte ratio (NLR) was calculated from obtained values.

Polyp count: At tissue collection the colon was carefully dissected distal to the cecum and proximal to the anus. Mesentery adipose tissue was removed with forceps. The colon was opened longitudinally, and polyps were counted and measured using a dissecting microscope.

RNA isolation and qPCR: Tissue samples were homogenized in 1 mL TRIzol reagent (Life Technologies, GIBCO-BRL, Carlsbad, CA) reagent using mechanical bead beating. After incubating for 5 min at room temperature, 200µl of ultrapure chloroform was added, samples were mixed, and then incubated at room temperature for 5 minutes. Samples were then centrifuged at 14,000g for 15 min at 4^0C and the resulting supernatant was removed and mixed with equal volume (~500 µl) ultrapure isopropanol to precipitate RNA. After precipitation at room temperature for 5 minutes, samples were centrifuged at 14,000g for 15 min at 4^0C to pellet RNA. After pellets were obtained, the supernatant was discarded, and pellets were washed twice with 70% ultrapure ethanol. Samples were centrifuged at 7,500g for 6 min between washes. After washes, pellets were dried and dissolved in 100 µl ultrapure RNase free water. To further purify RNA, samples were incubated twice with 10 µl of 8M Lithium Chloride on ice for 1 hr and centrifuged at 14,000g for 20 min between incubations. After the final incubation, pellets were dissolved in 100 µl ultrapure RNase free water and RNA was precipitated in 10 µl 3M

Sodium Acetate and 200 µl ultrapure ethanol. After precipitation, samples were centrifuged at 14,000g for 20 min at 4^0C. After centrifugation, the supernatant was discarded and the resulting pellet was washed with 800 µl of 75% ultrapure ethanol and recentrifuged at 14,000g for 10 min at 4^0C. Pellets were then dried and dissolved in 80 µl ultrapure RNase free water. RNA sample quality and quantities were verified using a Nanodrop One Microvolume Spectrophotometer (Thermofisher, San Diego, CA) and determined to be of good quality based on A260/A280 values (>1. 8) prior to cDNA synthesis using QuantiTect Reverse Transcription kit (Qiagen 205313). Quantitative RT-PCR analysis was carried out as per the manufacturer's instructions (Applied Biosystems) using Taq-Man Gene Expression Assays. We utilized groups of 3 color gene expression assays consisting of FAM, VIC, and JUN fluorophores. Data were normalized to vehicle treated controls and compared to five reference targets (B2M, TBP, HPRT, HMBS, and H2AFV), which were evaluated for expression stability using the GeNorm algorithm.[98,99]

Histopathology:

Hematoxylin & Eosin staining (H&E)

Transverse sections (~5µm) were cut from the paraffin embedded tissues on a rotary microtome. Cut tissues will be allowed to expand on a 40^0C -45^0C water bath and then attached to (+) charged saline coated microscope slides. Excess paraffin is removed by placing slides in a 65^0C oven for 1hr and then stored at 4^0C until staining. Sections were warmed to room temperature for 5-10 min. In cases of polyp analysis, tissue morphology was analyzed by observation and comparison to healthy tissue control sections. Sections were deparaffinized using the following washing progression; 3x5min

xylene washes, 2x5min 100% EtOH, 1x3min 95% EtOH, and 1x3min 70% EtOH. Sections were then washed for 5min in dH_2O, stained with filtered hematoxylin for 5min, then again washed 6x5 in dH_2O. Sections were washed in acid alcohol mix (160mL 100% EtOH, 1mL acetic acid, and volumed to 200mL with dH_2O) for 6 dips then again washed in dH_2O for 4 dips. Sections are then washed in Ammonia H_2O (0.6mL Ammonium OH volumed to 200mL with dH_2O) for 6 dips and then again washed in dH_2O for 10min. The sections were then be stained with Eosin for 2min and dehydrated in the following alcohol progression; 1x2min 70% EtOH, 1x2min 95% EtOH, 2x3min 100% EtOH, and 2x5min xylene. Sections were allowed to air dry for 30min and then mounted for viewing with Permount mounting media. Digital photographs will be taken from each section at 4x, 10x, 20x and 40x with a Nikon E600 Widefield Epifluorescence and Darkfield Microscopy System at the University of South Carolina School of Medicine, and morphology examined. All histopathological analyses were performed by a board-certified pathologist at the University of South Carolina School of Medicine (Dr. Ioulia Chatzistamou, M.D. Ph.D.).

Immunohistochemistry: Transverse sections (~5μm) were cut from the paraffin embedded tissues on a rotary microtome. Cut tissues will be allowed to expand on a 40^0C -45^0C water bath and then attached to (+) charged saline coated microscope slides. Excess paraffin is removed by placing slides in a 65^0C oven for 1hr and then stored at 4^0C until staining. Sections were warmed to room temperature for 5-10 min. Sections were deparaffinized using the following washing progression; 3x5min xylene washes, 2x5min 100% EtOH, 1x3min 95% EtOH, 1x3min 70% EtOH, and finally washed for 5min in dH_2O. To unmask antigens, sections were incubated in citrate unmasking

solution (Vector Labs) for 30 min at 95^0C and then cooled for 20min at room temperature. Sections were then washed in PBS for 5 min then blocked in 10% serum from the host species of the dedicated secondary antibody (i.e. Goat serum) in a humid chamber. After blocking, primary antibodies were diluted 1:100 in 5% goat serum and incubated overnight at 4^0C. The next day, sections were washed with PBS for 5 min and then incubated with an HRP-conjugated secondary antibody for 1 hour at room temperature in a humid chamber and finally washed in PBS. DAB solution was used to develop HRP-conjugated secondary antibodies. After DAB development, sections were washed with dH_2O and counterstained with acidic Harris Hematoxylin solution for 30s -1 min. After briefly washing in dH_2O, sections were dehydrated quickly through 95% EtOH and 100% EtOH. Sections were allowed to air dry for 30min and then mounted for viewing with Permount mounting media. Immunohistochemistry stains were imaged at 4x, 10x, 20x and 40x with a Nikon E600 Widefield Epifluorescence and Darkfield Microscopy System at the University of South Carolina School of Medicine.

Fecal transplantation: For the fecal transplantation experiment (Fig. 1B), 35 mice were randomly divided into four groups: Donor Vehicle, Donor 5FU, Recipient Vehicle (Vehicle FMT), Recipient 5FU (5FU FMT) (n=5 per Donor group and n=10–15 per Recipient group). The Donor 5FU group was injected with 40 mg/kg 5FU for 5 consecutive days as described earlier. All Donor mice were sacrificed 9 days after initial injection and a mucosal scrape was performed of the distal enteric tract (cecum to anus) to harvest the microbiota for fecal transplantation. Fecal materials were suspended in sterile 10% glycerol/PBS, allowed to settle by gravity for 10 min, and aliquoted into daily requirements for Recipient groups. To perform the FMT study we adopted a protocol by

Reikvam et al. 2011[95]. Recipient mice were pretreated with the following antibiotic cocktail every 12 h for 10 days prior to FMT: Vancomycin (50 mg/kg), Neomycin (100 mg/kg), Metronidazole (100 mg/kg), and Amphotericin-B (1 mg/kg) via oral gavage supplemented with Ampicillin (1 mg/ml) in the drinking water given ad libitum. All antibiotics were purchased from ACROS Organics, New Jersey. FMT was administered via oral gavage for 14 days with 150 µl respective fecal suspension from PBS or 5FU injected mice.

Microbiota sequencing and PICRUSt analysis: All Microbiome analysis and sequencing was performed by the University of North Carolina Microbiome Core. Fecal evacuates were collected from each mouse at the conclusion of the study and were chosen at random for 16S rRNA sequencing, at least one sample from each cage was used to prevent a cage effect in the data. A final n=5/group was obtained and used for 16S rRNA sequencing. DNA was isolated from fecal evacuates homogenized with bead-beating using the Qiagen Qiamp Fast DNA Stool Mini Kit (Qiagen #51604) and was used for 16S rRNA gene targeted sequencing using the V4 region on an Illumina MiSeq sequencer[100,101]. Amplification of the 16S rRNA V4 hypervariable region was carried out using the 16S V4 515F forward (5′ TCGTCGGCAGCGTCAGATGTGTATAAGAGAC AGGTGCCAGCMGCCGCGGTAA 3′) and V4 806R reverse primer (5′ GTCTCGTGG GCTCGGAGATGTGTATAAGAGACAGGGACTACHVGGGTWTCTAAT 3′) with added Illumina adapter overhang nucleotide sequences. The PCR conditions used were initial denaturing step at 95 °C for 3 min, followed by a cycling of denaturing of 95 °C for 30 s, annealing at 55 °C for 30 s and a 30 s extension at 72 °C (25 cycles), a 5 min extension at 72 °C and a final hold at 4 °C. Each 16S amplicon was purified using the

AMPure XP reagent (Beckman Coulter, Indianapolis, IN). In the next step each sample was amplified using a limited cycle PCR program, adding Illumina sequencing adapters and dual index barcodes (index 1(i7) and index 2(i5)) (Illumina, San Diego, CA) to the amplicon target. The thermal profile for the amplification of each sample had an initial denaturing step at 95 °C for 3 min, followed by a denaturing cycle of 95 °C for 30 s, annealing at 55 °C for 30 s and a 30 s extension at 72 °C (8 cycles), a 5 min extension at 72 °C and a final hold at 4 °C. The final libraries were again purified using the AMPure XP reagent (Beckman Coulter), quantified and normalized prior to pooling. The DNA library pool was then denatured with NaOH, diluted with hybridization buffer and heat denatured before loading on the MiSeq reagent cartridge (Illumina) and on the MiSeq instrument (Illumina).

Automated cluster generation and paired–end sequencing with dual reads were performed according to the manufacturer's instructions. Multiplexed paired-end fastq files were produced from the sequencing results of the Illumina MiSeq using the Illumina software configure BclToFastq. The paired-end fastq files were joined into a single multiplexed, single-end fastq using the software tool fastq-join. Demultiplexing and quality filtering was performed on the joined results. Quality analysis reports were produced using the FastQC software. Bioinformatics analysis of bacterial 16S amplicon sequencing data was conducted using the Quantitative Insights Into Microbial Ecology (QIIME) software[102]. Operational taxonomic units (OTUs), an operational definition used to classify groups of closely related individuals[103], were picked from the quality filtered results using pick_de_novo_otus.py. Chimeric sequences were detected and removed using ChimeraSlayer. Alpha diversity and beta diversity analysis were performed on the

data set using the QIIME routines: alpha_rarefaction.py and beta_diversity_-through_plots.py, respectively. Summary reports of taxonomic assignment by sample and all categories were produced using QIIME summarize_taxa_through_plots.py and summarize_otu_by_cat.py[103]. Samples were rarefied at 10,000 reads/sample. FastTree2 (Price MN, Dehal PS, Arkin AP FastTree 2- approximately maximum-likelihood tress for large alignments) to build the phylogenetic tree. Finally, we used an open reference method for OTU picking. Phylogenetic Investigation of Communities by Reconstruction of Unobserved States (PICRUSt) was used to predict the functional gene content in the fecal microbiota based on taxonomy obtained from the Greengenes reference database. PICRUSt and LefSe were performed online in the Galaxy workflow framework.

Specific Aim #2 will determine the safety and efficacy of dietary emodin on reducing toxicity of 5 fluorouracil chemotherapy.

Rationale: Emodin is a natural anthraquinone found in various Chinese medicinal herbs. Recent evidence has demonstrated that emodin has many health benefits, including anti-inflammatory, anti-viral, and anti-bacterial properties, among others. In this aim, we will first characterize the safety and pharmacodynamics of emodin and then use emodin as a complementary therapeutic to attenuate the toxicities of 5FU.

Experimental design for specific aim #2.

Primary Outcomes

Pharmacodynamics: Emodin will be measured in the plasma of male and female mice given a 20 mg/kg and 40 mg/kg dose at specific time points to determine the peak concentration and rate of clearance.

Histopathology and Toxicology: A broad tissue analysis will be performed to evaluate the systemic toxicity of emodin after 3 months of continuous feeding.

Functional Testing: Functional tests will be employed to evaluate the effect of 5FU on quality of life measures associated with non-specific toxicities attributed to 5FU toxicity.

Inflammation: The inflammatory response to 5FU will be evaluated systemically and in major organs.

Secondary outcomes:

Microbiome: The effect of 5FU on the gut microbiome and microbial ecosystem will be evaluated by 16S rRNA sequencing.

Specific Methodology Aim #2:

Animals: For experiment 1; we performed a subchronic (12 week) toxicity study using 3 different doses of emodin (~20 mg/kg, 40 mg/kg, and 80 mg/kg) infused into the AIN-76A diet of male and female mice (n=5/group/sex).

For experiment 2; we evaluated chronic (n=5-20/group) and acute (n=20/group/sex) interventions to 5FU.

Emodin Preparation: Emodin was purchased from Nanjing Zelang Medical Technology Co., Ltd, (Nanjing, China). Emodin was independently analyzed by the Mass Spectrometry Center at the University of South Carolina prior to the initiation of the experimental study. LC-UV-MS and NMR was performed to confirm the purity of Emodin and the molecular structure. Emodin was delivered intraperitoneally (I.P.) or by oral gavage (P.O.) at 20 mg/kg or 40 mg/kg doses. For I.P., emodin, dissolved in DMSO

was made in a large batch, aliquoted, and stored at -20^{0}C until used for injections. It was subsequently diluted in PBS (1% DMSO) and administered to mice I.P. at doses of 20 mg/kg (0.5mg/mL) or 40 mg/kg (1mg/mL). To deliver emodin P.O., we utilized a 20G 30-mm flexible plastic tubal oral gavage needle (Instech, #FTP-20). To prevent aspiration of the emodin bolus, mice were briefly anesthetized with 2% isoflurane prior to gavage and held upright until consciousness was regained. Emodin was prepared fresh on the day of administration. Briefly, emodin was mixed in pure propylene glycol (VWR, #97061) for 6-8 hours at room temperature while protected from light. The emodin solution was delivered to mice at 20 mg/kg (6 mg/mL) and 40 mg/kg (12 mg/mL) doses. We used 1% DMSO in PBS (I.P.) or pure propylene glycol (P.O.) for vehicle controls.

Specific Aim #2: will determine the safety and efficacy of dietary emodin on reducing toxicity of 5 fluorouracil chemotherapy.

Table A.3 Animal treatment groups for experiment #1.

Strain	Treatment	Age (Weeks)	N
C57BL/6J	AIN Diet	10	5/sex
C57BL/6J	Low Emodin Diet	10	5/sex
C57BL/6J	Medium Emodin Diet	10	5/sex
C57BL/6J	High Emodin Diet	10	5/sex

Table A.4 Animal treatment groups for experiment #2.

Strain	Treatment	Age (Weeks)	N
C57BL/6J	Control + Vehicle	10	5
C57BL/6J	Control + 40 mg/kg Emodin	10	5
C57BL/6J	5FU + Vehicle	10	20
C57BL/6J	5FU + 40 mg/kg Emodin	10	20
C57BL/6J	5FU + Vehicle	10	20/sex
C57BL/6J	5FU + 20 mg/kg	10	20/sex
C57BL/6J	5FU + 40 mg/kg	10	20/sex
C57BL/6J	5FU + 80 mg/kg	10	20/sex

Solid Phase Extraction and LC-MS/MS Analysis:

Whole blood was collected in EDTA coated tubes from the inferior vena cava and centrifuged at 4,000 RPM for 10 min. Plasma was aliquoted and stored at -20^{0}C until solid phase extractions. For free emodin quantification, 50 µl plasma was mixed with equal 0.2M sodium acetate buffer with 1% ascorbic acid (pH 5.0). For emodin glucuronide quantification, 50 µl plasma was mixed with half volume of 0.2M sodium acetate buffer with 1% ascorbic acid and 1000 units of β-glucuronidase (Millipore Sigma #G2174). D4-emodin (1 ng/µl) was used as an internal standard (Santa Cruz #218302). Both tubes were then incubated at 37^{0}C for 2hr. After incubation, the mixture was extracted with 600 µl ethyl acetate three times. The ethyl acetate layer was evaporated under N_2 gas to dryness and reconstituted in 5% ammonia water. Solid phase extraction was performed using a vacuum manifold (Supelco #SU57250-U) with Oasis MCX cartridges (Fisher #186000254) and was eluted with 3 mL 5% formic acid-methanol.

After elution, the eluent was evaporated under N_2 gas to dryness and reconstituted in 400 µl 5% ammonia methanol.

Emodin samples were analyzed and quantified by LC-MS/MS using electrospray ionization in negative ion mode. Chromatorgraphic separation was performed on a Waters Acquity UPLC system using a binary solvent gradient. Solvent A was water containing 0.1% formic acid and solvent B was methanol. The LC column was a Waters XBridge C18 reversed phase column (2.1mm X 100mm containing 3.5um particles) running at a flow rate of 0.2 mL/min. The solvent gradient started at 50%B, ramped to 95%B over 10 minutes and was maintained at 95%B until 14 minutes. The gradient then returned to initial conditions. The mass spectrometer was a Waters Premier XE triple quadrupole instrument. Data was collected in multiple reaction monitoring (MRM) mode. Two precursor/product ion pairs were monitored; one pair for emodin (269 daltons > 225 daltons) and one pair for the internal standard deuterium labeled emodin (273 daltons > 229 daltons). According to the standard curve of emodin in 5% ammonia methanol, the concentration of emodin was calculated relative to the D4-emodin internal standard. Total emodin was measured from the tube containing the β-glucuronidase, free emodin was measured from the tube without β-glucuronidase, and glucuronidated emodin was calculated as the difference between total emodin and free emodin.

Histopathology:

Hematoxylin & Eosin staining (H&E)

H&E staining was performed as described in Aim 1.

Alcian Blue staining

Goblet cells were observed using Alcian blue staining. Transverse sections (~5μm) were cut from the paraffin embedded tissues on a rotary microtome. Cut tissues will be allowed to expand on a 40^0C -45^0C water bath and then attached to (+) charged saline coated microscope slides. Excess paraffin is removed by placing slides in a 65^0C oven for 1hr and then stored at 4^0C until staining. Sections were warmed to room temperature for 5-10 min. Sections were deparaffinized using the following washing progression; 3x5min xylene washes, 2x5min 100% EtOH, 1x3min 95% EtOH, 1x3min 70% EtOH, and finally washed for 5min in dH_2O. Sections were then stained with Alcian Blue solution (1% Alcian blue, 3% acetic acid) for 30 min and then washed with tap water, then dH_2O. After washing, sections were counterstained with Nuclear Fast Red solution (0.1% nuclear fast red, 5% aluminum sulfate) for 5 minutes and then washed in tap water. Sections were then washed with dH_2O and dehydrated quickly through 95% EtOH and 100% EtOH. Sections were allowed to air dry for 30min and then mounted for viewing with Permount mounting media. Digital photographs will be taken from each section at 4x, 10x, 20x and 40x with a Nikon E600 Widefield Epifluorescence and Darkfield Microscopy System at the University of South Carolina School of Medicine.

Trichrome staining

Transverse sections (~5μm) were cut from the paraffin embedded tissues on a rotary microtome. Cut tissues will be allowed to expand on a 40^0C -45^0C water bath and then attached to (+) charged saline coated microscope slides. Excess paraffin is removed by placing slides in a 65^0C oven for 1hr and then stored at 4^0C until staining. Sections were warmed to room temperature for 5-10 min. Sections were deparaffinized using the following washing progression; 3x5min xylene washes, 2x5min 100% EtOH, 1x3min

95% EtOH, 1x3min 70% EtOH, and finally washed for 5min in dH_2O. Sections were then re-fixed in Bouin's solution for 1 hr at 56^0C and then washed in dH_2O for 10 min. Sections were then stained in Biebrich scarlet-acid fuchsin solution for 10-15 minutes and then washed in dH_2O. Sections then were differentiated in phosphomolybdic-phosphotungstic acid solution for 10-15 minutes. Sections were then placed directly (without rinsing) into aniline blue solution for 5-10 minutes, rinsed briefly in dH_2O and differentiated in 1% acetic acid solution for 2-5 minutes. Sections were then washed with dH_2O and dehydrated quickly through 95% EtOH and 100% EtOH. Sections were allowed to air dry for 30min and then mounted for viewing with Permount mounting media. Digital photographs will be taken from each section at 4x, 10x, 20x and 40x with a Nikon E600 Widefield Epifluorescence and Darkfield Microscopy System at the University of South Carolina School of Medicine, and morphology examined. All histopathological analyses were performed by a board-certified pathologist at the University of South Carolina School of Medicine (Dr. Ioulia Chatzistamou, M.D. Ph.D.).

Plasma Cytokine Analysis: Plasma was analyzed for common markers of major organ toxicity/physiological impairment including ALT (Cayman Chemical, 700260) and creatinine (Cayman Chemical, 700460) and according to manufacturer's instructions.

Functional Testing:

Peripheral nociception assessment

All experimental mice were utilized to evaluate the effects of 5FU treatment on peripheral neuropathic nociception. After 3 consecutive days of habituation to the testing apparatus, right hind-paws were tested for neuropathic nociception by a single experimenter blinded to experimental conditions using Von Frey filaments (North Coast Medical, Morgan Hill, CA). Each Von Frey filament was tested for 5 consecutive

measurements, data was calculated as the paw withdrawal threshold in grams of force. Threshold was determined by 3 consecutive reactions to the stimulus. Measurements were performed by the same investigators through the entirety of the study (A. Sougiannis). Total stimuli were also summed to interpret total sensitivity to the touch test.

Grip strength assessment

Grip strength assessment was performed as described in Aim 1.

Run-to-fatigue assessment

Run-to-fatigue assessment was performed as described in Aim 1.

Blood Panel Analysis: Blood panel analysis was performed as described in Aim 1.

RNA isolation and qPCR: RNA isolation and qPCR were performed as described in Aim 1.

16S rRNA *in-situ* hybridization: Colons were excised whole from the rectum to the anus, opened longitudinally without disturbing opened tissue, and fixed for 24hrs in Carnoy's solution (6:6:1 – Ethanol:Acetic Acid:Chloroform) then processed and embedded into paraffin blocks by standard techniques. 5μm section were placed on SuperFrost slides for FISH studies. The oligonucleotide probe (EUB338: 5'-GCTGCCTCCCGTAGGAGT-3') was purchased from EuroFins synthesized with carbocyanite dye (Cy3) added to the 5'-end. Sections were deparaffinized and dehydrated with 4x3 min washes in xylene followed by 4x3 min washes in 100% EtOH. Bacterial cell walls were opened by washing sections in ultrapure chloroform for 15 min, air dried for 1 min, then put in a 50^0C oven for 30 min. Hybridization buffer was prepared with 1% formamide and prewarmed before hybridizations. 2 mL preparations were as follows: 20μl, 1,580 μl dH_2O, 360 μl 5M NaCl, 40 μl 1M Tris HCl (pH7.4), and 10 μl 10% SDS. Samples were

incubated with EUB338 probe diluted 1:100 in buffer for 1 hr at 50^0C in a humid chamber. After incubation, samples were washed with dH_2O and incubated for 5 min at room temperature with 1 μg/mL DAPI solution and washed again. Diluted hybridization buffer was used as a mounting media and imaged immediately using a Leica DM2500 fluorescent microscope.

Western Blotting: Whole cell protein extracts were obtained by homogenizing bone marrow isolates in 300μl Mueller Buffer. Homogenates were centrifuged at 14,000 RPM for 15 min and then supernatants were aliquoted to new microcentrifuge tubes. Total protein per μl was quantified using the Bradford method. Tissue homogenates were separated on had casted 10-12% SDS-PAGE gels and transferred to nitrocellulose membranes. The gels are transferred to nitrocellulose membranes for 1hr at 12V in room temperature transfer buffer. After transfer, membranes were washed with dH_2O and stained with ponceau S to ensure equal loading and proper transfer. Membranes were then blocked with TBS with 0.1% Tween 20 and 5% non-fat milk (5% TBST) for 1 hr at room temperature and then placed in primary antibody at dilutions of 1:600-1:1000 overnight at 4^0C. The next day, after 3x10 min wash with TBST, secondary anti-rabbit IgG-conjugated secondary antibodies were incubated with the membranes at 1:2000 for 1 hr in 5% TBST at room temperature. Enhanced chemiluminescence was used to visualize the antibody-antigen interactions and develop the blot using autoradiography. Autoradiographs were scanned to digital files and were analyzed by measuring the integrated optical density of each band using Image J software (NIH, Bethesda, MD). Obtained data was normalized to the total protein loaded in each lane which was

determined by quantification of each lane after membranes were stained with Amido Black solution and scanned to digital files.

Flow Cytometry: Flow cytometry was performed using the BD FACS ARIA II machine located and operated by the UofSC School of Medicine Instrument Resource Facility. Bone marrow was flushed from both left and right femurs of mice using PBS and passed through 70μm cell strainers. An aliquot of cells was fixed in 70% EtOH for 24hr at-20^0C prior to staining with Ki67 and Propidium Iodide (PI) for cell cycle analysis. Remaining unfixed cells were resuspended in flow buffer (PBS with 5% FBS) and blocked with FC block (anti-CD16/CD32) for 30min at 4^0C. After blocking cells were stained with macrophage panel (CD11b – FITC, F4/80 – PE, and CD45 – PE/Cy7) for 1hr at 4^0C. Cells were then washed twice with sterile PBS and then resuspended in 1mL PBS for flow cytometric analysis. Analysis was performed using FlowJo_v10.6.2 software by identifying CD45+ immune cells, then gating for CD11b+ monocytes and F4/80+ to identify double positive cells as mature macrophages.

Specific Aim #3 will determine the efficacy of dietary emodin on preventing colorectal cancer.

Rationale: There is emerging evidence that emodin may have anti-tumor properties. We will use the AOM/DSS and $Apc^{min/+}$ models of colorectal cancer to investigate the potential for emodin to be administered as a preventative agent to patients at risk for developing colorectal cancer.

Experimental design for specific aim #3. Aim 3 will contain two separate animal experiments to test the efficacy of emodin as a preventative agent against the development of colorectal cancer.

Primary Outcomes

Polyp Count: The total polyp number will be evaluated.

Inflammation: The inflammatory response to 5FU will be evaluated systemically and in major organs.

Secondary outcomes:

Microbiome: The effect of emodin on the gut microbiome and microbial ecosystem will be evaluated by 16S rRNA sequencing.

Specific Methodology Aim #3:

Animals: $Apc^{min/+}$ mice were purchased from Jackson Laboratories at 4 weeks of age and were habituated to AIN-76A diet for 1 week prior to the start of the experiment. At 5 weeks of age mice were randomized into two groups: $Apc^{min/+}$ + Vehicle (n=8) and $Apc^{min/+}$ + 80 mg/kg emodin (n=8). Mice were euthanized at 16 weeks of age and tissues were collected. For chemical induction of CRC (AOM/DSS model) *C57BL/6J* mice from Jackson Laboratories were randomized into four groups at approximately 12 week of age: Control (n=5), AOM/DSS + Vehicle (n=20), AOM/DSS + 40 mg/kg emodin (n=20), and AOM/DSS + 80 mg/kg emodin (n=20). Control mice received a 200µl dose of sterile PBS and AOM/DSS mice received a 10 mg/kg dose of AOM prepared in sterile PBS. After one week, AOM/DSS mice received 2% DSS drinking water *ad libitum* for one week followed by two weeks of recovery. After two weeks of recovery, AOM/DSS mice received 1% DSS drinking water *ad libitum* for one week followed by 2 weeks of

recovery. Mice were euthanized after 12 weeks of treatment and tissues were collected. Symptom scores were determined using the same method as in Aim 1.

Emodin Preparation:

Emodin was prepared as described in Aim 2 and administered orally.

Specific Aim #3: will determine the efficacy of dietary emodin on preventing colorectal cancer.

Table A.4 Animal treatment groups for experiment #2.

Strain	Treatment	Age (Weeks)	N
C57BL/6J	Control + Vehicle	10	5
C57BL/6J	AOM/DSS + Vehicle	10	20
C57BL/6J	AOM/DSS + 40 mg/kg Emodin	10	20
C57BL/6J	AOM/DSS + 80 mg/kg Emodin	10	20
$Apc^{min/+}$	Vehicle	4	8
$Apc^{min/+}$	80 mg/kg Emodin	4	8

Genotyping: All $Apc^{min/+}$ mice were genotyped using a tail snip and DNA PCR. At 4-5 weeks of age; animals will be weaned, numbered, and a small tail snip (~1-2mm) collected. The tail snip is digested in 200µL of tail digest buffer and 5µL of proteinase K. Tails are incubated overnight in a water bath set at 55OC. After incubation, samples are heat shocked at 95OC in a dri-bath for 10 minutes. Heterozygosity of the *Apc* gene will be determined *via* a PCR reaction (*Apc* forward 5' TGAGAAAGACAGAAGTTA 3', reverse 5' TTCCACTTTGGCATAAGGC 3'). PCR products are run out on a 5%

polyacrylamide gel and exposed to UV light. Presence of a band indicates heterozygosity of the *Apc* gene.

Polyp count: Intestinal polyps from $Apc^{min/+}$ mice were counted by staining in methylene blue. Formalin fixed intestinal sections from all $Apc^{min/+}$ mice were rinsed in deionized water, briefly stained in 0.1 % methylene blue, and counted by the same investigator who was blinded to the treatments. Polyps from AOM/DSS mice were counted during surgical resection without methylene blue. Polyps were counted under a dissecting microscope, using forceps to pick through the villi and crypts to identify polyps. Polyps were categorized as small (< 1 mm), medium (1-2 mm), or large (> 2 mm). After polyps were counted, methylene blue stained intestinal sections were washed with 70% ethanol and embedded in paraffin for further analysis.

Flow Cytometry: Flow cytometry was performed using the BD FACS ARIA II machine located and operated by the UofSC School of Medicine Instrument Resource Facility. Bone marrow was flushed from both left and right femurs of mice using PBS and passed through 70μm cell strainers. Cells were resuspended in flow buffer (PBS with 5% FBS) and blocked with FC block (anti-CD16/CD32) for 30min at 4^0C. Lamina propria was isolated from whole excised colons using the Miltenyi Biotech Lamina Propria Dissociation Kit, Mouse (Miltenyi# 130-097-410). After blocking, cells were stained with macrophage panel (CD11b – FITC, F4/80 – PE, CD206 - APC, CD11c – APC/Cy7, Ly6C – PerCP/Cy5.5, and CD45 – PE/Cy7) for 1hr at 4^0C. Cells were then washed twice with sterile PBS and then resuspended in 1mL PBS for flow cytometric analysis. Analysis was performed using FlowJo_v10.6.2 software by identifying CD45+ immune cells, then gating for CD11b+ monocytes and Ly6C+ activated cells to identify F4/80+

cells as mature macrophages. Mature macrophages were then gated and analyzed for CD11c and CD206 expression to identify M1- and M2-type macrophages, respectively.

RNA isolation and qPCR:

RNA isolation and qPCR were performed as described in Aim 1.

Histopathology:

Hematoxylin & Eosin staining (H&E)

H&E staining was performed as described in Aim 1.

Western Blotting:

Western blotting was performed as described in Aim 2.

APPENDIX B

EMODIN PRODUCT INTEGRITY

Principal Investigator: Alexander T. Sougiannis
Re: 1 F31 AT009820-01
Product Information: Emodin

D. Refined Products

D1. Name the supplier of the product. *

Nanjing Zelang Medical Technology Co., Ltd.

D2. Present data on the characterization of the product (e.g., chemical profile or fingerprint) as thoroughly as the state of the science allows.

a. **Indicate the purity if the product is a single component.**
b. **Provide concentration of major and minor components if the product is a mixture.**
c. **Information from suppliers MUST be confirmed through independent analysis either by a third-party lab or by the investigator (if they have appropriate facilities and expertise). Provide conformational data (e.g. chromatograms and/or spectra) or a plan regarding how this will be obtained.**

Purity: *Emodin is a single component with >98% purity.*

Independent verification: *Nanjing Zelang Medical Technology Co., Ltd. will perform preliminary identification of Emodin sample using in-house LC-UV-MS techniques. Nanjing Zelang Medical Technology Co., Ltd. will provide a certificate of analysis (see Appendix, documents in Chinese and English) with identity and impurity test results and source information. Emodin will be independently analyzed by the Mass Spectrometry Center at the University of South Carolina prior to the initiation of any experimental study (see Appendix). LC-UV-MS and NMR will be performed to confirm the purity of Emodin and the molecular structure (see Appendix). All chemicals and reagents used for standardization at the University of South Carolina will be HPLC-grade.*

D3. Provide data on the analysis of the product for contaminants/impurities such as pesticides, heavy metals, and residual solvents.

Product information: *Nanjing Zelang Medical Technology Co., Ltd. follows the guidelines of the China Food and Drug Administration (CFDA) which includes testing of heavy metals, impurities, and other toxins (see Appendix).*

Independent verification: *After receiving Emodin, I will send the Emodin powder to be tested for microbial aflatoxin, heavy metal, and pesticide presence to NP Analytical Laboratories (St. Louis, MO, USA). Microbial analysis will detect the presence of total microbial counts, yeast and most counts, gram-negative bacteria, E. coli, and salmonella. Emodin will also be tested for aflatoxin B1 presence. The presence of arsenic, cadmium, lead, and mercury heavy metals will be verified. Additionally, a pesticide screen will be performed.*

D4. Provide data on batch-to-batch reproducibility. These data may be required separately for the agent alone, the vehicle alone, and the final products as appropriate.

I will use the same batch of Emodin for the entire study, thus I do not expect to have any problems with batch-to-batch reproducibility. In the case that I need a new batch of Emodin, special attention will be given to the lot number. Further, I will perform NMR and LC-UV-MS to confirm the purity and molecular structure of the new batch. Data presented in the appendix indicates our streamlined ability to validate the Emodin extract (see NMR and MS appendix).

D5. Present a plan to monitor stability of product samples from all batches used during the study. The plan should include:

a. **How you plan to store the test agents, vehicle, and/or final product**
b. **What analyses will be conducted, the methods to be used, and how frequently and by whom the analyses will be done**
c. **Investigator's tolerances for chemical and/or biological variability, and what will be done if variability exceeds those limits. In addition, sufficient material must be retained from each batch to allow independent analysis, should NCCIH request samples. Samples should be maintained a minimum of 1 year after all results arising from the study have been published.**

Storage: *Emodin will be stored at -20 degrees Celsius as a dry powder once it arrives from the Nanjing Zelang Medical Technology Co., Ltd. Solutions of Emodin extracts will be prepared at 100mM (27 mg/ml) in DMSO and will be stored at -20 degrees Celsius.*

Stability Testing: *Before conducting a new experiment, or every 3 months, 27 mg/ml of Emodin powder will be dissolved in DMSO, aliquoted, and stored at -20 degrees Celsius. An aliquot will be used for Emodin stability testing (anti-inflammatory capacity) against a freshly prepared aliquot. Remaining aliquots will be stored at -20 degrees Celsius.*

After confirming the stability of Emodin using LC-UV-MS, I will verify the anti-inflammatory capacity of Emodin utilizing freshly harvested bone marrow derived macrophages. Briefly, bone marrow derived macrophages will be harvested and allowed to grow in the presence of 15% L929 conditioned media for 7 days. Cells will be plated on a 12-well cell culture plate at a density of $0.5x10^6$ cell/ well for 24 hours to allow for adherence. Then, cells will be treated with Emodin at 0, 50, 100, and 200 μg/ml for 24 hours. After Emodin treatment, cells will be stimulated with LPS at 100 ng/ml for 24 hours. Media and cells will be harvested and assayed for TNFα, IL-6, IL-1β, IFNγ, and CXCL2 RT-PCR assays. Results should show a dose-response of Emodin's ability to decrease TNFα, IL-6, IL-1β, and IFNγ expression in bone marrow derived macrophages stimulated with LPS. CXCL2 expression will be used as a negative control, as Emodin does not change CXCL2 expression after LPS treatment. The PI, Alexander Sougiannis, will perform all stability and cell culture experiments (see attached paper from Fan laboratory (dissertation committee member)).

Tolerances and Contingency for Variability: *Emodin aliquots that show less than 10% variability in anti-inflammatory capacity test will be used for experimental studies. If Emodin aliquots fail to reduce TNFα, IL-6, IL-1β, and IFNγ expression, shows greater than 10% variability, or does not show a dose response curve, these aliquots will not be used in any of the experiments and new Emodin aliquots will be analyzed prior to any experiments and a new LC-UV-MS fingerprint will be compared to the original chromatogram. In the event the Emodin fingerprint is not comparable to the original chromatogram, new Emodin will be ordered from the Nanjing Zelang Medical Technology Co., Ltd. and the stability protocols will be performed as described above prior to any experimentation.*

Voucher samples: *We will store voucher specimens of Emodin, and any new orders of Emodin (2 x 100g). Emodin will be stored at -20 degrees Celsius as previously described. The raw material will be confirmed taxonomically by Nanjing Zelang Medical Technology Co., Ltd. A voucher specimen will be submitted to the University of South Carolina A.C. Moore Herbarium (http://herbarium.biol.sc.edu//). The A.C. Moore Herbarium at the University of South Carolina, founded in 1907, contains over 100,000 specimens making the herbarium the largest in the state of South Carolina. The majority of material stored is native to the Southeastern United States and more specifically from South Carolina.*

D6. Provide information relevant to the manufacturing process assuring reasonably consistent material suitable for scientific study (including process control, as well as chemical standardization of ingredients).

a. **Provide information on the formulation of the final product (e.g. excipients, solvents, buffers, chow/feed composition).**
b. **Provide documentation to show product was manufactured under GMP guidelines.**

Final Product Formulation: *Nanjing Zelang Medical Technology Co., Ltd. uses crude material from Rheum palmatum to extract Emodin. As described above (sections D2, D3, and D5), we will confirm the chemical fingerprint (LC-UV-MS and NMR) and characterize Emodin upon arrival to ensure we have received a purified compound.*

GMP guidelines: *Nanjing Zelang Medical Technology Co., Ltd. follows the guidelines of the China Food and Drug Administration (CFDA). The Emodin extract to be used in our studies will be purchased from the Nanjing Zelang Medical Technology Co., Ltd. and will only be used in animal studies. The extract will be well characterized (see section D2, D3 and D5) to allow similar human studies to be performed in a GMP compliant laboratory in the future.*

D7. When the product is combined with a diet, a Certificate of Analysis and specifications for the vehicle will also be necessary to assure purity, consistency, absence of bioactive components and/or reproducibility of the vehicle. Furthermore, analysis of the formulated diet may be required to assess consistency, stability, etc., of the product in this matrix.

Not applicable. Emodin will be given by oral gavage and will be prepared fresh on the day of delivery to the animal.

南京泽朗医药科技有限公司
Nanjing Zelang Medical Technology Co., Ltd

检 验 报 告 单
Certificate of Analysis

Product Name	品名：	Emodin	大黄素
Botanical Name	植物名称：	Rheum palmatum L.	蓼科植物掌叶大黄
Batch Number	批号：	ZL130306582	
Quantity	数量：	100g	
Manufacture Date	生产日期	2013 年 3 月 08 日	
Certificate Date	报告日期	2013 年 3 月 15 日	

Analysis	分析	Specification	规格	Results	
Assay (HPLC)	含量	大黄素≥98%		98.05%	
Physical & Chemical Control		理化指标			
Identification	鉴别：	Positive reaction	呈正反应	Verified	确认
Appearance	性状：	Powder	粉末	Complies	符合规定
Color	颜色：	Orange	桔红色	Complies	符合规定
Loss On Drying	干燥失重：	≤5.0%	3.07%	Complies	符合规定
Taste	味觉：	Special taste	特殊味道	Complies	符合规定
Mesh Size	网筛孔径：	80mesh	80 目	Complies	符合规定
Heavy Metals	重金属：	≤20ppm	10ppm	Complies	符合规定
Microbiological	微生物指标				
Total Plate Count	细菌总数：	≤1000cfu/g		Complies	符合规定
Yeast & Mold	霉菌及酵母菌：	≤100cfu/g		Complies	符合规定
Salmonella	沙门氏菌：	Negative	阴性	Negative	阴性
E. Coli	大肠杆菌：	Negative	阴性	Negative	阴性
Shelf life	保存期：	36 Months	36		
贮藏 Storage	贮藏于阴凉干燥处，避免高温和强烈阳光照射 Store in a cool and dry place, keep away from strong sunlight & heat				

Analyst 分析师 ：万冬梅

Audit 审核人：

南京泽朗医药科技有限公司 质检专用章

Figure B1. Certificate of Analysis from Zelang

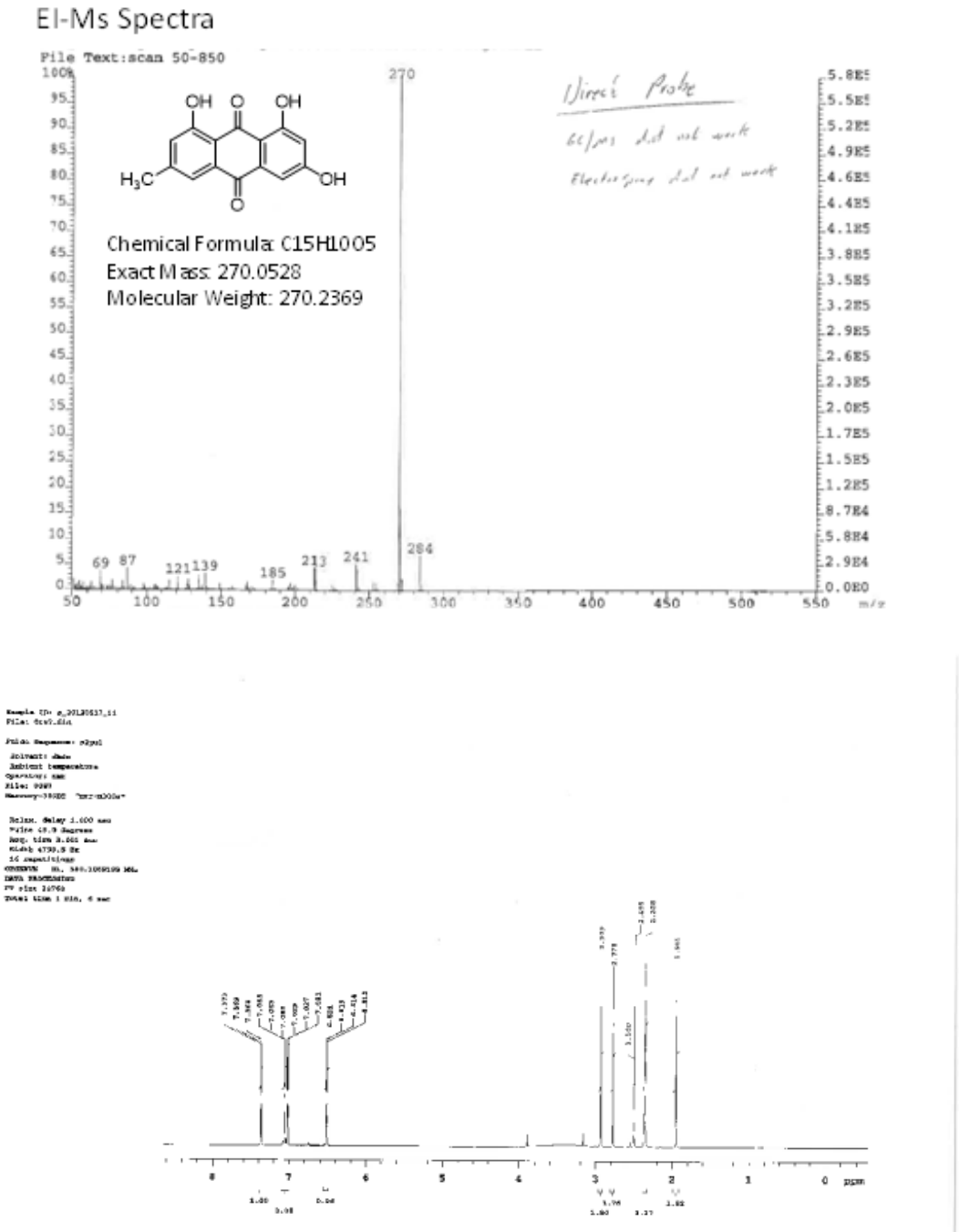

Figure B2. Chromatograms of Emodin

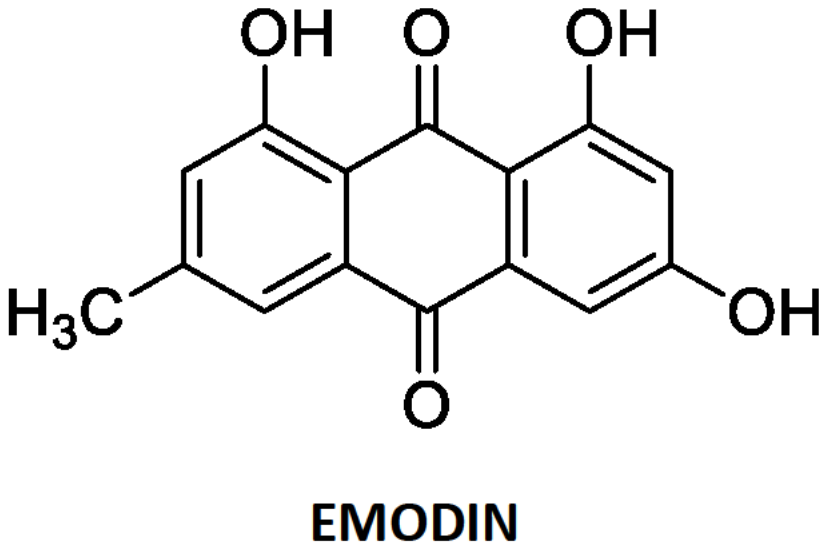

Figure B3. The chemical structure of Emodin.

References Cited

1) Iwanowycz, S., Wang, J., Altomare, D., Hui, Y. & Fan, D. Emodin Bidirectionally Modulates Macrophage Polarization and Epigenetically Regulates Macrophage Memory. *J. Biol. Chem.* **291,** 11491–503 (2016).

Emodin Bidirectionally Modulates Macrophage Polarization and Epigenetically Regulates Macrophage Memory*[S]

Received for publication, November 2, 2015, and in revised form, March 7, 2016. Published, JBC Papers in Press, March 23, 2016, DOI 10.1074/jbc.M115.702892

Stephen Iwanowycz[1], Junfeng Wang[1], Diego Altomare[2], Yvonne Hui[1], and Daping Fan[1]

From the [1]Department of Cell Biology and Anatomy, University of South Carolina School of Medicine, Columbia, South Carolina 29209 and the [2]Department of Drug Discovery and Biomedical Sciences, South Carolina College of Pharmacy, University of South Carolina, Columbia, South Carolina 29208

Macrophages are pleiotropic cells capable of performing a broad spectrum of functions. Macrophage phenotypes are classified along a continuum between the extremes of proinflammatory M1 macrophages and anti-inflammatory M2 macrophages. The seemingly opposing functions of M1 and M2 macrophages must be tightly regulated for an effective and proper response to foreign molecules or damaged tissue. Excessive activation of either M1 or M2 macrophages contributes to the pathology of many diseases. Emodin is a Chinese herb-derived compound and has shown potential to inhibit inflammation in various settings. In this study, we tested the ability of emodin to modulate the macrophage response to both M1 and M2 stimuli. Primary mouse macrophages were stimulated with LPS/IFNγ or IL4 with or without emodin, and the effects of emodin on gene transcription, cell signaling pathways, and histone modifications were examined by a variety of approaches, including microarray, quantitative real-time PCR, Western blotting, chromatin immunoprecipitation, and functional assays. We found that emodin bidirectionally tunes the induction of LPS/IFNγ- and IL4-responsive genes through inhibiting NFκB/IRF5/STAT1 signaling and IRF4/STAT6 signaling, respectively. Thereby, emodin modulates macrophage phagocytosis, migration, and NO production. Furthermore, emodin inhibited the removal of H3K27 trimethylation (H3K27me3) marks and the addition of H3K27 acetylation (H3K27ac) marks on genes required for M1 or M2 polarization of macrophages. In conclusion, our data suggest that emodin is uniquely able to suppress the excessive response of macrophages to both M1 and M2 stimuli and therefore has the potential to restore macrophage homeostasis in various pathologies.

Macrophages are a heterogeneous population of innate immune cells found in most tissues of the body (1, 2). They are capable of displaying a variety of functional phenotypes along a broad spectrum, at the extremes of which are classically activated M1 and alternatively activated M2 macrophages (3, 4). Macrophages are induced to a proinflammatory M1 state by Th1 cytokines (such as IFNγ and TNFα) and bacterial products (such as LPS). M1 macrophages play major roles in host defense against bacteria or tissue remodeling after injury through production of proinflammatory cytokines (such as IL12, TNFα, and IL1), reactive oxygen species and NO, and proteases (such as MMP 2 and 9). IFNγ and TNFα activate the JAK/STAT cascade and lead to STAT1 activation, whereas LPS activates the NFκB and MAPK cascade upon ligation with TLR4 (4, 5). A combination of stimuli, including Th2 cytokines (such as IL4, IL10, and IL13), growth factors (such as TGFβ and CSF1), glucocorticoids, and immune complexes, can polarize macrophages toward an anti-inflammatory M2 phenotype (6). M2 macrophages have major roles in tissue homeostasis and repair, inflammation resolution, and immune regulation. M2 macrophages are characterized by high expression of Arg1, YM1, Mrc1, and IL10 and low expression of proinflammatory cytokines (7). IL4/IL13 signal through the common IL4ra receptor and lead to STAT6 phosphorylation and activation, which, along with several other secondary transcription factors, including IRF4, PPARγ,[2] and KLF4, fine-tunes transcriptional responses in the cells (5, 8). Macrophage are also able to retain a memory for the signals to which they have been exposed through epigenetic modification, which results in increased transcription (priming) or repressed transcription (tolerance) upon future exposure (9–11). Cytokines cause the addition of the positive histone modifications H3K4me3 or H3K27ac to gene promoters that lead to increased expression. The mechanisms of tolerance are incompletely understood but could involve the loss of positive histone modifications and/or an increase in negative histone modifications (such as H3K27me3) (11). The different macrophage functional phenotypes need to be tightly controlled for a proper response to environmental stimuli.

An imbalance in macrophage phenotypes has been shown to contribute to the pathology of a large number of diseases (12–14). Chronic M1 macrophage activation promotes tissue damage in neurodegenerative disorders, arthritis, and autoimmune diseases (12, 15, 16). Although necessary for the initial stages of tissue repair, excessive M1 activation inhibits the healing of damaged tissue through excessive matrix degradation and inhibition of tissue regeneration (17, 18). Chronic M1 activation has

* This work was supported by National Institutes of Health Grants HL116626 and AT003963-04S5. The authors declare that they have no conflicts of interest with the contents of this article. The content is solely the responsibility of the authors and does not necessarily represent the official views of the National Institutes of Health.

[S] This article contains supplemental Tables 1–3.

[1] To whom correspondence should be addressed: Dept. of Cell Biology and Anatomy, University of South Carolina School of Medicine, 6439 Garners Ferry Rd., Bldg. 1, C36, Columbia, SC 29209. Tel.: 803-216-3806; Fax: 803-216-3846; E-mail: daping.fan@uscmed.sc.edu.

[2] The abbreviations used are: PPAR, peroxisome proliferator-activated receptor; me3, trimethylation; ac, acetylation; qPCR, quantitative PCR; IRF, interferon regulatory factor; iNOS, inducible nitric oxide synthase.

APPENDIX C

PERMISSION TO REPRINT

* Permission to reprint is obtained for Chapter 3 from the journal *Brain Behavior and Immunity*.

Obtained from https://www.elsevier.com/about/our-business/policies/copyright#Author-rights.